APPLICATION OF DATA FUSION FOR MINERALIZATION POTENTIAL MODELING, LYNN LAKE GREENSTONE BELT, MANITOBA, CANADA

Derek M. Rogge

A Thesis
Submitted to the University of Manitoba
In partial fulfillment of the requirements
For the degree of
Master of Science

Department of Geological Sciences
University of Manitoba
Winnipeg, Manitoba, Canada

THE UNIVERSITY OF MANITOBA

FACULTY OF GRADUATE STUDIES

*****

COPYRIGHT PERMISSION PAGE

APPLICATION OF DATA FUSION FOR MINERALIZATION POTENTIAL MODELING, LYNN LAKE GREENSTONE BELT, MANITOBA. CANADA

BY

Derek M. Rogge

A Thesis/Practicum submitted to the Faculty of Graduate Studies of The University of Manitoba in partial fulfillment of the requirements of the degree of

MASTER OF SCIENCE

ABSTRACT

Two quantitative data fusion combination methods, Dempster-Shafer belief theory and Fuzzy logic, have been used in this project to produce mineralization potential maps for shear-hosted gold and VMS deposit types within the southern portion of the Lynn Lake Greenstone Belt, northwestern Manitoba, Canada. An expert system, or knowledge driven approach, was adopted for this study. This approach makes use of theoretical principles to translate components of a conceptual model into a spatial model.

Ground truthing and comparison of known occurrences with potential maps were used to test the accuracy of the spatial models. Potential maps showing only the top 5% of potential value distribution were compared with known occurrences. Correlation between the known occurrences and potential maps showed an average accuracy of 74% and 57% for the shear-hosted and VMS spatial models respectively. Ground truthing noted that high strain fabrics, quartz-carbonate veining, silicification, and samples containing anomalous concentrations of gold correllated with the high potential zones defined in the shear-hosted model. For the VMS spatial model disseminated sulphides and chlorite-garnet and quartz-epidote alteration zones in subaqueous basalts and felsic volcanic units were found. Both the Burnt Timber gold mine and the Fox Lake VMS deposit were located within high potential zones in the shear-hosted and VMS potential maps respectively. In addition to the mineralization potential maps combination of data sets was also used to define major structural trends and high deformationa zones. The results from this analysis correlate well with known structure and have implications on future exploration in the belt.

The expert approach allows for experimentation and for numerous scenarios to be tested. This allowed for the evaluation of different proximity functions and tectonic scenarios. The output maps generated using the diffrent scenarios and proximity functions did show differences in the location and distribution of high potnetial zones. These differences indicate that this information can significantly effect the prioritization of exploration and should not be exclude form this type of combination.

Evaluation of the two combination methods has shown that time, scale, and missing data are the key factors in determining which method should be applied to study other areas using this appraoch to mineralization potential mapping. This project has

demonstrated how the expert system, or knowledge driven, approach can be used to translate theoretical principles defined in the conceptual model to produce a spatial model. In combination with the two data fusion methods this appoach has the ability to accurately prioritize areas for exploration.

ACKNOWLEDGEMENTS

First and foremost I would like to thank my advisor Norman Halden for his all of his support during my Masters and undergraduate work in the Department of Geological Sciences, University of Manitoba. For the always interesting discussions, both with respect to this work and more general topics. Along with Norman Halden this project could not have been completed without the help of Chris Beaumont-Smith, Manitoba Geological Survey, for all his support in the field and knowledge of structural geology; Ian Ferguson for his knowledge of geophysics and his critical comments that have resulted in a much improved thesis; and, Geoffrey DeVerteuil, Department of Geography, for his comments on the thesis.

I would also thank to thank David Leverington for his help with the SAR data; Sergio Mejia for keeping my computer running at top speed; to Paul Lenton, Manitoba Geological Survey, for helping acquire and put together the data sets; Roy Dixon, Manitoba Remote Sensing Centre, for helping to acquire the SAR data; Dianne Michalak for her help with GIS; and last but not least the staff and graduate students in the Department of Geological Sciences, University of Manitoba.

Table of Contents

List of Figures

List of Tables

1 INTRODUCTION

1.1 Introduction

Geoscientists collect a wide variety of data in order to solve, test, or simply observe a particular problem at hand. These data will include point, temporal, and spatial data, such as geochemical data, U - Pb zircon ages, and optical imagery from remote sensing platforms. Geological and geophysical data is commonly represented in a graphical format, because the information can be presented and understood more easily than the same data presented in a written format.

An exploration geologist commonly works with multiple sets of geological and geophysical spatial data in order to prioritize areas for future exploration. Analysis of the data sets allows a geologist to understand various patterns, which are relevant to processes involved in ore genesis. This interaction with the data sets allows the expert to determine how they will combine the available information. For instance, individual data sets may be weighted, based on the geoscientists experience, before combining the data sets to prioritize areas of potential economic interest. With more experience, there is greater interaction with the data, and subsequently, improved results. However, synthesis of information from the data sets is often done in an informal manner and is prone to personal bias.

The fusion of data is commonly completed instinctively. However, problems do exist with the combination or merging of multiple sets, or layers, of spatial data using only the human brain. Early interaction usually places the data in a spatial register, subsequently the user interacts with the data. For example, a geological map includes information on the various lithologic units within a given area. Interaction with this data

also allows the geologists to observe stratigraphic relations that may be indicative of a VMS deposit. VMS deposits are commonly conductive bodies, and therefore, the geologist may wish include the information available from local electromagnetic surveys. Further interaction allows the geologists to locate areas where stratigraphic relations indicative of a VMS deposit coincide with conductive bodies. The geologists has now narrowed their search for VMS potential in the given area. Additional data sets can further narrow the search. However, with more data sets we can quickly become overwhelmed with information and interaction becomes difficult, if not impossible. Depending on the geologists objective, individual data layers may include more useful information than other layers; more useful layers can given greater weight. This weighting of data layers adds to the problem of saturation. Accurate quantification of spatial relationships with the human brain is not always possible and the integration of theoretical information is also difficult to integrate while interacting with the data sets. Light tables were a simple way to cope with different layers of data, but again simple binary addition of layers produces only marginally better results than using only the human brain. These problems can be addressed with the increases in computer memory, processing speed, and availability spatial data software. Multiple sets of spatial data can be manipulated and displayed quickly and efficiently using statistical and numerical combination methods. Computers are capable of repeating tasks in an unbiased and reproducible way. So the problems of saturation, weighting of data, quantification of spatial relationships, and integration of theoretical information can now be applied during the combination of multiple data sets.

Data fusion is a framework in which information from multiple data sets from different sources are combined or merged using various tools to obtain information of greater quality (Wald, 1999). The terms "combination" and "merging" refer to any process that involves a mathematical operation performed on two or more sets of information. The method of combination and the use of the data are determined depending on the objective (Wald, 1999).

Geographical information systems (GIS) have been developed to put together and manage large sets of diverse spatial data. These programs are also capable of manipulating multiple data layers in order to analyze and model the interrelationships between spatial data sets (An et al., 1991; Moon, 1993; Bonham-Carter, 1994). The manipulation, or combination, of spatial data can be accomplished using statistical weighting methods, Boolean logic, fuzzy logic, Dempster-Shafer theory, and neural network methods. Data fusion can be used to locate areas of potential economic interest, define regional bedrock geology, or delineate major structural trends. However, this fusion of data must be done in a consistent and justifiable manner, otherwise the results will not be precise and technically accurate (Argialas and Harlow, 1990). Different spatial resolution, scale, formats, sources, and projections among data sets, along with incomplete and imprecise spatial data requires a proper quantitative method of combination to address these problems (Moon, 1993).

The objective of this project is to produce mineralization-potential maps using a GIS platform for shear-hosted gold and volcanogenic massive sulphide type deposits in the southern part of the Lynn Lake Greenstone Belt, northwestern Manitoba. This objective is accomplished by using a data fusion framework. Combining information

from two or more input data sets, with respect to a particular deposit style or occurrence, produces information that is less biased, which may therefore be deemed of greater quality. Potential maps may be used to assist future prioritization of exploration and land use management.

1.2 The Trans Hudson Orogen and the Lynn Lake Greenstone Belt

The Lynn Lake Greenstone Belt is an early Proterozoic magmatic arc that is part of the larger Trans Hudson Orogen (Hoffman, 1981) which extends from South Dakota northward through much of Manitoba, Saskatchewan, Nunavut, and eastward across Hudson Bay to the Cape Smith Belt, northern Quebec (Figure 1.1). The Chipewayan Batholith, located in the northern part of the orogen, is interpreted to represent a cordilleran-type continental margin. The batholith is bounded to the north by reworked Archean continental crust of the Rae-Hearne Province (Lewry and Collerson, 1990). The Churchill-Superior Boundary Zone is a major component of the Trans Hudson Orogen and comprises a narrow zone of mainly reworked Archean basement gneisses in the south and pillowed to massive tholeiitic to komatiitic basalts with coeval differentiated mafic-ultramafic sills forming the northern segment (Hoffman, 1990). The tectonic history of this boundary zone continues to be a source of debate.

An extensive zone of juvenile crust to the west of the Churchill-Superior Boundary Zone, known as the Reindeer Zone (Figure 1.2), comprises a collage of accreted magmatic arcs, volcanogenic clastic rocks and later molasse deposits (Lewry and Collerson, 1990). Felsic arc volcanic rocks and plutons have given dates ranging from 1910 to 1830 Ma with the majority of those dates between 1910 and 1875 Ma

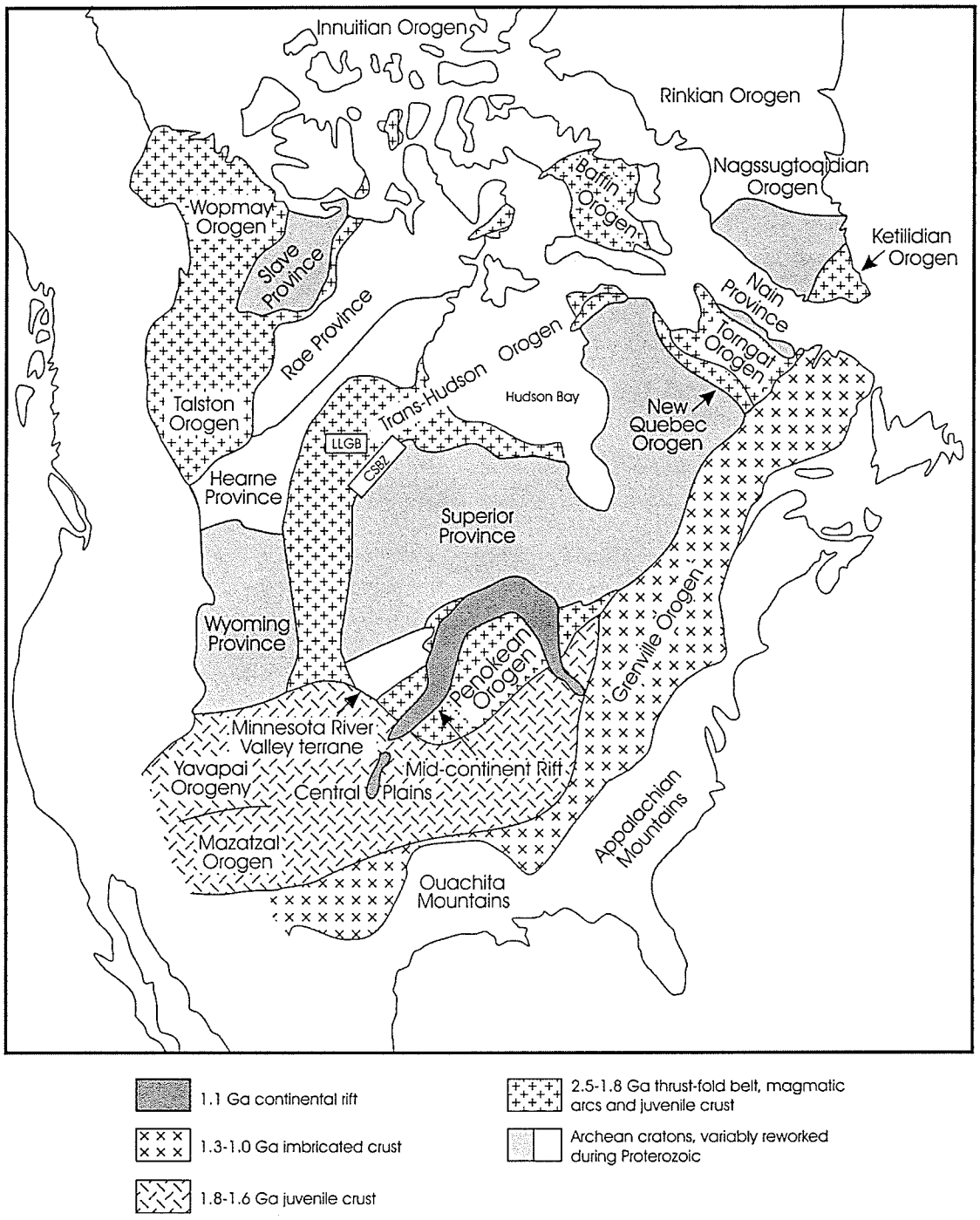

Figure 1.1 Early Proterozoic orogenic belts and Archean cratons in North America (after Card and Poulsen, 1998). The Lynn Lake Greenstone Belt (LLGB) lies within the central portion of the Trans Hudson Orogen. CSBZ - Churchill-Superior Boundary

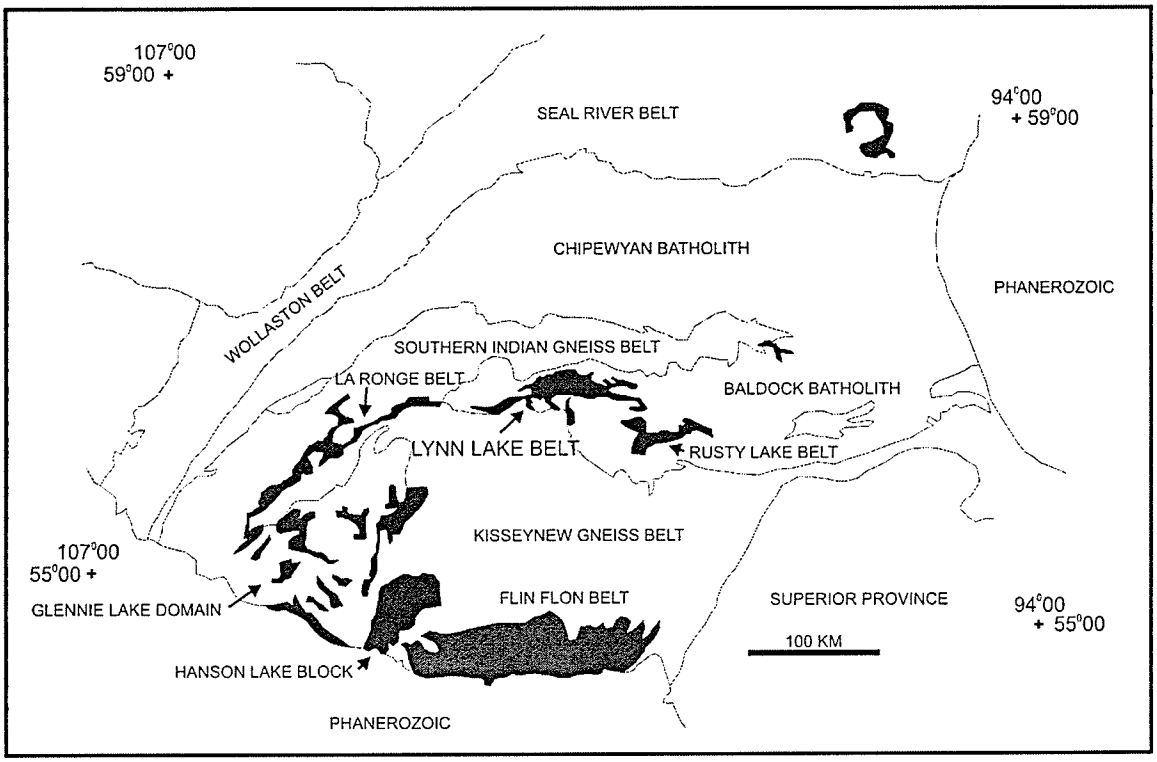

Figure 1.2 Major geological divisions of the southwestern Churchill Structural Province (after Baldwin et al., 1986). Supracrustal greenstone belts are shown in black.

(Baldwin et al., 1985; Lewry et al., 1987; Van Schmus et al., 1987; Gordon et al., 1990). Granitoid-greenstone terranes within the Reindeer Zone have arc-type geochemical characteristics. Major, trace element and Nd, Pb, and Sr isotopic data suggest an oceanic, subduction related arc setting with little material derived from adjacent Archean terranes (Watters and Pearce, 1987; Syme, 1990; Thom et al., 1990).

The Lynn Lake Greenstone Belt is part of the Proterozoic Trans-Hudson Orogen and is located in the northwestern part of Reindeer Zone (Figure 1.3). U - Pb ages from the belt range between 1910 and 1831 Ma (Baldwin et al., 1987; Turek et al., 2000). The greenstone belt is bounded to the north and south by the Southern Indian and the Kisseynew Gneiss belts, and to the east and west by the Rusty Lake and La Ronge

Greenstone Belts respectively. Upper greenschist to lower amphibolite facies metamorphosed volcanic, sedimentary, and plutonic rocks comprise the east trending 130 km by 60 km wide belt, which is divided into predominantly volcanic northern and southern segments separated by intrusive complexes. Geochemical data for the northern and southern segments of the Lynn Lake Belt show a distinctive volcanic arc origin, consistent with other belts within the Reindeer Zone. Similar volcanic assemblages occur along strike within the Lynn Lake Belt and may be related to several extrusive centres (Zwanzig et al., 1999).

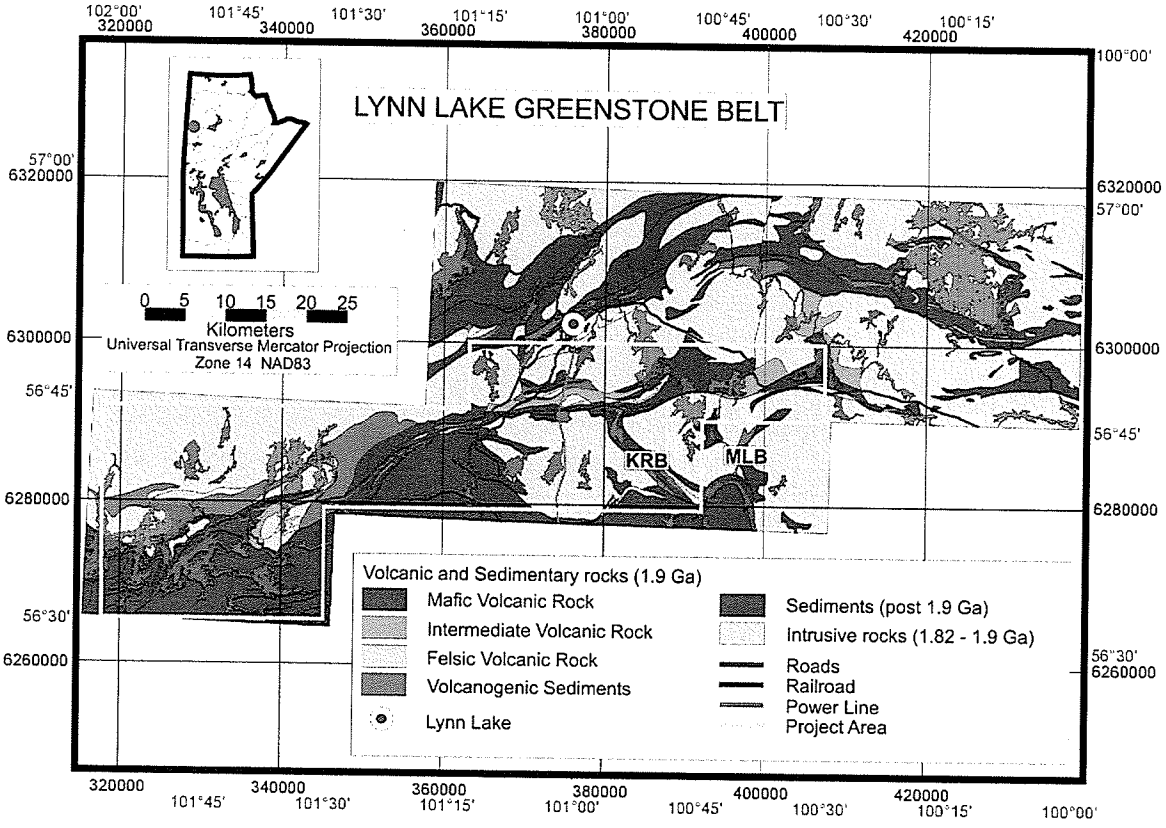

Figure 1.3 Generalized geology of the Lynn Lake Greentsone Belt. KRB - Keewatin River Belt; MLB - Miskwa Lake Belt.

1.3 Objective and Basic Methodology

The objective of this project is the development of mineralization potential maps for the southern part of the Lynn Lake Greenstone Belt, particularly with respect to the Johnson Shear Zone (JSZ) and associated structures (Figure 1.3). This will be accomplished by using data fusion, GIS, and theoretical principles of geology and geophysics. Five main stages are required to reach the objectives: 1) the development of a conceptual model; 2) compilation of a spatial database; 3) selection of a combination method; 4) translation of the conceptual model into a spatial deposit model; and 5) probability output and testing (modified from Wright and Bonham-Carter, 1996). The emphasis of this project is on the processes involved in producing spatial deposit models with predictive power that we can test.

1.3.1 Conceptual Model

The conceptual model is a compilation of generally excepted theoretical principles for a specific type of deposit. This is not to be confused with the conceptual model defined by Wright and Bonham-Carter (1996), which can be considered to be a type of exploration model. The exploration model includes the geological deposit model and those features that favor the occurrence of the specific type of deposit, such as lithological, structural, geochemical, and geophysical information compiled during regional exploration. Henley and Berger (1993) note that an exploration model is used to provide support for corporate or individual decision making, whereas the deposit model seeks to synthesis the major components of a suite of deposits with similar style. Thompson (1993) discusses ore deposit models as including both observational data and

theoretical concepts (the genetic or conceptual model). In this project a conceptual model will be defined using theoretical concepts. The development of a spatial deposit model from a conceptual model can be considered as the exploration model described by Wright and Bonham-Carter (1996).

1.3.2 Data Set

Compilation of a spatial database will be accomplished using GIS and image processing platforms. Data sets acquired for this study are geological field maps, lithogeochemical maps, total field (TF) and vertical gradient (VG) magnetic data, very-low frequency electromagnetic (VLF-EM) data, and synthetic aperture (SAR) data. These data sets have been made available from the Manitoba Geological Survey, Geological Survey of Canada, and RADARSAT International. The spatial coverage of the individual data sets vary and do not cover the entire greenstone belt. Differences in spatial resolution, scale, formats, sources, and projections also occur among the compiled data sets. Problems associated with these differences must be addressed prior to choosing a combination method and the development of the spatial model. The compiled spatial database is available on CD (Appendix A) and will form a basis for any further analysis and processing.

1.3.3 Combination Method

The combination method used for this project is determined by the objective and the data available. To reach the objective one can approach the problem from two points of view. First there is the statistically approach in which combination of data is

determined by one, or more, training areas. A training area is a known deposit or occurrence. The characteristics that define the training area are applied directly to the entire region of interest. This method is limited in that you are looking for an exact replica of the training site. This method is useful in areas where a great deal of information is known about a deposit, or a series of similar deposit types are found in close proximity.

The second method is an expert system approach in which theoretical principles of geology and geophysics, and good knowledge of the regional geology are used. The strength of this method depends on the "expert" or "experts". This method allows for more flexibility than the statistical method and numerous scenarios based on a general model may be developed. A training area may not be possible if exploration in an area is minimal, or if the data available is regional in scale. For this reason the expert systems approach method becomes very useful. This approach has been adopted for this study because it allows flexibility, or experimentation, and the data acquired is at a regional scale. Fuzzy logic and Dempster-Shafer methods are two such expert systems, or knowledge driven systems (Bonham-Carter, 1994), and will be used as the quantitative combination methods in this project.

1.3.4 Spatial Deposit Model

The conceptual model enables an expert to categorize spatial information into usable forms for meaningful reasoning (Moon, 1993). This spatial information must be translated into a spatial deposit model in order that the combination produces mineralization potential maps. This translation involves two main stages. The first stage

involves determining which data sets are relevant to a particular aspect, or component, of the conceptual model. The second stage requires that we determine how to present those relevant data sets in a spatial manner. The resultant spatial deposit model is also used to control the combination sequence of the various data layers.

1.3.5 Probability Output and Testing

A series of output maps are produced for the spatial deposit model, which reflect the various scenarios developed in the model. Two aspects are considered during the testing stage of this project. The first aspect of testing looks at the accuracy of the probability models. This is accomplished by comparing known occurrences with the potential maps and ground truthing of high potential sites. Ground truthing includes field reconnaissance and sample collection for geochemistry. The second aspect includes problems that occur during processing that are addressed during subsequent processing and combination stages. These problems may involve the application of theoretical principles, or translation of components in the conceptual model into the spatial model. Errors in the data or numerical calculations may also occur and can be found during testing.

2 GEOLOGY OF THE LYNN LAKE GREENSTONE BELT

2.1 Introduction

The La Ronge, Lynn Lake, and Rusty Lake Greenstone belts form a 400 km long semi continuous stretch of early Proterozoic supracrustal and plutonic rocks (Figure 1.2). The Lynn Lake belt lies between the La Ronge and Rusty Lake belts, separated by large granitoid intrusions and major faults, and by paragneiss, orthogneiss and plutonic rocks respectively. The three belts were previously considered to be part of a single structural subprovince of similar age. However, more recent U-Pb zircon ages show that there are two significant periods of magmatism (Baldwin et al., 1987; Bickford and Van Schmus, 1985; Turek, et al., 2000). Of the three belts the volcanic rocks within the Lynn Lake belt are the oldest, with an age of 1910+15-10 Ma, whereas granotoid plutons in the belt (1876+8-6 Ma) are coeval with the volcanic rocks within the Rusty Lake belt (1878+3-3 Ma). In the La Ronge belt volcanic rocks range from 1884+/-5 to 1877+/-8 Ma while the associated plutons were emplaced between 1866+/-12 Ma and 1849+/-12 Ma (Bickford and Van Schmus, 1985). Magmatism in the La Ronge, Rusty Lake and intrusive units in the Lynn Lake belts has ages similar to that of volcanic rocks in the Hanson Lake Block and Glennie Lake Domain to the south and southwest (Figure 1.2).

Within the Lynn Lake Belt volcanic and volcaniclastic rocks form two east trending segments that define northern and southern belts separated by large subvolcanic plugs (Figure 1.3). Geochemical subdivisions for volcanic rocks in the Lynn Lake Belt have been correlated with stratigraphic units and include calc-alkaline, arc tholeiite to E-MORB, enriched arc-tholeiite, komatiitic basalt, and depleted arc tholeiite respectively (Zwanzig et al., 1999). The various volcanic assemblages were brought together during

periods of extensional, compressional, and possible transcurrent faulting (Gilbert et al., 1980). Figure 2.1 shows a generalized stratigraphy for the Lynn Lake Greenstone Belt. Subsequent folding, which developed an early foliation, was followed by subvertical intrusion of the Lynn Lake gabbro and plutons of the Pool Lake Tonalite around 1876 Ma (Baldwin et al., 1987). The volcanic rocks have major-element, trace-element, and REE chemical signatures similar to Cenozoic intra-oceanic arcs (Syme, 1985) and have historically been termed the "Wasekwan Group" (Bateman, 1945). Recent work by Zwanzig et al. (1999) showed tholeiitic arc, calc-alkaline arc, MORB-like and OIB-like assemblages have distinct geochemical signatures within the Wasekwan Group. Zwanzig et al. (1999) suggest the term Wasekwan Group no longer be used to describe the diverse volcanic assemblages of the Lynn Lake belt. Instead the belt should be interpreted as being made up of assemblages amalgamated during tectonic processes similar to those in the Flin Flon Belt. Volcanic assemblages dated at 1.85 - 1.84 Ga (Ansdell et al., 1999) unconformably overly fluvial-alluvialarenties of the Sickle Group (Norman, 1933). The Sickle Group sediments occur predominantly to the south of the southern belt adjacent to the Kisseynew Gniess Belt. Quatzofeldspathic sandstone, pebbly sandstone, hornblende-bearing sandstone and pelite, and heterolithic conglomerate comprise the diverse stratigraphy of the Sickle Group. Basal units of the Sickle Group contain clasts of the underlying volcanic and plutonic rocks (Gilbert et al., 1980). Contacts between the volcanic assemblages of the southern belt and the Sickle group have been found at several locations. However, because of the regional deformation the exact nature of the unconformity is difficult to ascertain.

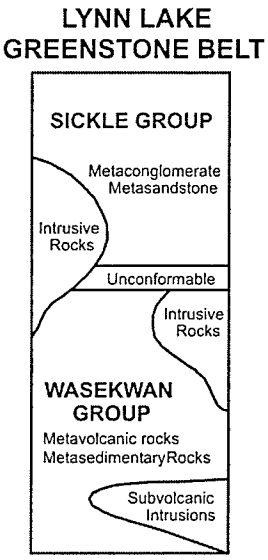

Figure 2.1 Stratigraphic outline for the Lynn Lake Greenstone Belt (after Baldwin et al., 1980).

The rocks of the Lynn Lake belt were metamorphosed at upper greenschist to upper amphibolite facies during polyphase deformation (Gilbert et al., 1980). Peak metamorphism in the belt occurred relatively late in deformational history. Greenschist facies metamorphism is dominant in the eastern part of the southern belt, specifically in the Cartwright Lake-Hughes Lake area (Figure 2.2). The metamorphic grade increases westward and a greenschist-amphibolite transition occurs near Moses Lake. Lower- to middle-amphibolite facies occur in the western part of the belt and in the Miskwa Lake and Keewatin River belts. Upper amphibolite facies metamorphism is restricted to the very western part of the belt near Dunphy and Laurie Lakes.

2.2 Northern Belt

The northern belt comprises a north facing homoclinal sequence of highly aluminous mafic volcanic rocks, commonly plagioclase-phyric basalt flows, breccias, and debris flows. The high-alumina characteristic of the northern belt basalt flows is distinct

from similar flows in the southern belt (Syme, 1985). Rhyolite pyroclastic rocks and flows form the base of the sequence and are overlain by high alumina basalt, basalt, andesite and rhyolite; a dominantly turbiditic sequence; more primitive high alumina basalt, basalt, and high magnesia basalt; and finally a sequence of basaltic tuff and volcanogenic sediments (Gilbert et al., 1980). Conglomerate and greywacke of the Southern Indian Gneiss Belt unconformably overlie the northern belt sequence. The northern and southern belt rocks contact one another in only one poorly exposed location north of Hughes Lake.

2.3 Southern Belt (Project Area)

Gilbert et al. (1980) have interpreted the tholeiitic aphyric flows near Cockeram Lake and porphyritic calc-alkaline basalts at McVeigh Lake and Fox Lake to be overlapping volcanic edifices with flanking aprons, which form the extensive mafic "platform" that comprises southern belt, which is the focus of this project (Figure 2.2). To the west, this platform is overlain by dacite and discontinuous units of sedimentary rocks near Fox Lake. Mafic, intermediate and felsic complexes are found in the central and eastern portion of the southern belt near Cockeram and Hughes lakes.

The Cockeram Lake anticline, which predates the Pool lake tonalite, exposes what are considered to be the oldest rocks in the Lynn Lake belt (Gilbert et al., 1980). This anticline and the Johnson Shear Zone (JSZ) (Bateman, 1945), are the dominant structural features of southern belt. The JSZ is a long-lived regional-scale ductile-brittle shear zone that extends along the southern margin of the belt. The shear zone has long been recognized as an important gold-bearing structure (Bateman, 1945; Milligan, 1960;

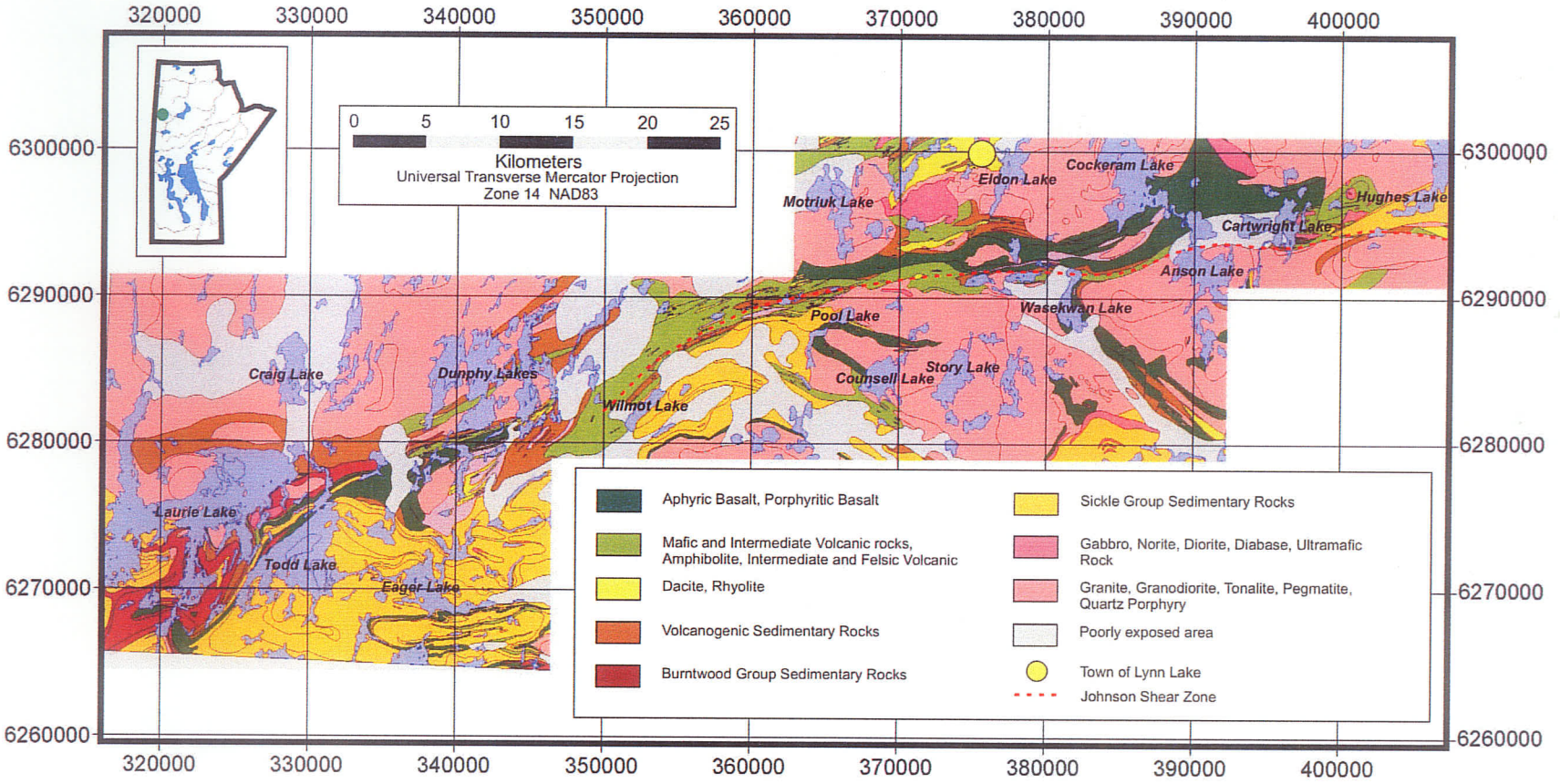

Figure 2.2 Geology of the southern segment (project area) of the Lynn Lake Greenstone Belt.

Gilbert et al., 1980; Kenaley, 1982; Peck, 1986; Fedikow et al., 1991; Peck, 1986; Peck and Eastwood, 1997, Peck et al., 1998; Richardson and Ostry, 1996; Sherman, 1992; Beaumont-Smith and Rogge, 1999; Jones et al., 2000). The shear zone is the focus of the shear hosted gold mineralization spatial models to be developed for this project. Near Fraser Lake and McVeigh Lake the stratigrahic and geochemical trends of the volcanic rocks are similar to that observed in the Fox Mine succession (Zwanzig et al., 1999). The Fox Mine succession was host to the past producing Fox Mine VMS deposit. A VMS spatial model will be developed for this project along with the shear-hosted spatial model. The two models will be applied to the southern belt, from Hughes Lake westward to Laurie Lake.

2.3.1 Deformation and Plutonism

Multiple deformational and plutonic events have occurred during the tectonic history of the Lynn Lake Greenstone Belt. Five deformational events were defined by Gilbert et al. (1980) and Beaumont-Smith and Rogge (1999) (Table 2.1). Synvolcanic intrusions, similar in composition to the volcanic host rocks, are generally small mafic and felsic bodies. These early plutons were folded along with the volcanic rocks during an early D_1 folding and faulting event primarily with an east-north easterly trend. These folds are truncated by large composite plutons of diorite, tonalite, granodiorite and granite, which intruded between the northern and southern belts (Gilbert et al., 1980). A second northwest trending deformation event (Gibert et al., 1980) resulted in uplift, erosion, faulting and tilting of the volcanic and synvolcanic intrusions. This sequence of rocks is truncated by the Sickle Group unconformity. Deposition of Sickle Group

conglomerates, comprising clasts of the underlying volcanic, plutonic and hypabyssal rocks; was followed by thrusting at the belt margins (D_3, Gilbert et al., 1980).

TABLE 2.1: Tectonic Evolution of the Lynn Lake Greenstone Belt

Event	Beaumont-Smith and Rogge, 1999	Baldwin et al., 1980
Volcanism and associated sedimentation; syn intrusions		
Folding and faulting (east-northeasterly); JSZ initializes	D1	D1
Uplift, erosion, faulting, and tilting; Intrusions of large plutons (tonalite, granite) between northern and southern belts		D2
JSZ; mineralization (?)	D2	D3
Sickle deposition		
JSZ; remobilization (?); peak metamorphism; North-east trending crenulation fabrics and folds	D3	D4
Cataclasis, open cross folding; Post-Sickle granodiorite, tonalite and gabbro	D4/D5	D5
Shallow-plunging recumbent folding	D6	

Intrusions of granodiorite, tonalite and gabbro occurred after the deposition of the Sickle Group sediments. Reactivation during the D_3 event produced the dextral shear fabrics (Beaumont-Smith and Rogge, 1999) representing the D_4 east and northeast trending shearing and faulting of Gilbert et al. (1980). The D_4 event of Beaumont-Smith and Rogge (1999) comprises open folds, which include narrow cataclasite zones, and conjugate kink bands and associated weak conjugate crenulations to fracture cleavages. This event may be related to the cataclasis and open cross folding described by Gilbert et

al. (1980). The final movement within the belt was largely brittle sinistral movement with the development of pseudotachylite and cataclasite.

The structural geometry of the greenstone belt is largely the product of the first two periods of deformation (D_1 and D_2), which culminated in the development of regional D_2 dextral shear zones (Beaumont-Smith, 2000). The Johnson Shear Zone (Bateman, 1945) is the dominant structural feature of the southern belt formed primarily during the D_2 event. The JSZ is a long-lived regional-scale ductile-brittle shear zone that extends along the southern margin of the greenstone belt. Intensive silicification and quartz-carbonate veining during the main D_2 event, characterize the gold mineralization within the approximately 300 m wide JSZ (Beaumont-Smith and Rogge, 1999). In the eastern part of the belt the shear zone is located along the supracrustal-plutonic contact, which may reflect a primary rheological control leading to the development of the JSZ (Beamont-Smith, 2000). In the west the shear zone is developed within the supracrustal rocks and not along a supracrustal-plutonic contact, this setting removes any time-stratigraphic control.

2.3.2 Cockeram, McVeigh, and Hughes Lake Assemblages

Tholeiitic, aphyric, pillowed and massive basalt flows form a 2100 m thick assemblage; the Cockeram Lake thoeleiitic sequence forms the base of the eastern sequence. The aphyric basaltic sequence was deposited in a subaqueous environment and is intercalated with the McVeigh Lake porphyritic basalt to the west. It is in structural contact with calc-alkaline andesites of the Hughes Lake suite along the eastern edge of Cartwright Lake. The Cockeram Lake basalt has chrondrite-normalized REE patterns

indicative of a prototypical arc tholeiite (Zwanzig, 1999), whereas the approximately coveal 1.5 km thick McVeigh Lake porhyritic basalt is a relatively primitive calc-alkaline arc sequence (Syme, 1985). The McVeigh Lake basalt comprises massive flows and autoclastic breccia with only minor pillowed flows.

The Hughes Lake suite predominantly comprises a thick lower aphyric to porphyritic basalt and basaltic andesite; and an upper plagioclase phyric and aphyric andesite, local rhyolite, and sedimentary rocks (Syme, 1985). However, a complete section of the Hughes Lake suite is unknown. Geochemical similarity between the Hughes Lake suite and small intrusions spatially restricted within the suite is consistent with the Gilbert et al., (1980) interpretation that the intrusions are synvolcanic. The calc-alkaline succession has been interpreted to represent a stratavolcano on the upper flank of the Cockeram Lake shield. Epiclastic and pyroclastic materials were deposited over the lower flank in a shallow subaqueous environment (Gilbert et al., 1980). The Hughes Lake basalt overlies the calc-alkaline suite and has been termed a transitional suite by Syme (1985). New data (Zwanzig et al., 1999) show the basalt has an enriched arc tholeiitic geochemical signature and is most similar to the mafic-intermediate rocks of the calc-alkaline suite. However, the tholeiitic character and an abrupt contact between the two suggest they are not petrogenetically linked.

In the western hinge area of the Cockeram Lake anticline the McVeigh Lake high-Al basalt lies along strike form the McVeigh Lake porphyritic basalt. They have steep REE and negative HFSE signatures similar to those of the underling calc-alkaline McVeigh Lake basalt. Zwanzig et al., (1999) describes these basalts as enriched arc

tholeiites. Stratigraphic and geochemical relations show that volcanism evolved towards higher Al and Fe during sedimentary basin development (Gilbert et al., 1980).

MORB-normalized REE patterns for the Gemmel-McVeigh Lake- low to high-Mg basalts are consistent with them being of volcanic arc origin (Zwanzig et al., 1999). These basalts are found from Franklin Lake to Gemmel Lake south of the JSZ, and from McVeigh Lake to Stear Lake respectively. Arc tholeiites with weak negative HFSE anomalies, separated from the southern belt by the Pool Lake pluton, are tentatively correlated with the Wilmot Lake normal- to high-Mg basalt and andesite rocks found further to the west. This unit is directly below the Sickle Group unconformity (Gilbert et al., 1980).

2.3.3 Fox Lake Assemblage

The calc-alkaline Fox Lake porphyritic basalt (which may be correlated with the McVeigh Lake porphyritic basalt because of its similar Fe-fractionation trend, enrichment in LREE, and low Zr/Th and high Th/Nb ratios, (Zwanzig et al., 1999)) is interpreted to be part of a small shield volcano (Gilbert et al., 1980). The amphibolite and high-Mg schist (Laurie Lake assemblage) located further to the west may also be correlated with the Fox Lake porphyritic basalt. This basal platform of pyroxene-phyric basalt is dominated by pillowed and massive flows, and autoclastic breccia and has a maximum thickness of about 1500 m. It is intruded by a gabbro and tonalite at Snake Lake and has been interpreted to be overlain by the Snake Lake dacite and Fox mine succession. However, fault contacts between these units cannot be ruled out (Gilbert et al., 1980).

Aphyric and porphyritic flows interlayered with mafic to intemediate breccia and minor sedimentary and felsic volcanic rocks comprise the 700 m thick Fox Mine succession. The Fox Mine succession has an arc tholeiitic signature; it includes the calc-alkaline Snake Lake dacite, which is provisionally interpreted to be related to the underling calc-alkaline Fox Lake basalt (Zwanzig et al., 1999). The dacite unit includes aphyric and plagioclase-phyric massive flows, autoclastic breccias, and tuff, which are locally overlain by sediments (Gilbert et al., 1980). The Fox Road turbidite, a coarse turbidite and mass flow deposit 1500 m thick, is located east of the Fox Lake mine and is considered to have filled a tectonic depression (Gilbert et al., 1999). The Wilmot Lake normal- to high-Mg basalt and andesite rocks were deposited above the turbidite

2.3.4 Tod and Hatchet Lake Assemblages

The Tod Lake aphyric basalt and the Hatchet Lake basalt (Gilbert et al., 1980) are located at the southwestern end of the Lynn Lake greenstone belt. They are separated by faults from the rest of the belt and have since been reclassified as part of the Granville Lake assemblage that extends along part of the north flank of the Kisseynew Domain (Zwanzig, 1990). Massive and pillowed basaltic flows and gabbro sills, locally overlain by pillow breccia and hyaloclastite, form two main thrust sheets. The two thrust sheets are stratigraphically similar and structurally overlie part of the Granville Lake Greywacke and Burntwood Group greywacke-mudstone turbidite. The tholeiitic contaminated MORB, or arc-rift Todd Lake basalt and the tholeiitic N-MORB or BABB Hatchet Lake basalt, are considered to part of the same marginal basin (Zwanzig et al., 1999).

2.3.5 Keewatin and Miskwa Lake Assemblages

The Keewatin River basalt and Miskwa Lake porphyritic basalt and aphyric basaltic andesite are located south of the JSZ. The two assemblages are surrounded by plutonic rocks and truncated to the south by sedimentary rocks of the Sickle Group. Mafic flows and tuff, dacite, and greywacke-siltstone comprise the arc tholeiites of the Keewatin River basalt. They contrast sharply with the porphyritic and aphyric mafic flows in the Miskwa Lake belt. Massive plagioclase phyric dacite flows and crystal-lithic tuff, overlain by greywacke and siltstone, represent the only felsic extrusive material in the Keewatin River and Miskwa Lake supracrustal segments. The stratigraphically unrelated Miskwa Lake porphyritic basalt contains a northwest-trending isoclinal anticline with a tonalite core (Gilbert et al., 1980). This depleted arc tholeiite includes pyroxene-plagioclase phyric, plagioclase phyric and aphyric mafic flows, whereas the aphryic mafic flows of the Miskwa Lake basaltic andesites are considered enriched arc tholeiites (Zwanzig et al., 1999).

3 CONCEPTUAL MODELS

3.1 Introduction

Gold occurs within the Lynn Lake belt in various styles and settings. In order to locate new areas of economic interest one must define a conceptual model that best represents a particular style of gold mineralization. In this project the shear-hosted gold and VMS conceptual models are defined by theoretical concepts of geology and geophysics as determined by research and exploration geoscientists. The more precise and complete the conceptual model is, the greater the ability it will have to predict the location of new occurrences. The conceptual model can be simplified by dividing elements of the model into components. Some of these components cannot be treated in a spatial sense. So, once a conceptual model has been defined it must be adjusted to represent the data available, and from this, a spatial deposit model can be developed. During the development of the shear-hosted gold and VMS conceptual models considerations are made with respect to the translation of the components into a spatial model. These considerations should take into account the scale of the project and the data sets available. Although the conceptual model is the first stage in the development of mineralization potential maps, the expert will already have an idea of which data sets are available, and therefore, which components of the conceptual model should be emphasized. Non-spatial information, such as the yield strength of various lithologies or heat loss from an intrusive body, can also be incorporated into the spatial deposit model. However, their influence is applied primarily in the weighting of the spatial data.

3.2 Introduction to Shear-hosted Gold Model

Shear-hosted gold deposits form in complex structural systems that may have been active in a number of fluid and stress regimes. Therefore, it is unreasonable to define a single model that represents all of the various components and sub-components of such deposits. However, there are a number of characteristics that are observed consistently in the majority of shear-hosted occurrences. In this project four major components are used to define the shear-hosted conceptual model. They are structure, source rock, fluid and heat source, and alteration.

Stuctural control, or deformation, is the dominant component of the shear-hosted gold conceptual model. Deformational zones, such as shear zones, represent conduits between a lower crustal site of ore fluid generation and the upper crustal site of ore deposition (Hodgson, 1993). Ore transport and deposition are fairly well defined processes, but source rock and ore-fluid generation are less specific (Hodgson, 1993). The location of a shear -hosted gold deposit is not specific to a particular lithology. The source of gold, however, may be specific with respect to lithology and geotectonic environment, and therefore, deposition and source of gold should be assessed separately. Metamorphic fluids, fluids formed by granulitization, magmatic hydrothermal fluids, and recirculating seawater are all possible sources for fluids in a shear-hosted system (Roberts, 1988). Rock-water interactions cause both wall rock and fluid composition to be altered with the result that fluids may be enriched in gold, or have a composition from which gold may preferentially be taken out of solution.

Factors relating to deformation, fluid movement, and composition may be significant at smaller scales. For example, small splays may trap a fluid enriched in gold or pH levels in the fluid may vary over just a few metres. In each case these small-scale features can significantly affect where gold may occur in economical quantities. However, owing to the regional scale nature of this study these features cannot be incorporated into the spatial model.

3.2.1 Structural Component

Shear zones are high strain regional scale structures, several kilometers to 100's of kilometers typically long with a length to width ratio of 5:1 (Ramsay and Huber, 1987). They commonly form in prograding arc-trench complexes in collisional tectonic settings (Hodgson, 1993). Regional scale metamorphism, magmatism, and faulting in collisional settings have been shown to be spatially and temporally associated with shear-hosted gold deposits (Murphy, 1989). Often the shear zones are caused by simple-shear and are considered detachment faults. These faults occur near major structural - lithological contrasts commonly 8-12 km within the crust at the brittle ductile transition zone (Kerrich, 1989). The width of a shear zone generally increases with depth as the conditions change from brittle to ductile behavior (Figure 3.1) (Sibson, 1989).

In greenstone belts similar structures may occur at various scales. The structural geology of gold deposits is commonly a scaled down version of the regional structure (Roberts, 1988). Greenstone belts throughout the Precambrian shields of the world commonly contain steeply dipping planar shear zones that are generally parallel or sub-parallel to the volcanic stratigraphy (Roberts, 1988). The distribution of gold deposits is

controlled at the belt scale by these ductile shear zones, whereas second or third order flanking brittle-ductile splays control local kilometer scale distribution (Burnsnall, 1989). The entire shear zone system commonly includes a major fault with a set of minor sub-parallel, intersecting, and complex anastomosing deformational zones (Hodgson, 1993). In shear zones and faults the protolith rock is commonly weakened or broken. Where erosion has exposed the shear zone or fault at the surface, preferential weathering occurs above these zones and results in a thicker layer of weathered overburden relative to adjacent areas.

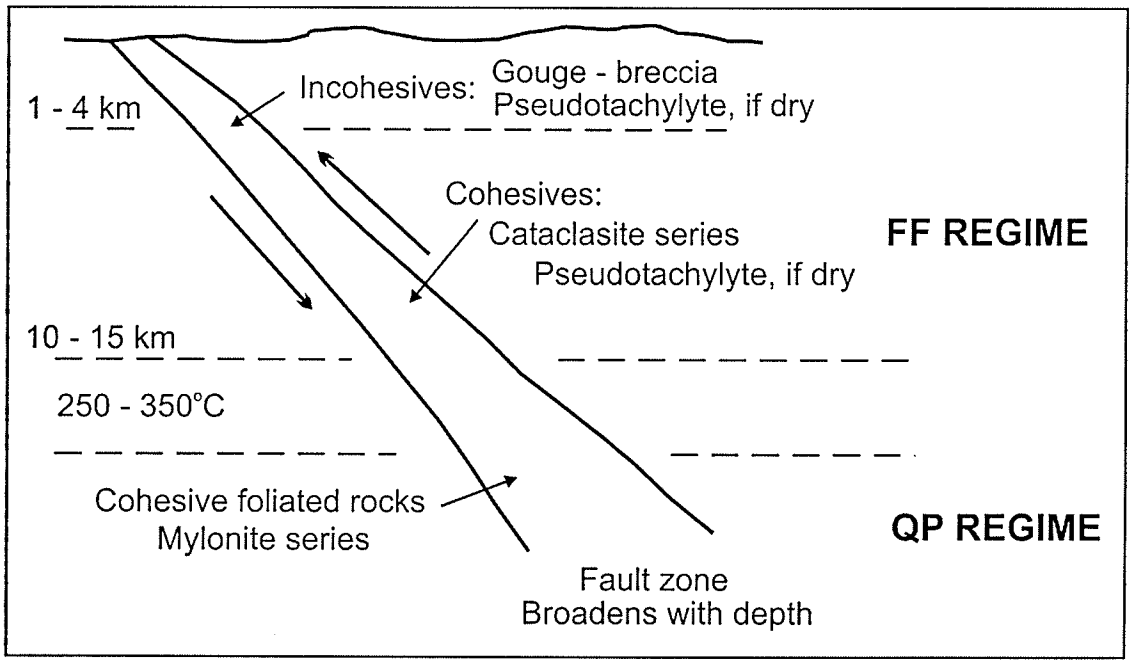

Figure 3.1 Variation in deformational behavior with depth within major crustal shear systems. FF - frictional faulting regime; QP - quasi plastic deformation regime. (After Sibson, 1989)

Shear zones act as the major fluid conduits for ore-fluids. These ore-fluids form vein and disseminated type deposits. Vein type deposits are related more to brittle fracturing, whereas ductile shearing has a tendency to produce disseminated deposits. Vein systems are part of the deformation process, and not created by fluids moving into existing open fractures (Roberts, 1988). Gold mineralization itself is primarily within vein sets or in the immediate wall rocks, but may also be found laterally outwards in less deformed rocks. Brittle and ductile behavior in the crust is controlled by a combination of lithological properties and local variables. Constraints on the rheological behavior of rocks include the mineralogy and grain size in the rock, as well as local variables such as temperature, confining pressure, stress, strain rate, fluid pressure, and differential stress (Kerrich, 1989). Deformation and vein formation are considered part of a continuous process in which fluid circulation, or the availability of fluids, exists over a long period of time (Roberts, 1988). Permeability in the rocks occurs as a result of shear stress and the reduction and fracturing of grains. High pore fluid pressures during prograde regional metamorphism can enhance the permeability (Etheridge et al., 1984). The deposition of gold is commonly a late structural event (Sibson et al., 1988).

Structure is the major control in shear-hosted gold deposits. The existence of shear zones, or high deformational zones, represents high potential for locating a deposit. Translation of the structural component of the conceptual model into the spatial model must consider 1) proximity to shear zones and faults; 2) the lateral extent of deformation associated with shear zones and faults; 3) brittle and ductile deformational characteristics; and 4) regional deformational history. The latter consideration can be derived from

structural knowledge specific to the project area. For instance, if the expert wishes to focus on a known mineralization event, such as the D_2 event for the JSZ, structures associated with the event could be assessed separately.

3.2.2 Fluid - Heat Component

Fluids are responsible for bringing gold into the shear zone vein system. The source of such fluids is still under debate. Magmatic hydrothermal and metamorphic fluids are generally considered to be the most likely source of the fluids in a shear-hosted system (Figure 3.2) (Hodgson, 1993). Magmatic fluid generation involves crystallization and evolution of magmatic fluid in spatially associated felsic intrusions. Metamorphic fluids generated by dehydration of supracrustal sequences at depth can be a major source of the fluids in a shear zone system. Low salinity, moderate CO_2 contents, δD, $\delta^{13}C$, $\delta^{18}O$, and $\delta^{34}S$ values, and Sr and Pb isotopic compositions of hydrothermal fluids in shear zones are consistent with metamorphic dehydration under amphibolite facies conditions (Kerrich, 1989b). Purely magmatic fluid generation is not consistent with these compositional characteristics, however, contributions from a magmatic source cannot be dismissed. In either case, Precambrian shear-hosted gold deposits occur in convergent margin settings with spatial and temporal links to syn- to post-tectonic felsic intrusions and regional metamorphism. It is then possible that both magmatic and metamorphic fluids are sources of the fluids in a shear zone system. High temperatures are commonly associated with regional metamorphism and magmatism. Hydrothermal fluids migrating through deformational zones, such as shear zones, may, therefore, be driven by regional metamorphism and plutonsim. Intrusive bodies are commonly

spatially associated with major shear-hosted gold deposits. These bodies can be considered an additional heat source of hydrothermal fluids migrating through the deformational zones.

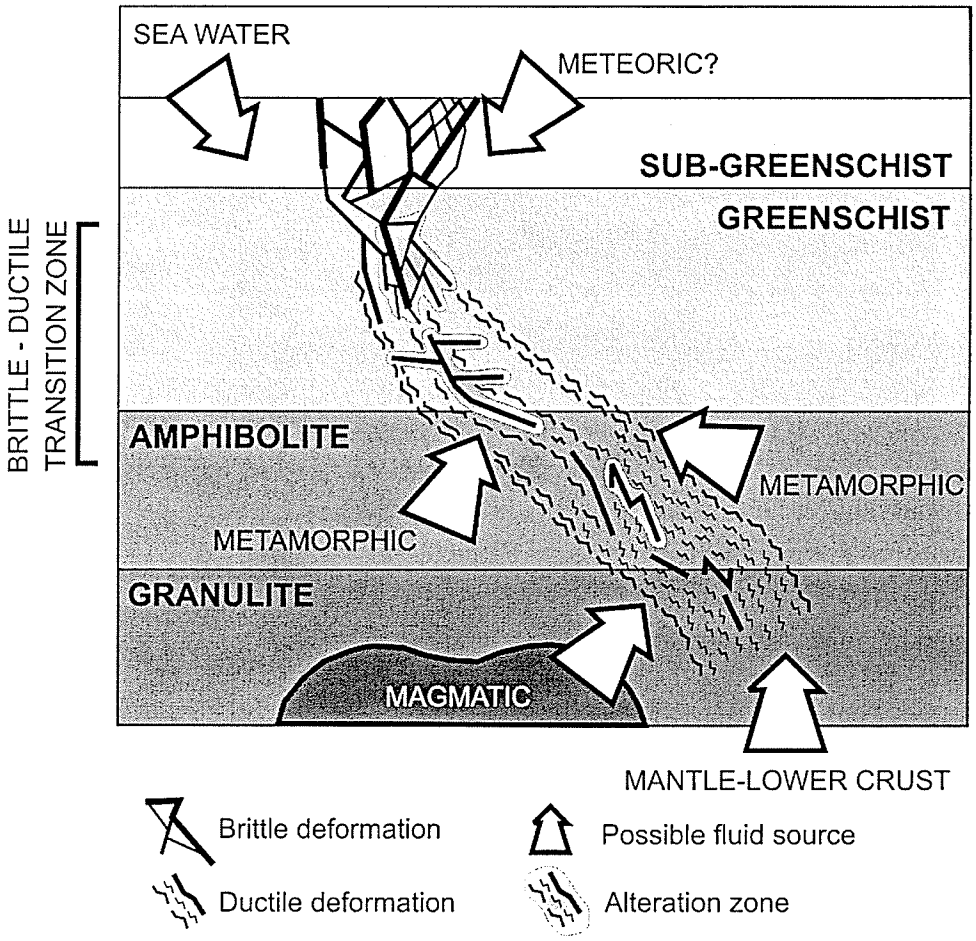

Figure 3.2 Schematic crustal profile of shear-hosted gold deposits and possible fluid sources (after Colvine et al., 1988).

The composition of fluid inclusions within parts of shear zones devoid of Au is similar to that found in parts where gold abundance is high. This would suggest that the source of barren and enriched fluids is likely derived from a similar region with the crust. During their ascent the gold-barren fluids are modified locally through reactions with the

wall rocks. This interaction between migrating fluids and wall rock may produce gold-bearing fluids that form economic deposits (Hodgson, 1993). As fluids migrate they interact with the adjacent rocks causing compositional changes in the fluid and wall rock. Changes in the fluid composition are important because they allow gold to enter the solution. Stable gold thio-complexes in neutral solutions with low concentrations of total sulphur enable gold to be transported in high concentrations (Roberts, 1988). Changes in fluid composition may eventually create the necessary conditions for gold to be taken out of solution. Oxidation, changes in pH, destabilization of the thio-complex by the reduction in the activity of reduced sulphur, decrease in temperature, or sudden release in pressure are possible mechanisms that may result in the precipitation of gold (Roberts, 1988). The composition of fluids associated with gold deposits is commonly a CO_2-rich, low-salinity brine (Roberts, 1988).

Considerations with respect to the fluid-heat component of the conceptual model should include 1) metamorphic grade across the project area, 2) composition of fluids trapped within the rocks, 3) proximity to intrusive bodies, which act as an additional heat and fluid source; and 4) history of plutonism within the belt. The metamorphic grade across the Lynn Lake Greenstone Belt ranges from upper greenschist in the east to upper amphibolite in the west. Integrating metamorphic grade into the shear-hosted deposit model, specifically with respect to fluid source, has proven to be a difficult task, and therefore, omitted. Integration of fluid composition has also been omitted owing to the scale of the project and the lack of available data for the project area. With respect to a magmatic source of fluid and heat, Bonham-Carter et al., (1993) and Wright and Bonham-Carter (1996) used proximity to subvolcanic intrusions and synvolcanic dikes to

represent a possible heat source in their VMS model. For this project intrusive bodies will be considered as an additional heat source to drive the hydrothermal system. Considerations with respect to the intrusive bodies must include 1) heat loss into the adjacent rocks, and 2) the lateral extent of heating adjacent rocks. There are multiple generations of intrusive bodies within the Lynn Lake Greenstone Belt and not all are necessarily associated with mineralization. For this reason the history of plutonism within the belt should also be considered during the translation stage.

3.2.3 Source of Gold

For the most part gold deposits in shear zones are not specific to a particular lithology. However, some rocks tend to be more susceptible to alteration or fracturing, and are therefore more probable sites for concentration. The source of the gold found within a shear zone is unlikely to be derived entirely from rocks directly adjacent to the deposit. Fluids that contain gold in solution are concentrated in gold during their migration through structural conduits, such as shear zones and faults. If the fluids were derived from metamorphic dehydration and magmatism within the greenstone belt this would suggest that the gold is, at least, derived locally from the supracrustal rocks of the greenstone belt (Roberts, 1988).

Saager et al., (1982) noted that gold distribution in volcanic rocks could be divided into a background population of about 1 ppb and an excess population with a threshold value of 6.8 ppb. The background population could be attributed to gold association with silicates and oxides, whereas in the excess population gold is associated with sulphides. Keays (1984) noted that in igneous rocks gold is scavenged by

immiscible sulphide melts, specifically high temperature magmatic rocks that have a greater capacity to dissolve sulphur, and hence gold, relative to low temperature magmatic rocks. Komatiites and magnesium-rich basalts, which are spatially associated with many major shear hosted gold deposits in Archean and Proterozoic terranes, are likely high temperature magmatic sources of gold. Primitive oceanic rock assemblages, which tend to have high magnesium contents, may also represent a possible source of gold (Hodgson, 1993). The source of gold can be considered separately from the deposition of gold. With this in mind translation of the conceptual model into the spatial model should consider the ranking, or weighting, of the various lithologies in terms of their potential for initially containing gold. This weighting can be based on: 1) the rock type, 2) genetic association, 3) geochemistry; and, 4) and timing of mineralization. The ultimate source of gold in this project will be considered to be from a magmatic source. All sediments are secondary, derived from intrusive and volcanic rocks, therefore, primary volcanic and intrusive units should be weighted the highest followed by volcanogenic sediments and reworked sediments. This does not take into account, for example, the ability of gold to be concentrated during fluvial sedimentation. For geochemistry units may be divided based on their Mg abundance and tectonic subdivisions based on trace element and REE data. Another aspect to consider is timing of mineralization. In the case of the JSZ, mineralization appears to be a predominantly D_2 event (Beamont-Smith, 2000). Depending on the deformational history and mineralization certain lithological units may not have existed, and therefore, should not be considered when combining information.

3.2.4 Alteration

Mineralogical changes caused by water-rock interaction as fluids equilibrate with the local surroundings commonly result in alteration zones that are useful in the exploration of gold (Figure 3.2). The degree of alteration may also be related to brittle and ductile behavior in rocks changing from greenschist to amphibolite facies. In more brittle rocks, fluids are able to migrate more rapidly to higher structural levels. At higher levels fluids have a markedly different composition than the local fluids. As the fluids and wall rock eqilibriate significant alteration occurs; in amphibolite grade regions with ductile characteristics continuous reactions are possible because of slower fluid movement. Significant alteration in these areas may be minimal (Murphy, 1989). Gold deposits within the Rae-Hearn Province occur in higher ambient metamorphic grades than most gold belts. These gold deposits commonly occur within ductile shear zones composed of recrystallized mylonite (Burnsnal, 1989). Shear-hosted gold deposits are also commonly associated with pyritic, carbonate, and potassic alteration, and regions of silicification (Kerrich, 1989). Considerations for the spatial model include 1) spatial association to alteration zones, and 2) mineralogical assemblages within the alteration zones. In this project an alteration data set is not available, therefore, translation of this component is not possible at this time.

3.2.5 Gold Deposits and Occurrences in the Southern belt

Appendix B is a list of known deposits and occurrences in the southern part of the Lynn Lake Greenstone belt and is compiled from the Mineral Deposit Series, Manitoba Energy and Mines; excluding the West Gemmel Lake occurrence. The occurrences have

been chosen based on the "Vein Type Deposit" classification given in the Mineral Deposit Series and include single vein, multiple veins or lenses, and stockwork vein systems. No shear-hosted classification is given. Some occurrences that are included are listed as "disseminated - not classified". Descriptions of the occurrences are compiled from Baldwin (1989), Ferreira (1993a, b), Ferreira and Baldwin (1997), Richardson and Ostry (1996), Fedikow et al., (1991). Figure 3.3 shows the locations of the known occurrences. Table 3.1 is a summary of key aspects of the occurrences listed in Appendix B and Table 3.2 lists the coordinates of the occurrences.

3.3 Volcanic-Hosted Massive Sulphide (VMS) Conceptual Deposit Model

Volcanic-hosted massive sulphide deposits occur as accumulations of sulphide and sulphate minerals on the sea floor, or beneath the sea floor. These accumulations are caused by hydrothermal fluids that circulate and react with adjacent rocks producing sulphide- and metal-rich fluids. Deposits of this type have occurred throughout geologic time in pre 3400 Ma volcanic strata of the Pilbara Block to present day black smokers in spreading arc and back arc tectonic settings (Franklin, 1993).

Massive sulphide ore on the seafloor, or immediately below the seafloor is the main mineralized component of the VMS deposit, however, disseminated stringer ore zones below the massive sulphide can also include economical concentrations of copper, zinc, and lead (Figure 3.4). Many VMS deposits also contain recoverable amounts of silver and gold. VMS deposits have been divided into two distinctive compositional groups based on the zinc/(zinc + lead) ratio (Lydon, 1988a). The first is the Cu-Zn group that comprises concordant to semi concordant, massive iron-sulphide rich bodies

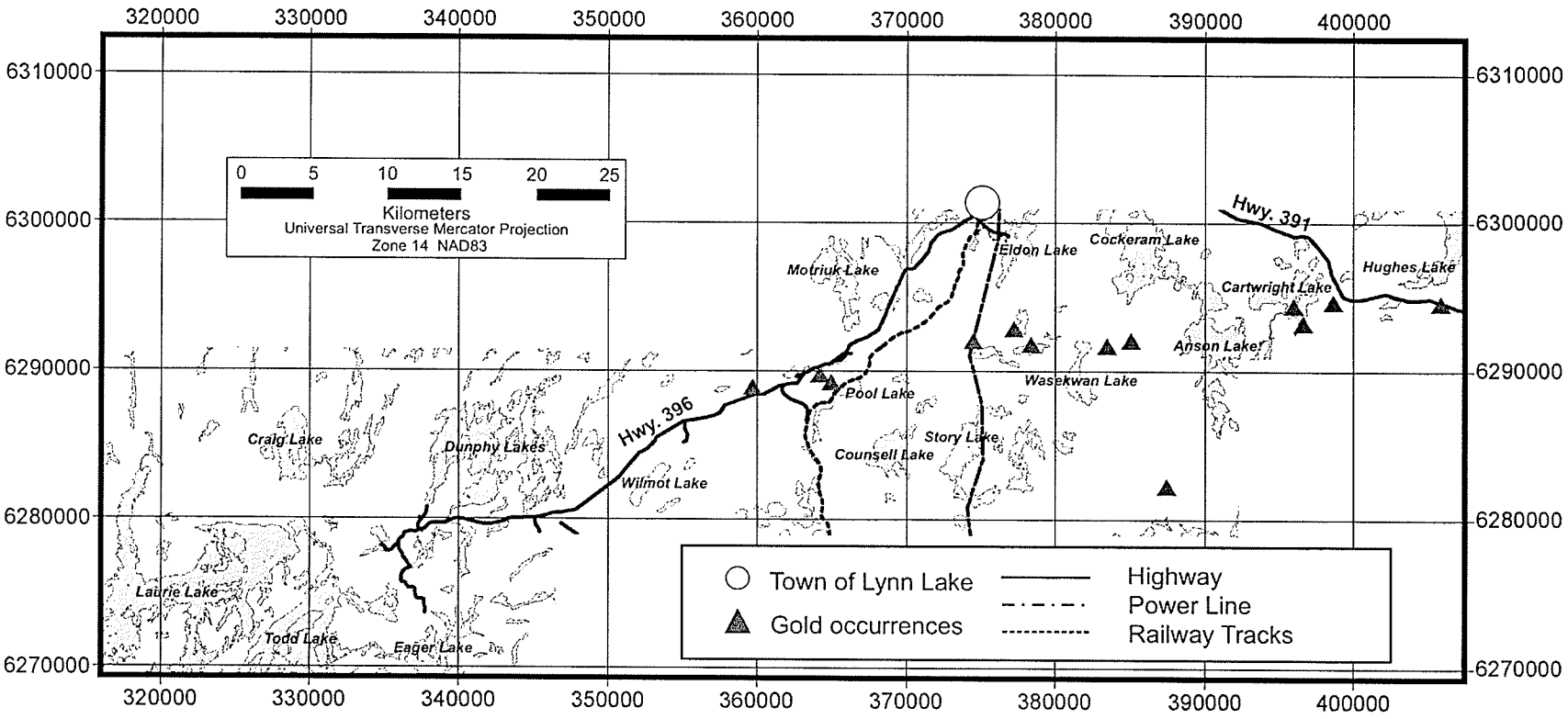

Figure 3.3 Gold occurrences in the southern segment (project area) of the Lynn Lake Greenstone Belt.

TABLE 3.1: Gold Deposits and Occurrences

Site(1)	Classification	Deformation	Mineralization	Alteration	Au
NTS64C/15 L1	Disseminated, not classified	Shear zone (JSZ) (2)	py, cp, ga, visible Au	Sericite schist	tr. 0.05 g/t
NTS64C/15 L3	Vein type; multiple veins and lenses	Shearing, cataclasite (JSZ)	py, ga, cp, asp, bn	Silicification, carbonatization, epidotization	160-10000 ppb
L4	Vein type; multiple veins and lenses	Shearing, cataclasite (JSZ)	minor py, tr. Ga	Altered tholeiitic basalt, chlorite, albite, quartz, epidote, calcite	62-3000 ppb
L43	Vein type; multiple veins and lenses	Cleavage planes and discontinuous mylonite zones, proximal to JSZ	py, asp	Quartz-carbonate-feldspar stringers	nil-2857 ppb
NTS64C/15 L6	Vein type; multiple veins	Shear laminated mylonite (JSZ)	py, minor ga, cp, sp	Silicification, carbonatization	Open pit mine produced 80000 ounces from 1993-1996
L36	Vein type; multiple veins and lenses	Drag folds, fold noses, proximal to JSZ	po, ga, tr. py, sp, Au	Minor carbonatization	tr. Au
NTS64C/14 L9	Single quartz vein	Shearing (JSZ)	py, ga, minor sp		
NTS64C/15 L35	Vein type; multiple veins and lenses	Pseudotachylite, fracture cleavage (JSZ)	po, tr. py, cp, rare asp	Chloritization, silicification	53-755 ppb
NTS64C/14 L8	Vein type; multiple veins	Pronounced schistosity	ga, sp, po, Au	silicification	tr.-91 g/t
NTS64C/11 L5	Vein type; multiple veins and lenses	Mylonitic, ductile and brittle deformation	py, cp, po, asp, mt, free Au	Biotite, tourmaline, chlorite, carbonate, k-spar; chlorite, biotite, tourmaline, carbonate, garnet, k-spar	up to 17g/t
West Gemmel Lake (3)	Shear hosted gold mineralization	Mylonitic fabrics (JSZ)	py, asp	Sericitized, silicified	1900 ppb
NTS64C/10 L1	Vein type; single vein	Proximal to major fault	Minor py, cp, sp, tr. ga	silicification	Reserves of 541 000 tones grading 8.23 g/t

(1) Compiled from the Mineral Deposit Series, Geological Services, Manitoba Energy and Mines, Government of Manitoba
(2) Spatially associated with the Johnson Shear Zone
(3) New occurrence (1999)

TABLE 3.2: Deposits and Occurrence Coordinates

Site	Easting(1)	Northing(1)
NTS64C/15 L1	380701	6307291
NTS64C/15 L3	396610	6293174
L4	395979	6294359
L43	398658	6294641
NTS64C/15	385060	6292028
L6		
L36	383477	6291672
NTS64C/14 L9	377461	6292641
NTS64C/15 L35	378381	6291752
NTS64C/14 L8	373523	6291869
NTS64C/11 L5	364926	6289196
West Gemmel Lake (2)	359727	6288835
NTS64C/10 L1	387431	6282164

UTM Coordinates Zone 14, Nad83 (coordinates from Mineral Deposit Series)

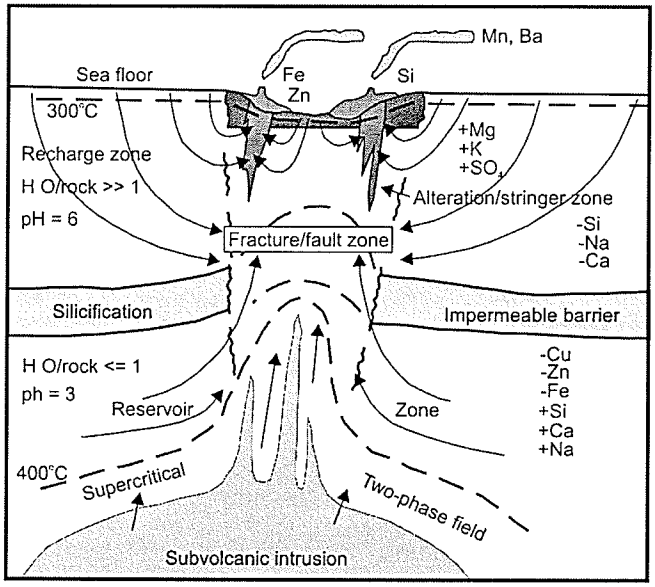

Figure 3.4 Model of VMS-producing hydrothermal system, incorporating elements of all subtypes of VMS deposits. Subvolcanic intrusion may contribute some metals and gases to the hydrothermal fluid. The blue areas under the massive sulphide deposits are alteration pipes. Copper precipitates within these and in the core of the massive sulphide mounds. This diagram is drawn perpendicular to the fracture system that controls hydrothermal discharge (after Franklin, 1993).

commonly underlain by vein systems, whereas the second group, Zn-Cu-Pb, is tabular concordant massive pyritic bodies. The Cu-Zn group deposits are generally of Archean and Proterozoic age and are dominated by mafic volcanic rocks with minor locally important felsic and sedimentary rocks. Zn-Cu-Pb deposits are underlain by less prominent stringer ore zones and are dominated by felsic volcanic sequences commonly Phanerozoic in age (Franklin, 1993). In this project the focus will be on the volcanic dominated Cu-Zn type of VMS deposit. The major components of the VMS conceptual model are, 1) ore-fluid source and alteration; 2) a heat source to drive the hydrothermal system; and, 3) stratigraphy.

3.3.1 Ore-Fluid Source and Alteration Component

Seawater comprises the main source of fluid in a VMS type system. Magmatic and meteoric fluids are considered a minor component, however, magmatic fluids contain much higher relative metal abundances than seawater (Franklin, 1993). Generation of ore fluids results from the heating of seawater and reaction between the fluid and adjacent rocks. Reactions between modified seawater and basalt at temperatures around 350^0C and 400^0C can cause sufficient depression of pH levels in the hydrothermal fluids to result in the mobilization of metals from the rock into the fluid (Seyfried and Janecky, 1985; Gibson et al., 1983). The reaction between basalt and seawater produce a sulphurous Na-Ca-Cl fluid that contains ppm concentrations of Fe, Mn, Zn, and Cu. Low pH levels can also be attained at lower temperatures through equilization with sedimentary and felsic rocks, which buffer the fluid. These hydrothermal fluids can

acquire enough sulphur and metals to produce a VMS deposit from virtually any volcanic and immature sedimentary rock (Franklin, 1993).

High temperature hydrothermal fluids can ascend quickly to the sea floor owing to the buoyant characteristics of high salinity seawater. As these high temperature fluids react with the adjacent wall rock, high temperature reaction zones result. Fluids that reach the surface, or near surface, precipitate sulphides primarily because of the rapid cooling of the hydrothermal fluid (Franklin, 1993).

Faults and fracture zones that are tectonically generated are considered to be fluid conduits that focus the flow of hydrothermal fluids (Franklin, 1993). Syngenetic faults that may act as conduits, can be good spatial indicators of VMS deposits, but only if the structure of an area is well known. Faults that are unrelated, or post date, the hydrothermal system should not be considered as spatial indicators of VMS deposits. Footwall hydrothermal alteration pipes occurring directly below the massive sulphide lens are the result of hydrothermal fluids reacting with wall rocks. These pipes commonly have distinctive alteration zones of inner chloritized cores surrounded by sericitized peripheries proximal to a massive sulphide lens. Another distinctive characteristic of VMS deposits is the decrease in chalcopyrite/(sphalerite+galena) ratio and increase in the Zn: Cu ratio upward and outward from the core of the massive sulphide lens (Lydon, 1988b). A lower semi-conformable alteration zone usually occurs hundreds of metres below the massive sulphide lens and may represent the reaction zone between fluid and wall rock. This reaction zone produces the sulfur- and metal-rich fluids that eventually ascend towards the sea floor (Hodgson and Lydon, 1977).

Considerations for the translation into a spatial model should include 1) rock types, 2) alteration zones; and 3) Cu and Zn background values. Seawater is considered to be the primary fluid source, and hence, lithological units such as subaqueous rocks types can be considered important spatial indicators of VMS deposits. The alteration zones associated with the interaction between the fluids and wall rock should also be useful spatial indicators of the presence of a VMS deposit. However, an alteration data set is not available, and therefore, the alteration component will be omitted. Most volcanic rocks and immature sedimentary rocks contain enough sulphur and metals to produce a VMS deposit, however, fluids circulating through units with higher background levels of Cu and Zn may have a higher probability of becoming an economic VMS deposit.

3.3.2 Heat Source Component

The hydrothermal fluids that are responsible for the transportation and deposition of metals that form a VMS type deposit require a long-term heat source (10^2 - 10^3 yr) to drive the system (Lydon, 1988b). The heat source also requires sufficient insulation to minimize heat loss in processes unrelated to the hydrothermal system (Hodgson and Lydon, 1977). In order to form a VMS deposit these hydrothermal fluids must also attain a sufficiently high temperature to dissolve metals in the order of parts per million (Cann et al., 1985). Rhyolite domes or plugs, sub-volcanic sills, felsic plutons, and spreading ridge magma chambers are possible sources of heat (Franklin, 1993). This heat source must be great enough to overcome the low temperature of seawater, the major source of the fluids, circulating through the permeable subaqueous volcanic rocks.

Observations of fluids exiting modern black smokers show they contain about 10 ppm Zn and Cu. Black smokers are considered to represent part of modern sea floor hydrothermal systems that capable of producing VMS type deposits. Substantial heat is required over long periods of time to generate a hydrothermal system capable of forming the average VMS deposit (Franklin, 1993). However, the average sized magmatic body does not produce enough heat over a given period of time if the fluids contain only 10 ppm Cu and Zn. It has been suggest by Cann et al., (1985) and Lowell and Rona (1985) that a vigorously convecting magma chamber may be able to produce enough heat to drive a hydrothermal system that could form a VMS deposit, assuming the metal abundance in the fluids is on the order of 100 ppm.

Another heat source proposed for the VMS deposits is derived from the stratal aquifer model (Gibson et al., 1983). In this model ore fluids are generated from pore water in a porous rock unit that is covered with an impermeable unit. This impermeable unit prevents the pore fluids from migrating and mixing with seawater. Burial of the pore fluids increases their temperature and pore-fluid pressure. Eventually the pore fluid pressure may exceed the lithostatic pressure and fractures develop, which allows for the release of high temperature fluids to react with adjacent wall rocks. This model allows for large quantities of fluid that have reacted with adjacent wall rock during upward release to be extruded onto the sea floor with minimal energy requirements (Lydon, 1988b).

A heat source is required for the creation of VMS deposits for two main reasons. First, high fluid temperatures are required to promote reactions between fluid and wall rock to mobilize metals. Heat is also required to drive the circulation of fluids through

the adjacent rock units and eventually heat loss leads to precipitation of metals on, or just below, the seafloor. Heating of the fluids may be caused by: 1) intrusive bodies, or 2) burial of pore fluids. Only the former will be considered here, owing to the inability to represent the latter case spatially. Spatial association to a heat source in the spatial model can be represented by proximity to intrusive bodies. Considerations with respect to the spatial model include 1) heat loss into the adjacent rocks, 2) the lateral extent of heating adjacent rocks; and 3) history of plutonism within the belt. These intrusive bodies are syn-genetic with the volcanic rocks. This fact is significant because it places constraints on which intrusive bodies may act as a heat source.

3.3.3 Stratigraphy

VMS deposits are not associated with a specific geotectonic environment; however, they do have similar stratigraphic characteristics. Cu-Zn VMS host rocks are commonly dominated by submarine volcanic or pyroclastic rocks. These deposits also occur within volcaniclastic rocks and marine sediments that do not have any genetic association with volcanic rocks. Clastic and chemical sedimentary units commonly overlie the volcanic host rocks. Massive sulphide lenses commonly occur along a single stratigraphic horizon, and are spatially related to structural and topographic features of the sea floor. Figure 3.5 shows an example of major VMS deposits in the Noranda massive sulphide district that occur primarily along one main horizon. Deposits are also spatially associated with rhyolite domes or felsic fragmental rocks (Lydon, 1988a).

Part of the development of a VMS deposit is an impermeable cap that confines the migration of hydrothermal fluids. Without an impermeable cap these fluids are free to

migrate to the sea floor over a large area and do not accumulate into large massive sulphide deposits. The impermeable cap may take the form of sedimentary units, massive submarine pyroclastic ash flows or felsic flows. Pervasive silicification formed by the hydrothermal system itself could also seal the rocks effectively (Franklin, 1993).

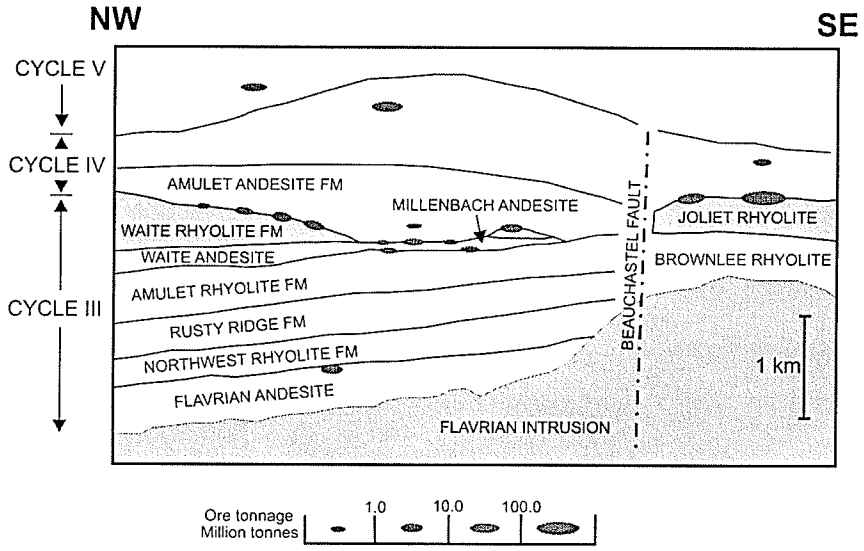

Figure 3.5 A schematic composite section of the Noranda massive sulphide district, showing stratigraphic relationships in the upper part of the Blake river Group and the stratigraphic positions of major VMS deposits (after Lydon, 1988a). Cycles refer to the andesite-rhyolite volcanic cycles of Spence and de Rosen-Spence (1975).

Consideration for the translation stage include 1) stratigraphic relations and lithological contacts, 2) timming of deposition; and 3) subaqueous rock types. VMS deposits are commonly found along one main stratigraphic horizon, which may represent the end of a volcanic cycle or hiatus in volcanic activity. Contacts then become important stratigraphic markers and can be represented in the spatial model. Timing of deposition is important because these deposits are syn-volcanic and, therefore, stratigraphic relations with post-volcanic sequences should not be considered.

3.3.4 VMS Deposits and Occurrences in the Southern belt

Appendix C is a brief summary of the VMS deposits and occurrences in the southern part of the Lynn Lake Greenstone belt compiled in the Mineral Deposit Series, Manitoba Energy and Mines. Deposits and occurrences have been chosen based on the classification given in the Mineral Deposit Series. In the Mineral Deposit Series the term massive sulphide deposit is used to reference the deposit type, not a sulphide rich rock. Deposits are defined where tonnage and grade are known. Figure 3.6 shows the locations of the known occurrences. Table 3.3 is a summary of key aspects of the occurrences and Table 3.4 lists the coordinates of the occurrences.

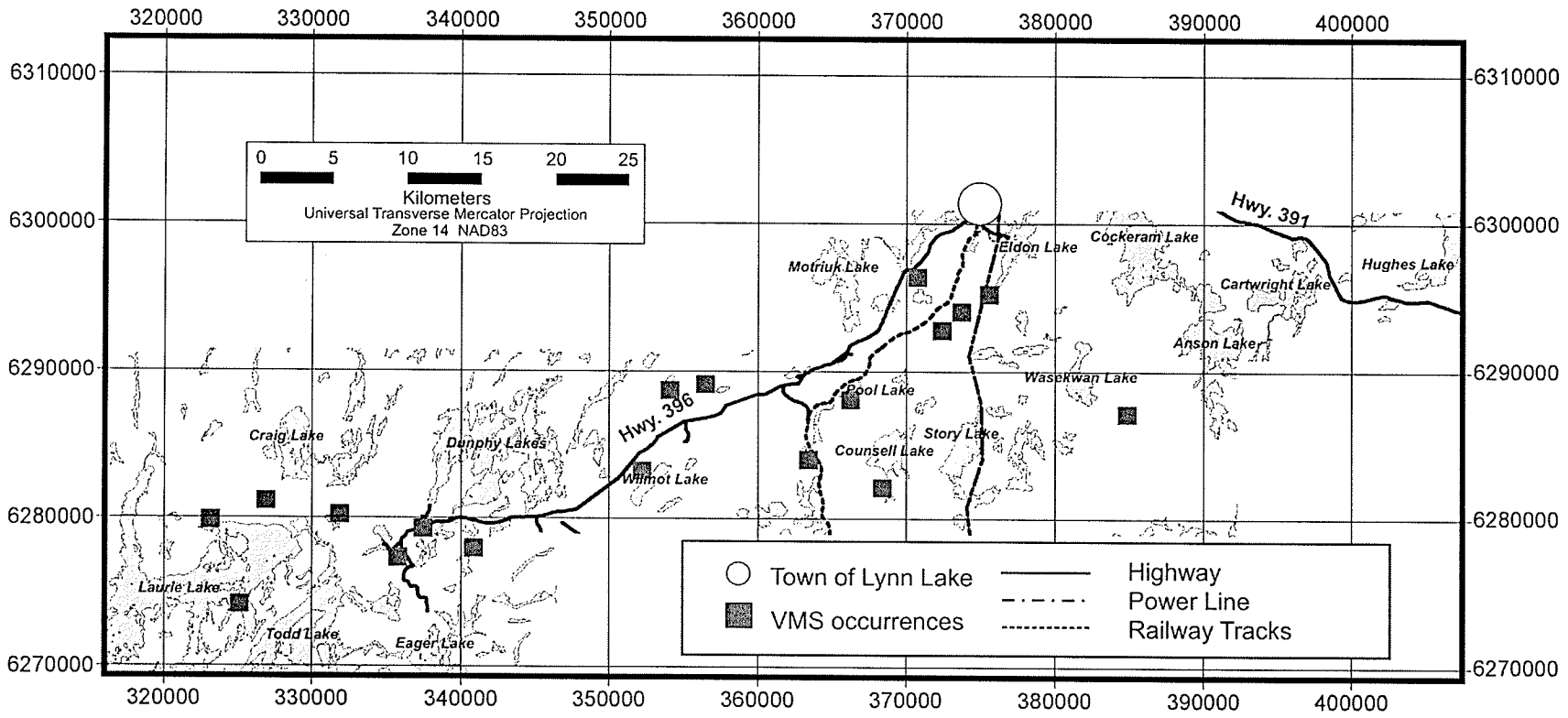

Figure 3.6 VMS occurrences in the southern segment (project area) of the Lynn Lake Greenstone Belt.

TABLE 3.3: VMS Deposits and Occurrences

Site	Classification	Mineralization	Alteration	Cu-Zn
NTS 64C/12 L1	SMSD-VRA (1)	py, cp, sp, po	quartz-sericite, quartz biotite, cordierite-anthophyllite, and biotite-phlogopite-talc-chlorite mineral assemblages	11 958 182 tonnes; grading 1.82% Cu, 1.78% Zn
L8	SMSD-AVR (2)	py, cp	Anthophyllite+cordierite+biotite±garnet	up to 3080 ppm Cu, 6180 ppm Zn
L15	SMSD-VRA	minor py, po	Garnet, biotite	tr. Cu and Zn
L18	SMSD-AVSR (3)	py, po, tr. cp	Anthopyllite+gedrite±garnet±cordierite±sillimanite±staurolite	up to 3789 ppm Cu from hand sample; 1.14% Cu and 0.02% Zn from DDH sample
L20	SMSD-VRA	py, po	Seritizied – quartz-biotite-garnet	up to 142 ppm Cu and 116 ppm Zn
L21	SMSD-VRA	po, py, sp, cp, mt, tetrahedrite	Cordierite-anthophyllite or anthopyllite-garnet-cordierite	Estimated 1361000 tonnes; grading 0.8% Cu and 2.15% Zn
L24	SMSD-AVR	py, cp	Garnet-anthophyllite	up to 2840 ppm Cu, 169 ppm Zn
NTS 64C/11 L4	SMSD-SRA (4)	py, po, cp, mt, asp, tr. sp	Garnet, chlorite	0.01% Cu, 0.17% Zn DDH sample
L8	SMSD-AVR		Chlorite-garnet±magnetite with minor staurolite, anothophyllite, kyanite, sillimanite, cordierite	3.7% Cu over 0.7 m from DDH
L9	SMSD-VRA	py, asp, po, cp	Ganet, chlorite	close to 1% Cu and Zn from DDH
L11	SMSD-AVSR	sulphides	Chlorite-garnet±magnetite	0.14% Cu over 25,4 cm; 3.65% Cu over 3..8 m from DDH
L18	SMSD-VSRA (5)	po, py, cp, sp, ga	Garnet, staurolite, chlorite, biotite	0.01 – 0.16 Cu; nil-0.17% Zn from DDH
L19	SMSD-VRA	po, py, cp, sp, ga	Garnet, staurolite, chlorite, biotite	0.08%Cu and 3.01% Zn over 6 cm; nil-0.03% Cu and 0.04-0.015% Zn over 30 cm; nil-0.08% Cu and nil-0.04% Zn from DDH
NTS 64C/10 L13	SMSD-VRA	py, po, cp	chlorite±sericite	No data available
NTS 64C/14 L13	SMSD-VRA	py, po, cp, sp		No data available
L14	SMSD-SRA	po, py, sp, cp	Potassic alteration	11-855 ppm Cu; 123-3530 ppm Zn
L48	SMSD-VRA	po		Nil-0.1% Cu; nil-0.2% Zn from DDH
L53	SMSD-VRA	py, cp, sp, po		

(1) Stratabound massive sulphide deposit, volcanic rock associated.
(2) Stratabound massive sulphide deposit, alteration with volcanic rocks.
(3) Stratabound massive sulphide deposit, alteration with volcanic and sedimentary rocks.
(4) Stratabound massive sulphide deposit, sedimentary rock associated.
(5) Stratabound massive sulphide deposit, volcanic and sedimentary rock associated.

TABLE 3.4: Deposits and Occurrence Coordinates

NTS Map Sheet	Location No.	Easting (1)	Northing (1)
NTS 64C/12	L1	337470	6279231
	L8	340833	6277899
	L15	335766	6277271
	L18	331881	6280191
	L20	326905	6281107
	L21	323118	6279802
	L24	325145	6274113
NTS 64C/11			
	L4	352229	6283146
	L8	363383	6283953
	L9	366238	6288010
	L11	368391	6282029
	L18	354083	6288639
	L19	356499	6289046
NTS 64C/10			
	L13	384827	6287061
NTS 64C/14			
	L13	370765	6296352
	L14	375621	6295172
	L48	373737	6293999
	L53	372440	6292739

UTM Coordinates Zone 14, Nad83 (coordinates from Mineral Deposit Series)

4 DATA SETS

4.1 Data Sets

A compilation of geological, geochemical, and geophysical data for the Lynn Lake Greenstone Belt has been developed and is in digital format. This compilation is also to be made available through the Manitoba Geological Survey as an Open File. The compiled data sets are listed in Table 4.1 and are available on the included CD (Appendix A). Only those data sets used in this project will be discussed. Issues to be addressed regarding differences in data format, resolution, scale, data set extent, and projection, will be discussed following the data set descriptions. GIS and image processing software used in this project included ArcView 3.2, ERMapper 6.1, and PCI 6.3.

4.2 Geological and Geochemical Data Sets

The 1:50 000 geological map of the Lynn Lake Greenstone Belt was compiled from five geological maps completed from 1976 - 1979 (Table 4.2). The map area covers 3500 km^2 and is bounded by longitudes 100020'W and 1020W, and latitudes 56030'N and 570N. At the time of regional mapping bedrock exposure was sporadic and averaged about 10% of the total surface area, however, large forest fires in the mid- and late 90's have resulted in large areas of well exposed, outcrop with limited lichen coverage. The geological map of the Lynn Lake Greenstone Belt was digitized in 1998 by Geological Services, Manitoba Industry Trade and Mines. The digitized map is in vector format (Figure 4.1). The 1:50 000 geological map includes major faults and the JSZ, both included as vectors. The extent of the JSZ had previously been mapped from Hughes Lake to Gemmel Lake. The western extent of the JSZ passed Gemmel Lake was mapped

during the 1999 and 2000 field seasons (Beaumont-Smith and Rogge, 1999; Beaumont-Smith, 2000) and was made possible owing to the recent forest fires.

TABLE 4.1: Compiled Data Sets for the Lynn Lake Greenstone Belt

Geological Map 1:50 000:	Revised 1980, digitized 1998 Geological Services, Manitoba Industry, Trade and Mines
Geochemical Units 1:250 000:	OF99-13-1 Lynn Lake Greenstone Belt, Geological Services, Manitoba Industry, Trade and Mines (1999)
Aeromagnetic Digital Data:	10500 Barrington lake (1) TF, VG, VLF-EM 13800 Lynn Lake 1982 (1) TF, VG, VLF-EM **(NU)** 17900 Lynn Lake 1988 (2) TF, TD-EM 18201 Lynn Lake 100 1985 (2) TF, VG, VLF-EM Geological Survey of Canada; Geological Services, Manitoba Energy and Mines
Syntetic Apature Radar Data:	RADARSAT_1, SAR Standard 3 Beam Mode, Canadian Space Agency, Manitoba Remote Sensing Centre (2000)
Geochemical Data:	Lynn Lake Greenstone Belt, Chris Beaumont-Smith, Manitoba Geological Survey (1999, 2000)
Geochemical Data:	Lynn Lake Greenstone Belt, Ground truthing, Derek Rogge and Manitoba Geological Survey (2000, 2001)
Regional Till Geochem **(NU)**	Open File 1204, Granville Lake (64C), Geological Survey of Canada (1989)
Regional Lake Sediment Geochem **(NU)**	Open File 999 Granville Lake (64C), Geological Survey of Canada (1989)

(NU) Data set not used in this project
(1) A "Joint Agreement" program between the Government of Canada and the Province of Manitoba.
(2) The Canada-Manitoba Mineral Development Agreement (MDA), 1984 – 1989

TABLE 4.2: Lynn Lake Greenstone Belt Geological Maps

Geological Maps (revised 1980), 1:50 000

GP80-1-1 Lynn Lake (64C-14)	H.P. Gilbert, E.C. Syme
GP80-1-2 Cockeram Lake (64C-15)	E.C. Syme, H.P. Gilbert
GP80-1-3 Laurie Lake (64C-12)	H.V. Zwanzig, M.W. Thomas, J.P. Keay
GP80-1-4 McGavock Lake (64C-11)	H.P. Gilbert, H.V. Zwanzig, B. McGill, H.D.M. Cameron, Oliver (1952), Milligan (1960)
GP80-1-5 Sickle Lake (64C-10)	E.C. Syme, H.V. Zwanzig, Fawley (1952), Milligan (1960)

Digital File: Digitized by Bonnie Lenton, Geological Services, Manitoba Industry, Trade and Mines (1998)

Samples collected and analyzed during regional mapping in the Lynn Lake Greenstone Belt (Gilbert et al., 1980; Gilbert, 1993) have been re-analyzed using ICP-MS (Activation Laboratories, 1999). The updated trace element data is included along with a 1:250 000 geochemical subdivision map in open file 99-13-1, Geological Services, Manitoba Industry, Trade, and Mines (Zwanzig et al., 1999). The new data has provided trace element and REE geochemical signatures for the stratigraphic components of the belt. From this data distinctive tectonostratigraphic assemblages have led to an improved the understanding of the geological history of the Lynn Lake belt. The data also has important implications for effective mineral exploration. The 1:250 000 geochemical subdivisions map is derived from the re-analyzed sample data and is in vector format (Figure 4.2). Sample data is also in vector format and is represented as point data.

Geochemical data was also collected during ground truthing of the mineralization potential maps, and during structural mapping conducted by the Manitoba Geological Survey. The data was collected during the 1999, 2000, and 2001 field seasons. This data is available in Appendix A. Sample data is in vector format and is represented as point

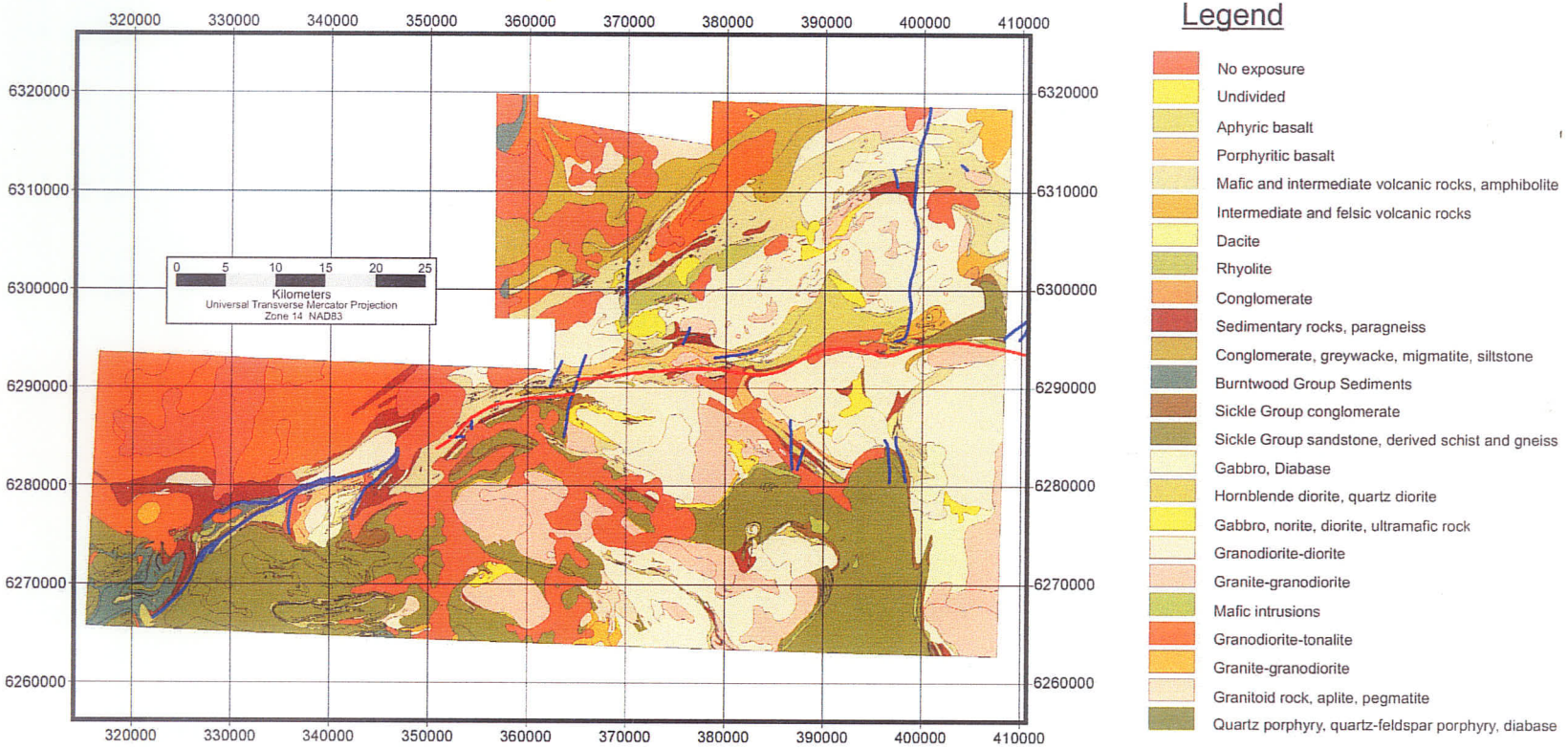

Figure 4.1 1:50 000 geological map of the Lynn Lake Greenstone Belt northwestern Manitoba (Geological Services, Manitoba Energy and Mines 1980, 1998). Known faults are shown in blue; JSZ is shown in red.

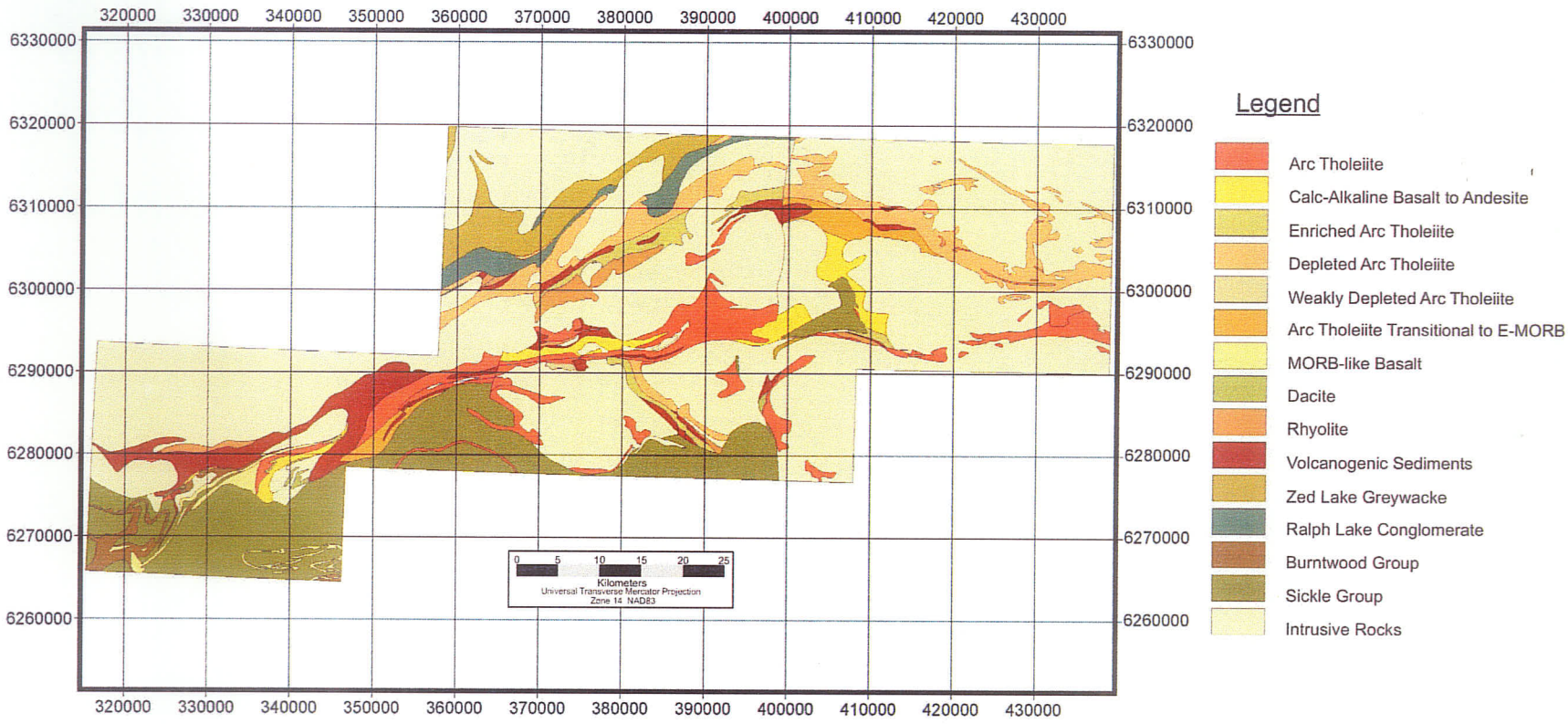

Figure 4.2 1:250 000 geochemical units map of the Lynn Lake Greenstone Belt northwestern Manitoba (OF99-13 Geological Services, Manitoba Energy and Mines 1999).

data. Figure 4.3 shows the locations for re-analyzed regional mapping samples, structural mapping samples, and ground truthing samples.

4.3 Aeromagnetic and VLF-EM Data Sets

Airborne geophysical data sets acquired for this project include total field magnetic data (TF), vertical gradient magnetic data (VG), very low frequency electromagnetic data (VLF-EM), and time domain electromagnetic data (TD-EM). Four surveys were flown and comprise the data set, however, only three surveys were used in this project (Table 4.3). Survey 17900 was not included because it did not include VG and VLF-EM data, which the three other surveys did include. Also the survey area did not cover a significant portion of the project area and also had < 10% overlap with the geological and geochemical data sets available. The surveys were flown under two separate agreements between the Government of Canada and the Province of Manitoba. VLF-EM and magnetic surveys measure 3-dimensional features within the subsurface and not simply the 2-dimensional surface. The TF, VG, and VLF-EM data sets are raster images in georeferenced tiff image format.

Magnetic surveys map magnetic anomalies in the Earth's magnetic field caused by the magnetic properties of the subsurface geology. Lithological units contain varying abundances of magnetic minerals, such as magnetite and pyrrhotite, which produce significant magnetic anomalies. These anomalies are superimposed on the normal magnetic field of the Earth. Aeromagnetic surveys can measure the Earth's total magnetic field as one or more of the field gradients. Magnetic surveys are primarily used for locating metalliferous mineral deposits such as VMS deposits. Regional scale

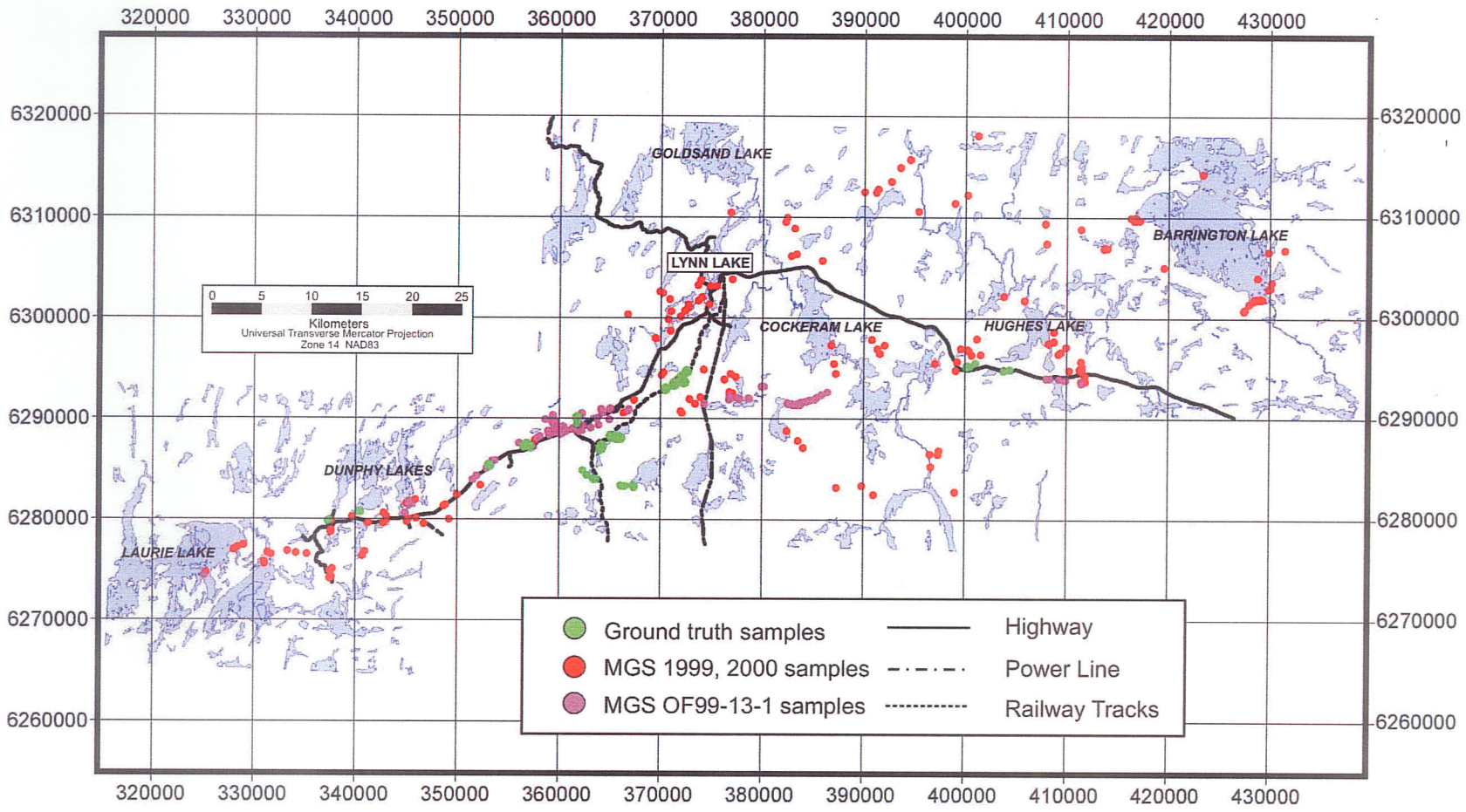

Figure 4.3 Locations of samples from OF99-13-1 Lynn Lake Greenstone Belt, Geological Services, Manitoba Energy and Mines (1999); Lynn Lake Greenstone Belt, Chris Beaumont-Smith, Manitoba Geological Survey (1999, 2000); and, Lynn Lake Greenstone Belt, Ground truthing, Derek Rogge and Manitoba Geological Survey (2000, 2001).

TABLE 4.3: Aeromagnetic Digital Data, Lynn Lake Greenstone Belt

Project Number	10500	Barrington lake (1)	TF, VG, VLF-EM
	13800	Lynn Lake 1982 (1)	TF, VG, VLF-EM
	17900	Lynn Lake 1988 (2)	TF, TD-EM
	18201	Lynn Lake 100 1985 (2)	TF, VG, VLF-EM

10500, 13800:

Data Acquisition	Digital
Platform	Fixed-Wing
Projection	UTM Nad27 – converted to Nad83
System (Mag)	2 Single Cell Self-Orienting/Optical Absorption VG Sensor Separation 2.05 m
System (EM)	HERZ TOTEM 1A Line Station: NLK SEATTLE 24.8 Ortho Station: NSS ANNAPOLIS 21.4
Open File Numbers	889, 1047

17900: NOT USED

Data Acquisition	Digital
Platform	Fixed-Wing
Projection	UTM Nad27 – converted to Nad83
System (Mag)	Varian Single cell split beam
System (EM)	GEOTEM / Time-Domain EM/135m cable

18201:

Data Acquisition	Digital
Platform	Fixed-Wing
Projection	UTM Nad27 – converted to Nad83
System (Mag)	SCINTREX /Optically Pumped/ VIM 2321 A1,A2 VG Sensor Separation 1.83 m
System (EM)	HERZ TOTEM 2A Line Station: NLK SEATTLE 24.8 Ortho Station: NSS ANNAPOLIS 21.4

(1) A "Joint Agreement" program between the Government of Canada and the Province of Manitoba.
(2) The Canada-Manitoba Mineral Development Agreement (MDA), 1984 – 1989

TF Total Field Magnetic
VG Vertical Gradient
VLF-EM Very Low Frequency Electromagnetic
TD-EM Time Domain Electromagnetic

magnetic surveys are also useful for studying geologic structure, such as faulting, shearing, and fracturing. These structures, specifically shear zones, are potential sites for stress-related mineralization.

Interaction between electromagnetic fields and the electrical conductivity structure of the subsurface is the basis behind the VLF-EM geophysical method. Electromagnetic fields generated using a coil or loop will induce secondary fields in the subsurface that may be detected in a receiving coil. Low frequency, 15-25 kHz, electromagnetic radiation generated from large transmitters around the globe is used as the primary electromagnetic source field (Kearey and Brooks, 1991). VLF-EM survey instruments can be mounted within a plane or towed behind. In mineral exploration VLF surveys are principally used for detection of metalliferous mineral deposits, which tend to have significantly different electrical properties than the adjacent rocks. Conductive sources also include shear zones, faults, graphitic units, and swamps. Linear conductors determined from VLF methods are good indicators of VMS deposits and may also indicate the existence of shear zones.

Magnetic and VLF-EM data was flow with 300 m line spacing. Perpendicular control lines were flow with spacing of 10 000 m. The data sets were received in GEOSOFT ASCII format, converted to NAD83 with a UTM projection calculated for a Central Meridian of 99.000W (Figures 4.4 - 4.7). The GEOSOFT ASCII format was converted to a flat ASCII file, which was subsequently interpolated and gridded, using ERMapper 6.1, to produce raster images. Minimum curvature was used to produce the raster images, with boundary tension, interior tension, convergence speed and limit, maximum iterations, and aspect ratio set to ERMapper 6.1 defaults. Acquired TF and

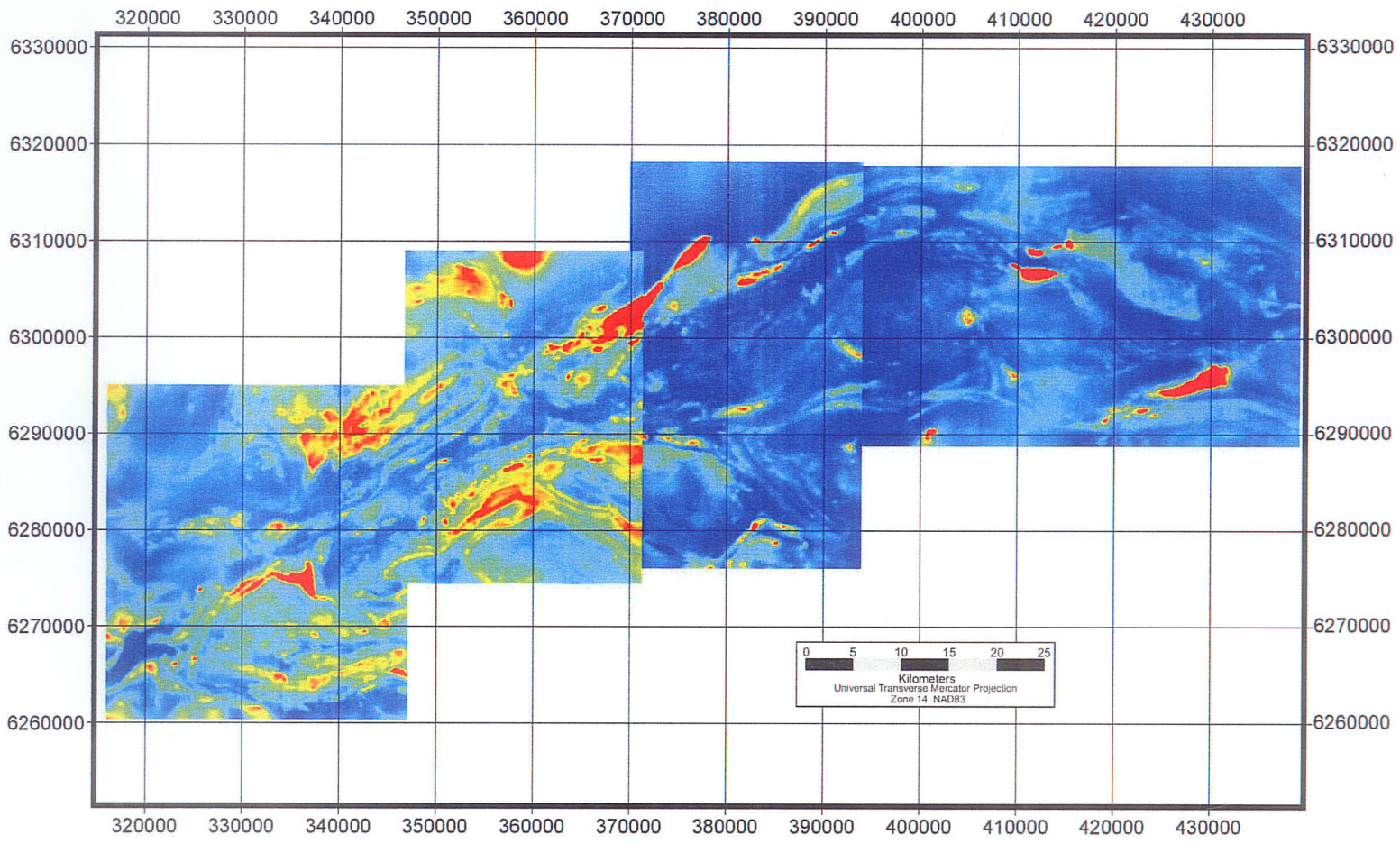

Figure 4.4 Total field magnetic surveys 105 (1), 138 (1), and 182 (2) of the Lynn Lake Greenstone Belt. Surveys are not leveled to each other. Red - magnetic high; Blue - magnetic low (linear scale). (1) A "Joint Agreement" program between the Government of Canada and the Province of Manitoba. (2) The Canada-Manitoba Mineral Development Agreement (MDA), 1984 1989

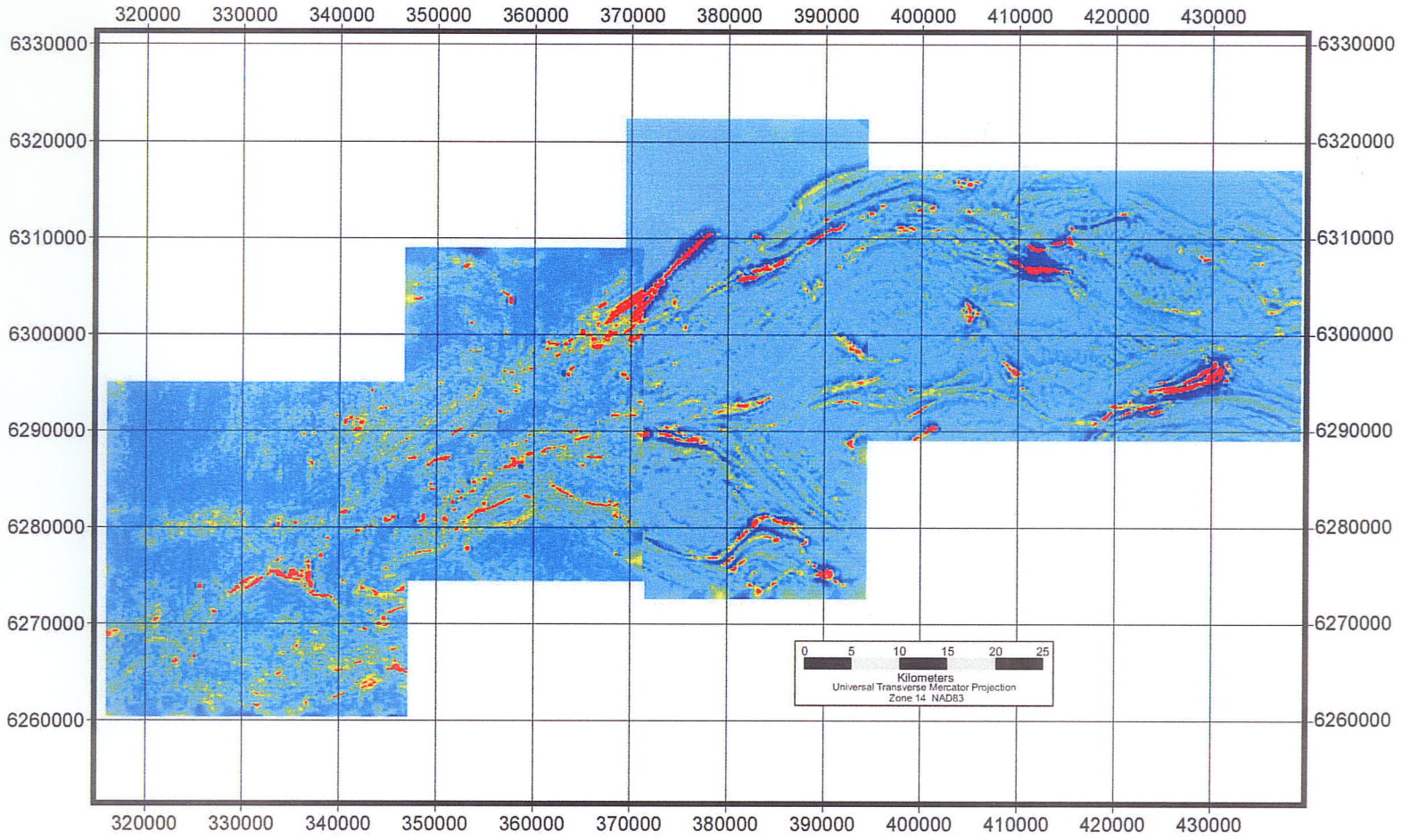

Figure 4.5 Vertical gradient magnetic surveys 105 (1), 138 (1), and 182 (2) of the Lynn Lake Greenstone Belt. Surveys are not leveled to each other. Red - magnetic gradient high; Blue - magnetic gradient low. (1) A "Joint Agreement" program between the Government of Canada and the Province of Manitoba. (2) The Canada-Manitoba Mineral Development Agreement (MDA), 1984

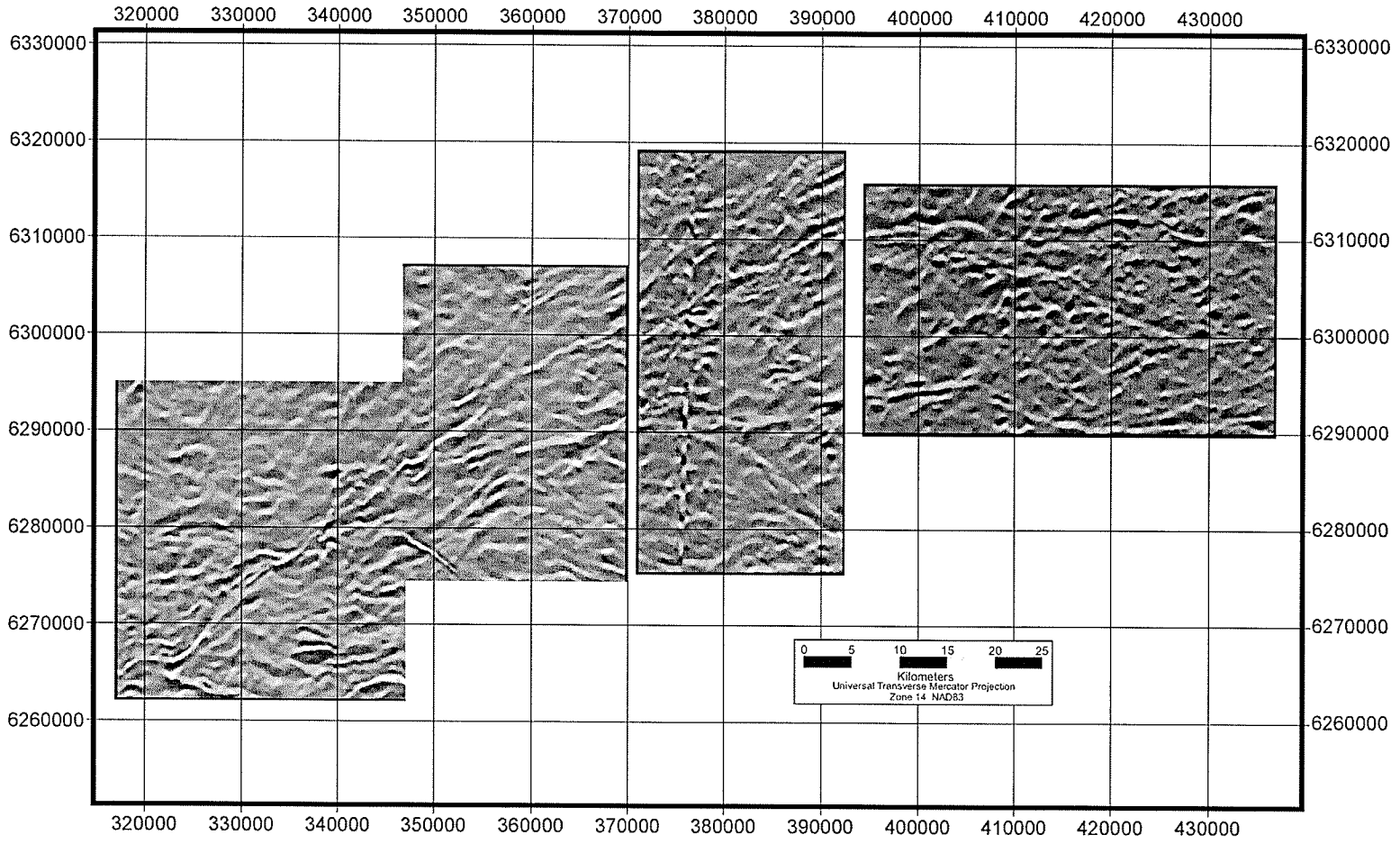

Figure 4.6 Very low frequency electromagnetic (line quadrature) surveys 105 (1), 138 (1), and 182 (2) of the Lynn Lake Greenstone Belt. Surveys are not leveled to each other. White - high conductivity; Black - low conductivity. Processed Fraser filter image (Fraser, 1969). (1) A "Joint Agreement" program between the Government of Canada and the Province of Manitoba. (2) The Canada-Manitoba Mineral Development Agreement (MDA), 1984 1989.

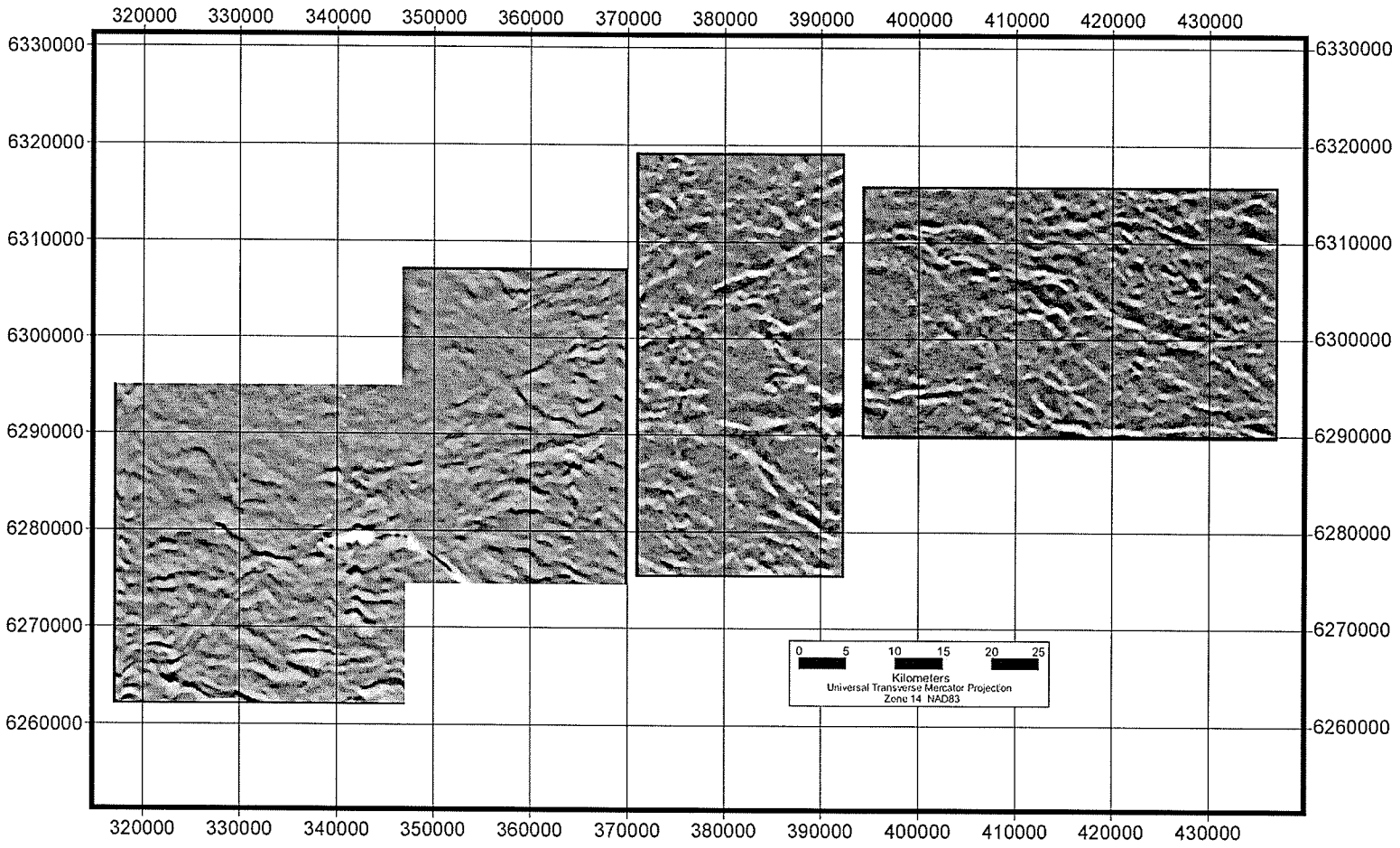

Figure 4.7 Very low frequency electromagnetic (ortho quadrature) surveys 105 (1), 138 (1), and 182 (2) of the Lynn Lake Greenstone Belt. Surveys are not leveled to each other. White - high conductivity; Black - low conductivity. Processed Fraser filter image (Fraser, 1969). (1) A "Joint Agreement" program between the Government of Canada and the Province of Manitoba. (2) The Canada-Manitoba Mineral Development Agreement (MDA), 1984 1989.

VG data was leveled to the survey, however, not to adjacent surveys. Raw quadrature and orthoquadrature VLF profiles show significant conductors as inflection points, which are difficult to interpret visually. For this reason a Fraser filter (Fraser, 1969) has been applied to the VLF-EM line quadrature and orthoquadrature channels before interpolation and gridding. This filtering method smooths the data followed by an alignment of maximum and minimum inflection points with conductivities.

4.4 RADARSAT Synthetic Aperture Radar

Synthetic Aperture Radar (SAR) is an active remote sensing method that sends microwave signals down to a planet's surface. These microwaves create backscatter signals that are received by the satellite, and are directly related to ground topography, dielectric properties, and surface roughness. RADARSAT is a side-looking instrument that allows for the enhancement of topographic features that are not parallel to the look direction. Look direction is the imaging direction and is perpendicular to the satellite orbital path. Linear features can be extracted from SAR imagery and can be used to aid in regional structural analysis (RADARSAT Geology Handbook, 1996). These linear features may be directly related to faults and fractures, dikes, and hydrothermally altered rocks in shear zones (Sharma et al., 1999).

SAR data was obtained from the Manitoba Remote Sensing Centre through an agreement between the Province of Manitoba and the Canadian Space Agency. In the agreement 218 pre-purchased satellite images collected over the lifetime of the satellite have been made available free of charge to users who wish to assess the SAR imagery for resource inventory and management purposes. The main purpose of the SAR imagery in

this project is for lineament analysis in combination with geophysical data analysis and regional structure mapping. The results will be used to help delineate the extent of the JSZ and to provide deformational zone potential, a key component of the shear-hosted model.

TABLE 4.4: RADARSAT Image Details

Platform	RADARSAT_1
Product Reference	Path Image (SGF)
Scene Orientation	11.3144102 °
Nominal Pixel Spacing	12.5 m
Nominal Line Spacing	12.5 m
Instrument	SAR Standard 3 Beam Mode - Incidence Angle Range (°) 30-37 - Approximate Resolution (m) 25 - Nominal Area (km) 100x100
Orbit Number	24367
Orbit Direction	Descending
Date Acquired	July 5, 2000
Date Processed	July 13, 2000
Coordinates (Lat, Lon)	Upper Left: 57.238489N, 102.234094W Upper Right: 57.041831N, 100.438290W Lower Left: 56.473970N, 102.498897W Lower Right: 56.278904N, 100.739554W
Projection	UTM
Central Meridian	101.476305W

SAR images were received in Path Image format, in which data has been converted to ground range and the image remains oriented in the direction of the orbit path. SAR image information is listed in Table 4.4. The standard 3 beam mode was chosen based on an analysis of incident angles for geological applications by Singhroy and Saint-Jean (1999) and the RADARSAT Geology Handbook (1996). Resolution of the SAR data is 25 m, re-sampled to 12.5 m. Processing of the image before lineament extraction included speckle reduction and geo-referencing. Microwaves emitted by SAR are in phase, however, each image pixel is the average of a large number of randomly

distributed scattering elements. This causes speckle, or noise, which can be suppressed. An 11x11 frost speckle reduction filter was chosen based on comparisons of speckle filters by Lopes et al., (1990) and Shi and Fung (1994) for extraction of linear features. Geo-referencing was completed using lakes, digitized from topographic maps, as ground reference points. The SAR data set is a raster image in georeferenced tiff image format. Figure 4.8 is the processed SAR image.

4.5 Multiple Data Platforms

Combination of multiple data sets that have different data format, resolution, scale, data set extent, and projection can cause serious problems, or result in useless mineralization potential maps, if these issues are not addressed. In this project the data acquired includes raster and vector data sets. To produce the mineralization potential maps for this project fuzzy logic and Dempster-Shafer numerical combination methods will be used. A complete discussion on these techniques is given in chapter 5. The two combination methods used in this project require the data sets be in raster format. During combination, data sets must be in the same format. Raster format enables multiple maps to be combined pixel by pixel; the resulting map represents a quantitative two-dimensional pixel array assessment of a mineral potential theme (Chung and Fabbri, 1993). Calculations will be applied pixel by pixel using the map calculator available in ArcView 3.2 Spatial Analysis.

Most geological maps are displayed in vector format, whereas geophysical and remote sensing data is primarily in raster format. Vector format is a data structure for representing points, lines, and graphical symbols. A point in this format is represented by

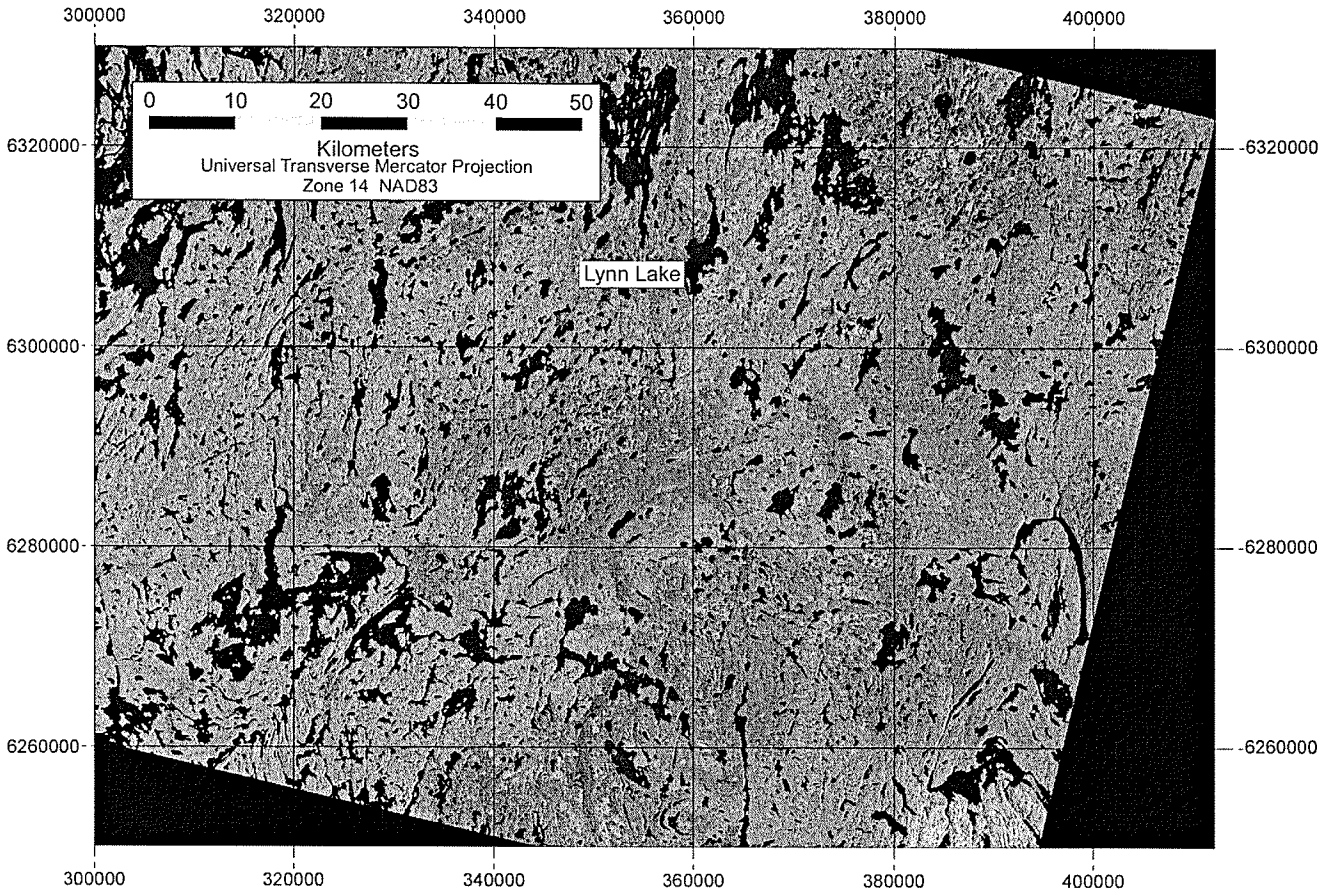

Figure 4.8 Synthetic Aperture Radar Data (SAR) RADARSAT_1, SAR Standard 3 Beam Mode, Canadian Space Agency, Manitoba Remote Sensing Centre (2000).

a pair of spatial coordinates, where lines and polygons are series of ordered points. Raster images are simply an array of pixels, or picture elements, where each pixel is a single rectangular cell, commonly square (Bonham-Carter, 1994). In this project the pixel arrays and vector maps are 2-dimensional. Ultimately the vector files must be converted into raster images for combination. Combination was completed in raster format with pixel size set to 50 m. Converting from vector to raster format can reduce the accuracy of the data. For example, geological contacts become a series of pixels that represent the line as closely as possible (Figure 4.9a). The smaller the pixel size the more precise the representation of the geological contact remains. It was considered that a 50 m pixel size for a project area approximately 140 km^2 should be sufficient for re-sampling or conversion from vector to raster so that these problems did not have a significant effect on the output potential maps.

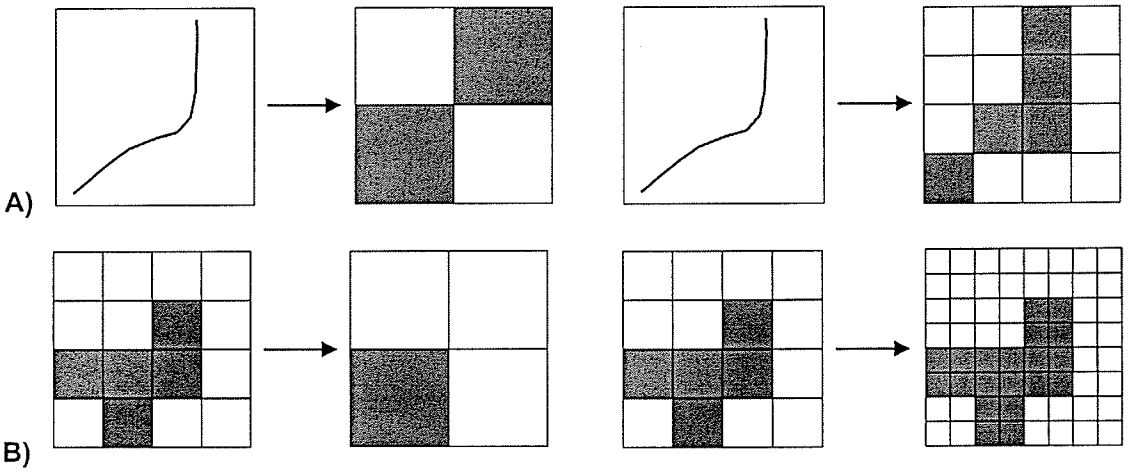

Figure 4.9 (a) The loss of accuracy in vector to raster transformation depends on the pixel size. (b) Increase in pixel size in a raster data set causing loss of accuracy in the original data set. Deacreasing the pixel size does not cause loss of accuracy in original data set.

The available data sets were received with various extents and in different resolutions and scales. These differences must also be considered during translation and processing. The project area extent was chosen, in part, by the data sets available. An area was chosen where all of the available data sets overlapped each other. This was done to minimize missing data from one or more of the data sets. The approach resulted in there being a few small gaps in the output potential maps (Figure 4.10). Differences in resolution result in the output being only as accurate (or less than) the input data set with the lowest resolution. Figure 4.9b shows how increasing the pixel size can cause loss of accuracy in the original data set. On the other hand, decreasing the pixel size will not affect the accuracy of the original data set. Geophysical data was originally gridded at 50 m resolution. The converted vector data was also set to 50 m. The SAR data has a resolution of 12.5 m. Increasing the pixel size would reduce the accuracy of the SAR data. However, the primary use of the SAR data was to extract lineaments, and therefore, the re-sampling is not necessary (see section 6.2.2). The geological and the geochemical subdivisions for volcanic rocks data sets are both in vector format, but have different scales. The polygons defined in the geochemical subdivisions map were digitized from the original 1:50 000 geological maps. The 1:50 000 geological data set was digitized separately from the original 1:50 000 geological maps. There are discrepancies between the two digital maps. However, they are considered minor and should not adversely affect the results.

Data sets with different projections should not be combined. In this project all of data sets were projected to UTM Zone 14 NAD 83 before translation and combination. Mineralization potential maps presented in subsequent chapters are also in UTM Zone 14

NAD 83. This was completed using projection utilities in ERMapper 6.1 and ArcView 3.2. Changing the projection of data sets can also cause the loss of accuracy of the original data. Shifts in the data during re-projection are considered small relative to the regional scale of the data sets, and should not adversely affect the results.

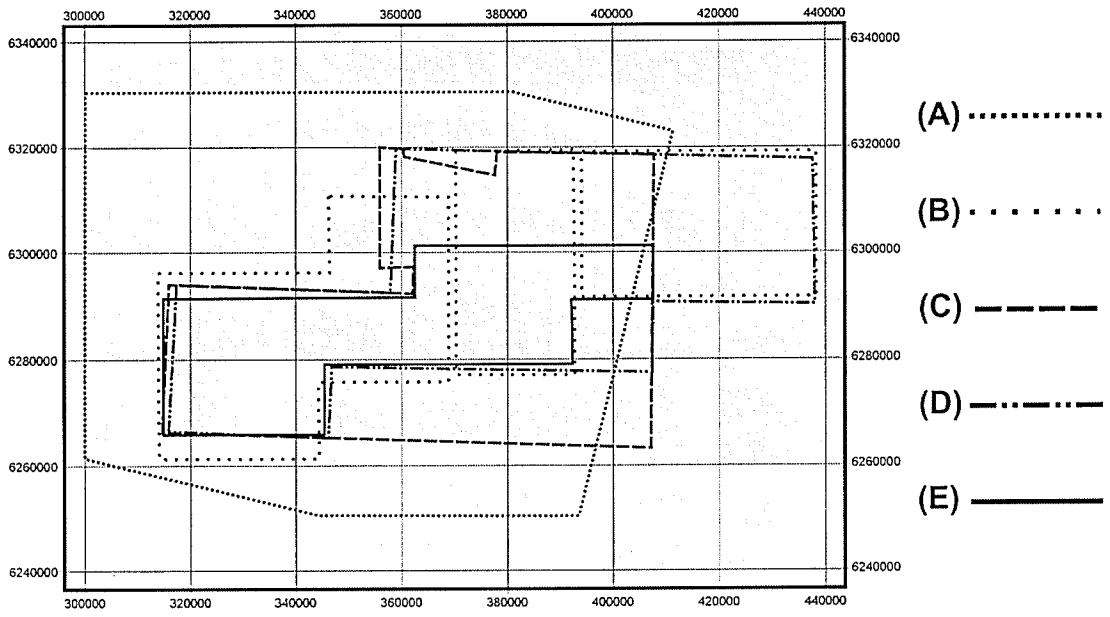

Figure 4.10 Coverage of regional base data sets. Note small gaps between geophysical surveys in the project area. (A) : SAR; (B) : VLF, TF, and VG geophysical surveys 105, 138, and 1 82; (C) : geochemical subdivisions; (D) : geological map: (E) : project area. Project area map project is UTM Zone 14, NAD83.

More specific problems with respect to the overall accuracy of the resulting mineralization potential maps include the extrapolation of geological contacts, compilation of regional geological maps, digitization, leveling of geophysical data sets, and depth of penetration for the TF, VG, VLF-EM, and SAR data sets. Geological maps represent real observations from a few small outcrops, which are used to interpret an area

as a whole (Chung and Fabbri, 1993). This interpretation results in uncertainty in the data. Extrapolation of units where no outcrop is exposed can result in minor shifts of geological contacts, or possible major errors where units are missed all together. Lithologies are mapped to a particular scale and many smaller, yet significant units, are not represented. Grouping lithological units can simplify a map, making it easier to interact with, however this grouping can also reduce the accuracy of the potential maps. Compilation of the regional geological maps is done in such a way as to minimize any inconsistencies between the maps, such as lithological classification and aligning contacts at the edge of adjacent maps. Both the 1:50 000 geological map and the 1:250 000 geochemical subdivisions data sets were digitized from the original regional maps. Loss of accuracy during digitization depends on the skill of the digitizer. It is assumed that the prior steps taken to produce the digital data available to the project were completed in a rigorous manner as to limit the loss of accuracy.

Three separate surveys make up the VLF and VG data sets, whereas one SAR scene covers the entire project area. For the VLF and VG surveys the data have not been leveled relative to adjacent surveys. Geophysical surveys 105 and 138 were completed under the same contract and instrumentation; however, survey 182 was completed under a different contract and instrumentation (Table 4.3). For these reasons processing, analysis, and combination will be completed with respect to the individual surveys.

The depth of penetration for the TF, VG, VLF-EM and SAR data sets vary. SAR data is a measure of surface roughness and penetration is not significant. On the other hand, the geophysical data is primarily a product of subsurface geology. Magnetic surveys map magnetic anomalies in the Earth's magnetic field caused by the magnetic

properties of the subsurface geology down to the Curie isotherm. Magnetism of ferromagnetic minerals is lost at the Curie temperature, typically between 20 and 40 km in continental regions (Lowe, 1999). However, exploration geologists are commonly most concerned with more shallow magnetic sources. For VLF surveys the depth of penetration depends upon its frequency and the electrical conductivity of the subsurface material. If the subsurface material is conductive then penetration is greatly limited. High frequency surveys have shallow penetration, whereas very low frequency surveys can penetrate to a maximum depth of 500m (Kearey and Brooks, 1991). Magnetic, electromagnetic and SAR data sets can be considered to reflect subsurface, near surface, and surface data respectively. This must be kept in mind during the translation and combination stages of the project.

5 DATA FUSION COMBINATION METHODS

5.1 Spatial Combination

The use of computers for display and analysis of geological and geophysical data has become more common as processing speed and available memory have increased. Geographical information systems (GIS) have been developed to effectively overlay digital information and perform quantitative modeling of geological, geophysical, and remote sensing data (An et al., 1991; Moon, 1993; Bonham-Carter, 1994, Wright and Bonham-Carter, 1996, and Srivastav et al., 2000). Data sets represent information that can be used by an exploration geologists to find areas of economic interest. However, the use of multiple data sets in combination can significantly increase our ability to find these potential areas. GIS platforms can be used to combine various geological, geophysical, and remote sensing data sets, but there are problems associated with different resolution, spatial extent, and the degree of uncertainty in the data sets (An et al., 1991; Moon, 1993; An et al., 1994ab). To overcome these problems a proper quantitative method is required that is independent of spatial resolution. Such methods should also be adequately able to deal with missing or zero value data, and addresses uncertainty in the data sets (An et al., 1991; Moon, 1993, An et al., 1994ab). Quantitative combination methods allow for a more thorough, analytical, less subjective and more repeatable process than any manual method (Wright and Bonham-Carter, 1996).

Most geological maps are displayed in vector format, whereas geophysical and remote sensing data is primarily in raster format. During combination, data sets must be in the same format (Chung and Fabbri, 1993); this project was completed using raster format. These quantitative combination methods can be statistical or expert in their

approach, such as Bayes probability and weights of evidence, or, fuzzy logic and Dempster-Shafer Belief theory, respectively. The former are described by Bonham-Carter (1994) as data driven methods, whereas the later are considered knowledge driven. Fuzzy logic and Dempster-Shafer Belief theory methods have been selected for this project, because of their usefulness in areas where few occurrences are known, and the data sets are at a regional scale. The Dempster-Shafer method was also chosen because the method allows for an uncertainty function.

Both fuzzy logic and Dempster-Shafer methods require the data sets to be in raster format in order to perform numerical calculations. Each data set, or input map is combined with the other data sets pixel by pixel. These calculations are done using the map calculator available in ArcView 3.2 Spatial Analysis. The following is a simple example of combination using a 20x19 pixel area (Figure 5.1). The purpose of this example is to show how the two combination methods combine input maps. The example will also give a brief overview of how translation and combination are implemented in a knowledge-based expert system. The shear-hosted and VMS spatial models developed in chapters 6 are significantly more complex, however, they follow the same principles described in this chapter.

Simple binary combination (0 or 1, yes or no, TRUE or FALSE) will also be considered in this example. Binary combination is included because it represents the most basic form of combination similar to what could be accomplished using a light table. Binary combination will be explained first followed by the Fuzzy logic (0 to 1, to some degree yes - to some degree no) and Dempster-Shafer Belief theory (0 to 1, to some degree yes - to some degree no - to some degree uncertain) methods will follow. The

conceptual model for this example states that a deposit is associated with volcanic rocks and to a lesser degree sedimentary rocks; it occurs on or close to faults, and is associated with magnetic anomalies. Geology, fault, and magnetic anomaly data sets will be considered in this example. The geology and fault maps are in vector format, whereas the magnetic map is in raster format. Input maps generated from the data sets are used as positive evidence that a deposit will occur.

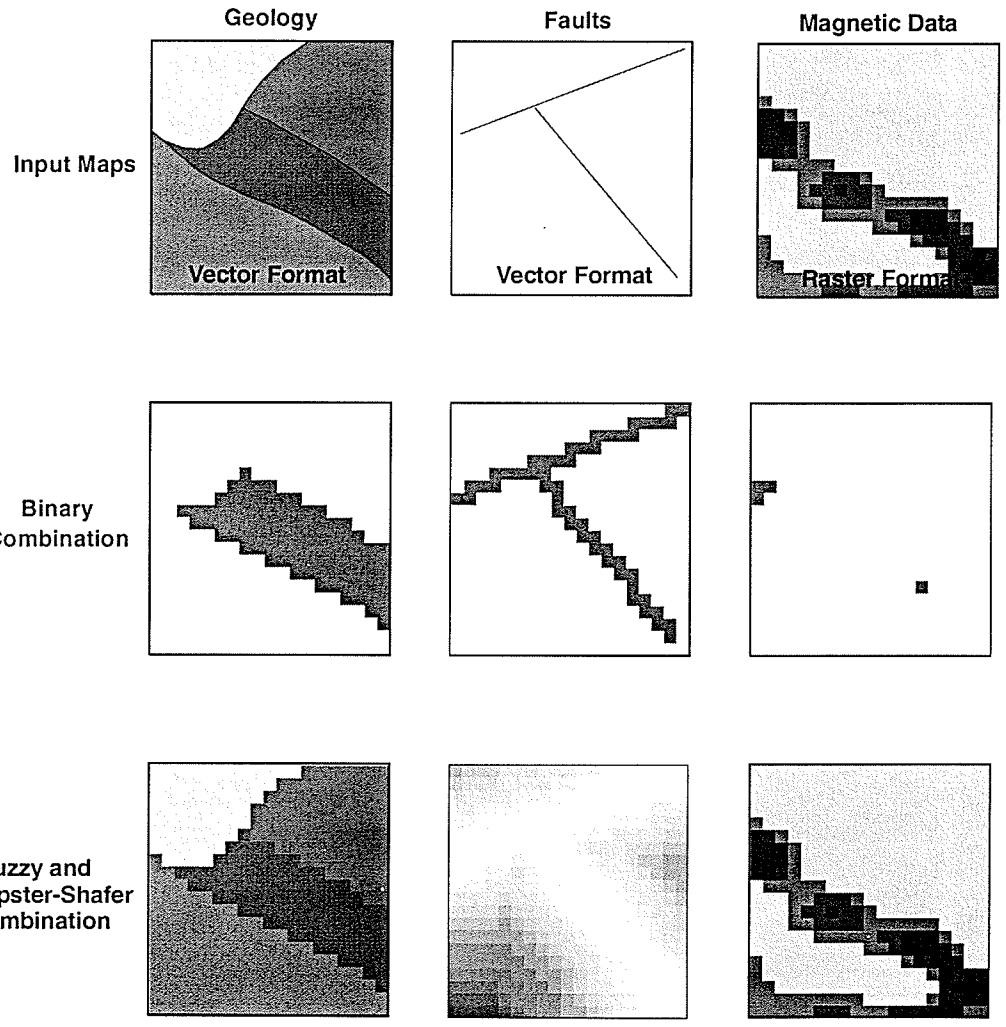

Figure 5.1 (a) Inputs include geology and fault data sets in vector format; and, magnetic data in raster format. (b) Input maps for binary, and (c) fuzzy logic and Dempster-Shafer combination example.

5.2 Binary Combination

With binary combination only two possible cases occur, these are yes a deposit exists or no a deposit does not exist. For binary combination attributes of the data sets are set to either 0 or 1 (Figure 5.1) (Table 5.1). The fault map has two attributes, fault or no fault. Where a fault occurs, pixels will be assigned 1, and where no fault occurs pixels are assigned 0. The geology map contains four attributes, volcanic rocks, sedimentary rocks, intrusive rocks and missing data. Volcanic rocks are associated with deposits and are reclassified as 1, whereas sediments, intrusive rocks, and missing data are reclassified as 0. The reclassified data sets can then converted into raster format. The magnetic map is already in raster format, however, the magnetic map includes five relative levels of magnetic strength. Deposits are associated with magnetic anomalies so pixels with the highest magnetic level are reclassified and set to 1, whereas all other pixels are set to 0. Three raster input maps have now been created from the geology, fault, and magnetic data sets and are now ready for combination.

Combination is completed pixel by pixel according to the following logic.

$$(((\text{IF } (x_i, y_j)_{\text{fault}} = 1) \text{ AND } (\text{IF } (x_i, y_j)_{\text{geology}} = 1) \text{ AND } (\text{IF } (x_i, y_j)_{\text{magnetic}} = 1))$$

$$\text{THEN } (x_i, y_j)_{\text{output}} = 1) \text{ ELSE} = 0 \qquad (1)$$

This combination can be completed by multiplying (x_i, y_j) from each of the three input maps,

$$(x_i, y_j)_{\text{output}} = ((x_i, y_j)_{\text{fault}}) ((x_i, y_j)_{\text{geology}})) ((x_i, y_j)_{\text{magnetic}})) \qquad (2)$$

The resulting output map is a binary raster image in which pixels with a value of 1 indicate potential sites for a deposit to occur (Figure 5.2). The output map generated from the binary method shows only one pixel as a potential site for a deposit. It is the

TABLE 5.1: WEIGHTS FOR COMBINATION EXAMPLE

MAGNETICS	BINARY	FUZZY1	FUZZY2	BELIEF	DISBELIEF	UNCERTAINTY
High	1	0.80	0.60	0.30	0.40	0.30
	0	0.67	0.50	0.25	0.45	0.30
	0	0.56	0.42	0.21	0.49	0.30
	0	0.44	0.34	0.17	0.53	0.30
	0	0.33	0.26	0.13	0.57	0.30
	0	0.21	0.18	0.09	0.61	0.30
Low	0	0.10	0.10	0.05	0.65	0.30
GEOLOGY	BINARY	FUZZY1	FUZZY2	BELIEF	DISBELIEF	UNCERTAINTY
No Data	0	0.00	0.00	0.00	0.00	1.00
Volcanic	1	0.90	0.80	0.40	0.40	0.20
Sedimentary	0	0.50	0.45	0.23	0.57	0.20
Intrusive	0	0.10	0.10	0.05	0.75	0.20
FAULT	BINARY	FUZZY1	FUZZY2	BELIEF	DISBELIEF	UNCERTAINTY
Proximal	1	0.80	0.70	0.35	0.35	0.30
	0	0.74	0.65	0.33	0.37	0.30
	0	0.69	0.60	0.30	0.40	0.30
	0	0.63	0.55	0.28	0.42	0.30
	0	0.57	0.50	0.25	0.45	0.30
	0	0.51	0.45	0.23	0.47	0.30
	0	0.46	0.41	0.20	0.50	0.30
	0	0.40	0.36	0.18	0.52	0.30
	0	0.34	0.31	0.16	0.54	0.30
	0	0.29	0.26	0.13	0.57	0.30
	0	0.23	0.21	0.11	0.59	0.30
	0	0.17	0.16	0.08	0.62	0.30
Distal	0	0.10	0.10	0.05	0.65	0.30

only pixel in which volcanic rock, a fault, and the highest magnetic level were found. The major problem with this approach is the assumption for each pixel is only a yes or no proposition, resulting in only the one pixel showing potential. However, an expert is aware that a fault, a volcanic rock, or a high magnetic signature is not 100% positive

evidence of a deposit. Each input map has attributes that are to some degree positive evidence of a deposit. This problem can be addressed using Fuzzy logic combination methods where each data set can be reclassified using a continuous scale from 0 - 1.

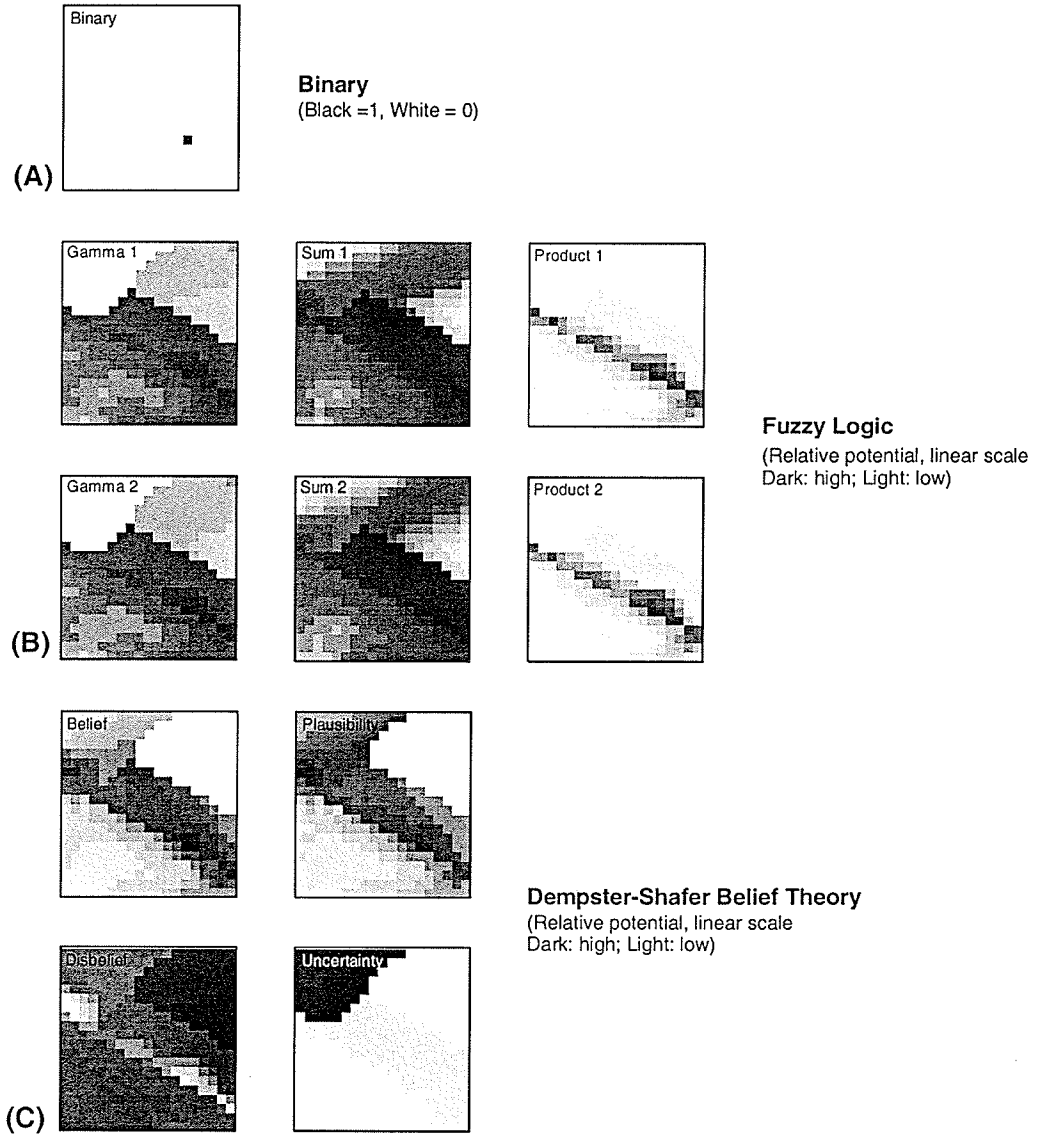

Figure 5.2 Potential output maps for (a) binary, (b) fuzzy logic and (c) Dempster-Shafer combination methods. Fuzzy logic outputs include fuzzy gamma, algebraic sum, and algebraic product; Dempster-Shafer outputs include belief, plausibility, disbelief, and uncertainty. The two sets of outputs for the fuzzy logic method are for weights given in Table 5.1.

5.3 Fuzzy Logic Combination

The Fuzzy-logic method utilizes a continuous scale from 0 to 1, or a fuzzy membership function. Full non-membership of a fuzzy set is 0 and full membership is 1 (Figure 5.3). Attributes in a given data set may indicate high potential for a deposit to occur. A pixel containing this attribute can be assigned a high fuzzy membership. In the case of Figure 5.3 the evidence value represents attributes of a data set. Fuzzy-set theory enables the user to develop a set of attributes for a particular spatial data set, whereby membership functions can be expressed as linear or nonlinear, depending on the problem at hand (Bonham-Carter, 1994). For example, if the target deposit is banded iron formations, magnetic data would be useful in locating the deposit. High magnetic values would be given a high fuzzy membership, whereas low magnetic values would be given a low fuzzy membership. The range from high to low magnetic values could be shown as a linear function. If, on the other hand, lithological units defined in a geological map are assigned a fuzzy membership values, the fuzzy membership function shown in figure 5.3 may be non linear. The function may also be determined by a mathematical function, such as an exponential or logarithmic function. The advantages of the fuzzy-logic method are its straightforward implementation and its ability to develop mineralization-potential maps in areas that are not well explored. The major disadvantage of this method is its inability to deal with missing or zero value data.

Before combination, the three input maps must be in raster format with fuzzy membership values ranging from 0 to 1. Fuzzy membership values are assigned to individual pixels. These pixel values can be considered weights, or the degree of belief that the particular attribute is evidence of a deposit. In the binary combination approach

translation of the conceptual model into the spatial model in limited, owing to the fact that attributes in each data set can be assigned either 0 or 1. In the Fuzzy logic method the attributes can be assigned different values. This allows for a more detail model, and hence, a more involved translation stage. In the case of the magnetic anomaly map, magnetic levels are reclassified relative to their strength using a linear function. Volcanic rocks are weighted the highest followed by sedimentary rocks. Missing data must be assigned a value, or weight, of zero. Proximity to faults can be included where pixels are weighted relative to distance from a fault.

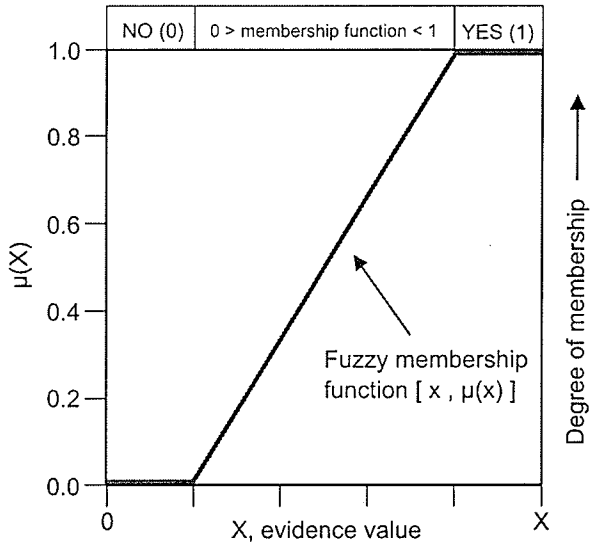

Figure 5.3 Fuzzy membership function for a hypothetical input data set. Fuzzy membership can, in some cases, be expressed as an analytical function, not necessarily linear as shown here, in other cases membership is defined more readily as a table (after Bonham-Carter, 1994)

The weights assigned in to each input map do not have to range the full 0 - 1. For instance a value of 1, or full membership, can be assigned to the fault attribute. In this case faults are considered 100 % positive evidence of a deposit, but there is also some degree of disbelief that a deposit will occur along a fault. An expert can consider the

occurrence of a fault to be only 80% positive evidence of a deposit. Disbelief is then equal to 20%; the negative evidence that a deposit exists. So, for the fault input map pixels along the fault are assigned a fuzzy membership of 0.8. Away from the fault pixels are progressively assigned a lower fuzzy membership value to a minimum of 0.1. Weighting can also be applied to the input data sets themselves, where geology may be a better indicator of a deposit than both the occurrence of a fault or a high magnetic signature. The expert can then assign a maximum fuzzy membership to each input map, with the attributes of each input map based on the maximum fuzzy membership value.

Another factor to consider when weighting the various attributes is full non-membership, or 0. Although intrusive rocks are not a likely lithology to contain a deposit, based on the given conceptual model, they are not 100% negative evidence of a deposit existing. Disbelief that a deposit will occur in an intrusive rock is 0.95, and therefore, belief = 1 - 0.95, or 0.05. Assigning a pixel a zero value will have the same affect as missing data. An attribute may not necessarily be good positive evidence of a deposit, but sometimes may be a good indicator that a deposit does not exist. This negative information about a deposit occurring can sometimes be as useful as positive evidence. Table 5.1 shows the weights of the three input maps in which the first column (FUZZY1) lists weights ranging from 0.1 to 0.8 for all input maps. The second column (FUZZY2) takes into account the weighting of each input map relative to each other and list weight ranges of 0.1 - 0.8, 0.1 - 0.7, and 0.1 - 0.6, for the geology, fault, and magnetic input maps respectively. Two sets of weights were used to demonstrate the difference between assigning a similar maximum weight to all the input maps versus given more weight to a particular input map.

The weights assigned to the input maps that are determined by an expert may be derived by statistical methods or by theoretical principles. In this example and in subsequent chapters weights are determined by theoretical principles. Initially these weights are subjectively determined based on the experience of the expert, however, during combination of multiple input maps the Fuzzy logic method is quantitatively precise (An et al., 1991).

The fuzzy logic method is based on fuzzy set theory first formulated by Zadeh (1965) in which a fuzzy set A is a set of ordered pairs:

$$A = \{ x , \mu (x)\} \text{ where } x (X \qquad (3)$$

where x is a member of X and $\mu(x)$ is the membership function. Methods of map combination include, fuzzy AND, fuzzy OR, fuzzy algebraic product, fuzzy algebraic sum and the gamma operation (Zimmerman and Zysno, 1980). The fuzzy AND operator is the membership function ($\mu_c(x)$ of the intersection $C = A \cap B$, whereas the fuzzy OR operator is the membership function ($\mu_c(x)$ of the union C = AUB. Fuzzy AND and OR represent the minimum and maximum fuzzy membership values occurring for each pixel respectively. These methods are useful if the input maps include decisive evidence of a proposition existing. In geological exploration, input data sets, excluding actual rock samples, are not decisive. Therefore, fuzzy AND and OR have not been used in this project. The output from fuzzy algebraic product, sum and gamma operations express all input from each of the data maps. A discussion of these fuzzy methods can be found in Zimmermann and Zysno (1980), An et al. (1991), Moon (1993), Bonham-Carter (1994), and Wright and Bonham-Carter (1996).

Given a set of map inputs, $U = \{x_1, x_2, \ldots, x_n\}$, the algebraic product is defined as

$$\text{Ucombination}\ (x_1, x_2, \ldots, x_n) = (x_1)\,(x_2) \ldots (x_n) \qquad (4)$$

The output is less than or equal to the smallest contributing membership value and therefore represents the minimum potential (Figure 5.4). The algebraic sum,

$$\text{Ucombination}\ (x_1, x_2, \ldots, x_n) = 1 - \{(1 - (x_1))\,(1 - (x_2)) \ldots (1 - (x_n))\} \qquad (5)$$

results in a maximum potential that is equal to or greater than the largest contributing factor (Figure 5.4):

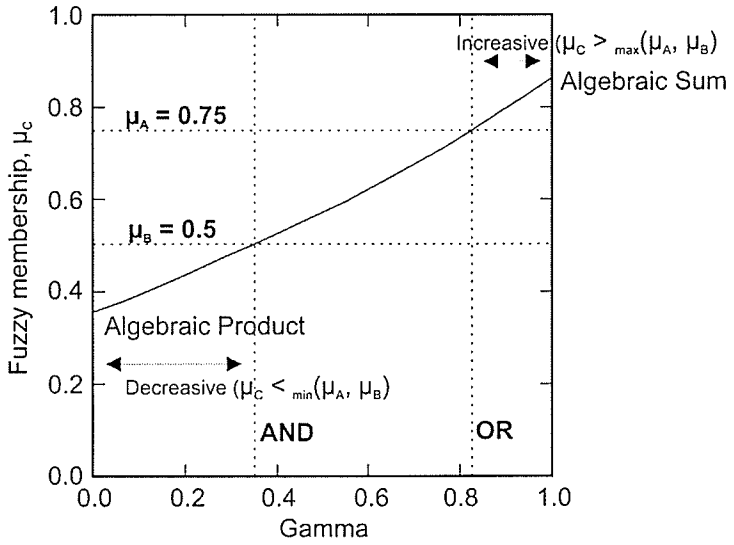

Figure 5.4 Fuzzy membership, μ_c, obtained by combining two fuzzy memberships, $\mu_A$and μ_B versus . This shows the effect of variations in γ for the case of combining two values, $\mu_A = 0.75$ and $\mu_B = 0.5$. When $\gamma = 0$, the combination equals the fuzzy algebraic product; when $\gamma = 1$, the combination equals the fuzzy algebraic sum (after Bonham-Carter, 1994).

The last method is the gamma operation, in which a parameter gamma is used to ensure a flexible compromise between the maximum potential of the algebraic sum and the minimum potential of the algebraic product (Figure 5.4). The value of gamma can range between 0 and 1, where 0 would result in the output being equal to the algebraic

product, and 1 would result in the output being equal to the algebraic sum. With a gamma value of 0.75 used in this combination example, the gamma operation can be defined as:

$$\text{Ucombination } (x_1, x_2, \ldots, x_n) =$$

$$(\text{(fuzzy algebraic sum)}^{0.75}) \; (\text{(fuzzy algebraic product)}^{1 - 0.75}) \qquad (6)$$

Six output maps are shown in Figure 5.2 and represent the fuzzy algebraic sum, product, and gamma operation for the two sets of weights given in Table 5.1. All six output maps show the high probability area defined by the binary output map, however, they also show an extension of the high probability feature to the southeast. The output maps generated for the two sets of weights (FUZZY1 and FUZZY2) are similar, however differences are visible. The results for this example are the combination of only three input maps. In the subsequent spatial models presented in chapter six up to 200 input maps were combined. The differences in mineralization potential maps using relative weights from 200 inputs should be far greater than observed in this simple example. The approach of relative weighting of input maps will be adopted for this study. The three fuzzy logic combination methods are able to express varying degrees of belief in each of the data sets. The gamma operation can act as compensation, or ones total confidence, in all the input data sets combined (An., 1991). A gamma value of 0.9 will be used during the combination stage of the shear-hosted gold and VMS spatial models developed in the next chapter. This gamma value was chosen based on earlier combination phases and gamma values used in other mineralization potential mapping projects (e.g. An et al. (1991), Moon (1993), Bonham-Carter (1994)). The Fuzzy logic method does not consider the uncertainty in each of the individual data sets, or the given attributes. For

the gamma operation missing or full non-membership is carried through the calculations and results in a value of 0 for that particular pixel or location. Uncertainty in data sets and missing data are considered in the next combination method, Dempster-Shafer Belief theory.

5.4 Dempster-Shafer Combination

The Dempster-Shafer method also utilizes a continuous scale from 0 to 1, however, it allows each map of evidence to include two independent "belief functions". An upper belief function, plausibility, is considered an optimistic assessment that the evidence supports a proposition, whereas the lower belief function, belief, is a conservative estimate. Uncertainty in this project can be defined as the degree of confidence in an evidence map and the processes involved in translation. The resulting probability maps represent a confidence band (figure 5.5). The method is useful in areas that are not well explored and is capable of dealing with missing or zero value data. The potential disadvantage of the method is the difficulty in conceptualizing belief, disbelief, and uncertainty. A detailed discussion on the formulation of the Dempster-Shafer method can be found in Dempster (1968) and Shafer (1976).

The basis behind the Dempster-Shafer method is

$$\text{Belief} + \text{Disbelief} + \text{Uncertainty} = 1 \qquad (7)$$

Belief in the Fuzzy logic and Dempster-Shafer methods represents the positive degree of evidence for the existence of a deposit. In the Fuzzy logic case Disbelief = 1 - Belief. The Dempster-Shafer method introduces the concept of uncertainty during combination.

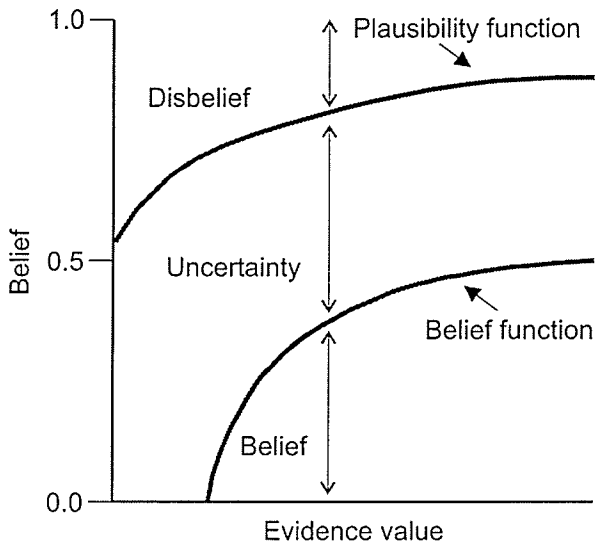

Figure 5.5 Idealized diagram of belief functions. Note that when plausibility and belief are equal, uncertainty is zero and belief plus disbelief equals 1 (after Wright and Bonham-Carter, 1996).

Theoretical principles are used to define the conceptual models in this project. However, the conceptual models derived from these principles are not perfect, hence the need for some explicit expression of uncertainty. As noted in section 4.5 geological maps represent real observations from a few small outcrops, which are used to interpret an area as a whole (Chung and Fabbri, 1993). This interpretation results in uncertainty in the data. The geologist or geochemical labs that process the data, for example, are prone to some degree of error. Geophysical and remote sensing data rely on instrumentation that is limited by our technology and our theoretical understanding of the processes involved. These degrees of uncertainty must be carried through any spatial combination, just as errors are carried through a numerical set of calculations.

The application of Dempster-Shafer belief theory with respect to geological exploration, has been discussed by An et al. (1994a,b), Moon (1990), Moon (1993),

Chung and Fabbri (1993), and Wright and Bonham-Carter (1996). The concept of Dempster's orthogonal sum is reviewed in Richards (1993). In the Fuzzy Logic combination method described earlier, the three data sets were assigned weights for the attributes in each input map. The same relative weights, or belief in the existence of a deposit, can be assigned to the input maps with the Dempster-Shafer approach. However, a level of uncertainty is also assigned. Belief function values for the Dempster-Shafer method are calculated relative to the assigned Fuzzy logic value. The calculation is necessary to allow for both disbelief and uncertainty functions in the Dempster-Shafer method. For this example weights assigned to the Dempster-Shafer Belief function are 1/2 those of the fuzzy belief values. For the shear-hosted and VMS models the Belief value is calculated as (FuzzyWeight * FuzzyMaximum).

For this example the geology map is assigned an uncertainty of 0.2, with the basalt attribute assigned a belief value of 0.45. Disbelief is calculated from the assigned belief and uncertainty and is equal to 0.35. Plausibility, the optimistic assessment that the evidence supports a proposition, can be calculated as,

$$\text{Plausibility} = 1 - \text{Disbelief} \tag{8}$$

Therefore a pixel that has a basalt attribute has an upper, 0.55, and a lower, 0.45, potential of a deposit occurring. If there is no uncertainty in the input map then,

$$\text{Belief} + \text{Disbelief} = 1 \tag{9}$$

Which is the same as the case for the Fuzzy logic method. More importantly if there is no data for an input map for a particular area then belief and disbelief are equal to 0, and therefore, uncertainty is equal to 1.

Combination, using Dempster' rule of combination, is accomplished pixel-by-pixel, as with the binary and Fuzzy logic methods. With this method we wish to obtain a combined belief, disbelief and uncertainty from two input maps, where,

$$Bel_{combination} + Dis_{combination} + Unc_{combination} = 1 \quad (7)$$

Dempster's rule of combination can be expressed as:

$$Bel_{combination} = (Bel_A\ Bel_B + Bel_A\ Unc_B + Bel_B\ Unc_A) / (1 - Bel_A\ Dis_B - Bel_B\ Dis_A) \quad (8)$$

$$Dis_{combination} = (Dis_A\ Dis_B + Dis_A\ Unc_B + Dis_B\ Unc_A) / (1 - Bel_A\ Dis_B - Bel_B\ Dis_A) \quad (9)$$

$$Unc_{combination} = (Unc_A\ Unc_B) / (1 - Bel_A\ Dis_B - Bel_B\ Dis_A) \quad (10)$$

The rule of combination is applied recursively in a pairwise fashion allowing for all input maps to be combined two by two. The combined belief, disbelief, and uncertainty can be used to calculate plausibility, where,

$$Pls_{combination} = 1 - Dis_{combination} \quad (11)$$

The above calculations can be derived using an orthogonal sum. This can be accomplished by constructing a unit square, with horizontal and vertical partitions representing given classes of the two input maps (Richards, 1993) (Figure 5.6). Rectangle A represents the orthogonal sum from pixel coordinates (x_{14} , y_{15}), whereas rectangle B is for pixel coordinates (x_2 , y_7). Belief and disbelief are the given classes. Each rectangle in the unit square represents combined evidence from the given classes. Combined belief is the sum of all rectangles that represent the class belief, including the rectangles containing uncertainty combined with the class belief. The same is applied to combining disbelief. The bottom right rectangle is attributed to uncertainty from both

sources after all evidence has been combined. Rectangles that include belief and disbelief classes are considered contradictory and not used for combination. In order to satisfy equation (7) a normalizing factor is calculated, which is the sum of all non-contradictory rectangles. If uncertainty = 1 (Figure 5.6) for input map B, such as in the case of missing data, equations 8 to 11 become:

$$Bel_{combination} = Bel_B\ Unc_A \tag{12}$$

$$Dis_{combination} = Dis_B\ Unc_A \tag{13}$$

$$Unc_{combination} = Unc_A\ Unc_B \tag{14}$$

$$Plsc_{ombination} = 1 - Dis_{combination} \tag{15}$$

Figure 5.2 show the belief, disbelief, uncertainty, and plausibility output maps for this given example. The Dempster-Shafer Belief theory method enables an expert to apply a degree of uncertainty during map combination. This degree of uncertainty is a quantitative assessment of the total combined uncertainty from all input maps. Belief and plausibility are also quantitative assessments of the upper and lower potential of a deposit occurring. Overall the gamma operation output, and the belief and plausibility outputs show similar characteristic features. The major difference is the handling of missing data. The Dempster-Shafer method can effectively deal with the missing data. Both the Belief and Plausibility output maps show a high potential zone at about left-centre. This zone is not visible in the gamma output maps. The Fuzzy logic and Dempster-Shafer method produce output maps that contain significantly more information that the binary output maps. Overall the Fuzzy logic method was easier to implement that the Dempster-Shafer method. Both methods have been adopted for the shear-hosted and VMS spatial models. The resulting output maps will be compared to assess their ability to highlight

high potential zones within the southern part of the Lynn Lake Greenstone Belt. From the comparison an evaluation of the two methods can be made with respect to applying the methodology used here to other areas.

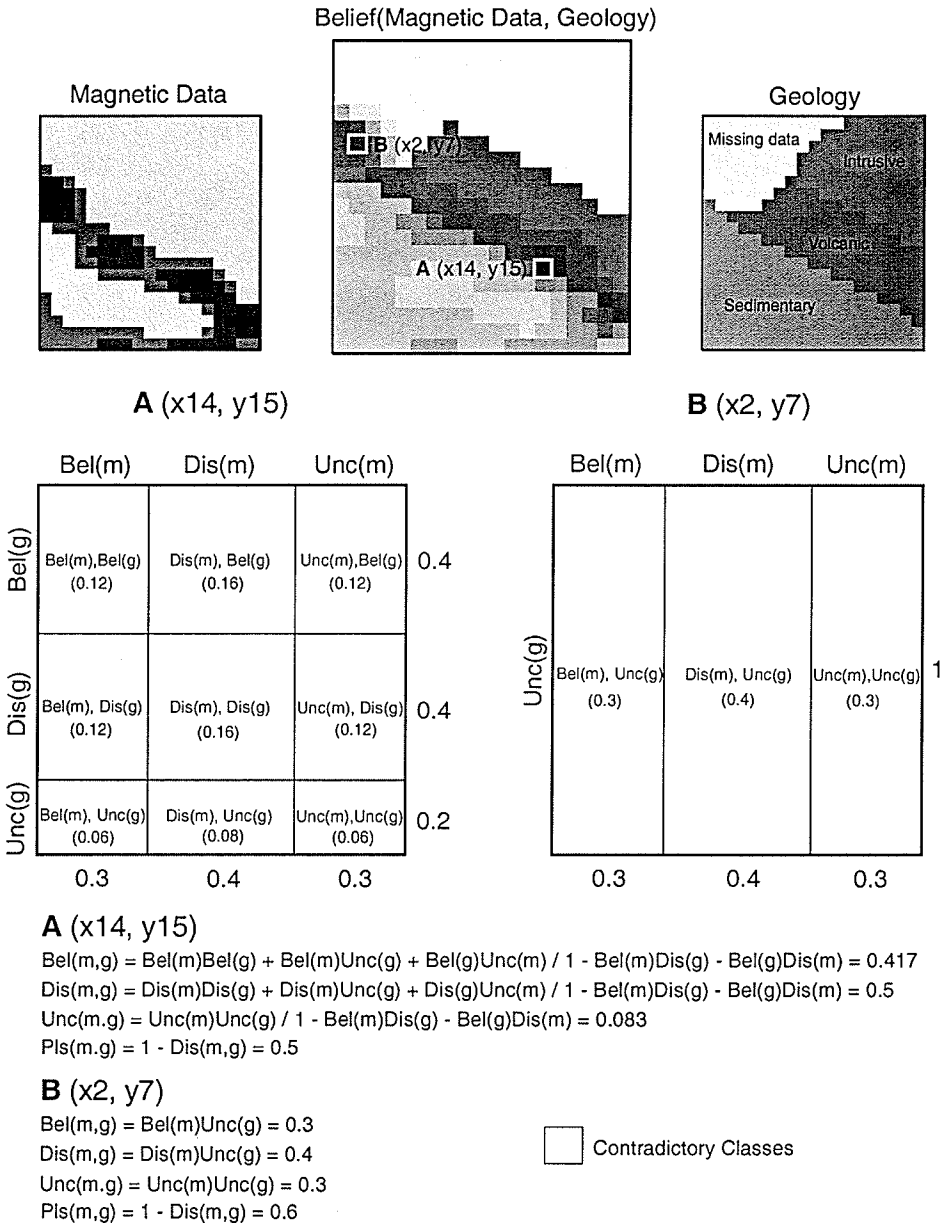

Figure 5.6 Dempster-Shafer combination of magnetic and geological input data sets using an orthogonal sum. Calculations for two pixels, (x14, y15) and (x2, y7), are shown as examples of the method. Note that for pixel (x2, y7) the geological input data set is missing data, therefore, uncertainty = 1. m: magnetic input map; g: geology input map.

6 SPATIAL MODELS

6.1 Introduction

The translation of components of the conceptual model into a spatial model is the next stage in producing mineralization potential maps. The translation stage of this project seeks to replicate the manual processes in which an expert follows during their interaction with multiple data sets to locate potential areas for exploration. These manual processes are replicated in two main steps: 1) determining which of the base data sets are relevant to a particular component of the conceptual model; and 2) determine how to present those relevant data sets in a spatial manner.

Base data maps are original data sets that have not undergone any modification. The relevance of each, with respect to the components of the conceptual model, may be determined to be either direct or indirect. Directly relevant data, for instance magnetic anomalies, can be incorporated into the spatial model without modification. Indirectly relevant data, such as proximity to a fault, involves the analysis and modification of one or more of the existing base data maps into a derivative data-map or maps before incorporation into the spatial model. This modification falls into the second stage of translation in which sub-components, or theoretical information, are presented spatially. Genetic links between various components of the conceptual model must also be considered in the second stage of translation. Combination of all the input maps could be completed in a single step. However, sub-spatial deposit models representing individual components of the conceptual model can be combined to produces a series of mineralization sub-potential maps. These sub-potential maps can then be combined in different ways to produce a set of mineralization potential maps. This allows for multiple

scenarios to be tested. The other advantage of translating components of the conceptual model separately is the ability to modify, or extract entirely, a single component without having to modify the model as a whole.

Structure, fluid-heat source, source rock, and alteration are the four major components of the shear-hosted conceptual model discussed in chapter 3. The major components of the VMS model include: 1) ore-fluid source and alteration; 2) a heat source to drive the hydrothermal system; and, 3) stratigraphy. For each component considerations were made with respect to the translation stage. These considerations took into account the scope of the project, such as the data sets available and the scale of the project area. Translation of the major components of the conceptual model will focus on these considerations. However, as noted in chapter 3, some of the considerations are omitted from translation, owing to the lack of an available data set, or the inability to accurately represent the component. If a specific consideration cannot be represent accurately it should not be included in the spatial model. Base data layers used for the shear-hosted model include the geological map, geochemical subdivisions for volcanic rocks, major faults including the JSZ, VG and VLF geophysical survey data, and one SAR scene. Translation of the VMS conceptual model into a spatial model makes use of the geological map, geochemical subdivisions for volcanic rocks, TF magnetic survey data, and VLF-EM survey data.

Input maps generated during the translation stage must be weighted before combination. This weight is the degree in which the expert considers the input map to be evidence of a deposit occurring. Weights are determined subjectively from the conceptual model. These values have no real quantitative meaning, however, they do

represent relative differences. Weights are assigned to individual pixels, or groups of pixels, of an input map; and to the input map as a whole. For an individual input map weights are applied either directly to each pixel having a specific value, or are set by maximum and minimum values that make use of a specific function, such and logarithmic or exponential functions. The maximum value is the weight assigned to the input map as a whole. Weights are between 0 - 1 and set for the fuzzy logic and Dempster-Shafer combination methods. Uncertainty for the Depster-Shafer method is determined at this point and is based on the degree of confidence in the input maps. The uncertainty value is determined by two factors: 1) the base data set, or sets; and 2) by the translation stage. The 1:50 000 geological map can be used as an example of the first factor in determining uncertainty. For the geological map the first issue is the knowledge of the geologist, or geologists, who mapped the area. It assumed here that the geological maps are accurate. Ten geologists were involved in the regional mapping project for the Lynn Lake Greenstone Belt. With multiple geologists mapping an area problems could arise with respect to the consistency of identifying lithological units. During compilation the maps were revised to correct for possible inconsistencies. Outcrop exposure is another issue to consider in determining uncertainty for the geological data set. For instance, extrapolation of contacts must be made in areas of poor, or little, exposure. The scale of the map is also important. Based on the regional scale of the project area and the factors above, uncertainty in the geological base data set should be low. Base data sets that have high uncertainty should be avoided.

Translation and processing of base data sets is the second factor in determining the uncertainty of input maps. How a component is translated form the conceptual model

into the spatial model is used to determine a level of uncertainty. This translation requires processing of a data set, or sets. Processing may be straight-forward involving only a single step. Processing may also be more complex and require multiple processing steps. If a component of the conceptual model is well represented in the spatial model, uncertainty may be considered low. Uncertainty is then the combined level of confidence in the data and processing steps used in translation.

6.2.1 Shear-Hosted Spatial Model: Structure Component Translation

In a shear-hosted model a shear zone, such as the JSZ, will be given high weight and will become a region of high potential for locating shear-hosted gold deposits as discussed in chapter three. Considerations for the structural component include: 1) proximity to shear zones and faults; 2) the lateral extent of deformation associated with shear zones and faults; 3) brittle and ductile deformational characteristics; and 4) regional deformational history. Input data sets that can be used to indicate the presence of a deformational zone include known faults and shear zones, VG and VLF, and SAR data sets.

Known faults and shear zones are mapped indicators of deformation, however, VG, VLF, and SAR data sets may also be used to locate deformational zones. VLF measures conductivity, which may be caused by the presence of water saturated clays resulting from weathering or hydrothermal activity and associated mineralization (Palacky, 1987). Weathering intensity is commonly higher in fractured zones and a thicker conductive weathered layer can be detected by VLF surveys. These linear features can be determined from VLF crossover anomalies. The presence of conductive

clays can be a guide to finding hydrothermal related deposits, such a shear zones (Keating, 1999). Much of the structure and lithological relations within the Lynn Lake Greenstone Belt shows the rocks are steeply dipping. VLF may also be used to detect conductive structures that have steeply dipping boundaries, such as faults and shear zones. Lineaments defined by VLF data may be cryptic evidence of a mineralized fault, or clay-rich weathered zones directly above fracture zones.

Magnetic surveys can be used to directly locate ore deposits such as banded iron formations. Magnetic surveys are also useful for delineating basement features such as lineaments, faults, shear zones, and lithological contacts that may be indirectly related to an ore deposit. Magnetic anomalies may also reflect alteration of magnetic minerals related to fluid migration through a shear zone. Delineation of these features requires lateral contrasts in magnetic properties. Sharper resolution of lineaments, faults, shear zones, and lithological contacts is possible using vertical gradient surveys, or vertical derivatives derived from total field magnetic data (Lowe, 1999). Linear features defined in a VG survey may, therefore, potentially be evidence of faults, shear zones, and/or lithological contacts. The term lineament is used to refer to the geological trend of lithological and brittle and ductile structural features. In this project the term will be applied to linear features observed in the VG, VLF, and SAR data sets.

SAR imagery has been shown to be a useful tool in providing geological, lithological and structural information in areas where there is dense forest cover (Sharma et al., 1999). SAR lineaments may indicate, faults, shear zones, lithological contacts, dikes, hydrothermally altered rocks, and eskers. Topography is primarily controlled by bedrock geology and structural trends in a region. Low topographic areas commonly

reflect areas of preferential erosion controlled by lithology or where existing faults or shear zones are located. Cliffs, or steep relief, may reflect faults or contacts between contrasting lithologies. Well-defined linear features in SAR images may, therefore, be an additional indicator of the presence of faults or shear zones.

Linear structures defined in the VLF, VG, and SAR data sets all indicated to some degree the presence of faults or shear zones. Not all linear features are associated with deformational processes. Eskers for example, are a surficial feature that should be visible in the SAR data. However, they are not likely to have a strong magnetic response or be highly conductive. By combining the data sets, linear features that are not directly associated with deformation, such as eskers, can be removed. Lithological contacts are features that may produce a strong linear trend in each of the 3 inputs data sets, but do not necessarily indicate a deformational zone. Contacts, however, are commonly sites of contrasting rheological characteristics, which in turn are preferential locations for structural movement, or shear zones. They are also possible sites for preferential fluid movement. Magnetic data is commonly used with VLF to prioritize conductors that may be associated with ore bodies, specifically VMS deposits (Ascough, 1999).

It is noted here that VG, VLF, and SAR represent sub-surface, near-surface, and surface measurements respectively (see 4.5). Combining these input data sets with known structure produces the structural component of the spatial model. This is accomplished in two stages. In the first stage proximity maps relative to known faults and the JSZ are developed. In the second stage, extracted lineaments defined by VG, VLF, and SAR input data sets are used to produce a second set of proximity maps.

Combining these proximity maps results in a deformation, or "shear zone potential output map".

6.2.1.1 Known Faults and the Johnson Shear Zone

Information on mapped faults and on the extent of the JSZ has been compiled from Gilbert (1980), Zwanzig et al. (1999), Beamont-Smith and Rogge (1999), and Beaumont-Smith (2000). The extent of the JSZ has been defined largely through field observations and, in part, air photographs. In areas of good exposure the width of the shear zone is about 300 m. Deformation is visible outside the 300 m zone, but is less intense. Faults were also defined during regional field mapping, but the extent to which air photographs and geophysics were used in their definition is not known. The JSZ and the faults have in places been extrapolated across lakes or through areas of thick cover. For this reason there is a degree of uncertainty in the data set.

Faults and shear zones can be considered the results of brittle and ductile shear-strain on rocks (Ramsay, 1980). Faults and shear zones display both ductile and brittle characteristics depending on the scale at which the rocks were assessed or mapped, and the depth of exposure. Brittle deformational zones are generally narrow, whereas ductile zones tend to be more laterally extensive (Bursnall, 1989). George and Bonham-Carter (1989), Watson and Rencz (1989), Bonham-Carter (1994), Rogge et al. (2000), and Srivastav et al. (2000) made use of proximity to faults and lineaments in their GIS and data fusion approaches to mineral exploration. In this project a lateral extent of deformation associated with the known faults and the JSZ will be based on the 5:1 length

to width ratio defined in the conceptual model. The brittle and ductile characteristics of the known faults and the JZS will be addressed during weighting of proximity zones.

The faults and JSZ data sets are in vector format. In order to set the lateral extent of deformation using the 5:1 ratio, faults and the JSZ must be grouped into unit length ranges. Unit length ranges are in intervals of 1000 m, excluding the first unit length range, which is 500m. Vectors greater than 10000 m are grouped into a single unit length range. Proximity zones relative to each fault for each of the unit length ranges were created using ArcView 3.2. Each proximity zone is set to 100 m width, with a pixel resolution of 50 m. The resulting proximity maps were reclassified with a maximum lateral extent defined by the ratio for the given unit length range. A lateral extent of 2000 m is applied to all faults greater than 10000 m in length. Figure 6.1 shows the sequence of producing a proximity map for a given unit range length.

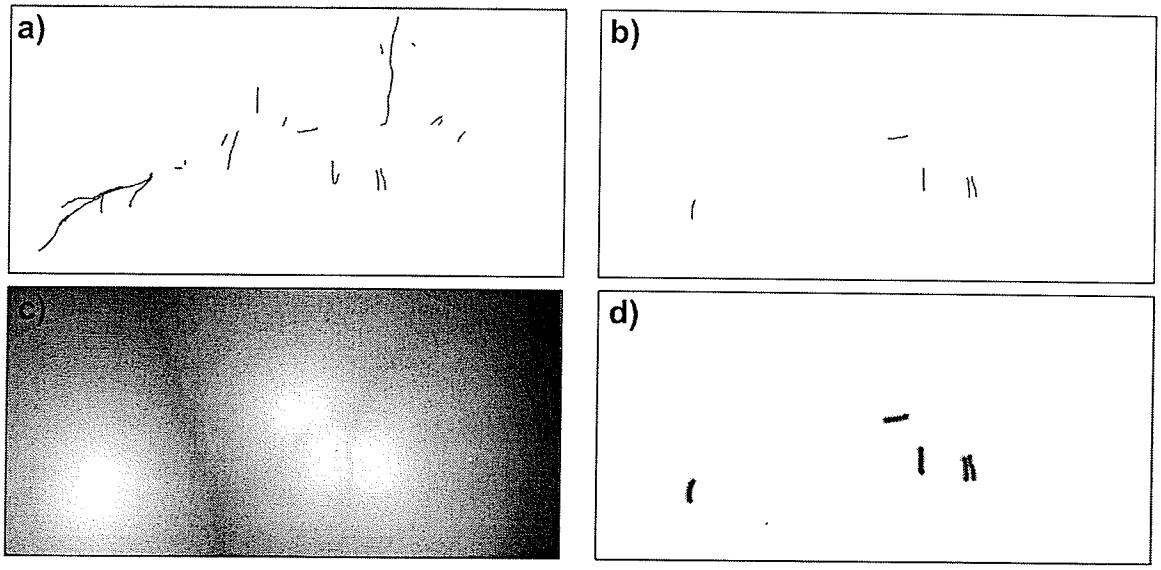

Figure 6.1 Sequence of steps to produce a fault proximity map for the 5000 - 6000 m unit length range: (a) known faults; (b) 5000 - 6000 m unit length range faults; (c) proximity zones from fault; (d) reclassified proximity zone with maximum extent set to 1000m.

Once proximity to faults has been set for each unit length range, weights are given to the individual proximity zones. Weighting of the proximity zones can be approached several different ways. For instance, statistical methods may use known deposits to determine which proximity zone has the highest potential for the object of interest (Bonham-Carter, 1994). Watson and Rencz (1989) and Rencz et al. (1994) weighted their linear structures based on orientation. Orientation has been considered in this project. However, a consistent method of implementing orientations based on the five major deformational events defined by Beaumont-Smith and Rogge (1999) is not within the scope of this project, and is therefore not considered further.

In this project linear, exponential, and logarithmic functions were used in various mineralization potential modeling phases. These functions are used to express the decrease in finite strain across a fault or shear zone. Ramsay and Graham (1970) developed methods for computing the finite strain across a shear zone. From their analysis a consistent variation in finite strain across a shear zone was determined (Figure 6.2). For faults the finite strain is minimal away from the fault plane. Faults and shear zones show elements of both ductile and brittle deformation depending on the scale at which they were mapped. The JSZ is dominated by ductile deformation, however, little information is available on the ductile and brittle characteristics of the major faults. For this reason the assumption is made that the faults have associated deformation. In this project two functions have been adopted to represent the finite strain across faults and shear zones, logarithmic and exponential functions. The logarithmic function can be considered to represent ductile, or shear zone characteristics, whereas the exponential

function represents more brittle deformation. The resulting output maps generated using exponential and logarithmic functions will be compared.

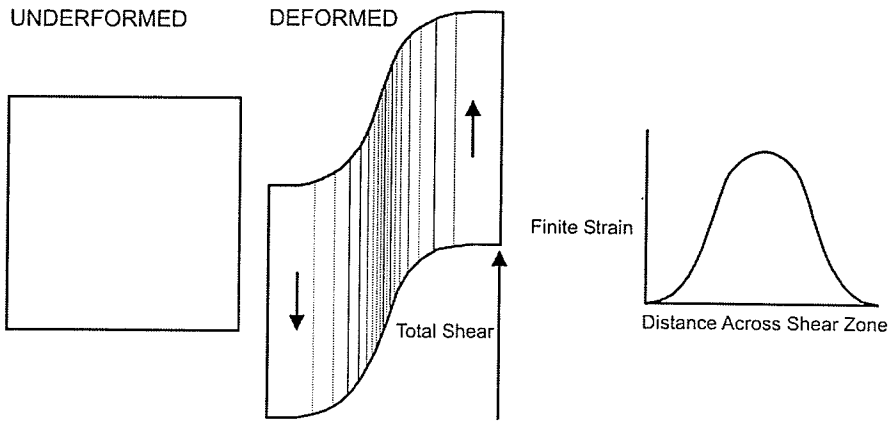

Figure 6.2 Variation of finite shear through a shear zone with heterogeneous shear strain (Ramsay and Graham, 1970).

Weighting of proximity zones is the highest near a fault, or shear zone. Progressively away from a fault, or shear zone, weighting decreases to a minimum of 0.01. The area outside of the maximum lateral extent of deformation is considered to have the lowest potential for deformation relative to the given unit length proximity map. These areas are not 100% evidence of deformation not occurring, and therefore, a minimum weight of 0.01 is set for all areas outside of the maximum lateral extent of deformation. The JSZ is a known shear zone with associated gold occurrences, and therefore, is considered good evidence of a deposit occurring. The faults, on the other hand, are not considered to be shear zones, but may have associated deformation. For this reason the maximum weight for the JSZ is 0.9, whereas the maximum weight for the faults is 0.8. Uncertainty for the JSZ and fault input maps are set to 0.1. Table 1 lists the maximum and minimum values for all major components of the shear-hosted spatial model.

TABLE 6.1: Shear-hosted Spatial Model Weighting

Component	Maximum Weight FL(1)	DS (B, D, U) (2)	Minimum Weight
Structure			
Faults	0.8	0.64, 0.26, 0.1	0.01
JSZ	0.9	0.81, 0.09, 0.1	0.01
VG	0.8	0.64, 0.16, 0.2	0.01
VLF (3)	0.85	0.73, 0.07, 0.2	0.01
SAR	0.7	0.49, 0.31, 0.2	0.01
Fluid/Heat			
Felsic Intrusions	0.6	0.36, 0.34, 0.3	0.01 (4)
Mafic Intrusions	0.4	0.16, 0.54, 0.3	0.01 (4)
Source Zone			
Lithology	0.6	0.36, 0.34, 0.3	0.01
Geochem			
MgO	0.6	0.36, 0.24, 0.4	0.01
Primitive vs Evolved	0.6	0.36, 0.24, 0.4	0.01

(1) Fuzzy Logic weight
(2) Dempster-Shafer weight (Belief, Disbelief, Uncertainty
(3) VLF includes line quadrature and ortho quadrature
(4) A weight of 0.1 is assigned to the area within an intrusive unit

6.2.1.2 Lineament Analysis

Unlike the known faults and JSZ, the lineament analysis of VLF, VG, and SAR input data sets, is a more indirect approach to finding potential areas of deformation. The input files have been pre-processed (see chapter 4) and are raster images in georeferenced tiff image format. In this analysis the first stage is the extraction of linear features in each of the input data sets.

Processing included an 11x11 median filter applied to the VLF data to smooth out the Fraser filtered (Fraser, 1969) preprocessed images. A 5x5 median filter was applied to the VG images. For the SAR image three processed images were used for lineament

extraction. They include the Frost 11x11 speckle reduction filter (see section 4.4); Frost 11x11 and median 11x11 filters; and, Frost 11x11, threshold adjustment, and average 11x11 filters.

Lineament extraction was completed using the lineament extraction algorithm included with PCI image processing software version 6.3.0. The algorithm extracts linear features from a radar image and saves the lines as polylines in a vector segment. Lineaments are distinguished by analyzing image intensity and gradients. Edge detection filters are applied to the image to produce a gradient image, which is subject to a threshold filter to create a binary edge. The resulting edges are extracted and saved as vectors. Various parameters that can be adjusted control the line extraction process (Table 6.2).

Numerous tests were applied to the VLF, VG, and SAR images to find the set of parameters that best fit those observed under visual inspection. This linear extraction algorithm was chosen over visual inspection because of its more rigorous quantitative approach to line selection. Of the three input SAR images tested, polylines extracted from the Frost 11x11 filtered image were used for subsequent analysis and combination. VLF data includes ortho and line quadrature data sets. Lineament extraction was applied to ortho and line quadrature data sets. The polylines from VLF, VG, and SAR were exported as ArcView Shape files and brought into ArcView 3.2. Figure 6.3 shows the combined extracted lineaments for VLF, VG, and SAR images.

The polylines were checked visually for correlation with artificial features. For example there are two major power lines that exist in the area, which were detected in the VLF data. These polylines were removed from the data set. Many of the SAR polylines

can be correlated with lake edges. In order to address this problem two factors were considered and used to visually remove polylines. First, if a polyline was > 50% represented by a lake edge it was removed from the data set. Second, if a polyline crossed part of a lake, > 50% of the polyline must occur on land on one or both sides of the lake. Any lineaments associated with other artificial features, such as roads, or artifacts of the image resulting from processing, were also removed.

TABLE 6.2: Lineament Extraction Parameters

Parameter	Description (1)
Radius of filter in pixels (RADI)	Specifies the radius of the edge detection filter (in pixels). It roughly determines the smallest-detail level in the input image to be detected. A large RADI value means less detail can be detected and also less noise.
Threshold for edge gradient (GTHR)	Specifies the threshold for the minimum gradient level for an edge pixel. It should be in the range of 0 to 255.
Threshold for curve length (LTHR)	Specifies the minimum length of curve (in pixels) to be considered as lineament or for further consideration (e.g. linking with other curves)
Threshold for line fitting error (FTHR)	Specifies the maximum error (in pixels) allowed in fitting a polyline to a pixel curve. Lower FTHR values give better fitting, but also shorter segments of polyline.
Threshold for angular difference (ATHR)	Specifies the maximum angle (in degrees) between segments of a polyline. Otherwise, it is segmented into two or more vectors. It is also the maximum angle between two vectors for them to be linked.
Threshold for linking distance (DTHR)	Specifies the minimum distance (in pixels) between the end pints of two vectors for them to be linked.

Descriptions from PCI Image processing software version 6.3.0

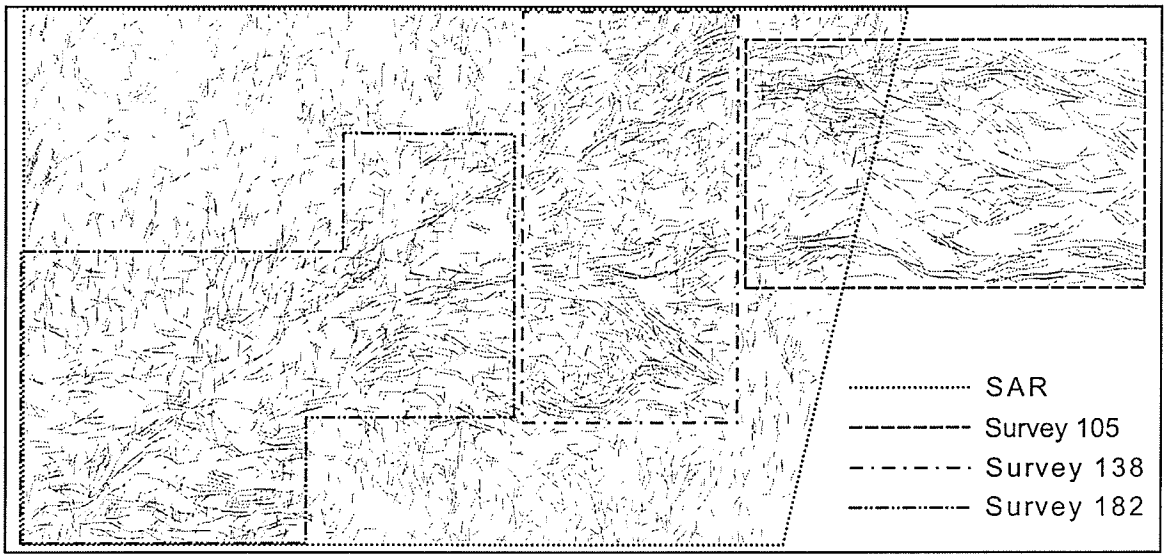

Figure 6.3 Extracted lineaments from VG, VLF, and SAR data sets using the PCI lineament extraction algorithm. Areas represent the extent of the three geophysical surveys (see Table 4.3)and the SAR image.

The polylines derived from the lineament extraction process on the VLF, VG, and SAR data sets are not necessarily shear zones, however, for this analysis they are assumed to represent fault structures with associated deformational zones. The resulting deformation potential maps can be tested during ground truthing. If the output maps are accurate in predicting the location of high deformational zones, this approach becomes a useful tool to map detailed structure in a given area. The process of producing proximity maps with a maximum lateral extent of deformation can be applied to the extracted lineaments from the VG, VLF, and SAR data sets. Proximity zones with a length to width ratio of 5:1 were developed for a series of unit length ranges with a minimum of 500 m up to a maximum of 10 000 m. The range of each unit length range is 1000 m except for the 500 - 1000 m unit length range. Lineaments greater than 10 000 m were set to a lateral extent of 2000 m.

Logarithmic and exponential function functions were used for weighting the proximity zones with maximum values nearest to the lineaments. Maximum weights of 0.85, 0.8, and 0.7 were used for VLF, VG, and SAR respectively. Lower weight is given to the SAR lineaments owing to the fact that the project area includes numerous glacial deposits, such as eskers. Extracted lineaments from the SAR data may also include these glacial features, which are not of interest in determining potential deformational zones. Major linear features extracted from the VG magnetic data may be caused by features at significant depth. These deeper features are still good evidence of high deformational zones, however, the data sets used in this project and the resulting output potential maps are 2-dimensional. Therefore, VLF is weighted slightly higher than the VG proximity maps because of its shallow penetration depth. Minimum weights for maximum extent and areas outside the proximity zones were given a value of 0.01. Uncertainty values for the Dempster-Shafer method are 0.2 for VLF and VG, and 0.35 for SAR. The SAR input maps are assigned a higher uncertainty than the VG and VLF primarily based on the fact the SAR lineaments were extracted from only one SAR scene. For SAR lineament extraction it is best if two scenes are used with near perpendicular look angles. Two scenes were acquired for this project, however, the look angles were only 20 degrees apart. The second image was also sub-parallel with the main structural feature of interest, the JSZ, and was therefore excluded. Future lineament analysis using this approach should make use of perpendicular look angles.

6.2.1.3 Deformation Potential Combination

Figure 6.4 is a flowchart that shows the stages of processing, analysis, and combination for the known faults, JSZ, and lineament analysis. The resulting output maps are reclassified to 64 levels. The number of levels was dependent on the capabilities of the software used. Reclassification at various sub-stages for structure, fluid-heat, and source zone are necessary owing to the limited number of decimal places available in ArcView Spatial Analysis. Subsequent calculations using both combination methods result in progressively smaller numbers. For the entire shear-hosted deposit model over 70 input layers were created, therefore, a single combination stage was not implemented. Sub-stages have also been used here because they allow for numerous scenarios to be developed and enable one to analyze the spatial relations between known occurrences and each of the major components of the shear-hosted model.

The algebraic sum, product and gamma operation of the fuzzy logic method were tested during the combination stage. Using the high number of input maps for the structural component, the algebraic sum resulted in most pixel values quickly approaching 1.0. The algebraic product, on the other hand, resulted in most pixel values having low potential. The gamma operation allows for a compromise between the "increasive" and "decreasive" effects (see section 5.3) of the algebraic sum and product. An et al. (1991) used a gamma value of 0.975 in their application of fuzzy logic combination of geological, geophysical, and remote sensing data of the Farley Lake area, Lynn Lake Greenstone Belt. Two gamma values were tested in this project, 0.75 and 0.9, and it was found that 0.9 kept the output values within a reasonable range. However, because of the distribution of high and low potential values for the VLF, VG, and SAR

output maps, a log transform was applied to the output maps before reclassification to 64 levels. The transform was applied to stretch the high potential values and condense the lower values. VLF, VG, and SAR input maps are primarily low potential except near lineaments. Combination of multiple inputs resulted in a small range of high potential values, and, because high potential areas are or interest the log transform was applied to the VLF, VG, and SAR output maps.

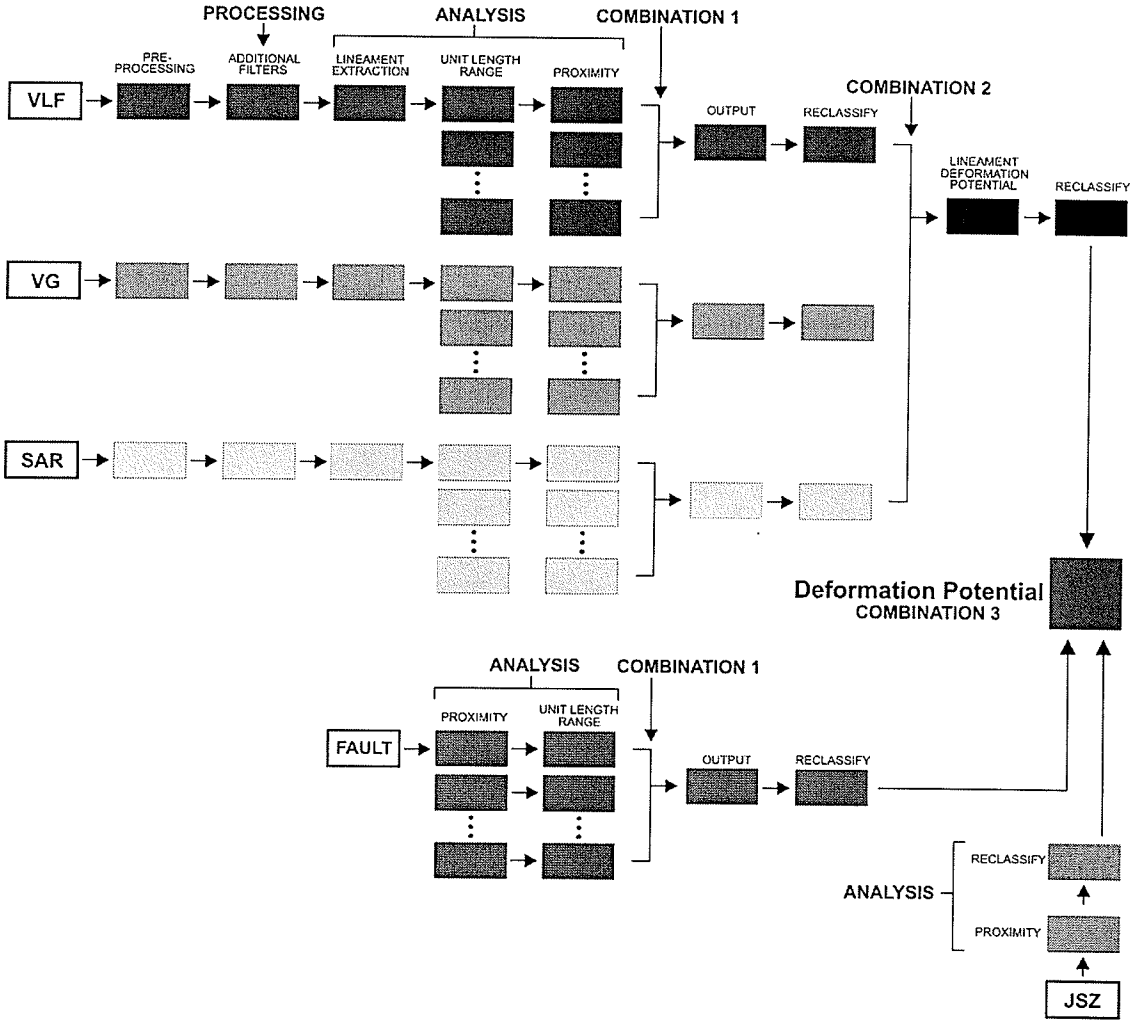

Figure 6.4 Flowchart of processing, analysis, and combination stages of deformation potential combination. VLF input includes line quadrature and ortho quadrature data sets.

Dempster-Shafer output maps for fault and JSZ input data sets are shown in figure 6.5. All outputs are shown with respect to the logarithmic deformation function. Dempster-Shafer outputs are shown with respect to belief. In the case that fuzzy and Dempster-Shafer combination methods produce virtually identical results, Dempster-Shafer output maps will only be shown. Fuzzy logic combinations for each component of the shear-hosted spatial model will make use of the gamma operation. A gamma value of 0.9 will be used. Appendix A is a list of all the output maps generated during combination, which can be viewed on the CD in Appendix A.

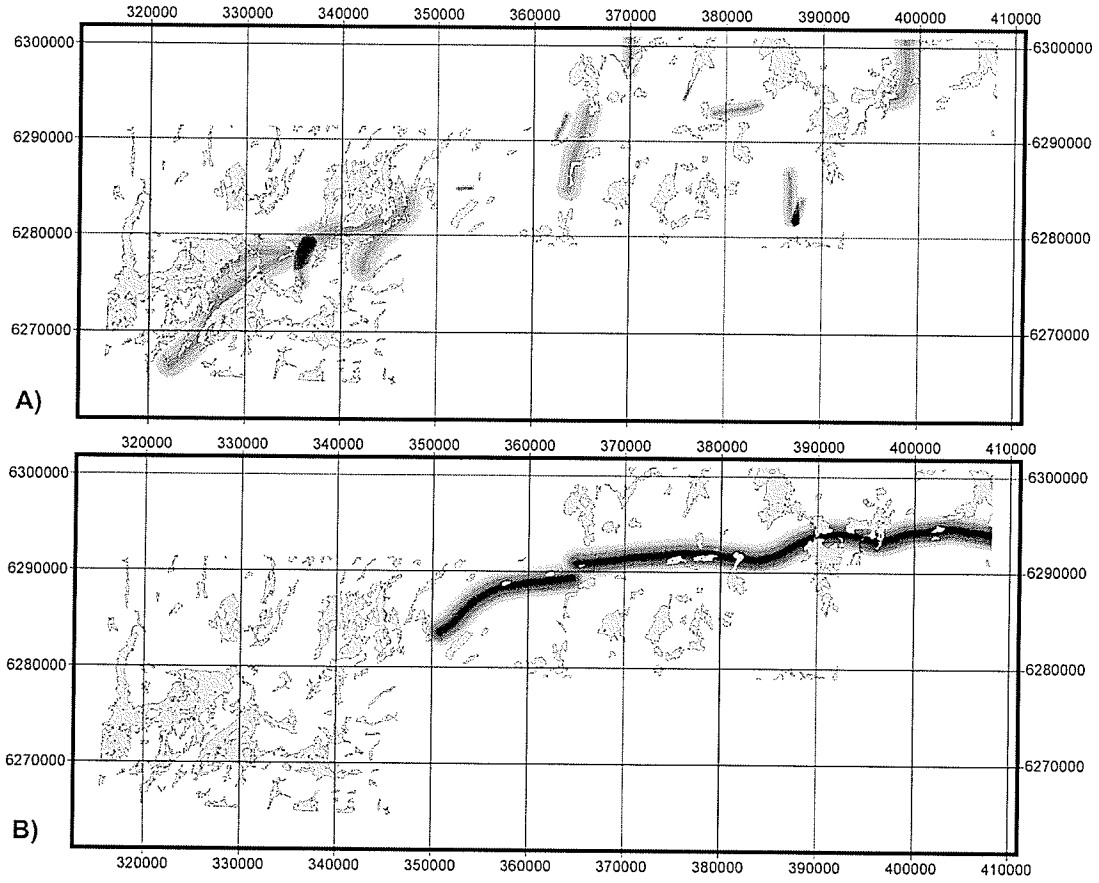

Figure 6.5 Output maps for fault and JSZ input data sets. Dempster-Shafer belief output for fault (a) and JSZ (b) data sets are shown. White indicates low relative potential; black indicates high relative probability (linear scale). Project area map projection is UTM Zone 14, NAD83.

VLF ortho and line quadrature proximity maps were joined in a single step. Dempster-Shafer and fuzzy logic output maps for VLF, VG, and SAR are shown in figure 6.6. VLF, VG, and SAR output maps were reclassified to 64 levels and combined into a single lineament deformation potential (Figure 6.7). The lineament deformation potential is subsequently combined with the combined fault and JSZ potential output maps.

6.2.2 Shear-Hosted Spatial Model: Heat Component Translation

Considerations with respect to the fluid-heat component of the conceptual model include 1) metamorphic grade across the project area, 2) composition of fluids trapped within the rocks, 3) proximity to intrusive bodies, which act as an additional heat and fluid source; and 4) history of plutonism within the belt. Integrating metamorphic grade and the composition of trapped fluids into the shear-hosted deposit model have been omitted (see section 3.1.2). Intrusive bodies acting as an additional heat source to drive the hydrothermal system and timing of intrusive events are included, and will comprise the heat potential component of the spatial model. Considerations with respect to the intrusive bodies as an additional heat source include 1) heat loss into the adjacent rocks, and 2) the lateral extent of heating adjacent rocks.

There are multiple generations of intrusive bodies within the Lynn Lake Greenstone Belt and not all are necessarily associated with mineralization. For this reason five different scenarios have been constructed to correspond to different stages in the tectonic evolution of the belt. The five scenarios are based on the tectonic history put forth by Gilbert et al. (1980) and the deformational stages defined by Beamont-Smith and

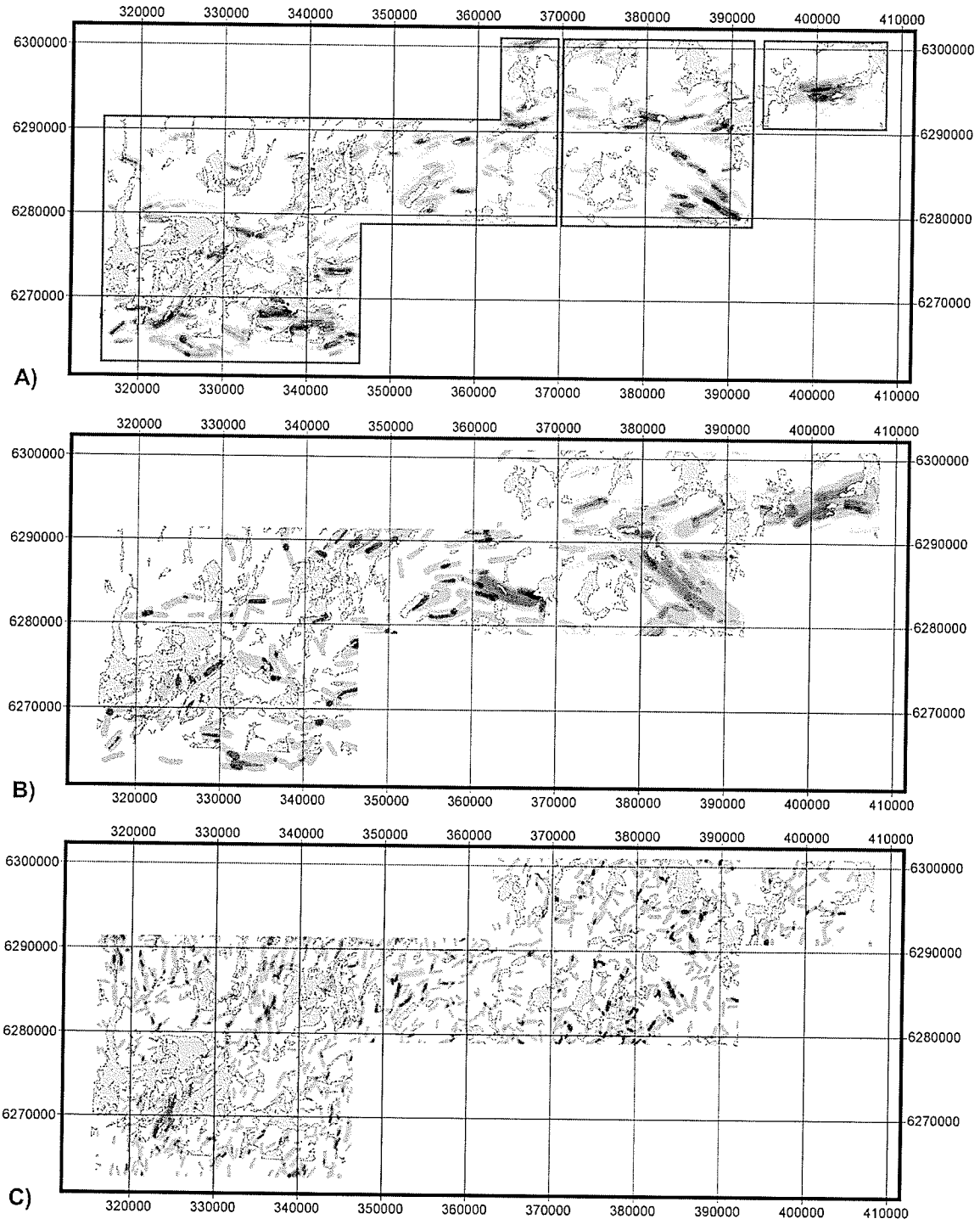

Figure 6.6 Output maps for VLF, VG, and SAR input data sets. Dempster-Shafer belief output for VLF (a), VG (b), and SAR (c). Fuzzy logic output for VLF (d), VG (e), and SAR (f). White indicates low relative potential; black indicates high relative protential (linear scale) for parts of the three geophysical surveys used (outline in (a)).

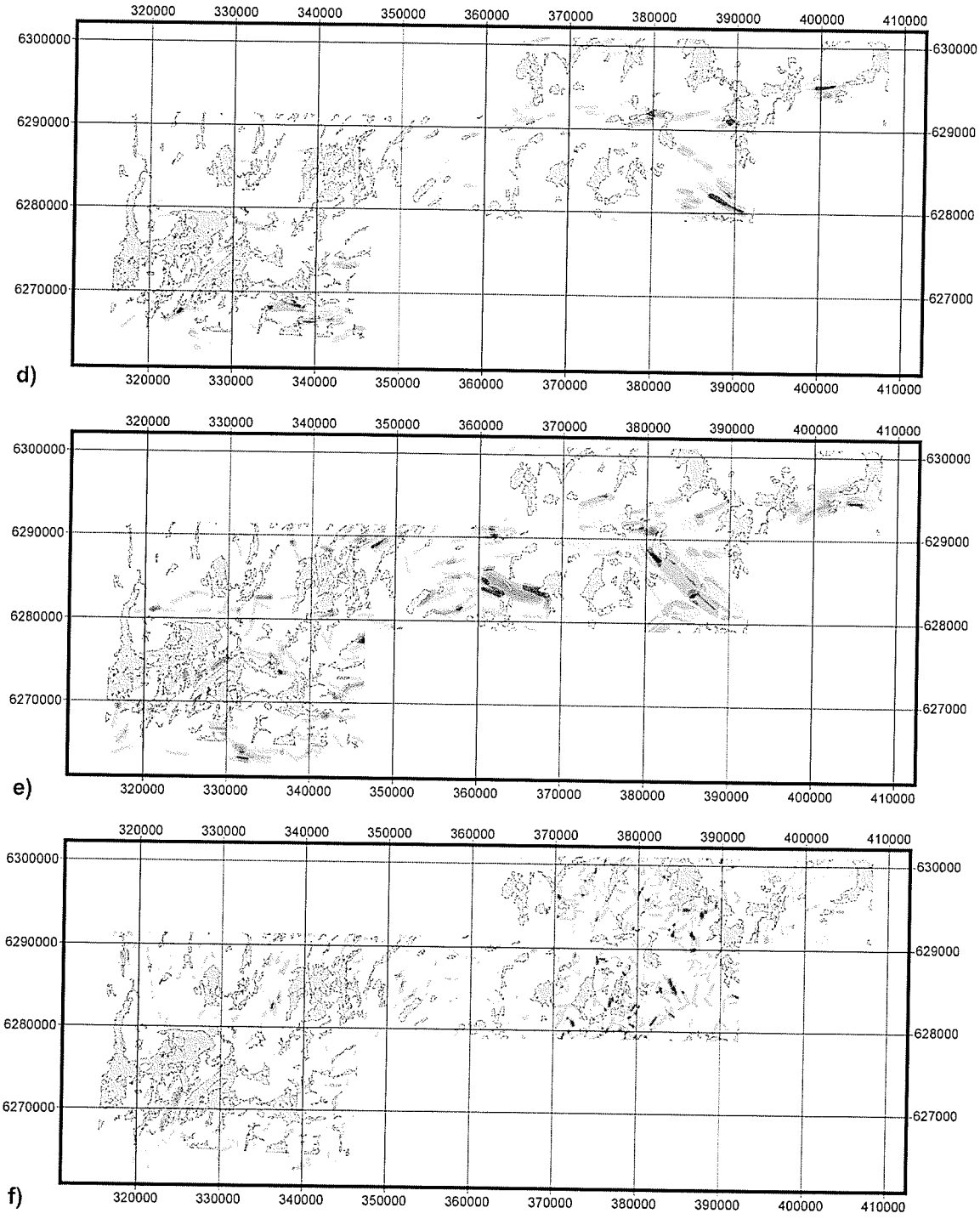

Figure 6.6 cont'

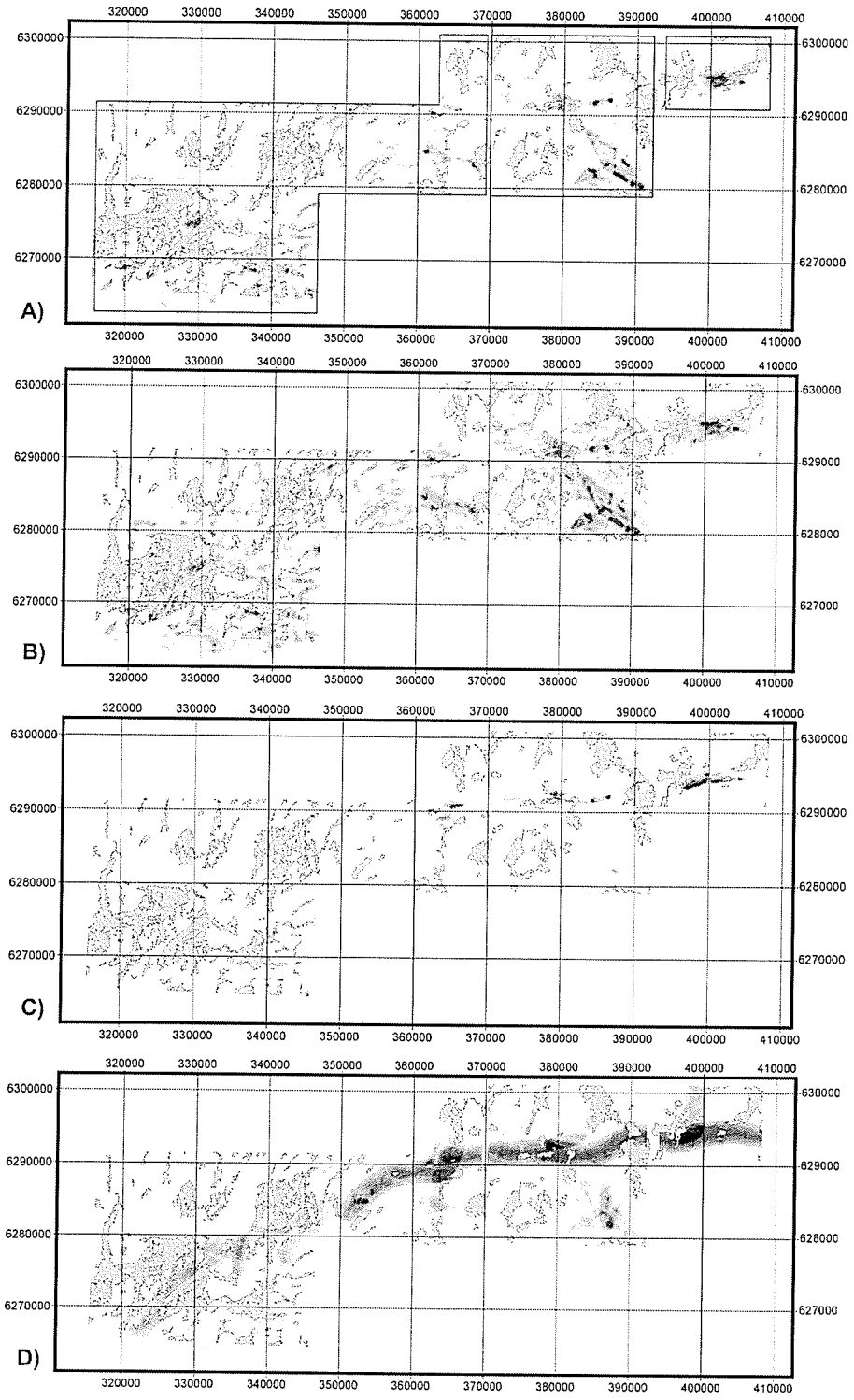

Figure 6.7 Dempster-Shafer belief (a) and fuzzy logic (b) output maps for combined VLF, VG, and SAR inputs. Dempster-Shafer belief (c) and fuzzy logic (d) output maps for combined VLF, VG, and SAR output with fault and JSZ. White indicates low relative potential; black indicates high relative potential (linear scale) for parts of the three geophysical surveys used (outline in (a)).

Rogge (1999) (Table 6.3). These scenarios will also be applied to source rock component of the spatial model. The base data set to be used for the heat component is the 1:50 000 geological map.

TABLE 6.3: Scenarios for Shear-Hosted Spatial Model

Event	Deformation (1)	Scenario	MFH Units (2)	SR Units (3)
Volcanism and associated sedimentation; syn intrusions				
Folding and faulting (east-northeasterly); JSZ initializes	D1	4	14,15	1 – 11
Intrusions of large plutons (tonalite, granite) between northern and southern belts				
JSZ; mineralization (?)	D2	3	14 –18	1 – 11
Sickle deposition				
JSZ; remobilization (?); peak metamorphism; North-east trending crenulation fabrics and folds	D3	1&2	14 – 18	1 - 13
Cataclasis, open cross folding; Post-Sickle granodiorite, tonalite and gabbro	D4/D5	5	All (4)	All (4)

(1) Beaumont-Smith and Rogge, 1999
(2) MFH: Magmatic fluid-heat input from 1:50 000 geological map
(3) SR: Source rock input from 1:50 000 geological map (see Table 6.4)
(4) Cumulative effects of all units

Proximity to intrusive bodies will be used to represent the heat component in the spatial model. Heat from an intrusive body increases the temperature of the adjacent rocks, which can be transferred by conduction or advection. Within the intrusive body heat loss may also be cause by convection. The amount of heat dissipation into the

country rock during an intrusive event is not constant over time. There are numerous factors that control heat loss over time and how far laterally from the body country rocks will be heated. For instance determining heat loss and the maximum extent for an intrusive body could be calculated by considering the 3-dimensional shape of the body, the initial temperatures of the body and host rock, the composition of the body, convective heat loss within the body, the thermal diffusivity of the host rocks, and so forth. Integration of this information could be applied to each of the intrusive bodies to determine heat loss and lateral extent of heating. The complexity of this task is beyond the scope of this project. For this project a more simplified model will be used to show the decay of heat into the adjacent country rocks. This decay function will be modeled using an exponential curve, which represents the temperature distribution near an intrusive body some time after intrusion (Philpotts, 1990) (Figure 6.8). This assumes that heat loss is constant within the intrusive body and the adjacent rocks, with rocks proximal to the body most affected.

The maximum extent of the effects of heat from an intrusive body on the adjacent rocks will also be defined using a simple model. Wright and Bonham-Carter (1996) made use of proximity zones in their VMS favourability mapping project. A maximum extent of 4 km was set for all subvolcanic sills and synvolcamic dykes. In this project the maximum extent will vary depending on the 2-dimensional surface area exposure of the intrusive body. Determining the 3-dimensional shape of an intrusive body is not possible based on the information available. So for this project an assumption is made that the bodies are circular to sub-circular, with the maximum extent calculated as 1 x radius, where $r = (\text{surface area} / \pi)^{1/2}$. The reasoning for using a variable maximum extent

instead of a set distance is based on the simple fact that larger bodies should have a greater effect on the surrounding rocks. It is noted here that the intension of the assumption is to create a set of proximity maps that are consistent with each other, with respect to maximum extent.

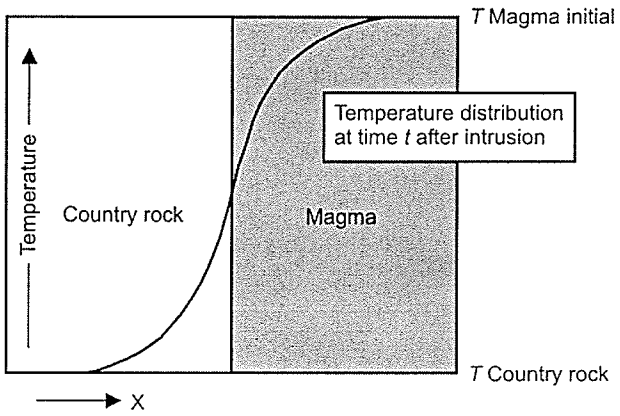

Figure 6.8 The temperature distribution in the vicinity of an igneous contact some time after intrusion (after Philpotts, 1990).

Owing to the fact that the solubility of water is generally higher in felsic melts, and, there is a spatial association between felsic bodies and Archean and Proterozoic shear-hosted deposits, felsic and mafic intrusive units in the 1:50 000 geological map were treated separately in the analysis. Each group of intrusive units was subsequently divided into unit area ranges based on the above assumption and calculated equivalent radius. Unit area ranges are 1000 m, excluding the 500 - 1000 m unit area range. Proximity maps for each of the unit area ranges were created using ArcView 3.2. The proximity maps are in raster format. Intrusive bodies with an "equivalent radius" value of < 500 m were not incorporated primarily because of the scale of potential maps being

produced. Intrusive bodies with an "equivalent radius" value of > 4000 m are given a maximum extent of 4000 m. Proximity zones are set at 100 m intervals.

Two main problems arose during this stage. They were: 1) how to weight the area within an intrusive body; and, 2) intrusions within or adjacent to other intrusions. The outer part of an intrusive body generally cools and solidifies first. As this outer part solidifies the inner liquid part continues to heat its surroundings. Over a given period of time the solid - fluid interface advances inward and proximity to heat source changes (Philpotts, 1990). Solidified portions of an intrusive body may, in turn, then be considered part of the adjacent rocks. However, for this project proximity is determined from the outer edge of a given intrusive body. Weighting is the highest at the edge of a given body and decreases to a value of 0.01 at the maximum extent. Areas outside the maximum extent are given a weight of 0.01. The area within an intrusive body is given a weight of 0.1 to reflect possible changes in the solid - fluid interface.

For the second problem intrusions within, or adjacent to other intrusions, can be accounted for by combining adjacent intrusive bodies into a single polygon. Proximity maps can be defined subsequently from the combined polygons. For this combination, however, the assumption was made that each polygon represents an intrusive phase that may have had an impact on the other adjacent bodies.

Prior to combination the five different scenarios corresponding to different stages in the tectonic evolution of the belt must be incorporated (Table 6.3). These scenarios allow the expert to include or extract elements of the spatial model that did not exist at the time of gold mineralization. For example, the effects of additional heat from post Sickle intrusive bodies should not be included in the combination stage if one suspects

gold mineralization is a D_2 event. Working at the scale of this project it is difficult to determine which, if any, intrusive units were an additional heat sources. However, it is possible to exclude bodies that were not in existence at the time of mineralization. The basis for the scenarios is derived from good knowledge of the project area. This information can significantly change the location of potential sites for exploration.

6.2.2.1 Heat Potential Combination

Figure 6.9 is a flowchart that shows the stages of analysis, and combination for heat component scenarios. For each scenario intrusive units were separated into felsic and mafic groups. Next, unit area ranges were set and proximity maps produced. All unit area ranges for a given scenario were combined in a single step and are shown in figure 6.10. Intrusive units for scenarios 1, 2, and 3 are the same. Maximum weighted values are 0.6 and 0.4 for the felsic and mafic bodies respectively (Table 6.1). A higher weight has been assigned to the felsic proximity maps, because of their association to shear hosted gold deposits. A minimum value of 0.01 is assigned to areas outside the maximum extent. Uncertainty in the geological map is minimal, however, the uncertainty in the representation of the heat component spatially is considered to be higher. The main factors were: 1) the assumption made about the shape of the bodies; 2) how to weight the area within an intrusive body; and, 3) intrusions within or adjacent to other intrusions. Uncertainty has been set at 0.3. Output maps were then reclassified to 64 levels before subsequent combination with the Source Zone Potential and Deformation Potential.

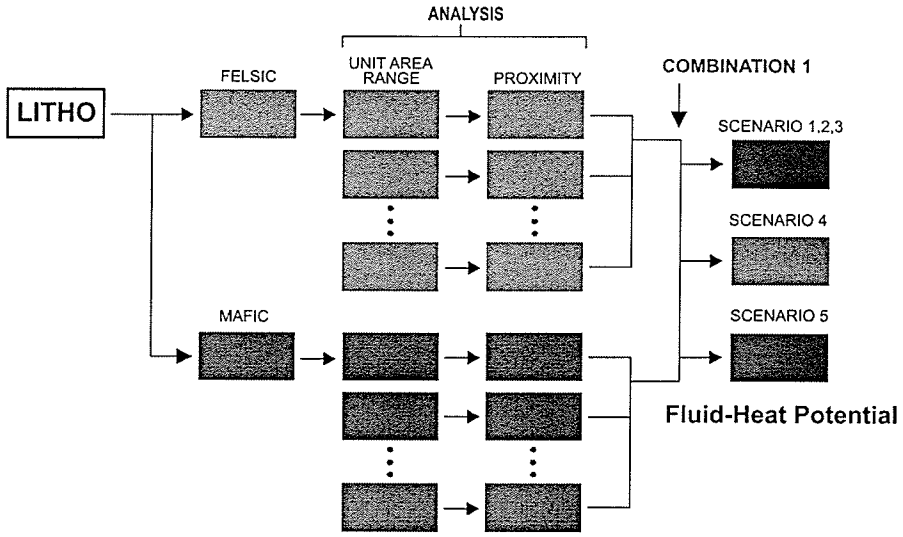

Figure 6.9 Flowchart of analysis and combination stages of fluid-heat potential combination. Base data set is the 1:50 000 geological map (LITHO). Intrusive units for scenarios 1, 2, and 3 are the same.

6.2.3 Shear-Hosted Spatial Model: Source Zone Component Translation

Source zone potential reflects the potential of a particular lithology, or tectonic assemblage, to initially contain gold. As noted in the conceptual model shear hosted deposits are not preferentially located in a particular rock type, however, it is considered that gold is derived locally from supracrustal rocks of the belt. Particular lithological units within the belt can be considered to have higher potential as a source of gold. This potential value can be represented by weighting the lithological units. Weighting can be based on 1) the rock type, 2) genetic association, 3) geochemistry; and, 4) and timing of mineralization. With respect to the conceptual model, high temperature magmatic rocks (e.g. komatiitic and Mg-rich basaltic compositions) and more primitive assemblages (e.g. oceanic assemblages) are considered to have high source zone potential. The geological map and geochemical subdivisions for volcanic rocks are the base data sets used for the source zone component.

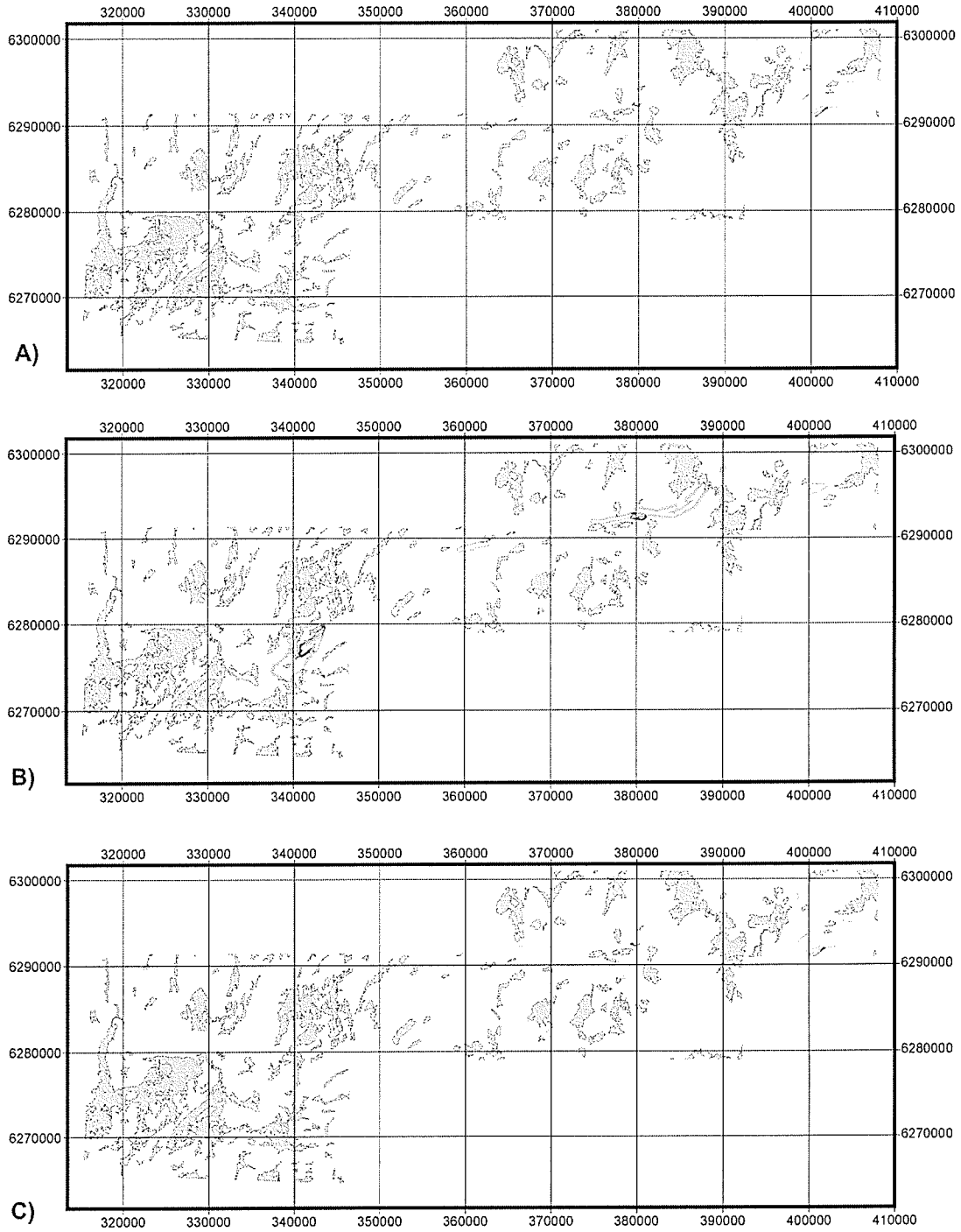

Figure 6.10 Dempster-Shafer belief output maps for Fluid-Heat scenarios. Scenario 1,2&3 (a), scenario 4 (b), and scenario 5 (c). Scenario 1,2&3 (d), scenario 4 (e), and scenario 5 (f). White indicates low relative potential; black indicates high relative potential (linear scale).

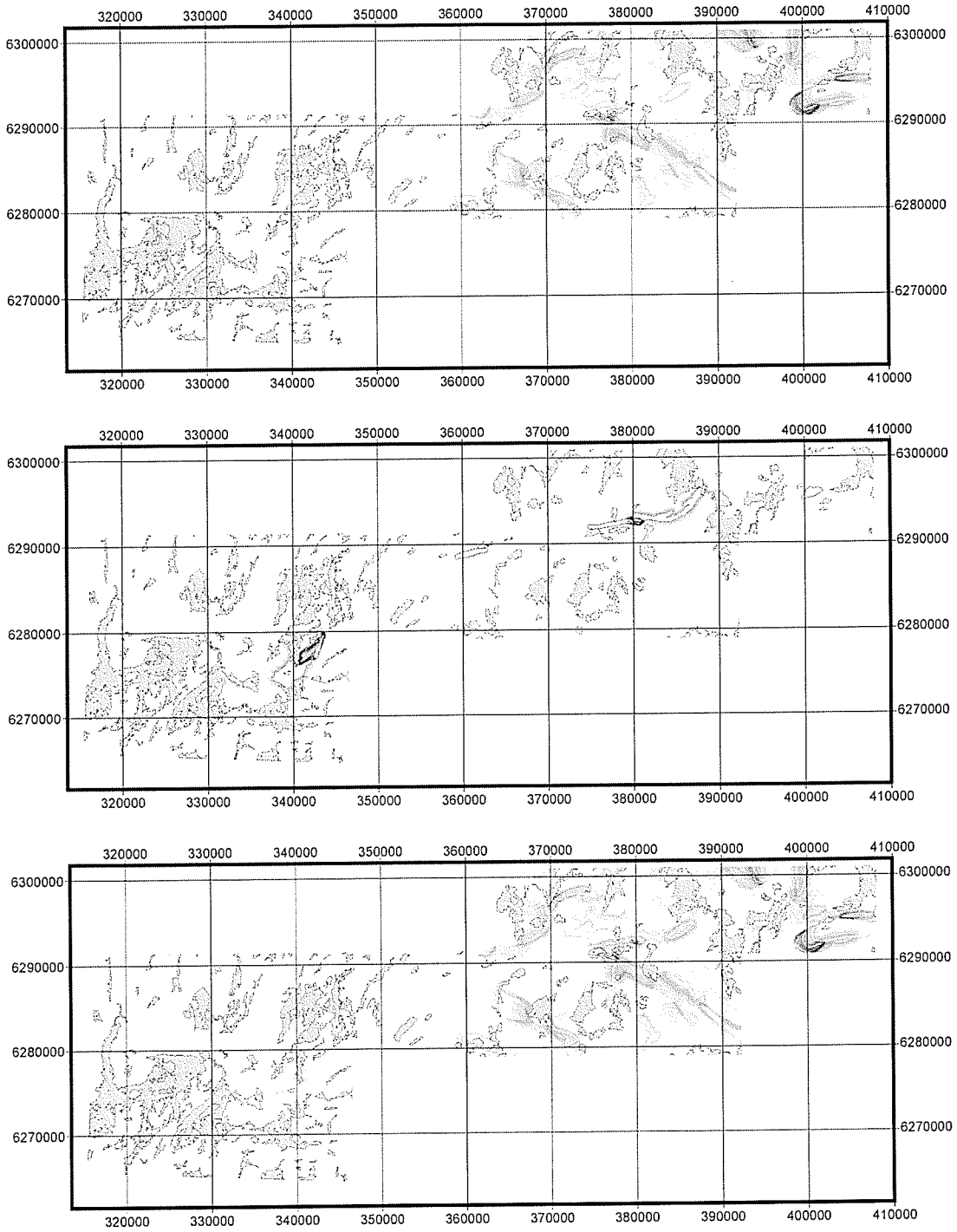

Figure 6.10 cont'

Another aspect to consider is timing of mineralization. In the case of the JSZ mineralization appears to be a predominantly D2 event (Beamont-Smith, 2000). Depending on the deformational history and mineralization, certain lithological units may not have existed at the time of formation, and therefore, should be excluded. For this reason five scenarios have been developed to account for the major tectonic events in the area, specifically related to the JSZ (Table 6.3). The five scenarios are applied to the lithological units, but not the geochemical subdivisions of the volcanic rocks. The same scenarios were used for the heat component.

6.2.3.1 Lithologic Units

The geological map for the Lynn Lake Greenstone Belt is in vector format. Weights were applied to each lithologic unit based on their potential of initially containing gold. Two main factors are considered in the weighting of units. First is genetic association and, second, is the type of rock. The ultimate source of gold in this project will be considered to be from a magmatic source. All sediments are secondary, derived from intrusive and volcanic rocks, therefore, primary volcanic and intrusive units are weighted the highest followed by volcanogenic sediments and reworked sediments. The weighting does not take into account, for example, the ability of gold to be concentrated during fluvial sedimentation.

Weights are listed in table 6.4 with mafic to ultramafic volcanic and intrusive rocks weighted the highest followed by volcanogenic sedimentary rocks and felsic intrusive rocks. Reworked sediments, such as the Sickle Group, are weighted the lowest. Volcanic rocks are weighted slightly higher, 0.05, than compositionally similar intrusive

rocks owing to subaerial and subaqueous alteration and possible primary concentration of gold.

TABLE 6.4: Source Zone (Lithology) Weighting

Unit (1)	Lithology	Unit (2)	Fuzzy	BEL	DIS	UNC
1	undivided	4	0.50	0.30	0.40	0.30
2	aphyric basalt	2	0.60	0.36	0.34	0.30
3	porphyritic basalt	3	0.60	0.36	0.34	0.30
4	M & I volcanic	4	0.50	0.30	0.40	0.30
5	I & F volcanic	5	0.40	0.24	0.46	0.30
6	Dacite	6	0.30	0.18	0.52	0.30
7	Rhyolite	7	0.30	0.18	0.52	0.30
8	Conglomerate	8	0.30	0.18	0.52	0.30
9	Sedimentary	9	0.30	0.18	0.52	0.30
10	Sed Uncertain age	10	0.15	0.09	0.61	0.30
11	Burntwood	11 and 1a	0.10	0.06	0.64	0.30
12	Sickle conglmerate	11 and 12	0.10	0.06	0.64	0.30
13	Sickle sandstone	12	0.10	0.06	0.64	0.30
14	Gabbro diabase	13	0.45	0.27	0.43	0.30
15	Diorite	13 and 14	0.45	0.27	0.43	0.30
16	Gabbro Ultra	15	0.45	0.27	0.43	0.30
17	Granodiorite	16	0.25	0.15	0.55	0.30
18	Granite Grano	16 and 17 (20)	0.25	0.15	0.55	0.30
19	Mafic intrusions	18	0.45	0.27	0.43	0.30
20	Grano tonalite	19	0.25	0.15	0.55	0.30
21	Granite grano	20	0.25	0.15	0.55	0.30
22	granitiod	19	0.25	0.15	0.55	0.30
23	quartz porhyry		0.20	0.12	0.58	0.30

(1) from 1:50 000 digital geological map (1998)
(2) from Gilbert et al., (1980)

The geological map is reclassified using the given weights. All units with the same weight are grouped together as a single classification. Proximity maps are then created for each classification. Proximity maps are created for two main reasons. First, shear-hosted deposits are not necessarily associated with a particular rock type, therefore,

proximity to potential source zones is important. Second, the 1:50 000 geological map contains areas of missing data. Proximity maps allow for coverage of the entire area of interest, including those areas of missing data. Proximity maps can also, to some degree, adjust for the three dimensional nature of the lithological units, however, this is not the intent of the proximity maps. A linear function was used for weighting the proximity zones with maximum values nearest to the lithological units. The maximum extent of the proximity zones for all volcanic units was 2000 m. Areas > 2000 m from the source were given a minimum weight of 0.01. The scale of this project is regional at scale. At this scale the 1:50 000 geological map will group together assemblages of rocks if the individual units are too small to be included separately. For instance pillow and massive basalts may be grouped with volcanogenic sediments or pyroclastic units. Weighting is applied based on the major lithology defined for a given assemblage. For this reason uncertainty is 0.4.

6.2.3.2 Geochemical Subdivisions of Volcanic Rocks

In section 3.1.3 it was noted that the geochemical subdivisions of volcanic rocks was put together using updated trace element geochemistry of the volcanic rocks in the Lynn Lake Greenstone Belt. This data has been incorporated into the shear-hosted spatial model. Each of the units were been defined using trace element and REE data for a selection of samples across the belt, and stratigraphic relationships within the belt (Zwanzig et al., 1999).

Mg-rich and less evolved volcanic rocks are considered to be probable sources of gold, therefore, two input maps have been developed to address these factors. The first

input map makes use of average MgO values for each of the volcanic sub-units. The second uses the tectonic subdivisions based on trace element and REE data. Weights applied to the volcanic subdivisions for MgO and tectonic input maps are shown in table 6.5. The input maps are reclassified based on given weights and proximity maps are created. Proximity maps are created for the same reasons noted in the lithology section. A linear function was used for weighting the proximity zones with maximum values nearest to the volcanic units. The maximum extent of the proximity zones for all volcanic units was 2000 m. Areas > 2000 m from the source were given a minimum weight of 0.01. Uncertainty is set 0.4 based on the limited number of samples available for each of the subdivisions.

6.2.3.3 Source Zone Combination Potential

Combination of lithological units and geochemical subdivisions for volcanic rocks is completed in two main stages (Figure 6.11). Proximity maps for the lithological units are combined in a single step with respect to the five scenarios (Figure 6.12), whereas MgO and tectonic input maps were combined separately and reclassified to 64 levels prior to combination with the lithological input scenarios (Figure 6.13). The Source Zone Potential output maps for the five scenarios are shown in figure 6.14 and were reclassified to 64 levels subsequent to combination with the Fluid-Heat Potential and Deformational Potential outputs.

TABLE 6.5: Source Zone (Geochemical) Weighting

Unit	Division	fuzzy MgO	BEL MgO	DIS MgO	UNC MgO	fuzzy tectonic	BEL tectonic	DIS tectonic	UNC tectonic
1a	ArcTholeiite	0.21	0.12	0.48	0.40	0.30	0.18	0.42	0.40
1b		0.30	0.18	0.42	0.40	0.30	0.18	0.42	0.40
1c		0.24	0.15	0.45	0.40	0.30	0.18	0.42	0.40
1d		0.18	0.11	0.49	0.40	0.30	0.18	0.42	0.40
2a	Calc-alkaline basalt to andesite	0.50	0.30	0.30	0.40	0.10	0.06	0.54	0.40
2b		0.49	0.29	0.31	0.40	0.10	0.06	0.54	0.40
2c		0.29	0.17	0.43	0.40	0.10	0.06	0.54	0.40
2d		0.16	0.10	0.50	0.40	0.10	0.06	0.54	0.40
3a	Enriched arc tholeiite	0.29	0.17	0.43	0.40	0.25	0.15	0.45	0.40
3b		0.13	0.08	0.52	0.40	0.25	0.15	0.45	0.40
3c		0.19	0.11	0.49	0.40	0.25	0.15	0.45	0.40
3d		0.18	0.11	0.49	0.40	0.25	0.15	0.45	0.40
4a	Depleted arc tholeiite	0.20	0.12	0.48	0.40	0.25	0.15	0.45	0.40
4b		0.19	0.12	0.48	0.40	0.25	0.15	0.45	0.40
4c		0.18	0.11	0.49	0.40	0.25	0.15	0.45	0.40
5a	Komatiitic basalt	0.47	0.28	0.32	0.40	0.01	0.01	0.59	0.40
6a	Weakly depleted arc tholeiite	0.24	0.14	0.46	0.40	0.35	0.21	0.39	0.40
6b		0.20	0.12	0.48	0.40	0.01	0.01	0.59	0.40
6c		0.17	0.10	0.50	0.40	0.35	0.21	0.39	0.40
7a	Arc tholeiite transitional - E-MORB	0.26	0.16	0.44	0.40	0.50	0.30	0.30	0.40
7b		0.11	0.07	0.53	0.40	0.50	0.30	0.30	0.40
7c		0.28	0.17	0.43	0.40	0.50	0.30	0.30	0.40
8a	MORB-Like basalt	0.35	0.21	0.39	0.40	0.60	0.36	0.24	0.40
8b		0.22	0.13	0.47	0.40	0.60	0.36	0.24	0.40
9a	Ocean island basalt-ultramafic	0.60	0.36	0.24	0.40	0.01	0.01	0.59	0.40
10a	Dacite	0.05	0.03	0.57	0.40	0.01	0.01	0.59	0.40
10b		0.07	0.04	0.56	0.40	0.01	0.01	0.59	0.40
11a	Rhyolite	0.01	0.01	0.59	0.40	0.01	0.01	0.59	0.40
11b		0.03	0.02	0.58	0.40	0.01	0.01	0.59	0.40
11c		0.05	0.03	0.57	0.40	0.01	0.01	0.59	0.40
11d		0.03	0.02	0.58	0.40	0.01	0.01	0.59	0.40
11e		0.03	0.02	0.58	0.40	0.01	0.01	0.59	0.40
11f		0.01	0.01	0.59	0.40	0.01	0.01	0.59	0.40
11g		0.01	0.01	0.59	0.40	0.01	0.01	0.59	0.40

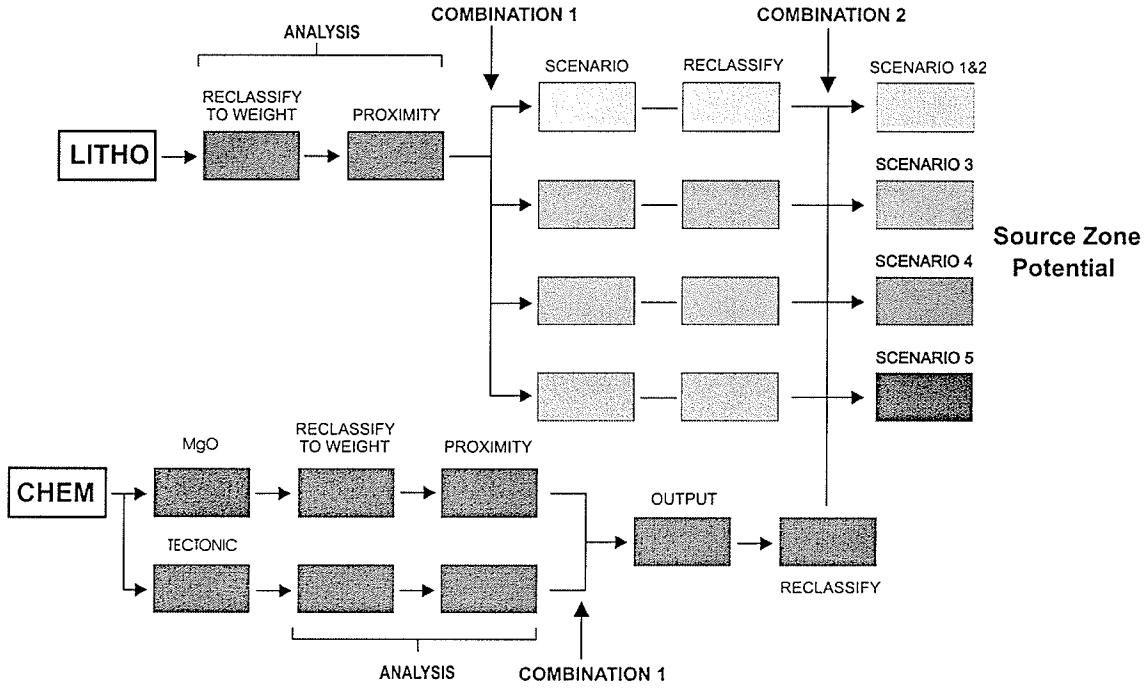

Figure 6.11 Flowchart of analysis and combination stages ofsource zone potential combination. Base data sets are the 1:50 000 geological map (LITHO) and 1:250 000 geochemical subdivisions map (CHEM). Lithological units for scenarios 1 and 2 are the same.

6.2.4 Shear-Hosted Spatial Model: Shear-Hosted Combination

The shear-hosted spatial model is made up of three main components; structure, fluid-heat, and source zone components. Sub-potential maps have been created for each of the three components. Each sub-potential maps represents the potential of a shear-hosted deposit occurring based on that particular component of the spatial model. Each component can be considered independent of the others and, therefore, the sub-potential maps can be combined different ways, such as by changing in the overall weighting of the given components, or by the extraction of one or more components.

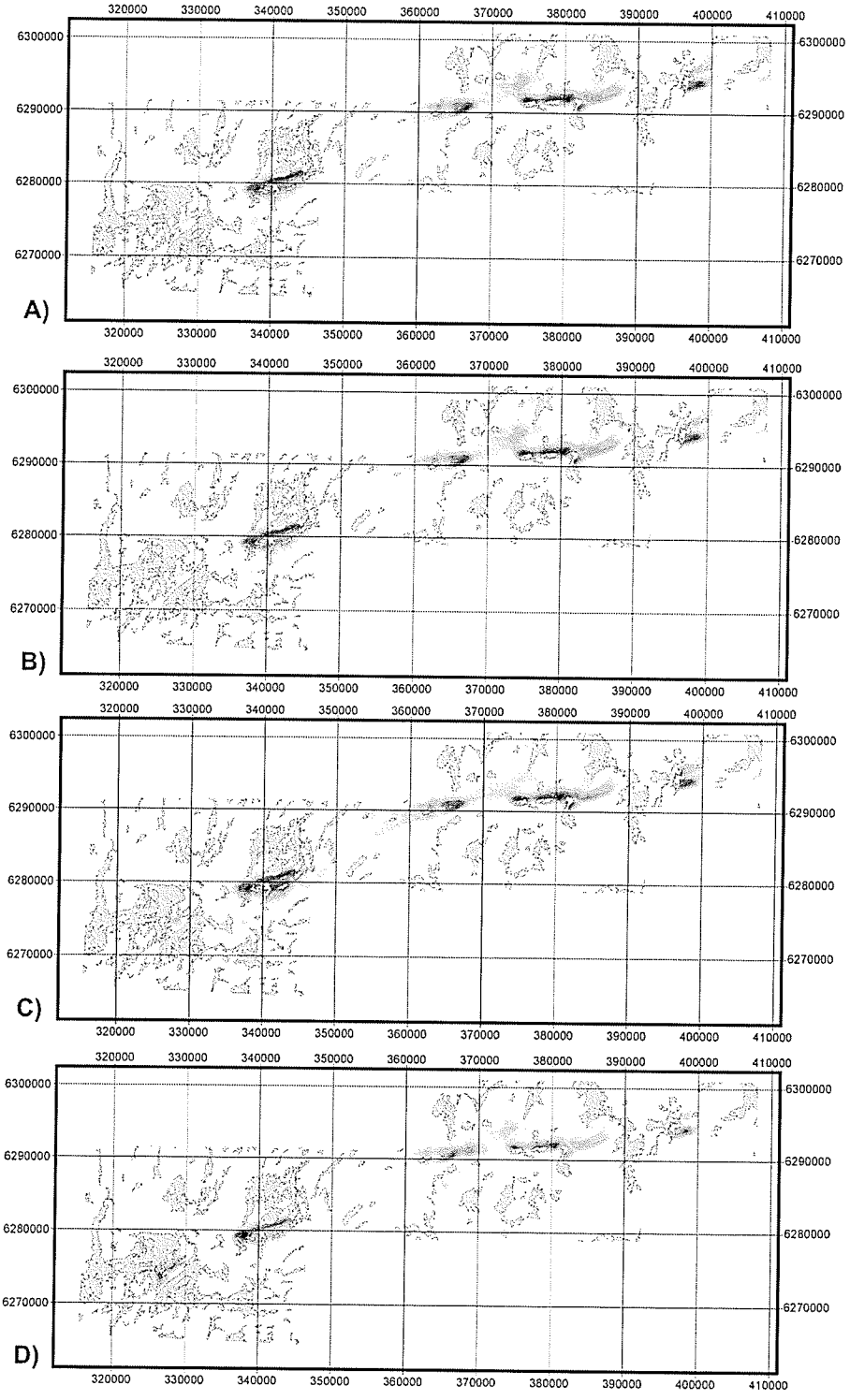

Figure 6.12 Dempster-Shafer belief output maps for Source Zone lithology potential. Scenario 1&2 (a), scenario 3 (b), scenario 4 (c), and scenario 5 (d). Scenario 1&2 (e), scenario 3 (f), scenario 4 (g), and scenario 5 (h). White indicates low relative potential; dark; black indicates high relative potential (linear scale).

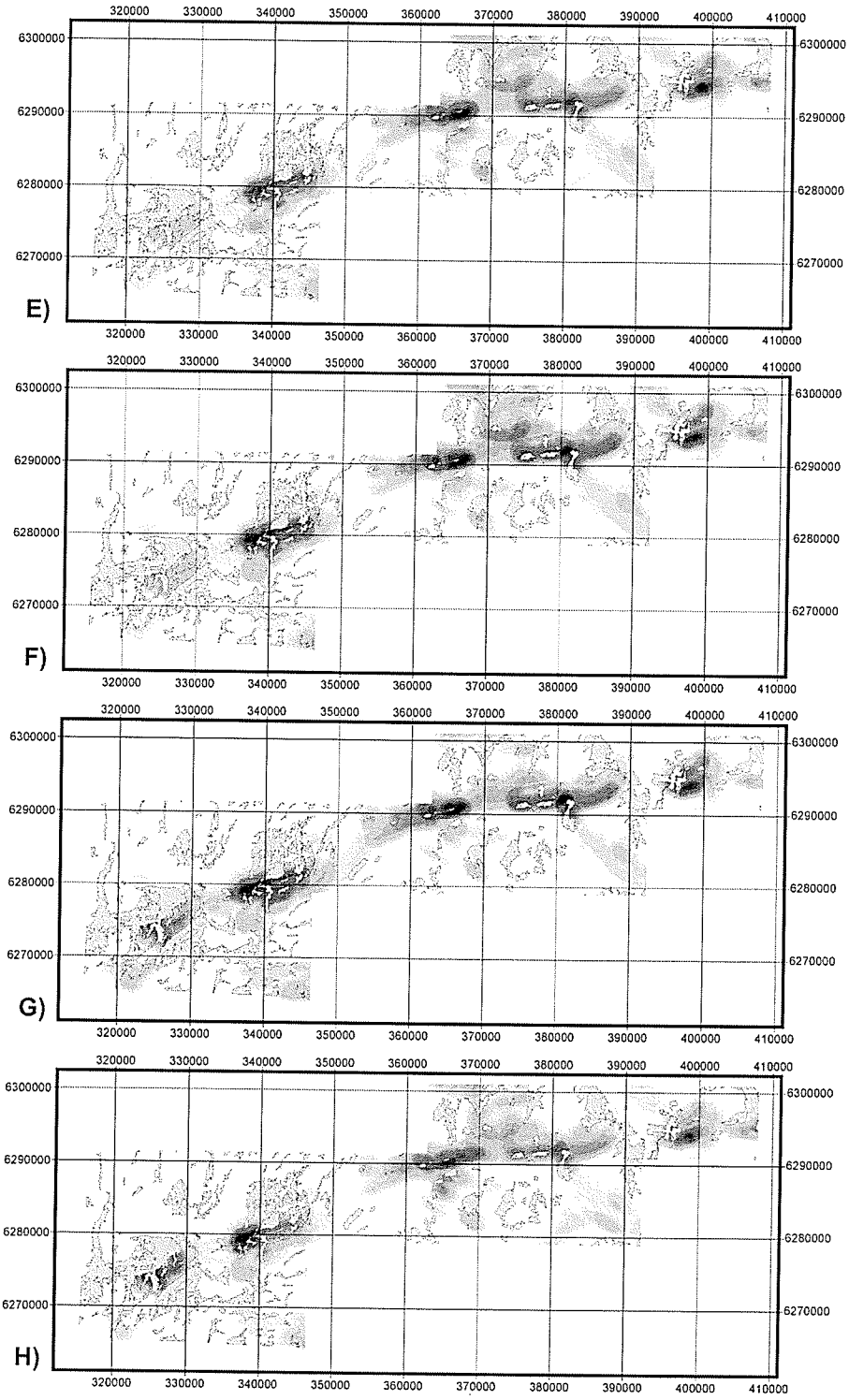

Figure 6.12 cont'

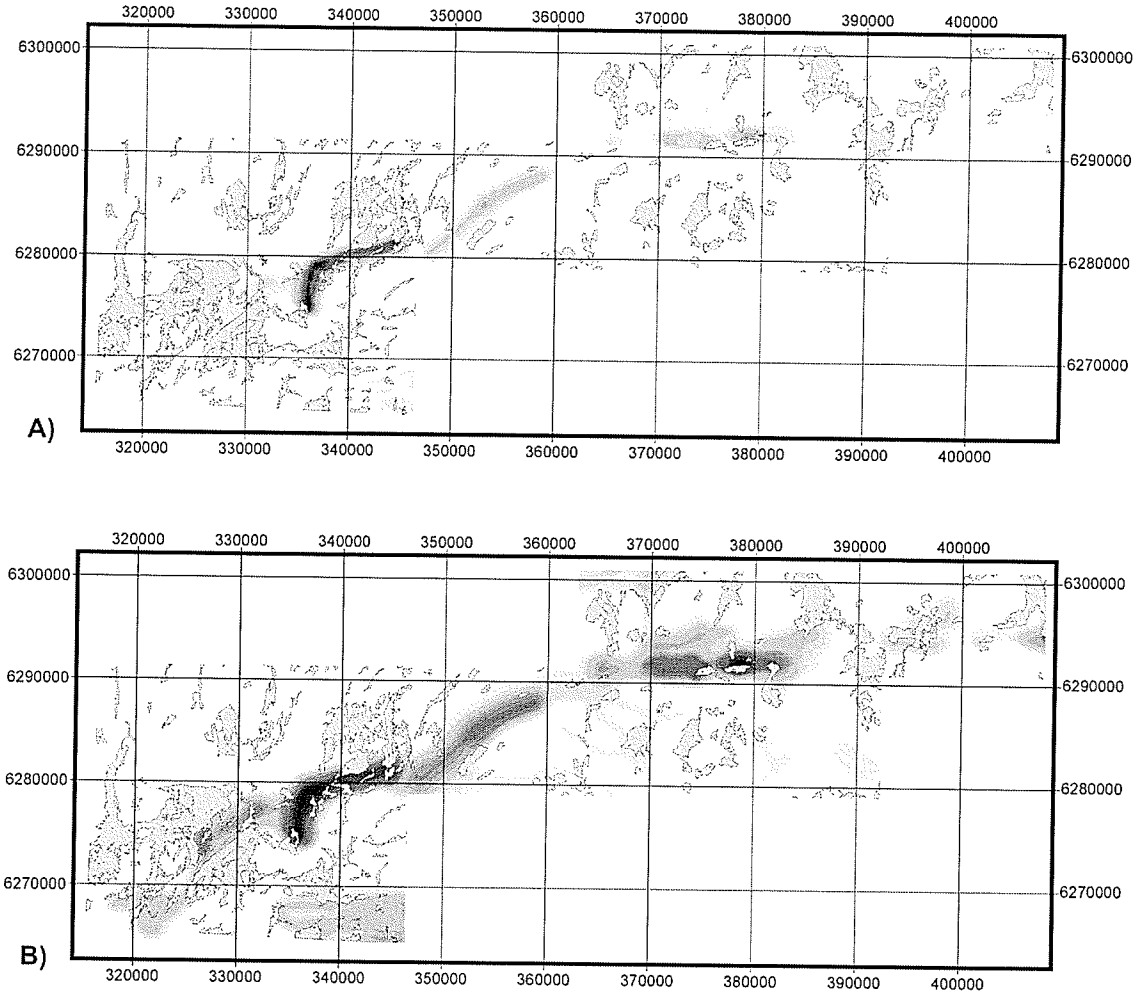

Figure 6.13 Dempster-Shafer belief (a) and Fuzzy logic (b) output maps for Source Zone geochemical potential. White indicates low relative potential; dark; black indicates high relative potential (linear scale).

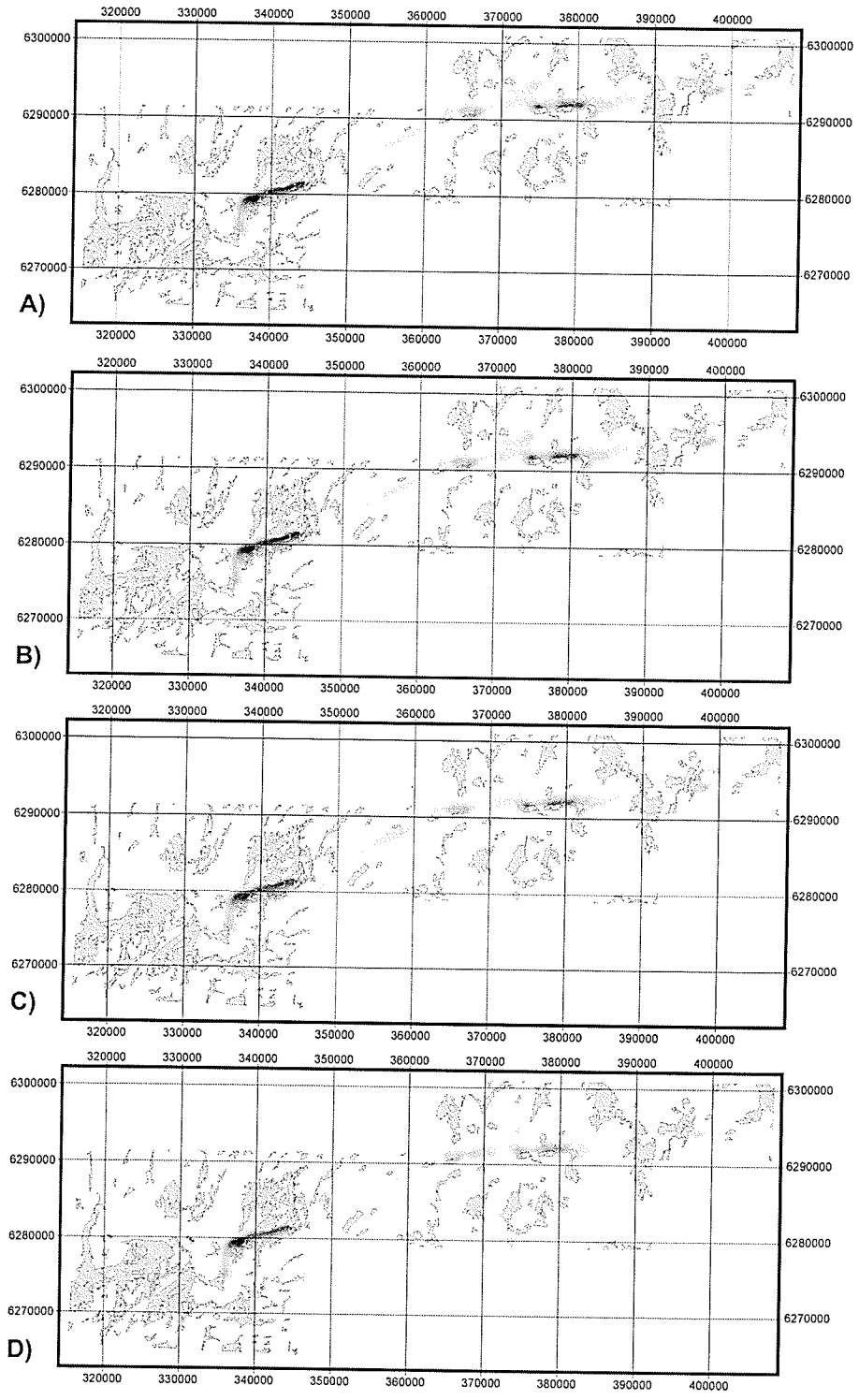

Figure 6.14 Dempster-Shafer belief output maps for Source Zone potential. Scenario 1&2 (a), scenario 3 (b), scenario 4 (c), and scenario 5 (d). Scenario 1&2 (e), scenario 3 (f), scenario 4 (g), and scenario 5 (h). White indicates low relative potential; dark; black indicates high relative potential (linear scale).

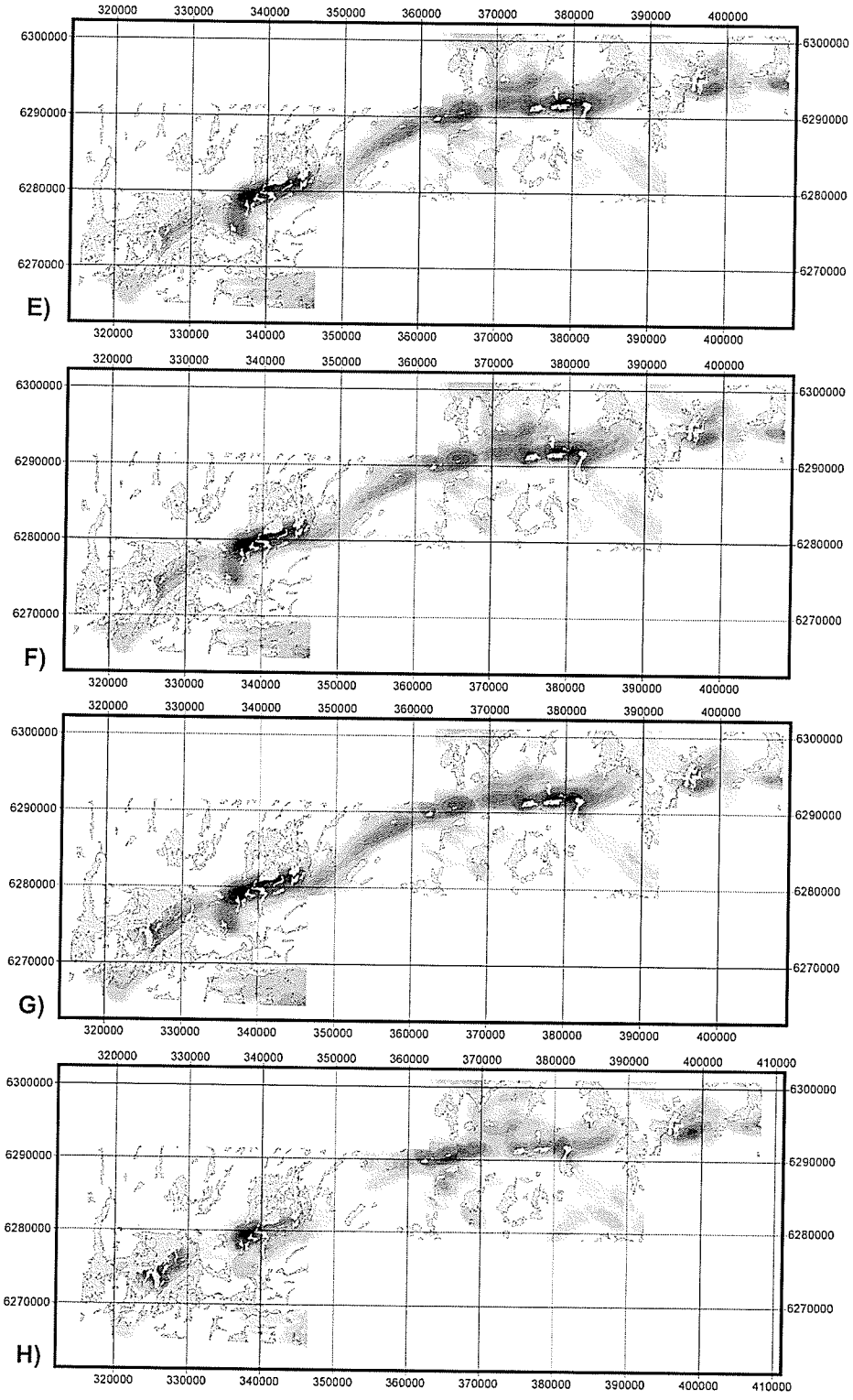

Figure 6.14 cont'

Weighting was applied to the various inputs that were combined to produce the component sub-potential maps. The resulting sub-potential maps were also weighted relative to each other. Structure is the dominant control on the location of shear-hosted gold deposits and is given the highest weight, with the heat and source zone components given the same maximum weight. Table 6.6 lists the maximum and minimum weights, and uncertainty values for each of the sub-potential maps.

TABLE 6.6: Shear-hosted Sub-Potential Weighting

Component	Maximum Weight FL(1)	Maximum Weight DS (B, D, U) (2)	Minimum Weight
Structure			
Lineament deformation	0.8	0.64, 0.16, 0.2	0.01
Structure deformation	0.8	0.64, 0.21, 0.15	0.01
Fluid/Heat	0.6	0.36, 0.34, 0.3	0.01
Source Zone	0.6	0.36, 0.34, 0.3	0.01

(1) Fuzzy Logic weight
Dempster-Shafer weight (Belief, Disbelief, Uncertainty

For this project all three components are included in the shear-hosted potential, however, the structural component will be combined with each of the scenarios for the heat and source zone components (Figure 6.15). The structural component will also be separated into lineament deformation potential and structural deformation potential. Lineament deformation potential will include the output potential maps from the lineament analysis. Structural deformation potential will combine the lineament deformation potential with the potential derived from the known faults and JSZ. Both lineament and structure deformation potential will include outputs for logarithmic and

exponential shear stress decay functions (see 6.2.1). Figure 6.16 shows a selection of shear-hosted potential maps using the lineament deformation and structure deformation inputs. For the structure deformation potential, regions with high potential are focused near faults and the JSZ, as might be reasonably expected. The fault and JSZ data sets have a low uncertainty with respect to the extent of the given faults and JSZ. The fault and JSZ data sets are, however, not a complete representation of the structure within the greenstone belt. A higher degree of uncertainty exists if one considers the possibility of other faults and shear zones in the greenstone belt. For this reason potential maps are also produced using lineament deformation potential, which can be considered to have no bias within the belt.

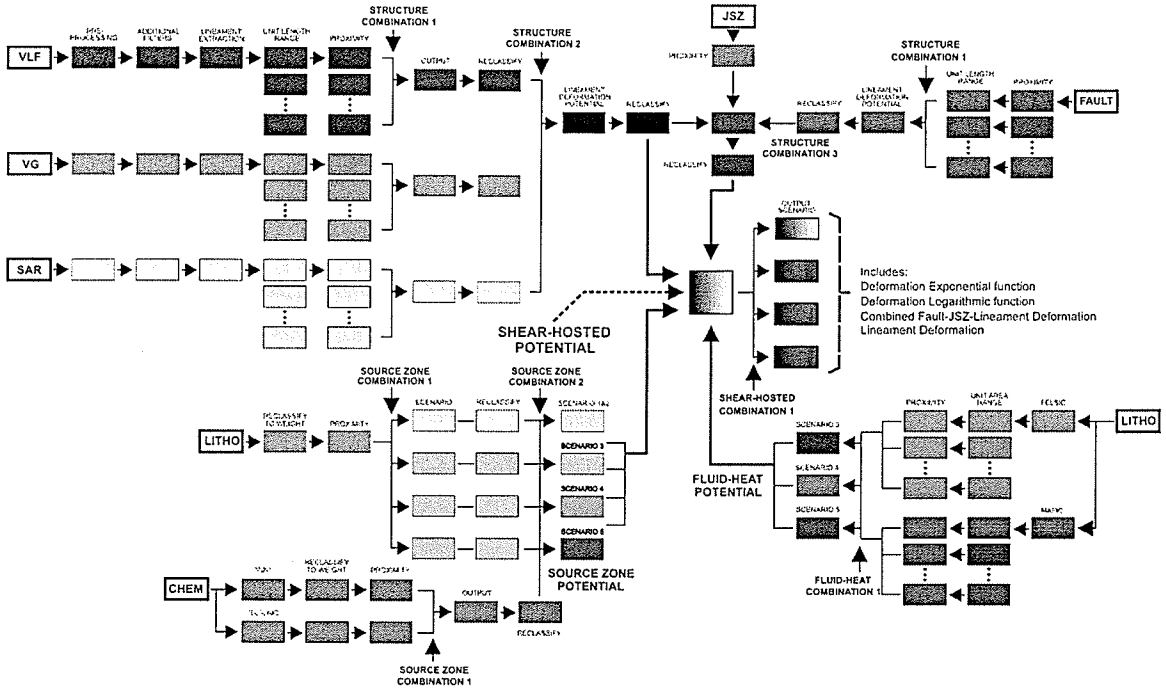

Figure 6.15 Flowchart of processing, analysis, and combination stages for the shear-hosted potential combination. Flow chart includes the structure, heat, and source components of the spatial model. Components are combined to generate output potential maps shown in Figure 6.16 and in chapter 7.

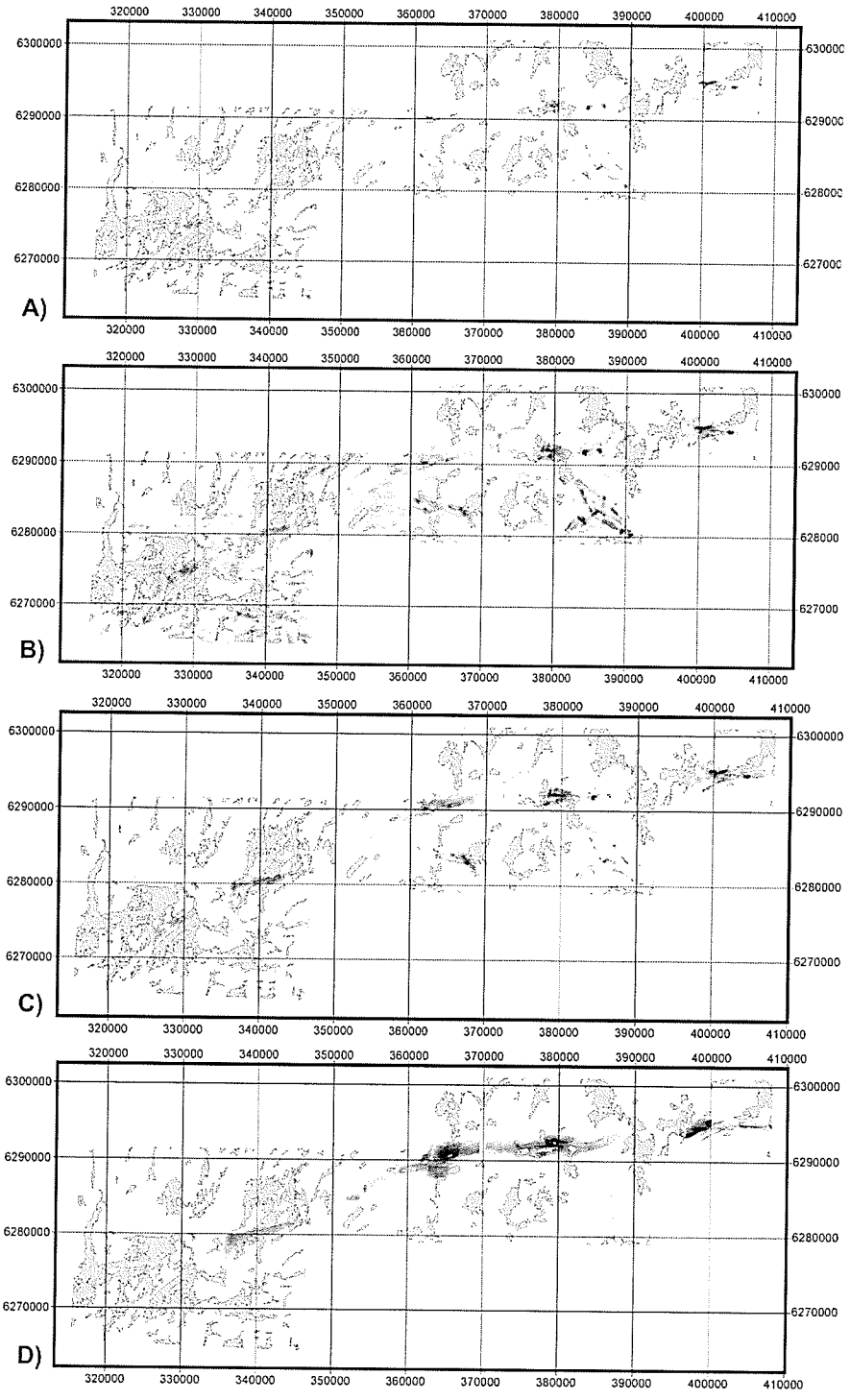

Figure 6.16 Selection of output potential maps for the shear-hosted spatial model. All output maps are for scenario 5 using a logarithmic decay function fo the structural component. Dempster-Shafer belief (a) and plausibility (b) output; Fuzzy logic gamma operation lineament (c) and structure deformation (d) output. White indicates low relative potential; dark; black indicates high relative potential (linear scale).

In total there are 32 potential output maps for the project area. Each of these maps have been divided into three zones based on the three geophysical survey areas. This has been done because the three geophysical surveys were not leveled to each other (see section 4.5). Only a selection of potential maps are shown in figure 6.16, however, all potential maps are listed in Appendix A and are available in Appendix A. From the potential maps four main high potential areas have been determined in the project area and are discussed in detail in chapter 7, Output and Testing.

6.3 VMS Spatial Model: Introduction

Translation of the VMS conceptual model into a spatial model makes use of the 1:50 000 geological map, 1:250 000 geochemical subdivisions for volcanic rocks, TF magnetic survey data, and VLF-EM survey data. In chapter 3 it was noted that the major components of the VMS conceptual model included, 1) an ore-rich fluid source; 2) a heat source to drive the hydrothermal system; and 3) stratigraphy. Seawater is considered to be the primary fluid source, and hence, lithological units such as subaqueous rocks types can be considered important spatial indicators of VMS deposits. However, differentiation of subaqueous and subaerial volcanic rocks at the scale of the geological map is not possible. The lithological data can be used to translate spatial and stratigraphic relations of VMS deposits into the spatial model as stratigraphic potential. It is assumed the dominant heat source that drives the hydrothermal system is associated with intrusive bodies. The geological map can also be used to show proximity to intrusive bodies, or by extension proximity to heat source. Not all intrusive bodies are

associated with VMS formation, therefore, the timing of intrusive events must be considered.

It was also noted in section 3.2.1 that most volcanic rocks and immature sediments have enough metals to produce a deposit, however, volcanic rocks do not necessarily contain equal quantities of Cu and Zn. For this reason the geochemical subdivisions for volcanic rocks data set will be used to find areas of high background Cu and Zn in volcanic rocks. The sulphide minerals that form the VMS deposits are generally good conductors, excluding ZnS, and include the magnetic mineral pyrrhotite. The VMS spatial model will include a geophysical factor that makes use of the TF and VLF-EM regional data sets. Alteration, which is an important spatial indicator of VMS deposits, will not be considered, because a compiled alteration data set for the belt is not available. The major components of the VMS spatial model will then include, 1) the heat source component; 2) the stratigraphic component; 3) Cu-Zn component; and, 4) a geophysical factor.

6.3.1 VMS Spatial Model: Heat Component

In the conceptual model (section 3.2.2) it was noted that a heat source is required for the creation of VMS deposits for two main reasons. First, high fluid temperatures are required to promote reactions between fluid and wall rock to mobilize metals. Heat is also required to drive the circulation of fluids through the adjacent rock units and eventually heat loss leads to precipitation of metals on, or just below, the seafloor. Heat from intrusive bodies and the stratal aquifer model were noted in section 3.2.2 as possible

sources of heating fluids. Only the former will be considered here, owing to the inability to represent the latter case spatially.

Proximity maps were used by Bonham-Carter et al. (1993) and Wright and Bonham-Carter (1996), to represent proximity to a heat source. This approach was adopted for the Shear-Hosted Spatial Model and will be used in the VMS spatial model. Considerations with respect to the heat component of the VMS spatial model include 1) heat loss into the adjacent rocks, 2) the lateral extent of heating adjacent rocks; and 3) history of plutonism within the belt. In the case of the Shear-Hosted Spatial Model five scenarios were used to represent different possible tectonic events and the related intrusive events. For the VMS spatial model only syn-volcanic intrusive bodies are considered to be a possible heat source for driving the hydrothermal system.

Felsic to mafic syn-volcanic intrusive units are selected from the 1: 50 000 geological map. As with the Shear-Hosted Spatial Model, the heating effects of an intrusive body on the adjacent rocks should have a maximum lateral extent. Proximity maps are created using the same assumption and principles defined in section 6.3 of the shear-hosted spatial model. Proximity zones are set at 100 m intervals to a maximum of 1000 m depending on the unit area. The intrusive units used for the VMS heat component comprise only the syn-volcanic units. For this reason intrusive units with a calculated equivalent radius of <500 m are included. Intrusive units with a calculated equivalent radius of < 250 m have a maximum extent of 250 m. Intrusive units with a calculated equivalent radius > 1000 m have a maximum extent of 1000 m. The largest syn-volcanic intrusive body has a calculated equivalent radius of < 2000 m. Heat dissipation into the country rock during an intrusive event is not necessarily constant over

time. For the VMS spatial model the distribution of heat into adjacent country rocks can be considered to fit an exponential curve (see 6.3).

TABLE 6.7: VMS Spatial Model Weighting

Component	Maximum Weight FL(1)	DS (B, D, U) (2)	Minimum Weight
Heat Source	0.7	0.49, 0.31, 0.2	0.01 (3)
Stratigraphy	0.8		
Felsic Volcanic	0.8	0.64, 0.16, 0.2	0.01
Intermediate Volcanic	0.75	0.57, 0.23, 0.2	0.01
Mafic Volcanic	0.7	0.49, 0.31, 0.2	0.01
Volcanogenic Sediments	0.65	0.42, 0.38, 0.2	0.01
Burntwood Group Sediments	0.55	0.30, 0.50, 0.2	0.01
Geophysics	0.7		
VLF	0.7	0.49, 0.31, 0.2	0.01
TF	0.65	0.42, 0.38, 0.2	0.01
Cu – Zn	0.5		
Cu	0.5	0.25, 0.35, 0.4	0.01
Zn	0.5	0.25, 0.35, 0.4	0.01

(1) Fuzzy Logic weight
(2) Dempster-Shafer weight (Belief, Disbelief, Uncertainty). Calculated from fuzzy weight.
(3) A weight of 0.1 is assigned to the area within an intrusive unit

6.3.1.1 Heat Source Potential Combination

A maximum fuzzy logic weight of 0.7 is given to proximity zones directly adjacent to the outer edge of a given intrusive unit. Within the intrusive units a value of 0.1 is assigned (see 6.3) and a minimum value of 0.01 is assigned to areas outside the maximum lateral extent. Table 6.7 lists the maximum and minimum values for all major components of the VMS spatial model. All weighting values are given with respect to the fuzzy logic method; values for the belief function for the Dempster-Shafer method are

calculated relative to the assigned Fuzzy value (see section 5.4). An uncertainty value of 0.2 was set for heat source potential based on three main factors: 1) the assumption made about the shape of the bodies; 2) how to weight the area within an intrusive body; and, 3) intrusions within or adjacent to other intrusions.

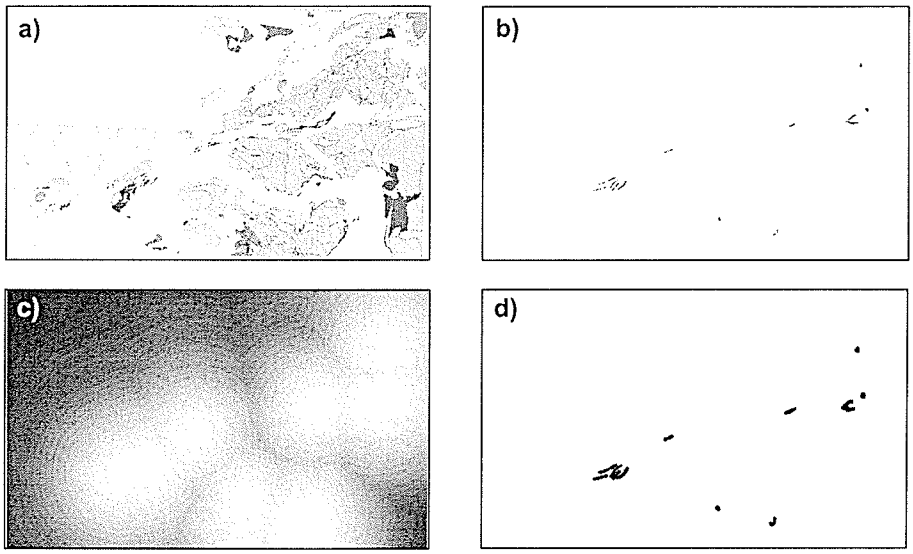

Figure 6.17 Sequence of steps to produce a heat source proximity map for the 250 - 500 m unit area range: (a) intrusive units from the 1:50 000 geological map; (b) 250 - 500 m unit area range intrusive bodies; (c) proximity zones from intrusive bodies; (d) reclassified proximity zone with maximum extent set to 500m.

Proximity maps are created by grouping the intrusive units from the 1:50 000 geological map into unit area ranges based on the 2 dimensional surface area of the units. Proximity maps are created for each group and set to a maximum extent depending on the given unit area range. Figure 6.17 shows the sequence of steps used to produce a heat source proximity map for a given unit area range. Combination of the heat source input layers is completed in a single stage (Figure 6.18). The heat source component output map was reclassified to 64 levels before subsequent combination with the stratigraphic

component, Cu-Zn component and geophysical factor. Figure 6.19 shows the heat source potential for the VMS spatial model. The figure includes outputs for the fuzzy logic gamma operation, with gamma set to 0.9, and the Dempster-Shafer belief function.

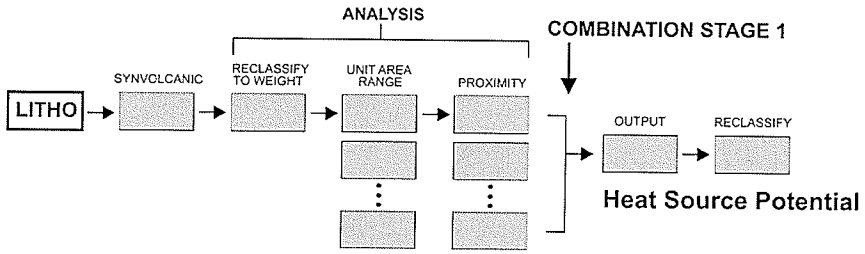

Figure 6.18 Heat Source Potential flow chart for analysis and combination. Base data set is the 1:50 000 geological map (LITHO).

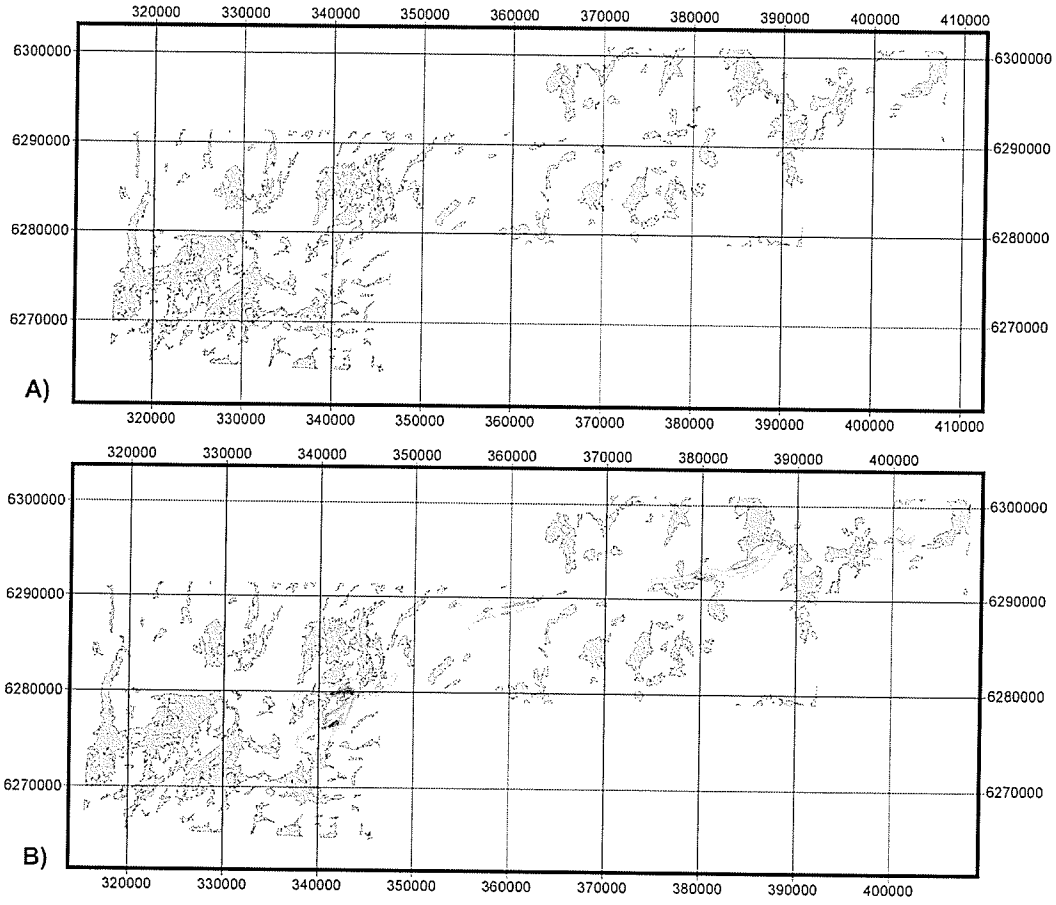

Figure 6.19 Dempster-Shafer belief (a) and fuzzy logic (b) heat potential output maps. White indicates low relative potential; black indicates high relative potential (linear scale).

6.3.2 VMS Spatial Model: Stratigraphic Component

Discussion of the stratigraphic component in the conceptual model has shown that the host rocks of Cu-Zn type VMS deposits are commonly subaqueous volcanic rocks, however, sedimentary rocks have also been found to host these deposits. Specific host rocks will not be used as evidence of a VMS deposit in this spatial model. Stratigraphic relationships, on the other hand, can help to locate areas of potential VMS deposits. Consideration for the translation stage include 1) stratigraphic relations and lithological contacts, 2) timming of deposition; and 3) subaqueous rock types. VMS deposits are spatially associated to subaqueous volcanic or pyroclastic rocks. These spatial associations can be represented in the VMS spatial model using proximity maps for lithological units in the 1:50 000 geological map.

Stratigraphic relations and lithological contacts are important stratigraphic markers and can be represented in the spatial model. For instance a proximity map generated for felsic volcanic rocks can be combined with a proximity map generated for volcanogenic sediments. If a felsic volcanic unit is in contact with a volcanogenic sedimentary unit the combined proximity maps will produce a zone of high potential along the contact. This high potential zone may reflect the end of a volcanic cycle or a hiatus in volcanic activity. This approach can be applied to the various volcanic and sedimentary rocks in the belt, however, timing of deposition must be considered. A complete set of stratigraphic top directions for the volcanic and sedimentary units in the southern part of the Lynn Lake Belt is not available. This does present a problem with respect to stratigraphic control. With the Dempster-Shafer a degree of uncertainty can be applied to account for this problem.

Weights for the lithological proximity maps are shown in Table 6.7. Volcanic rocks were weighted the highest, followed by volcanogenic sedimentary rocks, and sedimentary rocks of the Burnwood Suite. All other units are not included, because they did not exist during initial stages of the Lynn Lake belt. Felsic volcanic rocks were weighted slightly higher than mafic volcanic rocks for two reasons. First is the spatial association between VMS deposits and rhyolite domes or felsic fragmental rocks noted in the conceptual model. Second is the impermeable cap that confines the hydrothermal fluids, which commonly comprises felsic volcanic rocks. The Burntwood Suite sedimentary rocks are included in the stratigraphic potential section owing to a similar stratigraphic age with the volcanic rocks in the southwestern part of the belt (Gilbert et al., 1980).

6.3.2.1 Stratigraphic Potential Combination

Weights are assigned to each of the lithological units in the 1:50 000 geological map. Units with the same weight are combined into a single group. Proximity maps are created for each group and are given a maximum extent of 2000 m. Weighting is applied to the proximity zones with maximum weight within the lithological units. Weight decreases outwards using a linear function. Uncertainty is set at 0.2 for the stratigraphic potential owing to the lack of information on stratigraphic top directions (Table 6.7). Figure 6.20 shows the processing and combination stages of the stratigraphic potential component. The fuzzy logic and Dempster-Shafer method output maps (Figure 6.21) are reclassified to 64 levels prior to combination with other sub-potential maps.

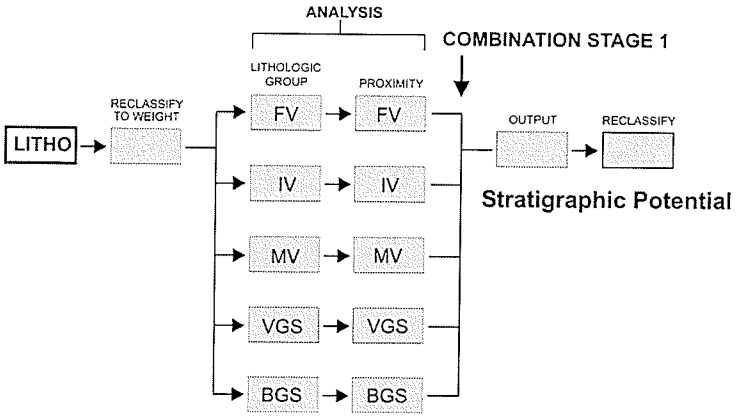

Figure 6.20 Stratigraphic Potential flow chart for analysis and combination. Base data set is the 1:50 000 geological map (LITHO). FV felsic volcanic; IV intermediate volcanic; MV mafic volcanic; VGS volcanogenic sediment; BGS Burntwood Group

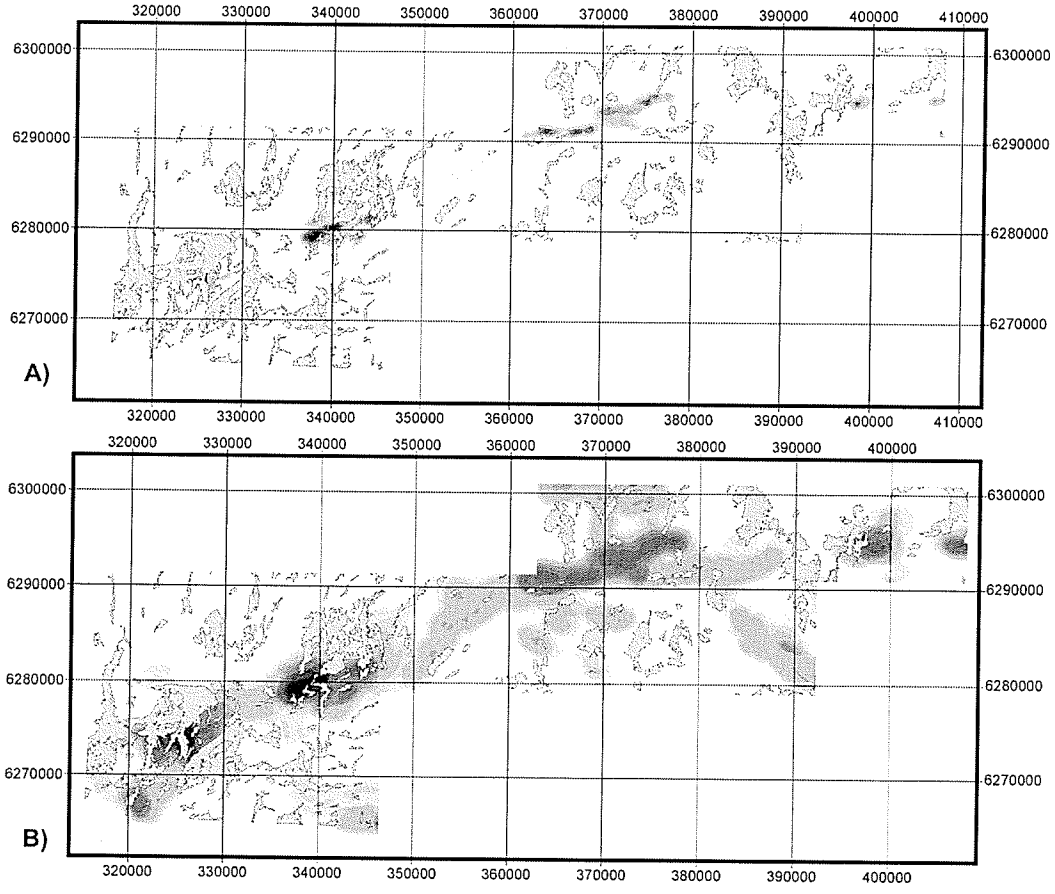

Figure 6.21 Dempster-Shafer belief (a) and fuzzy logic (b)stratigraphic potential output maps. White indicates low relative potential; black indicates high relative potential (linear scale).

6.3.3 VMS Spatial Model: Cu-Zn Component

Hydrothermal fluids circulating through a sequence of rocks react with the adjacent rocks and dissolve metals. Most volcanic rocks and immature sedimentary rocks contain enough sulphur and metals to produce a VMS deposit, however, fluids circulating through units with higher background levels of Cu and Zn may have a higher probability of producing an economic VMS deposit. Cu and Zn data from samples used to determine the geochemical subdivisions of volcanic rocks in the belt (Zwanzig et al., 1999) were used to locate areas of higher background Cu and Zn. The sample distribution is sparse, so no attempt was made to contour the data. Instead average values for all Cu and Zn for each volcanic subdivision were calculated. Anomalous values, those samples that significantly skew the mean, were excluded form the calculations. Average values for the geochemical subdivisions were calculated separately for Cu and Zn. Uncertainty in this approach is considered higher than the other components of the spatial model, because of the sparse number of samples for some geochemical subdivisions. A maximum weight of 0.5 and an uncertainty value of 0.4 were applied to the Cu-Zn potential.

Hydrothermal fluids may transport the metals in solution, so Cu - Zn bearing units are represented by proximity maps. Proximity zones were set at 200 m intervals with a maximum extent of 2000 m. Weighting is highest within the geochemical subdivisions and decreases outwards using a linear function.

6.3.3.1 Cu-Zn Potential Combination

Once averages were calculated for each geochemical subdivision, units were grouped together based on weight ranges. This process was completed separately for Cu and Zn (Figure 6.22). The proximity maps generated for each group were combined and the Cu and Zn output maps were reclassified to 64 levels. The two output maps were then combined to produce a Cu-Zn potential map, which were subsequently reclassified to 64 levels before combination with the other sub-potential maps. Figure 6.23 shows the Dempster-Shafer belief and fuzzy logic Cu-Zn potential output maps.

6.3.4 VMS Spatial Model: Geophysical Factor

Massive sulphide lenses commonly comprise pyrite, pyrrhotite, sphalerite, chalcopyrite, and magnetite. These minerals combine to give deposits distinctive electrical conduction characteristics, high magnetic susceptibility and high density (Ascough, 1999). For this reason geophysics has an important role in the detection of VMS deposits. Most Cu-Zn and Zn-Pb-Cu deposits are good electrical conductors and have significant electrical contrast with their host rocks. For VMS deposits to be good conductors they must have a high percentage of iron sulfides, > 60%, and the sulfides must be in contact with one another. If the iron sulfides are not in contact, the deposit may be a poor conductor. Magnetite and pyrrhotite are highly magnetic minerals and their presence in many VMS deposits commonly produces strong magnetic signatures relative to the surrounding rock. Combination of TF magnetic data with VLF-EM data can provide excellent prioritization of conductors, and therefore, VMS potential (Ascough, 1999).

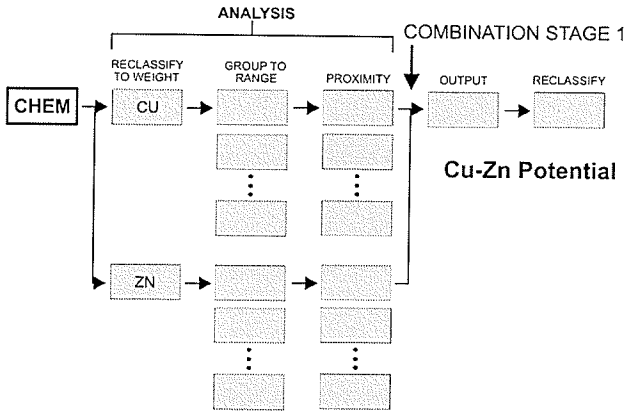

Figure 6.22 Cu - Zn Potential flow chart for analysis and combination. Base data set is the 1:250 000 geochemical subdivisions for volcanic rocks (CHEM). CU copper; ZN zinc.

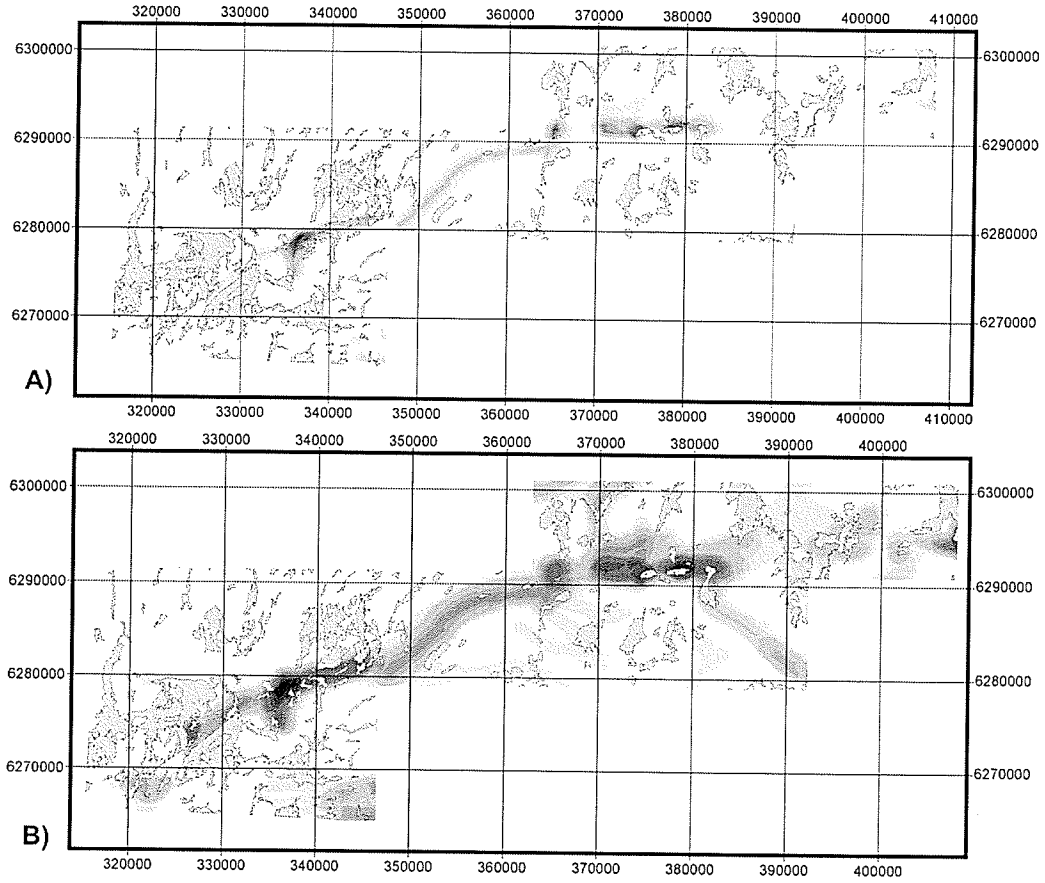

Figure 6.23 Dempster-Shafer belief (a) and fuzzy logic (b) Cu-Zn potential output maps. White indicates low relative potential; black indicates high relative potential (linear scale).

Magnetic and VLF data sets were set at 255 levels and weights were applied. Maximum weight for the VLF data was set to 0.7, whereas for TF magnetic data a maximum of 0.65 was used (Table 6.7). VLF data is weighted slightly higher than the magnetic data, because of a more shallow penetration depth (see section 6.2.2). VMS deposits are also commonly good electrical conductors. Uncertainty was set at 0.2 for the VLF and TF geophysical data sets. For the VLF data ortho and line quadrature channels were used. There are two major power lines that exist in the area and are visible in the VLF survey data. Combination of the ortho and line quadrature data sets partly decreased the effects of the power lines. Further combination with TF survey data and the heat, stratigraphic, and Cu-Zn potential maps show no significant effect of the power lines on the VMS potential output maps.

6.3.4.1 Geophysical Factor Combination

Combination of the ortho and line quadrature VLF data sets was completed using a straight multiplication of the two input maps. Multiplication was used because weighting of the two maps was not necessary. The resulting output VLF potential map was reclassified to 64 levels before combining with the TF magnetic data (Figure 6.24). The output for the geophysical factor was set to a maximum of 0.7 and reclassified to 64 levels for the three geophysical surveys. Uncertainty was set to 0.2 for both VLF and TF input maps. The uncertainty value is set relative to the three other components of the VMS spatial model. The degree of uncertainty for geophysical factor is considered low, and is set to the same value as the heat and stratigraphic components. Figure 6.25 shows the geophysical factor output for Fuzzy Logic and Dempster-Shafer methods.

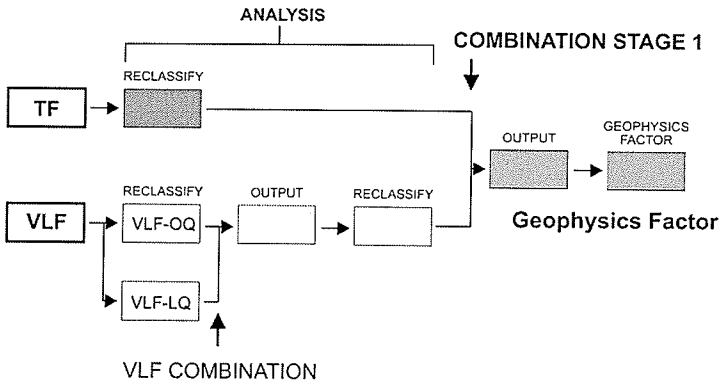

Figure 6.24 Geophysics Factor flow chart for combination. Base data sets are the total field (TF) and very low frequency electromagnetic (VLF) regional surveys 105, 138, and 182 (see Table 5.3). VLF-OQ orthoquadrature; VLF-LQ linequadrature.

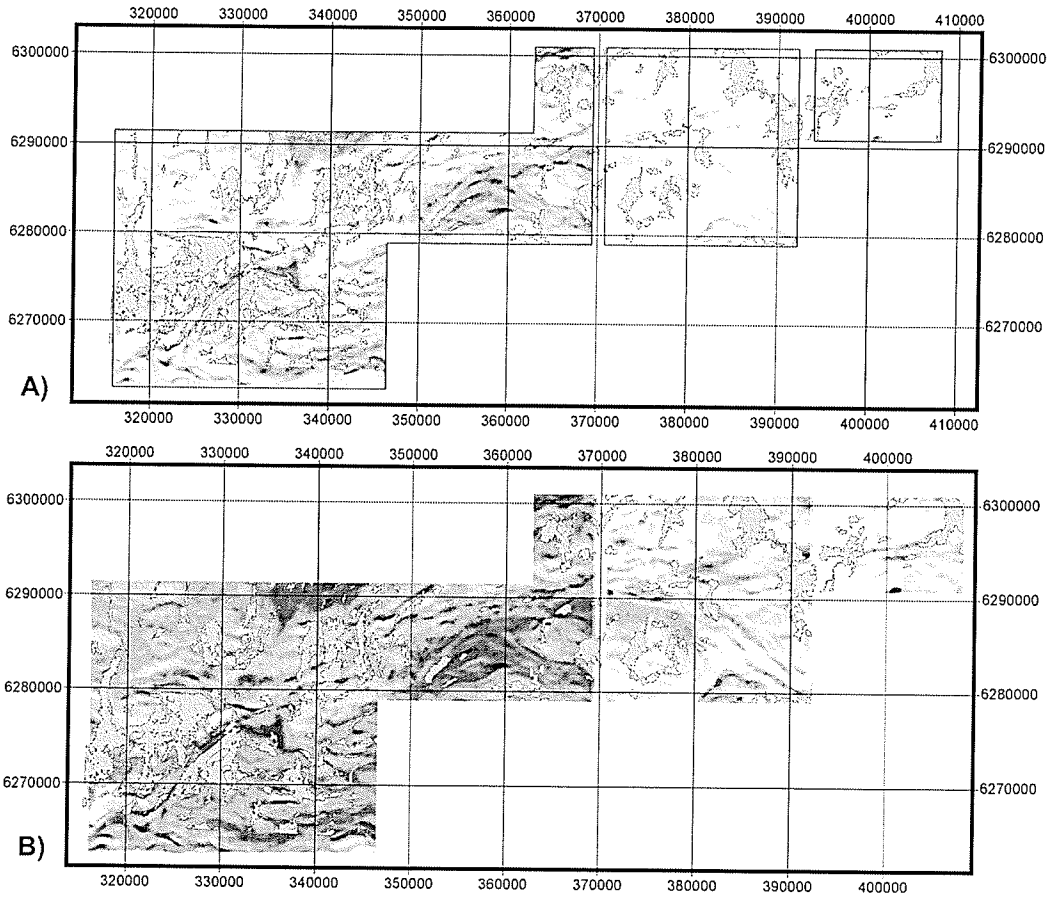

Figure 6.25 Dempster-Shafer belief (a) and fuzzy logic (b) Geophysical Factor potential output maps. White indicates low relative potential; black indicates high relative potential (linear scale) for parts of the three geophysical surveys used (outline in (a)).

6.3.5 VMS Spatial Model: VMS Combination

The VMS spatial model is made up of four main components; heat, stratigraphy, Cu-Zn, and the geophysics factor. Maximum weights are set for the heat source component, stratigraphic component, Cu - Zn component, and geophysical factor are show in Table 6.8. Combination of sub-potential maps includes two output VMS spatial model potential maps. The first combines all four sub potential maps, whereas the second does not include the Cu - Zn potential map (Figure 6.26). The Cu - Zn potential was left out in the second output owing to the confidence level in the Cu -Zn potential map. Comparisons between the two outputs show that the Cu - Zn potential did not change the output potential significantly. Figure 6.27 shows the VMS potential maps using the Fuzzy Logic and Dempster-Shafer data fusion methods respectively. Each of the maps are shown with respect to the three geophysical survey areas. High potential areas shown in figures 6.26 are discussed in detail in section 7.3 Output and Testing.

TABLE 6.8: VMS Sub-potential Spatial Model Weighting

Component	Maximum Weight FL(1) DS (B, D, U) (2)		Minimum Weight
Heat Source Potential	0.7	0.49, 0.31, 0.2	0.01 (3)
Stratigraphy Potential	0.8	0.64, 0.16, 0.2	0.01
Geophysics	0.7	0.49, 0.31, 0.2	0.01
Cu – Zn	0.5	0.25, 0.35, 0.4	0.01

(1) Fuzzy Logic weight
(2) Dempster-Shafer weight (Belief, Disbelief, Uncertainty). Calculated from fuzzy weight.
A weight of 0.1 is assigned to the area within an intrusive unit

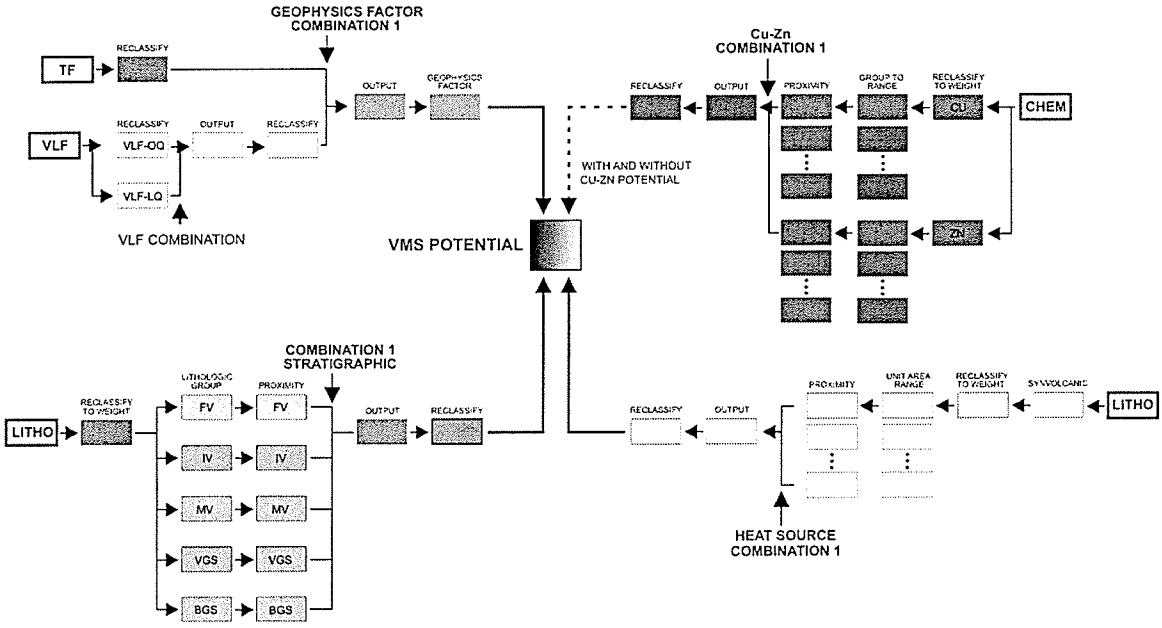

Figure 6.26 Flow chart for analysis and combination stages for the VMS potential combination. VMS potential includes outputs with and without the Cu-Zn sub-potential input map.

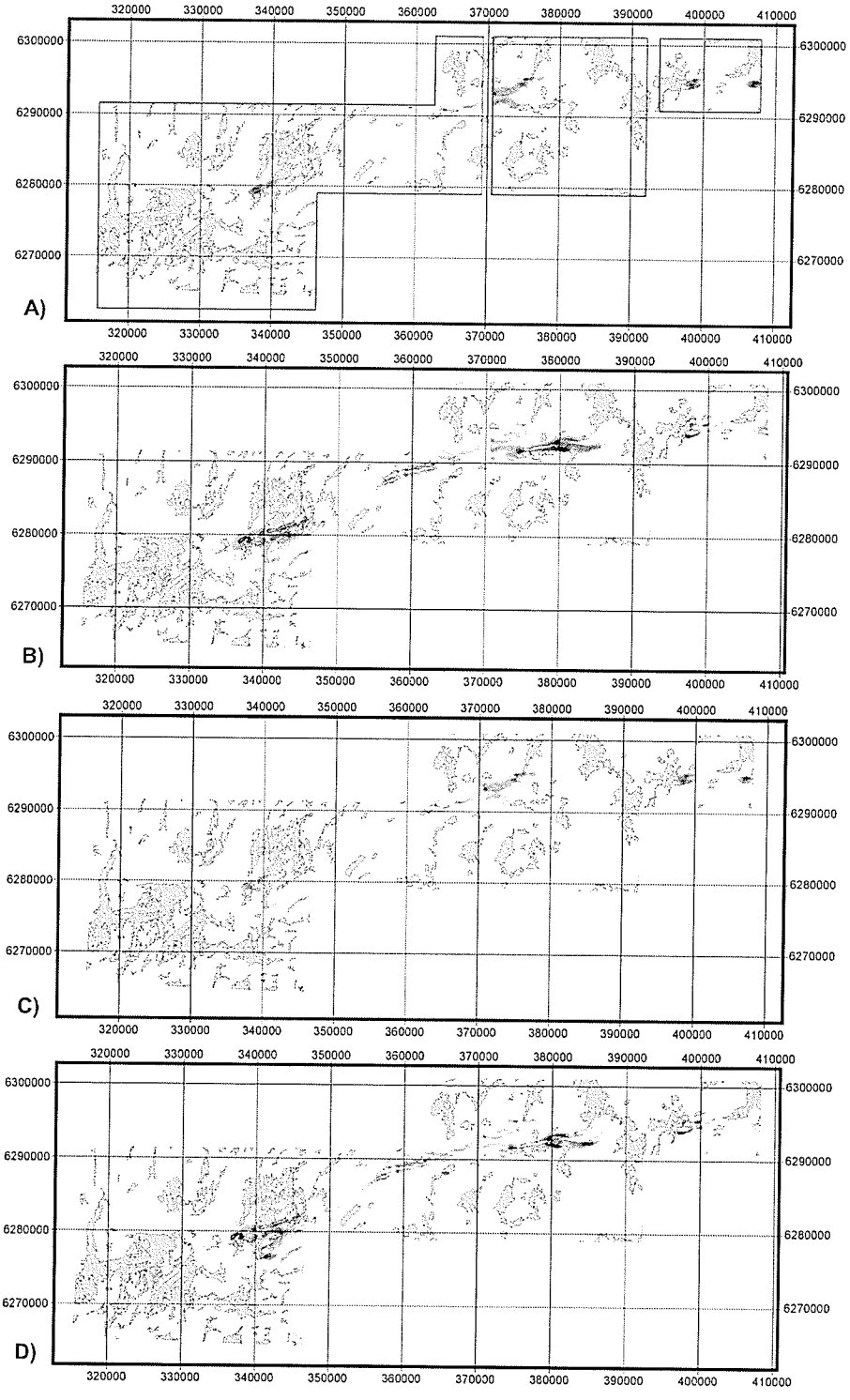

Figure 6.27 Dempster-Shafer belief (a) and fuzzy logic (b)VMS spatial model potential output maps including Cu-Zn sub-potential input. VMS potential maps (c) and (d) do not include Cu-Zn sub-potential input . White indicates low relative potential; black indicates high relative potential (linear scale) for parts of the three geophysical surveys used (outline in (a)).

7 OUTPUT AND TESTING

7.1 Introduction

The accuracy of the potential maps for the shear-hosted and VMS spatial models can be tested using major high potential zones that were accessible for ground truthing. Testing is done by comparing the high potential maps and the locations of known deposits and occurrences, and available literature on the area of interest. Major high potential zones include areas around Cartwright - Hughes Lake; Wasekwan Lake; Gemmel - Counsell Lake; and Dunphy - Laurie Lake areas. The majority of ground truthing focused on areas defined by the shear-hosted model. These areas are shown on potential output maps with respect to the five scenarios, lineament deformation potential with and without faults and the JSZ, and logarithmic and exponential shear-stress functions. Potential output maps that include only lineament deformation potential, as the structural component will be referred to as DL; those that include lineament deformation potential, faults, and JSZ input are referred to as DFJ. For the VMS model potential outputs with and without Cu-Zn potential in the Wasekwan Lake and Dunphy - Laurie Lakes areas will be discussed briefly.

Dempster-Shafer and fuzzy logic methods produce potential maps with similar high potential zones with the main differences occurring locally within those zones. The greatest difference between outputs is commonly between DL and DFJ outputs. This result is not unexpected, because potential maps that include DFJ input data tend to assign high potential near the faults and JSZ. Logarithmic shear-stress functions appear to define larger overall high potential zones with a smaller range of values. Exponential

functions, on the other hand, produce smaller areas of high potential with a greater range of output values.

The testing stage will compare the potential outputs of both Fuzzy Logic and Dempster-Shafer data fusion methods. In total there are 32 potential output maps for the project area. Each of these maps have been divided into three zones based on the three geophysical survey areas. For the shear-hosted spatial model only those potential maps that show significant differences in high potential will be presented. An emphasis will be given on output maps generated using scenario 3, which is considered to be the main mineralization event along the JSZ (Beaumont-Smith and Rogge, 1999). All potential maps are available on the included CD and are listed in appendix A. For a given output potential map pixel values for each of the three zones based on the three geophysical survey areas are displayed on a histogram. Figure 7.1 shows a selection of histograms for four output potential maps. From the histogram high potential zone are defined as the top 5% of the pixel value distribution. These pixels are shown in greyscale in the following potential maps. All other pixels are shown as white, or low potential.

Known occurrences and deposits noted in the following discussion are those described in chapter 3, and in Appendix B and C. Ground truthing data includes the reconnaissance work completed with Chris Beamont-Smith of the Manitoba Geological Survey (MGS) during the 1999 field season; and, additional field work completed during the 2000 and 2001 field seasons. References to sample data in the following sections included geochemical data from Open File 99-13 (Zwanzig et al., 1999), Geological Paper 80-1 (Gilbert et al., 1980), 1999 and 2000 MGS samples, and 2000 and 2001 ground truthing samples, all of which are available on the included CD. Samples

containing > 10 ppb Au are considered anomalous based on the 6.8 ppb threshold value determined by the distribution of gold in volcanic rocks (Saager et al., 1982). Samples that detected gold, but are < 10 ppb will be referred to as trace Au. Samples containing > 500 ppm Cu or Zn are highlighted in the VMS output potential maps.

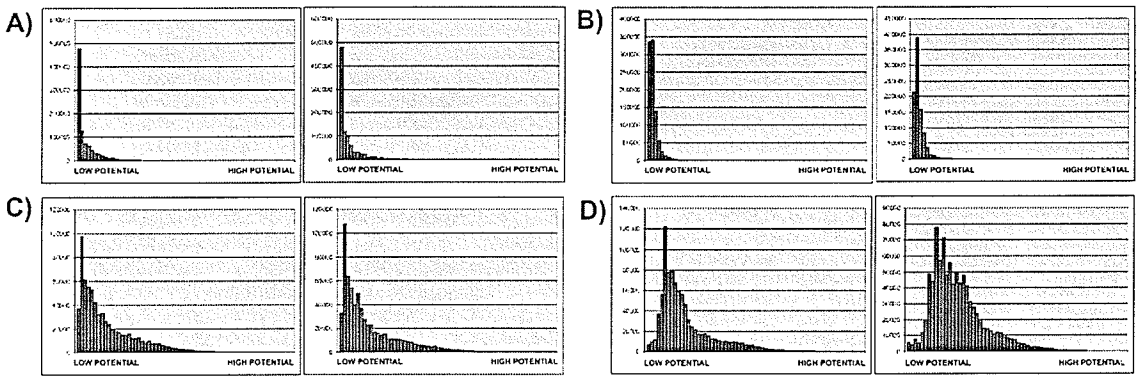

Figure 7.1 Selection of histograms for fuzzy logic and Dempster-Shafer potential maps showing typical distribution of high and low potential values. Shear-hosted (a) and VMS (b) Dempster-Shafer potential map histograms. Shear-hosted (c) and VMS (d) fuzzy logic potential map histograms.

7.1.1 Area 1: Cartwright - Hughes Lake

A semi-continuous high potential zone from the southern part of Cartwright Lake east towards Hughes Lake was present in each of the potential output maps. Three main high potential areas were determined. The extent of the high potential areas varies between the potential output maps. The first area is along the south and southeast shore of Cartwright Lake. The second area is just north of highway 391 between Cartwright and Hughes Lakes. The last main high potential zone is south of Hughes Lake along highway 391. Figure 7.2 shows potential output maps for scenarios 3 and 4 for fuzzy logic and Dempster-Shafer combination methods.

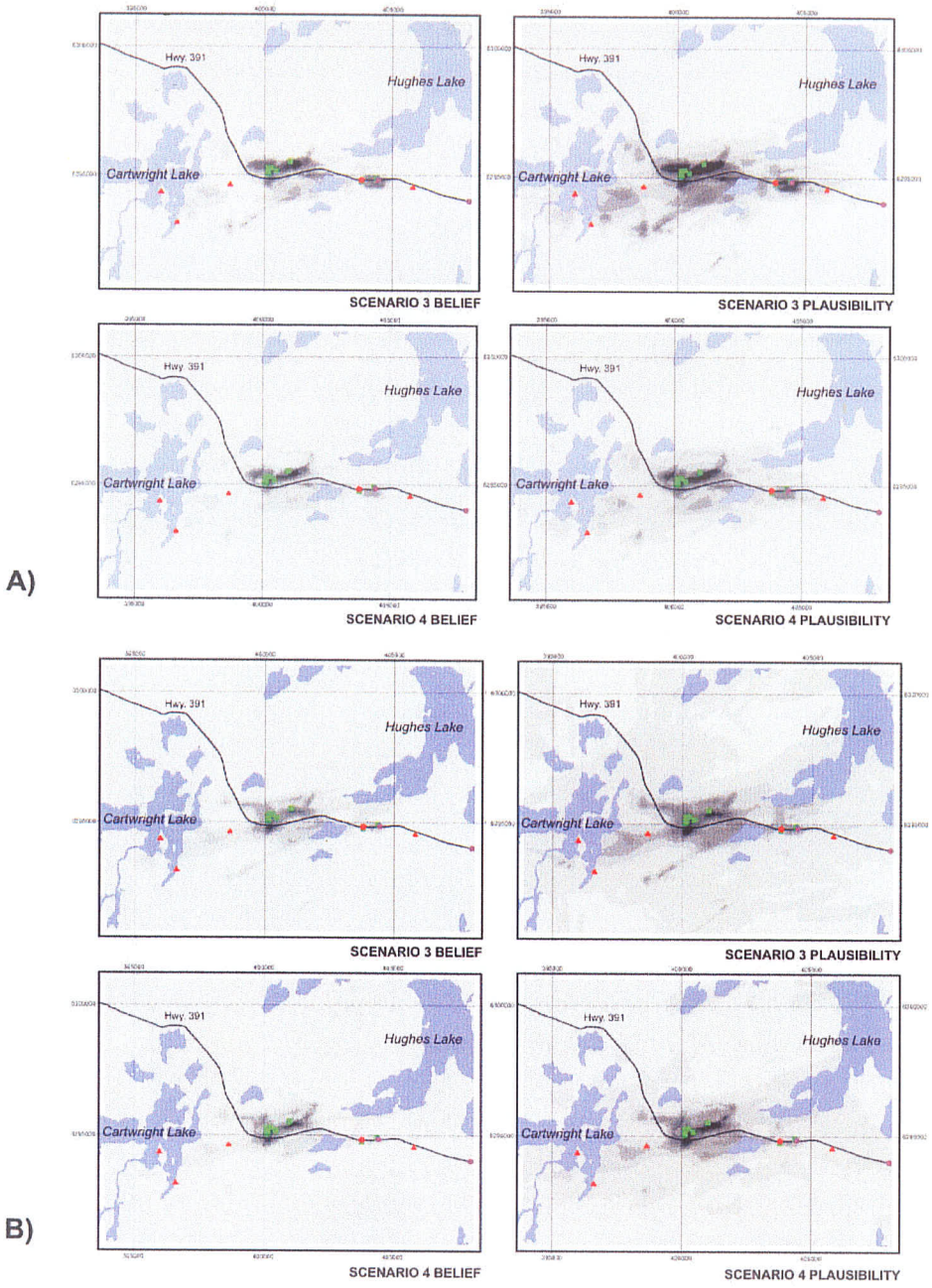

Figure 7.2 Dempster-Shafer combination outputs for Cartwright - Hughes area. Grey-scale levels represent top 5% of pixel value distribution, with relative scale being linear. White indicates low relative potential; black indicates high relative potential. (a) Structure component includes lineament deformation potential. Shear strain function is logarithmic. (b) Structure component includes lineament deformation potential. Shear strain function is exponential. Triangle (red) - known occurrences; Square (green) - ground truth locations; Square (red) - gold occurrences (>10ppb) from ground truth locations; Circle (purple) - Manitoba Geological Survey samples. Circle (red) - gold occurrences (>10ppb) from Manitoba Geological Survey samples.

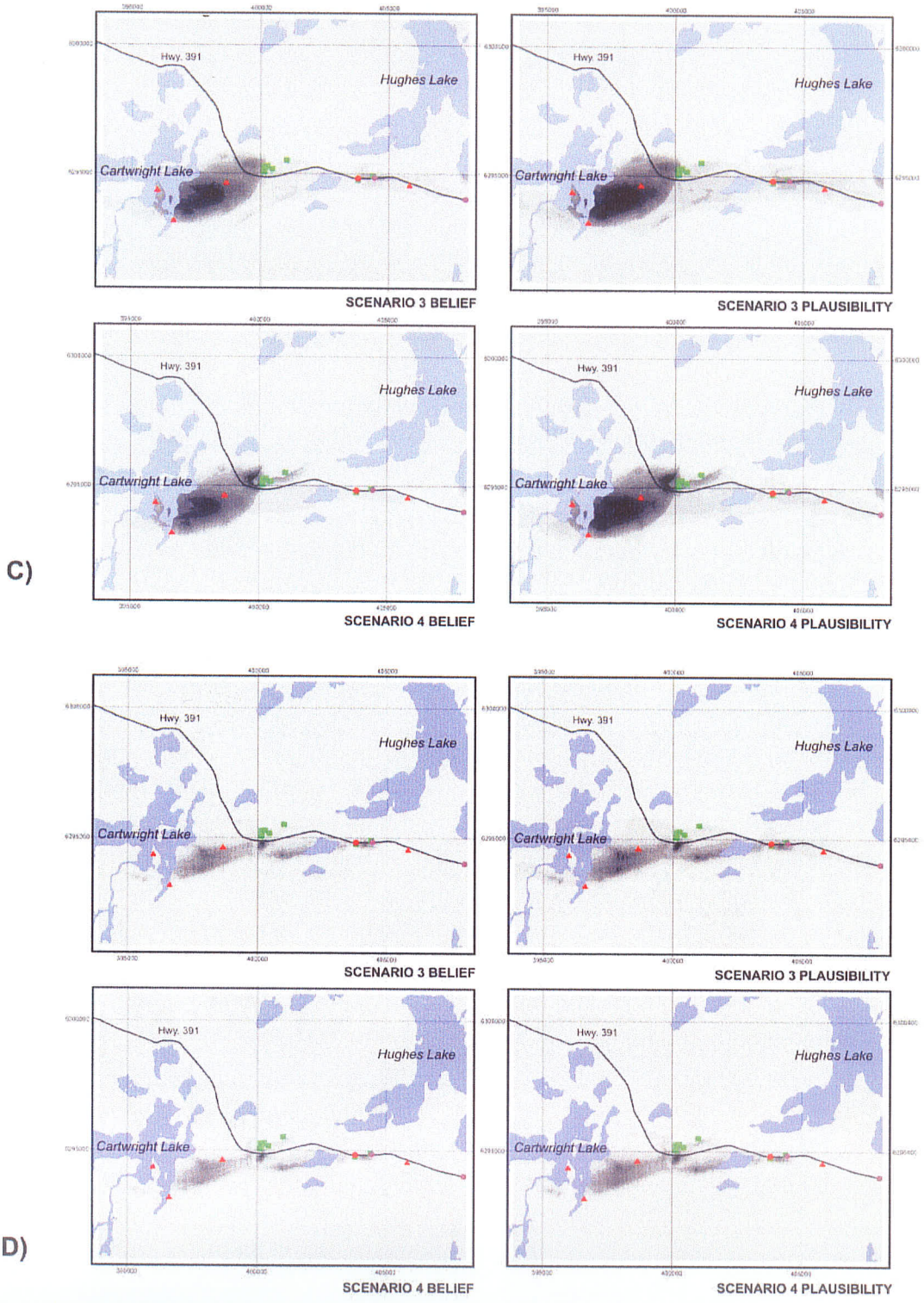

Figure 7.2 cont' Dempster-Shafer combination, (c) Structure component includes lineament deformation, faults and JSZ potential. Shear strainfunction is logarithmic. (d) Structure component includes lineament deformation, faults and JSZ potential. Shear strain function is exponential.

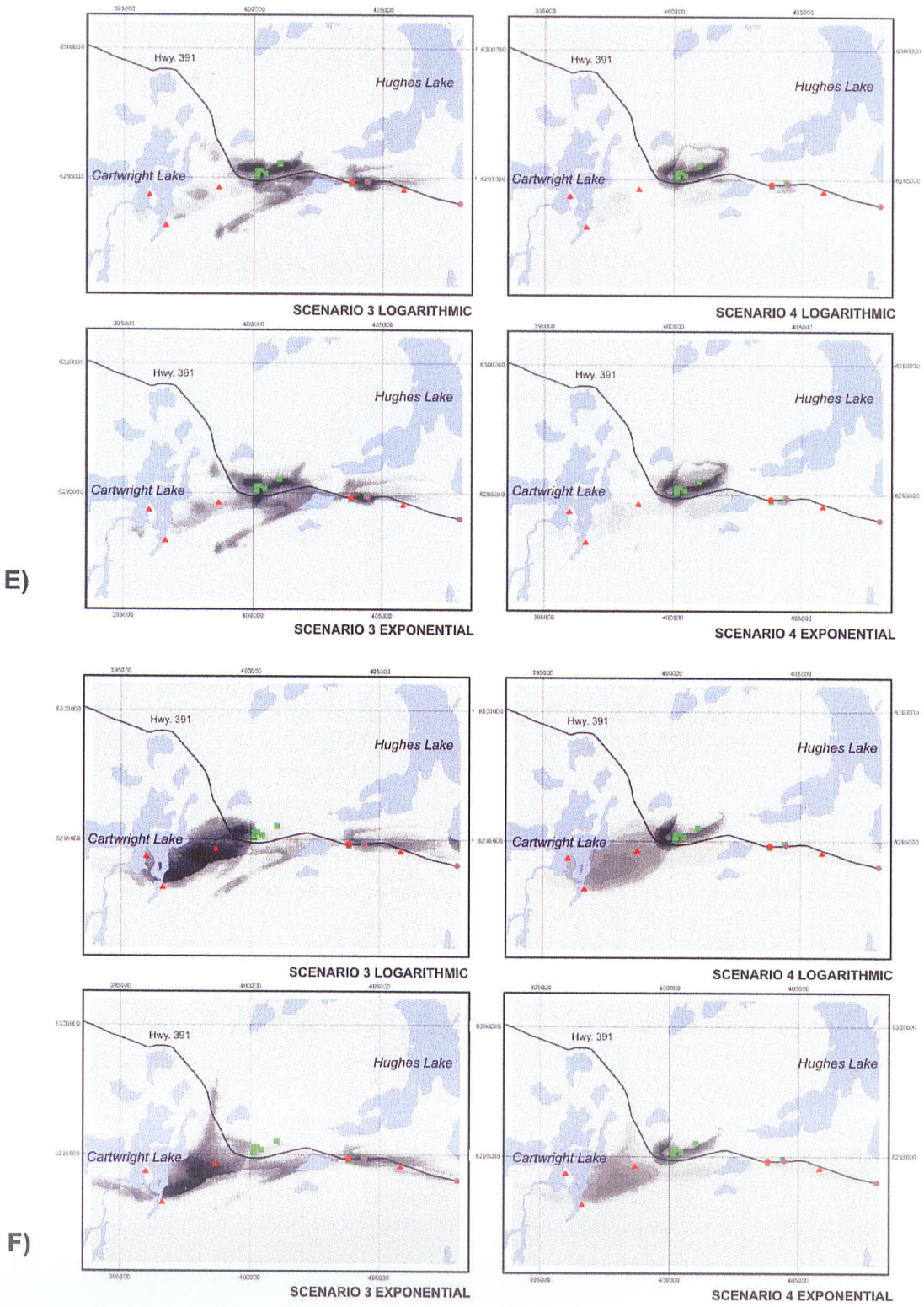

Figure 7.2 cont' Fuzzy logic combination, (e) Structure component includes lineament deformation potential. (f) Structure component includes lineament deformation, fault, and JSZ potential. Shear strain logarithmic and exponential functions.

Potential outputs from scenarios 3 and 5 of the shear-hosted spatial model are similar with only minor differences, as was the case for scenarios 1 and 4. Comparison of the logarithmic and exponential functions used for lineament deformation, faults, and the JSZ potential reveals a consistent difference in the range of output values. The exponential function generally produces a greater range in output values than the logarithmic function, specifically in the Dempster-Shafer potential maps. The major output differences were between DL and DFJ outputs. In this case the focus of high potential is shifted from just north of highway 391 (DL) (Figure 7.2 a, b, and e) to the area southeast of Cartwright Lake (DFJ) (figure 7.2 c, d, and f).

Four occurrences exist in the Cartwright - Hughes Lake area and are shown in figure 7.2. These occurrences are located more along strike of the JSZ. These occurrences lie within or directly adjacent to areas of high potential. Three occurrences are located in the southeast area of Cartwright Lake, an area of high potential that is well defined in the DFJ potential maps. This area is also shows high potential in the DL potential maps. However, the main high potential zone in the DL maps is shifted to the east along strike with the JSZ. Ground truthing in the area between the three occurrences was not possible because of a lack of exposure. The fourth occurrence is located along highway 391 south of Hughes Lake. This occurrence lies within or directly adjacent to the third high potential zone depending on the given potential map.

About 2 km west of the fourth known occurrence is the third high potential zone in the Cartwright-Hughes. Three grab samples taken from this high potential zone contained trace to 53 ppb Au. Two sites along the highway show similar shear-zone

mineralization as is present at the Burnt Timber (BT) open pit gold mine just east of Waskewan Lake (Peck et al., 1998). The area is a high strain zone in mafic and silicified rocks with quartz-iron carbonated veining throughout (Figure 7.3). Trace sulphides are disseminated within the host rock and within the quartz - iron carbonate veins. Coarse pyrite, 0.5 mm, can be found on freshly broken surfaces. North of the highway the strain level appears lower within alternating bands of siliceous units. Locally the rocks are fissile, whereas in other places brittle deformation is prominent (Figure 7.4). Quartz-feldspar veining occurs parallel to sub parallel to the main strain fabric. These veins are folded and are commonly well rusted (Figure 7.5).

Ground truthing was completed also north of highway 391 between Cartwright and Hughes Lakes (400000, 6295000; Figure 7.2). The first stop in this area was along a ridge of outcrop where Sickle conglomerate is in contact with mafic volcanic rocks. At the contact the basaltic rocks were highly strained, however, the strain level deceases quickly from the contact. Deformed pillows were found about 30 m north of the contact. Pseudotachylite was observed locally between the semi-deformed pillows and the contact. Coarse and fine sulphides were locally found within the basaltic rocks.

About 800 m west of the Sickle contact a ridge of good exposure was surrounded by thick overburden and swamp. This area included unstrained pillow basalts, high strain silicified rocks, and at least one quartz porphyry dike. Boudin structures, quartz veining, and pseudotachylite were found within the higher strain areas (Figure 7.6). The silicified rocks also contained iron carbonate veining. Coarse pyrite and fine disseminated sulphide mineralization was found in the silicified high strain fissile rocks proximal to a

quartz porphyry dike. Sulphides were also found within the quartz porphyry dike. Five grab samples were taken from the area with only one containing trace amounts of Au.

Figure 7.3 Shear zone fabric with quartz-iron carbonate veining similar to the BT open pit mine. Easting 404391, northing 6294885; UTM Zone 14, NAD83.

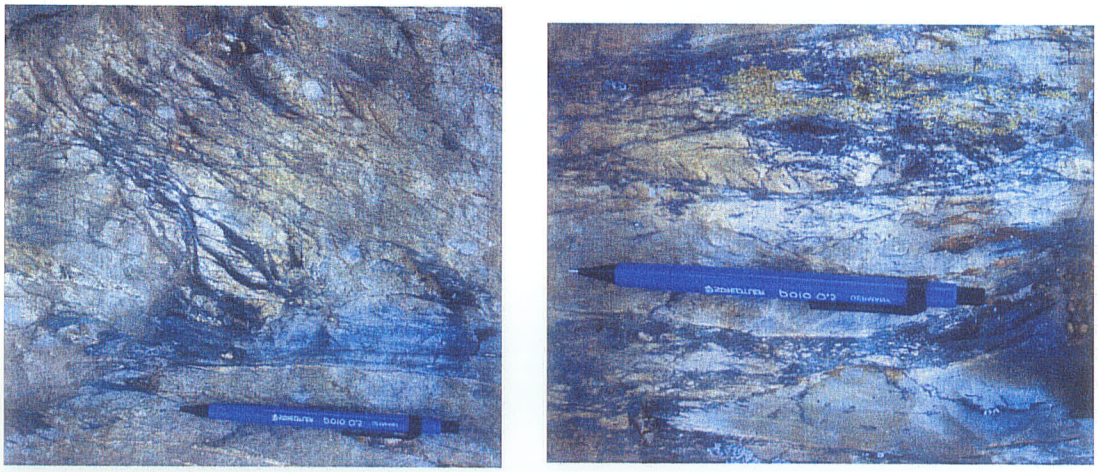

Figure 7.4 Brittle deformation in silicified units across highway from shear fabric shown in figure 7.3. Easting 404391, northing 6294885; UTM Zone 14, NAD83.

Figure 7.5 Quartz-feldspar-carbonate veins folded by main strain fabric. Easting 404391, northing 6294885; UTM Zone 14, NAD83.

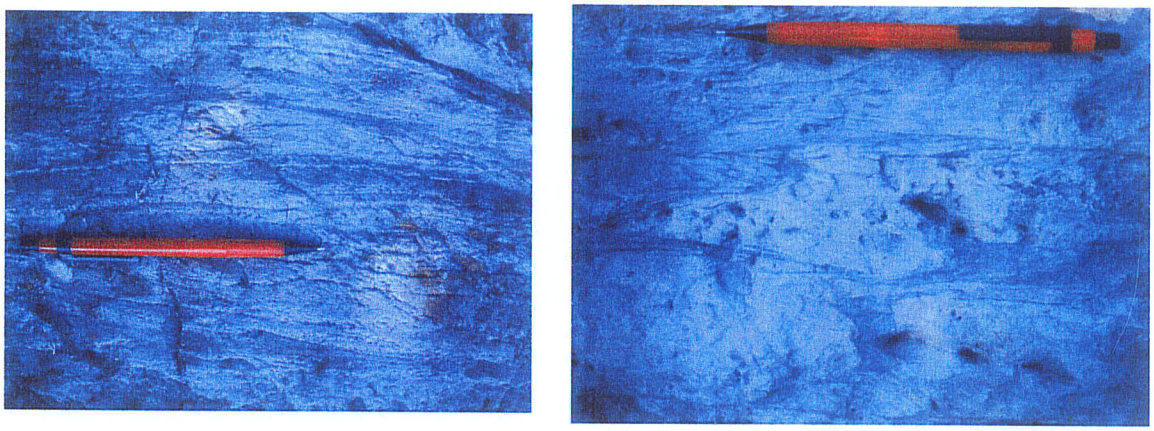

Figure 7.6 High strain fabric (a) and pseudotachylite (b) in silicified rocks. Easting 400150, northing 6295092; UTM Zone 14, NAD83.

7.1.2 Area 1: Wasekwan Lake

Three main areas of high potential are defined for the Wasekwan Lake area. They include; 1) along the north shores of Franklin and Foster Lakes trending towards Wasekwan Lake; 2) a continuation of 1) trending east from the northeast shore of Wasekwan Lake; and, 3) the southeastern part of the output area (Figure 7.7). The most

prominent zone in all output maps is 1); however, 2) is also well represented in each of the maps. Zone 3) occurs on all except four output maps, but is not always a prominent high potential zone. Logarithmic and exponential functions, used for lineament deformation, faults, and the JSZ, produce only minor differences in the Dempster-Shafer output potential maps. For this reason only logarithmic potential maps will be shown here (Figure 7.7 a and b). Exponential output maps are included in the appendix A. The fuzzy logic output potential maps shown will include both logarithmic and exponential functions (Figure 7.7 c and d). The only significant difference in high potential zones occurs between DL and DFJ potential maps. DFJ high potential is focused primarily north of Foster Lake next to McVeigh Lake, whereas all three areas are prominent on the DL outputs.

There are six known occurrences, one deposit, and a number of anomalous Au grab samples in the Wasekwan area (7.7). First and foremost is the location of the past producing Burnt Timber open pit gold mine. This deposit produced 80 000 ounces of gold from 1993 - 1996 and is hosted in shear laminated silicified and carbonatized volcanic and sedimentary rocks in the hanging wall of a post-mineralization fault. The mine is located just a few kilometers east of the north east shore of Wasekwan Lake along the east trending number 2) high potential zone (385000, 6292000: Figure 7.7). In a number of output maps this east trending high potential zone is highlighted by two high potential sub zones. The western sub zone is located directly adjacent to, or partially on, the BT pit. Also of interest in this area are two known occurrences and anomalous gold values obtained from groundwork completed during the 1999 field season.

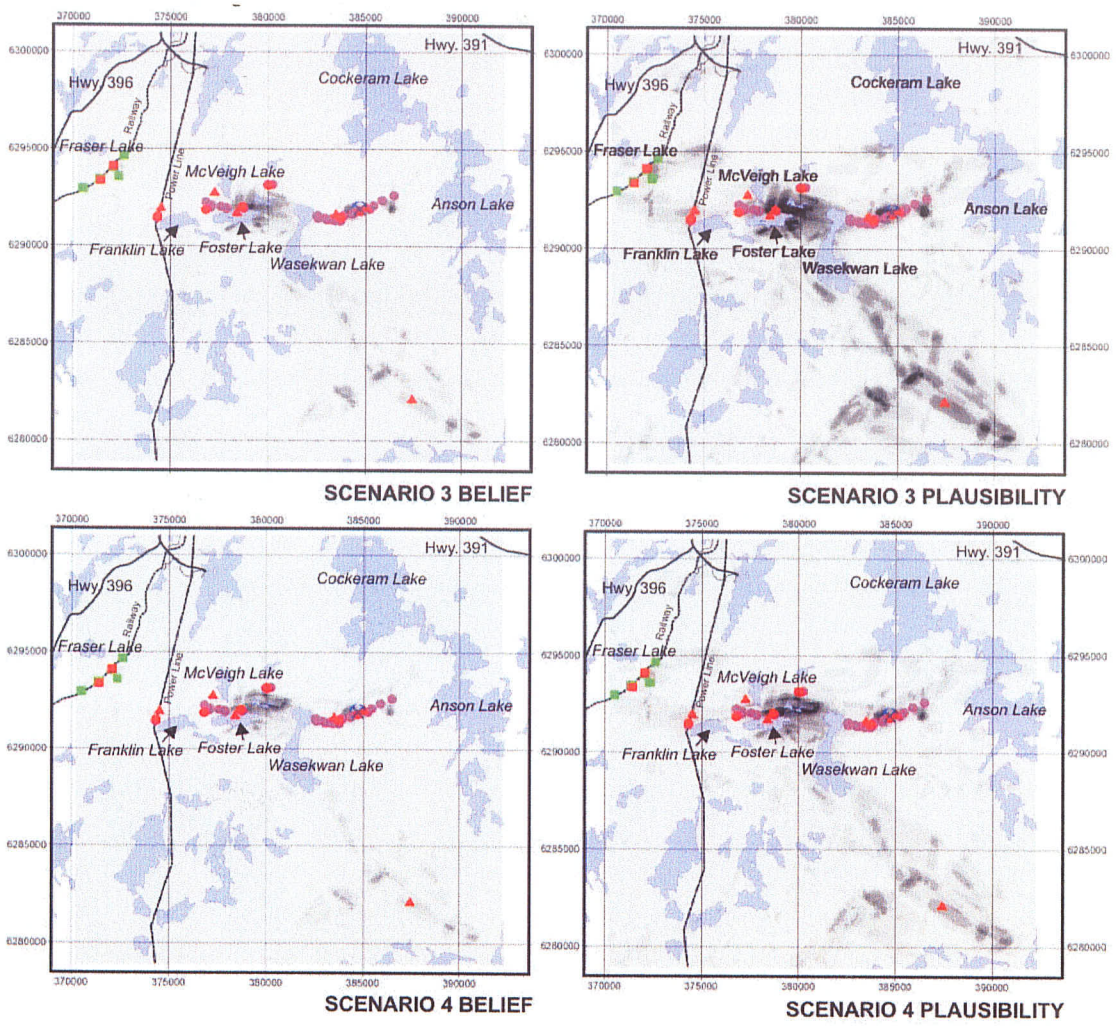

Figure 7.7a Dempster-Shafer combination outputs for Wasekwan Lake area. Grey-scale levels represent top 5% pixel value distribution, with relative scale being linear. White indicates low relative potential; black indicates high relative potential. Structure component includes lineament deformation potential. Shear strain function is logarithmic. Triangle (red) - known occurrences; Square (green) - ground truth locations; Square (red) - gold occurrences (> 10 ppb) from ground truth locations; Circle (purple) - Manitoba Geological Survey samples; Circle (red) - gold occurrences (>10 ppb) from Manitoba Geological Survey samples.

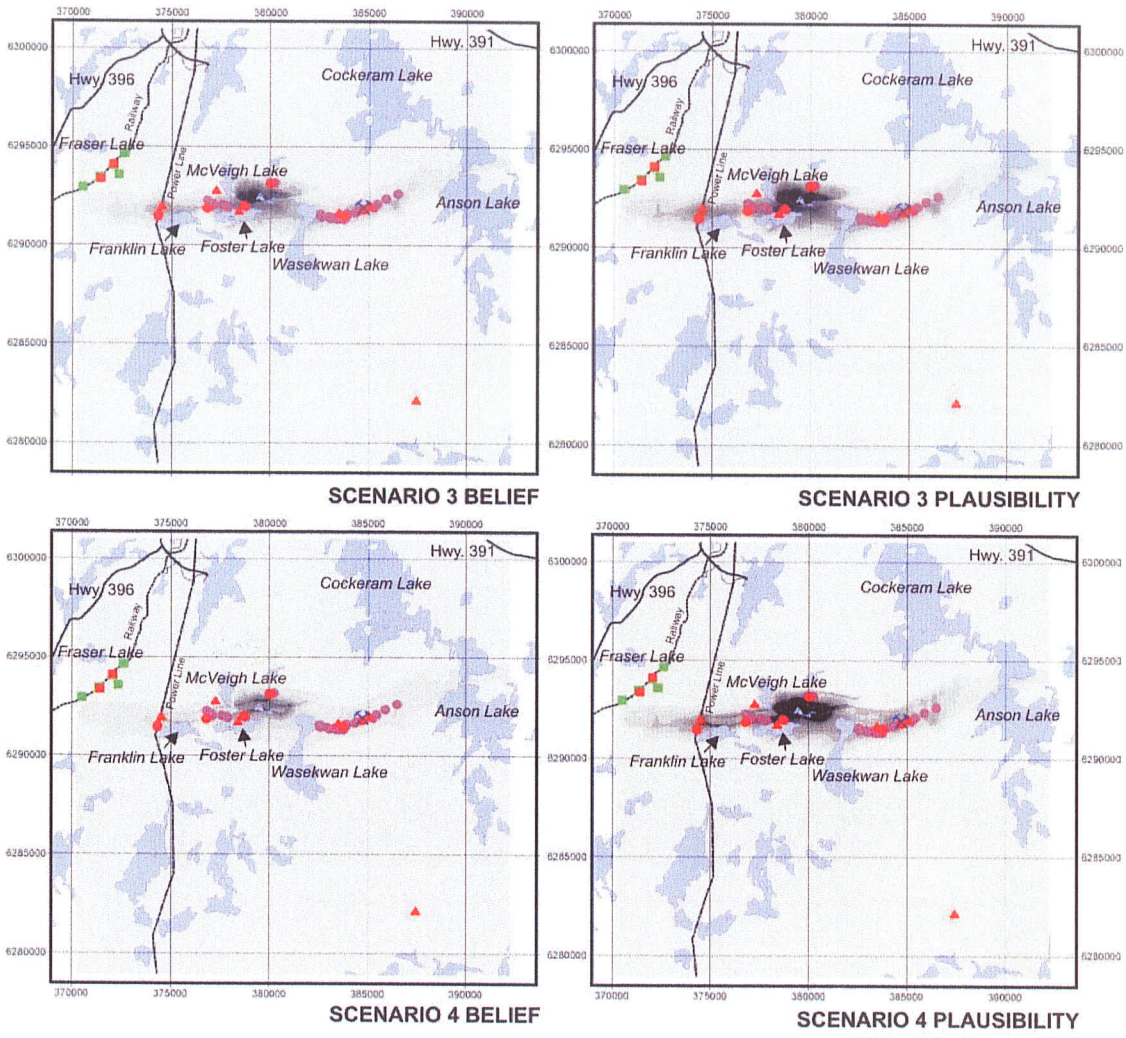

Figure 7.7b Dempster-Shafer combination. Structure component includes lineament deformation, faults, and JSZ potential. Shear strain function is logarithmic.

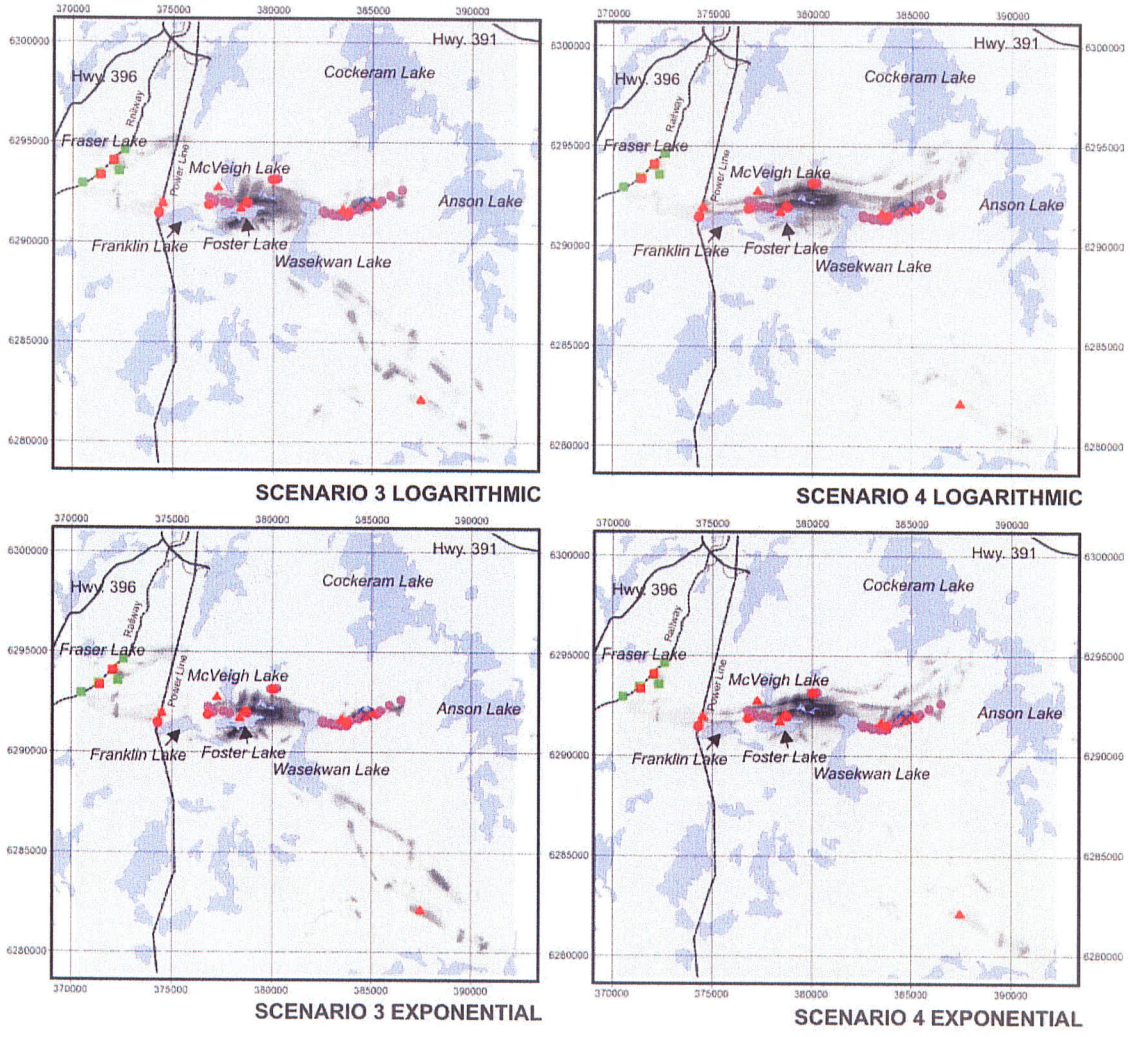

Figure 7.7c Fuzzy logic combination. Structure component includes lineament deformation potential. Shear strain logarithmic and exponential functions.

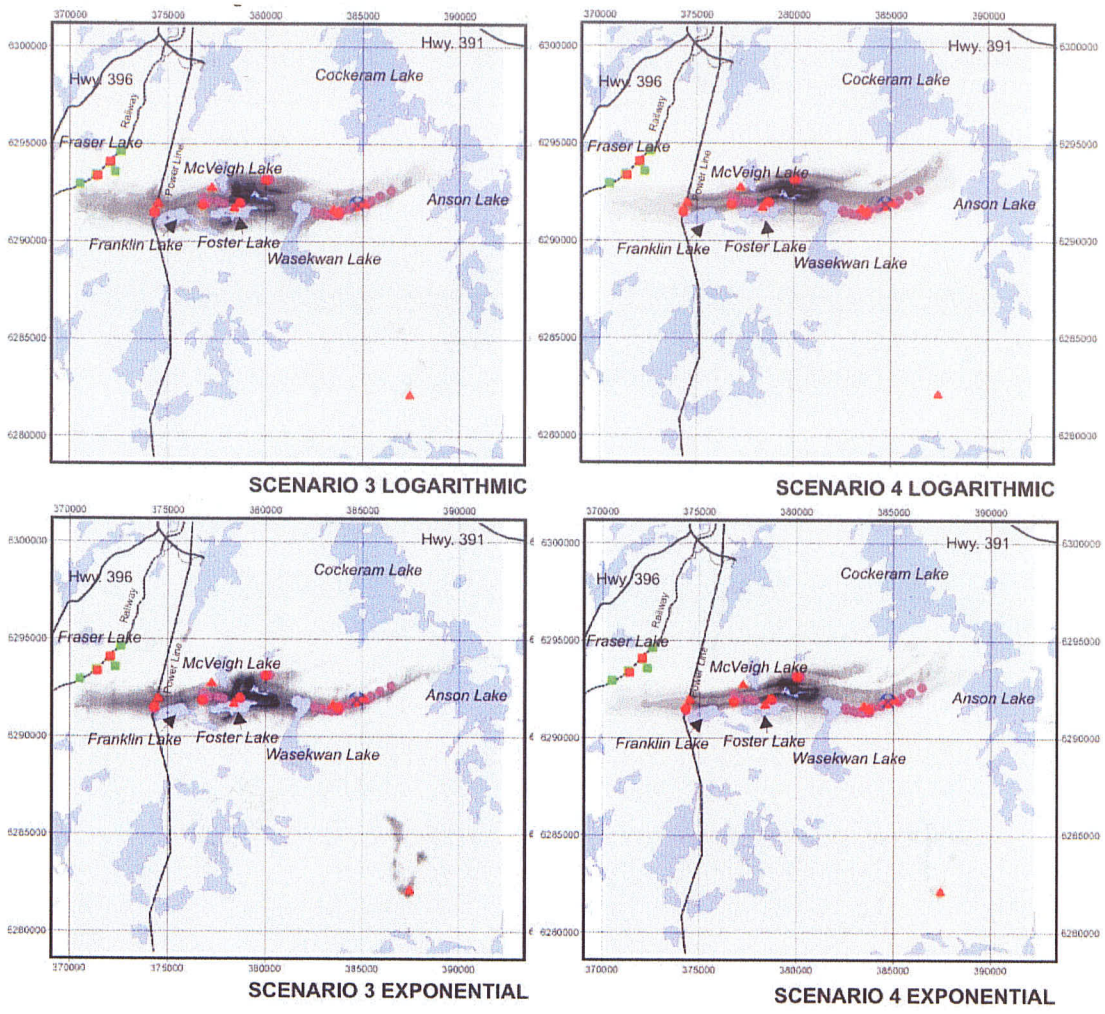

Figure 7.7d Fuzzy logic combination. Structure component includes lineament deformation faults, and JSZ potential. Shear strain logarithmic and exponential

A preliminary structural analysis and gold metallogeny investigation (Beamont-Smith and Rogge, 1999) was completed in and around the BT pit. The study area extended westward along the north shore of Foster and Franklin Lakes to the main Lynn Lake power line. Deformation in this area is controlled by the JSZ and gold mineralization appears to be related to dextral shearing during the D_2 event. From the BT pit westward to the northwest of Franklin Lake numerous occurrences of sulphide mineralization and quartz veining were observed in association with high strain ductile

deformation. In the area north of Franklin and Foster Lakes there are three known occurrences and anomalous grab samples containing trace to 32 ppb Au. High potential sites 1) and 2) lie along the main trend of the JSZ.

Another known occurrence is found about 8 km southeast of Wasekwan Lake in the Miskwa Belt (387500, 6282000: Figure 7.7). There is a high potential zone directly associated with the occurrence in most of the potential maps. There are also other high potential zones northwest along the main trend of the supracrustal rocks of the Miskwa Belt. Ground truthing was not completed in the area because there is no road access. Access is only possible be plane or by foot.

Six VMS output potential maps were produced and are shown in figure 7.8. There is a significant difference between the output maps for the fuzzy logic and Dempster-Shafer methods. In the fuzzy logic case the area of maximum potential is a high potential area between Waskewan, Foster and McVeigh Lakes, whereas for the Dempster-Shafer method the area of maximum potential is northwest of Franklin and McVeigh Lakes along the railway tracks. The area of maximum potential in the Dempster-Shafer output maps includes three known VMS occurrences. A fourth known occurrence is located a few kilometers south east of Wasekwan Lake. The Dempster-Shafer outputs show a small high potential zone at this location. Two samples, one collected just northwest of Franklin Lake in a high potential zone, and the other about 2.5 km west of Franklin Lake adjacent to a high potential zone, gave Cu values of 718 and 792 ppm respectively.

Ground truthing in the Wasekwan area focused on the area south of Fraser Lake along the railroad tracks. Moving from southwest to northeast nine stops were made

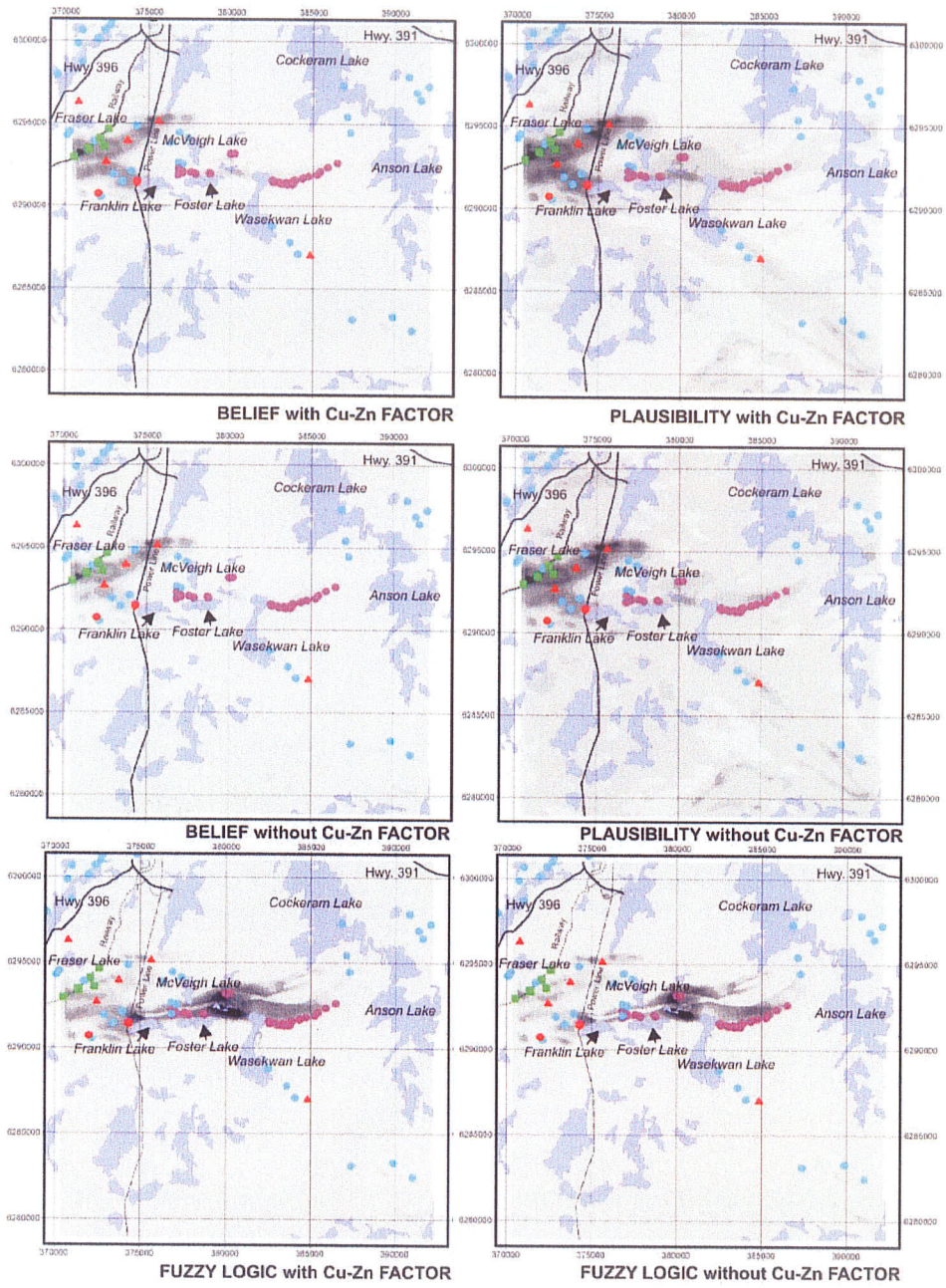

Figure 7.8 Dempster-Shafer and fuzzy logic combination VMS outputs for Wasekwan Lake area. Grey-scale levels represent top 5% of pixel value distribution, with relative scale being linear. White indicates low relative potential; black indicates high relative potential. Includes ouputs with and without Cu-Zn factor. Triangle (red) - known occurrences; Square (green) - ground truth locations; Square (red) - Cu or Zn occurrence (>500ppm) from ground truth locations; Circle (purple) - Manitoba Geological Survey samples. Circle (blue) - Open File 99-13 samples. Circle (red) - Cu or Zn occurrence (>500ppm) from Manitoba Geological Survey and Open File 99-13 samples.

along the tracks. Stop one included alternating siliceous and mafic units that were moderately strained. The siliceous units are porphyritic and aphanitic rhyolites, whereas coarse-grained basalt or amphibolite comprises the mafic units. Rusted zones are common and occur parallel to the main fabric. Disseminated sulphides were found within the some of the rusted zones, but only in trace amounts. The one sample taken from this location gave only 50 ppm Cu. No significant alteration was observed.

The next stop was about 900m northeast along the tracks where good exposure exists on both sides of the tracks. Lippilli-tuff and rhyolitic units are well rusted in places and include chlorite, garnet, and trace amounts of pyrrhotite. Cu and Zn values from one sample were 20 and 75 ppm respectively.

Alternating basalt and rhyolite units with sharp contacts are found another 900 m along the tracks. Elongate pillow basalts with aspect ratios of 10:1 to 20:1, are indicative of the higher level of strain in this location. Amygdales and 1-2 mm garnets occur within the basalts. Circular, centimetre to metre sized, epidote-quartz nodules were observed primarily throughout the basaltic units; they were also found locally in the rhyolitic units. Laterally extensive quartz-epidote zones have been documented stratigraphically under deposits in several massive sulphide districts (Galley, 1993). Rusted grab samples from this location contain 53 - 115 ppm Cu and 129 -161 ppm Zn.

At the last stop about 1 km farther north rhyolitic and mafic volcanic rocks are present. Quartz-epidote nodules elongate parallel with the main fabric were found in both rhyolitic and mafic units. One sample taken from a rusted, amphibole- and biotite-rich mafic volcanic rock with visible sulphides gave Cu and Zn values of 403 and 162 ppm respectively.

7.1.3 Area 3: Gemmel - Councell Lake

The Gemmel - Councell Lake area is divided into two main and one minor high potential areas (Figure 7.9). The first high potential area is a northwesterly trending zone extending from south of Councell Lake to an area about two kilometers northwest of Boiley Lake. The second area begins just east of Digney Lake and continues westward through Gemmel Lake on to Stear Lake. A small, minor high potential zone, was located along the northwest shore of Monique Lake. The Councell - Boiley Lake and Monique Lake areas were poorly defined in the fuzzy logic DFJ outputs (Figure 7.9 f) and they did not occur in the DFJ Dempster-Shafer outputs (Figure 7.9 c and d). This expected owing to the bias generated by including JSZ input into the combination stage (see section 6.5). What is more interesting is the fact that a high potential in the Councell-Boiley Lake area is highlighted on some of the DFJ outputs. DL output maps are shown in Figures 7.9 a, b, and e.

Ground truthing in the Councell - Boiley Lake area focused on an area at the south west corner of Councell Lake and along the southern shore of Boiley Lake. Mafic and intermediate volcanic units south of Councell Lake are in contact with granitic and granodioritic intrusive units to the east and northwest. Rocks in this area are moderately to highly strained. South of Councell Lake a highly silicified protoomylonite to mylonite unit was seen (Figure 7.10). This unit included 1-2% disseminated sulphide minerals with trace Au. About 100 m to the south of the protoomylonite a strong linear fabric occurs within fine bands of primarily mafic-rich material is intermixed with felsic bands. This unit is intruded by felsic dikes up to a metre in thickness and parallel to the main

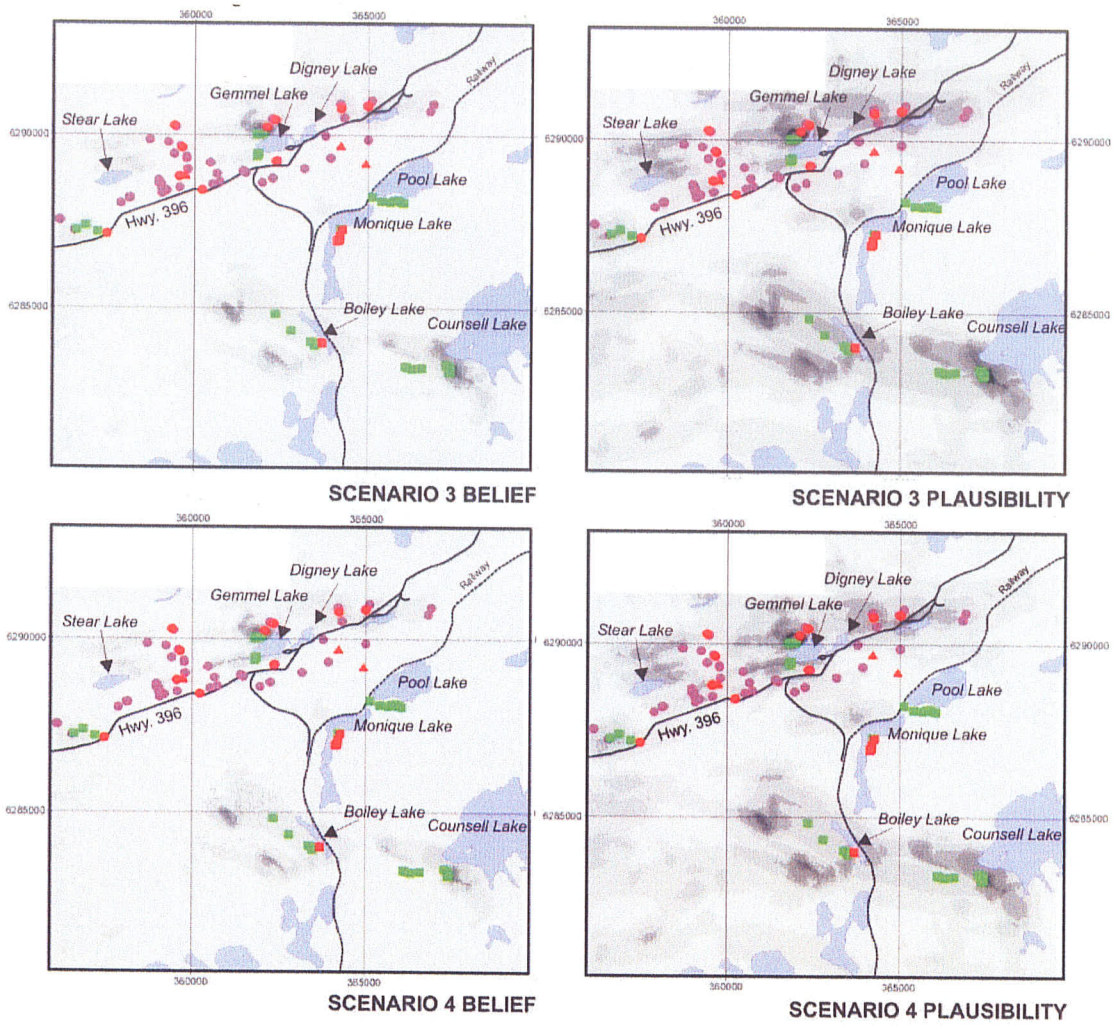

Figure 7.9a Dempster-Shafer combination outputs for the Gemmel-Counsell Lake area. Grey-scale levels represent top 5% of pixel value distribution, with relative scale being linear. White indicates low relative potential; black indicates high relative potential. Structure component includes lineament deformation potential. Shear strain function is logarithmic. Triangle (red) - known occurrences; Square (green) - ground truth locations; Square (red) - gold occurrences (>10 ppb) from ground truth location; Circle (purple) - Manitoba Geological Survey samples; Circle (red) - gold occurrences (> 10 ppb) from Manitoba Geological Survey samples.

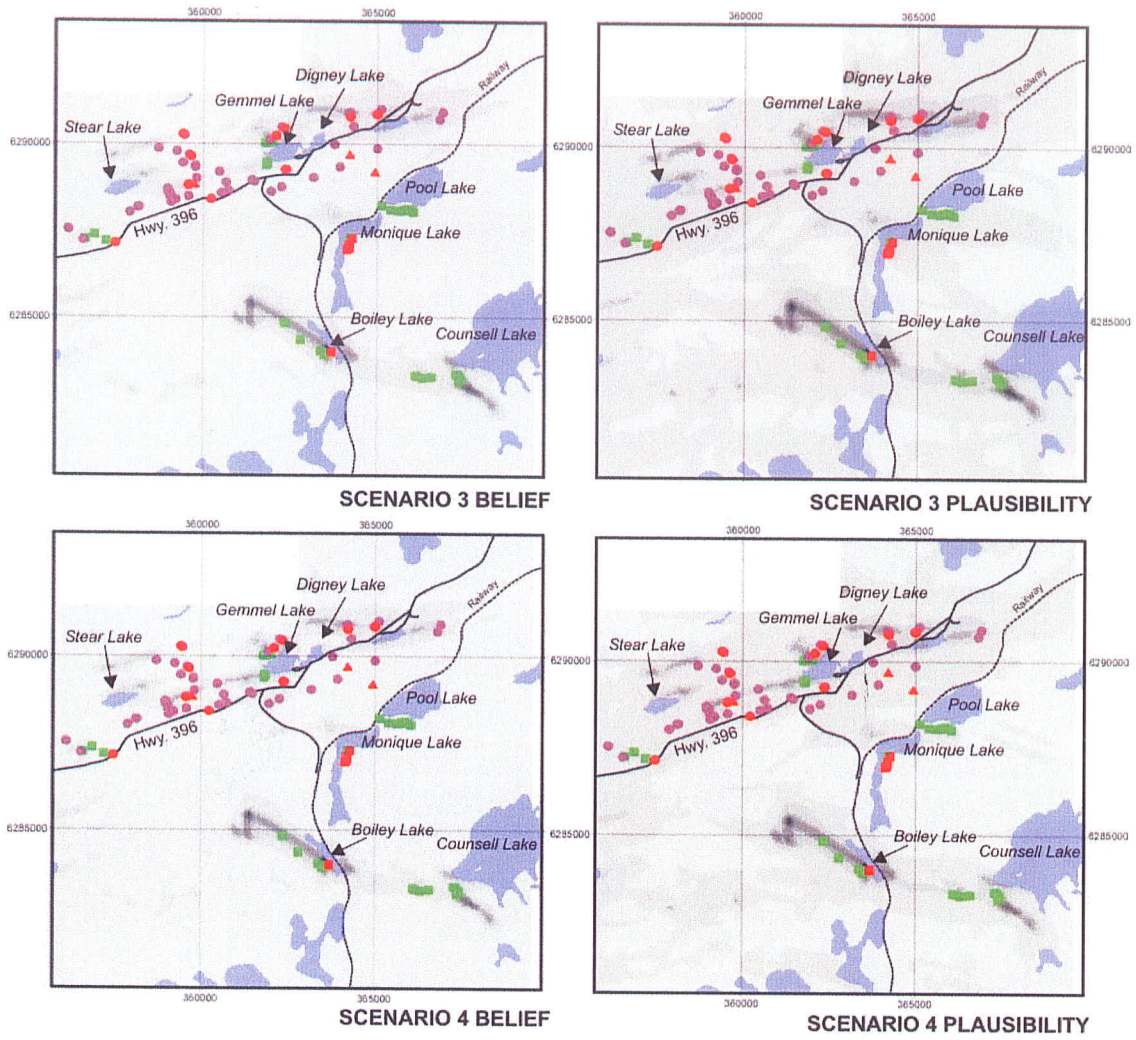

Figure 7.9b Dempster-Shafer combination. Structure component includes lineament deformation potential. Shear strain function is exponential.

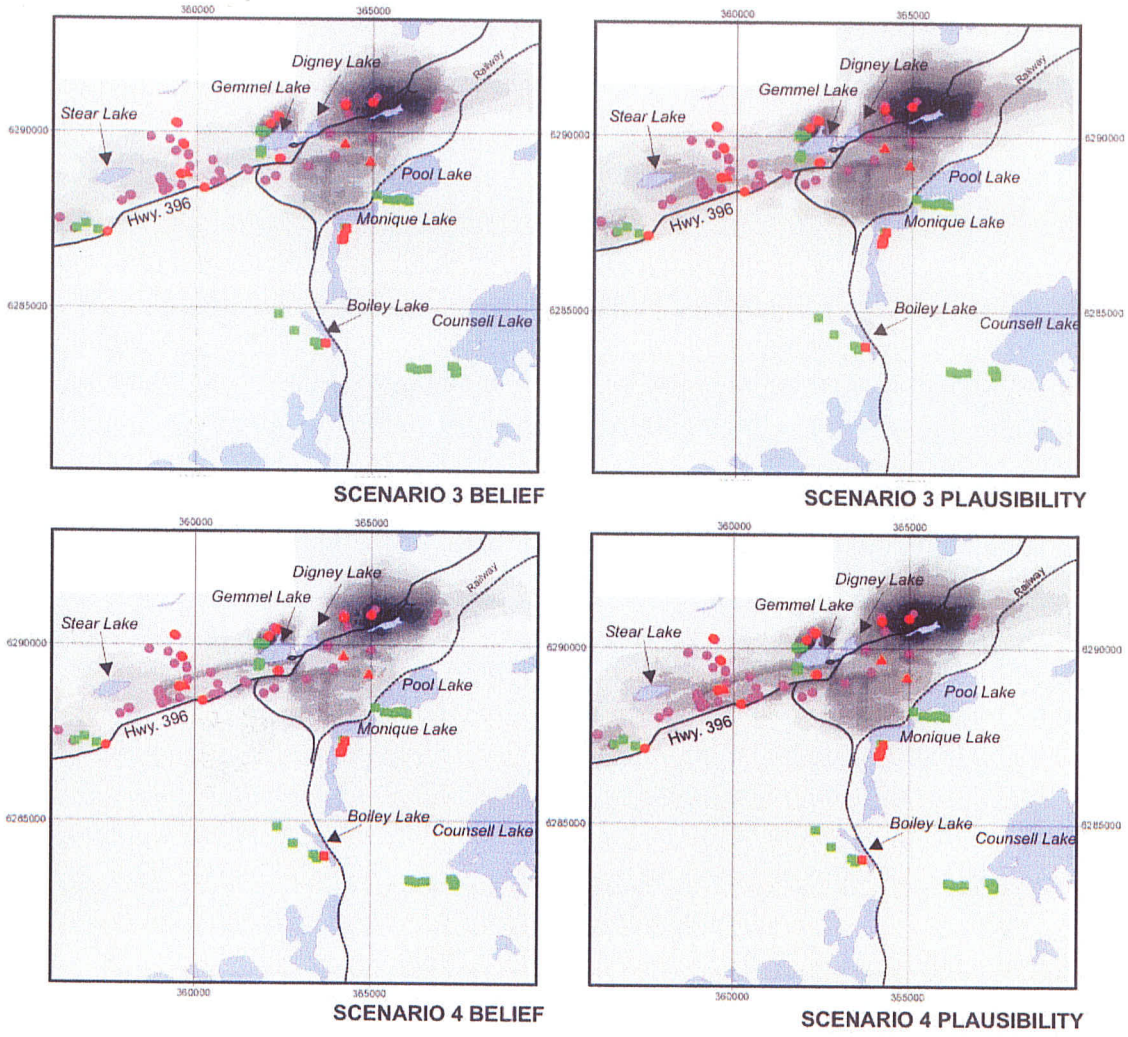

Figure 7.9c Dempster-Shafer combination. Structure component includes lineament deformation, faults, and JSZ potential. Shear strain function is logarithmic.

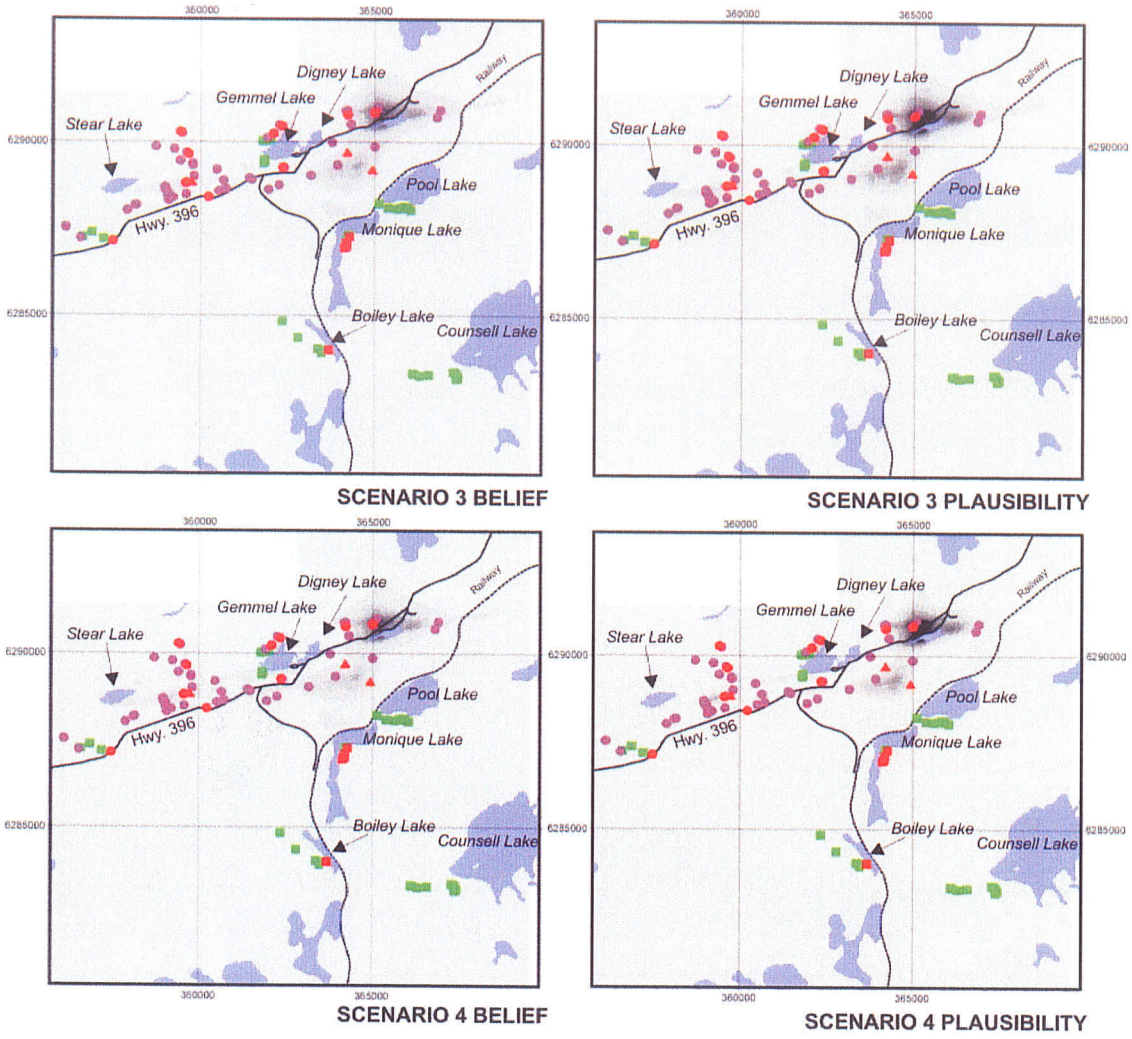

Figure 7.9d Dempster-Shafer combination. Structure component includes lineament deformation, faults, and JSZ potential. Shear strain function is exponential.

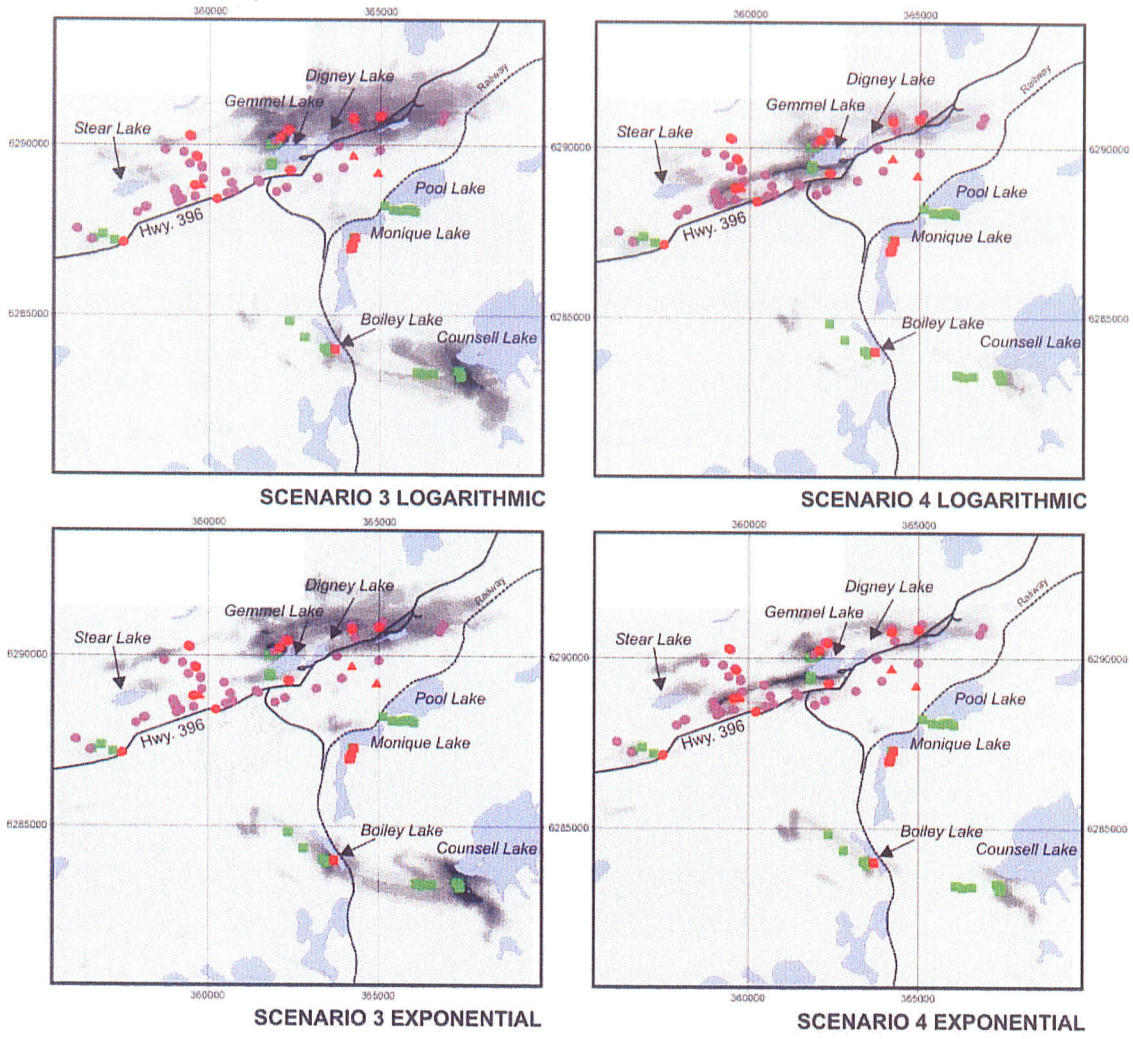

Figure 7.9e Fuzzy logic combination. Structure component includes lineament deformation potential. Shear strain logarithmic and exponential functions.

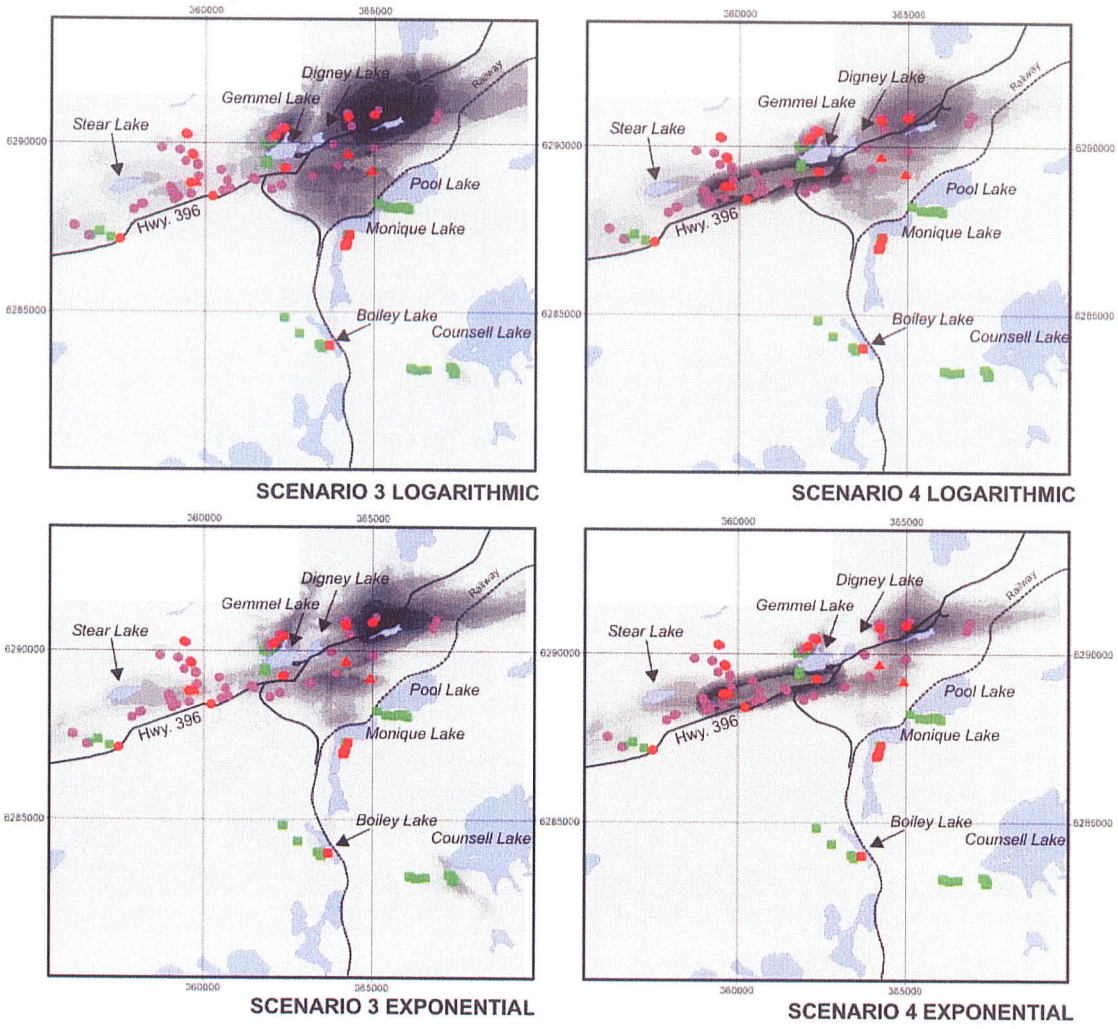

Figure 7.9f Fuzzy logic combination. Structure component includes lineament deformation, faults, and JSZ potential. Shear strain logarithmic and exponential functions.

fabric. Strain levels appear to decrease northward with distance into well-rusted iron-rich coarse-grained basalts. In places the basalts include trace sulphide minerals in biotite-rich bands. High strain fabrics were also observed about 1 km east along strike from the mylonitic unit. The predominantly thinly banded mafic-rich unit include garnet- and biotite-rich bands. Quartz veining is common throughout (Figure 7.11).

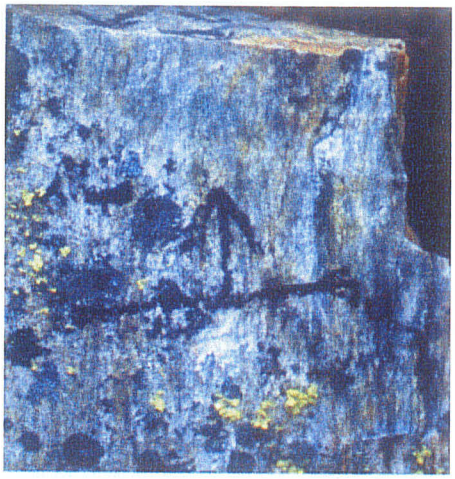

Figure 7.10 Highly siliceous pseudo mylonite to mylonite near Councell Lake. Includes 1-2% disseminated sulphide minerals and trace quantities of gold. Easting 367431, northing 6283210; UTM Zone 14, NAD83.

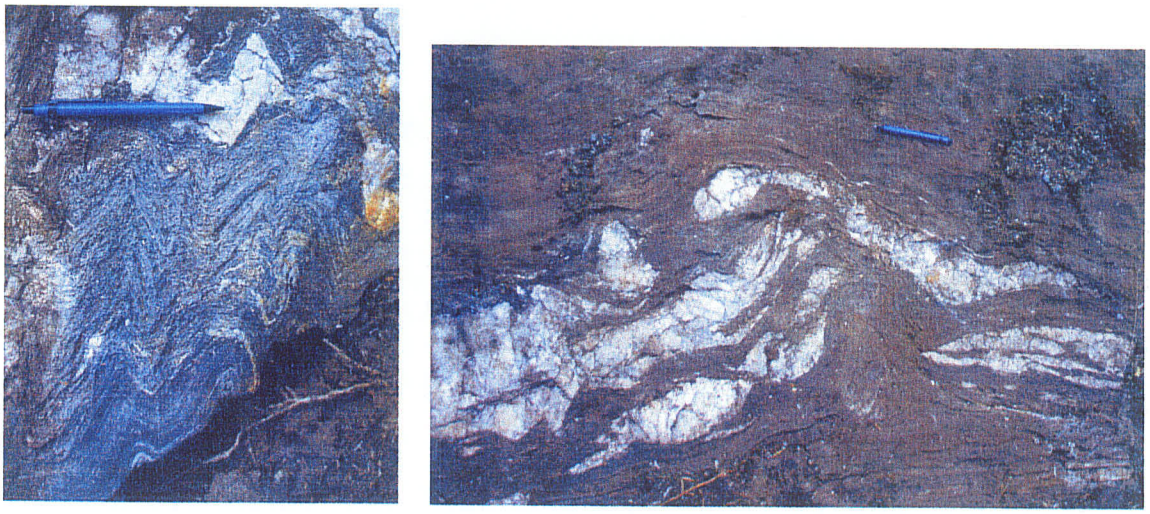

Figure 7.11 High strain fabric with quartz veining near Councell Lake. Easting 366160, northing 6283304; UTM Zone 14, NAD83.

Near the south shore of Boiley Lake a basaltic unit is in contact with a felsic intrusive unit. Quartz phenocrysts within the intrusive unit are elongate with a 5:1 length to width ratio. The basaltic unit shows varying degrees of strain and multiple generations of deformation (Figure 7.12). Included in the unit are discontinuous siliceous zones that are commonly rusted and are oriented parallel to sub parallel to the main fabric.

Disseminated sulphides, up to 2% in places, are found in both siliceous and more mafic sections. Garnet-rich zones, up to 50%, occur as 0.5-1 m wide bands parallel to the main fabric. Quartzofeldspathic veining and boudinage structures were also present in this location. One sample taken from a rusted silicified zone contained 13 ppb Au.

About 200 metres east of the discontinuous siliceous zones, strain fabrics are highlighted by garnets comprising up to 30% of the unit. Many of the garnets are rotated or stretched into Z folds along with the main fabric (Figure 7.13). Other garnets are equant whereas others are elongate with aspect ratios of 20:1. Large metre-sized boudinage structures and quartz veining were seen in the area (Figure 7.13). A silicified unit located about 100 m to the south of the garnet rich unit contained up to 10% pyrite. Au was not detected. High strain fabric and boudinage structures were observed for another 1.5 km trending northwest from Boiley Lake. Swamp and thick overburden did not allow for ground truthing in the high potential zone 2 km northwest of Boiley Lake.

An earlier phase of spatial modeling showed a high potential zone crossing through Monique Lake from southeast to northwest. Changes in the spatial model in the final phase of spatial modeling resulted in only the area on the northwest shore of Monique Lake showed high potential. However, because this area is covered by thick overburden the area along the southeast shore of Monique Lake, which has good exposure, was ground truthed. Samples from this location contained gold values ranging from 11 to 360 ppb. The sample with the highest Au concentration occurred within a moderate to strongly strained basalt with minor quartz and feldspathic veining. Highly strained areas are biotite-rich, whereas moderately strained areas are amphibole-rich. Pseudotachylite and boudin structures are locally developed. About 100 m to the north,

basaltic units show high strain fabrics with areas of quartz-tourmaline veining and silicification. Rusted surfaces were found locally and contained trace to 5% disseminated pyrite and pyrrhotite.

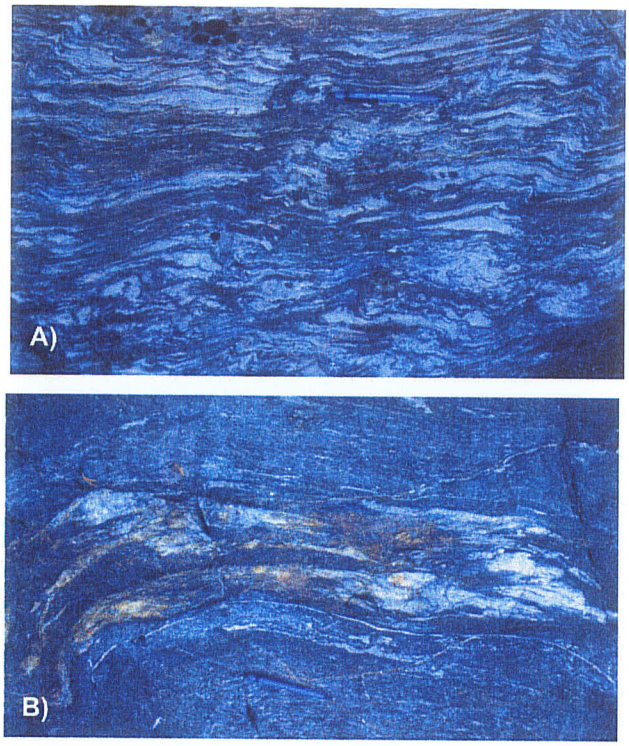

Figure 7.12 Multiple generation of strain fabrics (a) and discontinuous siliceous zones (b) parallel to sub parallel to main fabric. South shore of Boiley Lake. Easting 363675, northing 628400; UTM Zone 14, NAD83.

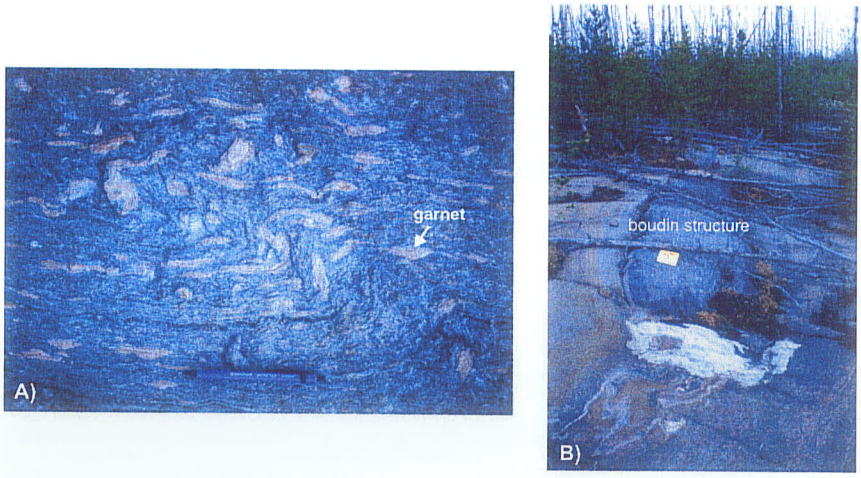

Figure 7.13 A typical garnet-rich zone (a) that is parallel to main fabric. Garnets are commonly highly deformed. Large boudinage structures 10 metres from garnet-rich unit. Easting 363479, northing 6284000; UTM Zone 14, NAD83.

A series of high potential sites occur from Digney Lake through Gemmel to Stear Lake. Known occurrences in the area include the Finlay McKinlay and Prospector gold occurrences, which are located to the northwest of Pool Lake. The two occurrences are located in high potential zones in the DFJ output maps (Figures 7.9 c, d, and f) and within 500 m of high potential zones in the DL output maps (Figures 7.9 a, b, and e). A third occurrence is located about 1.5 km east of Stear Lake. This occurrence was found during the 1999 field season and occurs within sericitized and silicified volcaniclastic dacite intercalated with porphyritic gabbro (Beaumont-Smith and Edwards, 2000). One sample collected in the area contained 1900 ppb Au. Delineation of the JSZ west of Gemmel Lake (Beamont-Smith and Rogge, 1999; Beamont-Smith, 2000) towards Stear Lake represents a different style of shear-hosted gold mineralization than previously recognized along the JSZ. However, gold mineralization near Stear Lake is still primarily controlled by deformation (Beaumont-Smith and Edwards, 2000).

Another high potential site along the northwest shore of Gemmel Lake was ground truthed during the summer of 2001. Six samples from four different locations were collected in 1999 and 2000 during ground truthing and MGS regional mapping. The six samples contained trace to 38 ppb Au. Quartz-carbonate veining in a 2-4 m wide high strain zone was seen over a distance of almost 300m during 2001 ground truthing. Boudinage structures were found throughout the length of the high strain zone. Iron-carbonate veining is found locally along foliation planes (Figure 7.14). Siliceous zones included about 1% disseminated sulphides. Another high strain zone was found about 100m southwest of Gemmel Lake. This zone was silicified with fine-grained disseminated pyrite and pyrrhotite up to 2%. Au occurred only in trace amounts in one

sample. Boudin structures were found along the length of the strain zone, in which multiple generations of deformation were documented. A sample from a third high strain zone, 300 m to the south of Gemmel Lake visited during the 1999 field season, included 10 ppb Au. Northwest of Digney Lake two samples containing 14 and 21 ppb Au, both of which lie within a high potential zone.

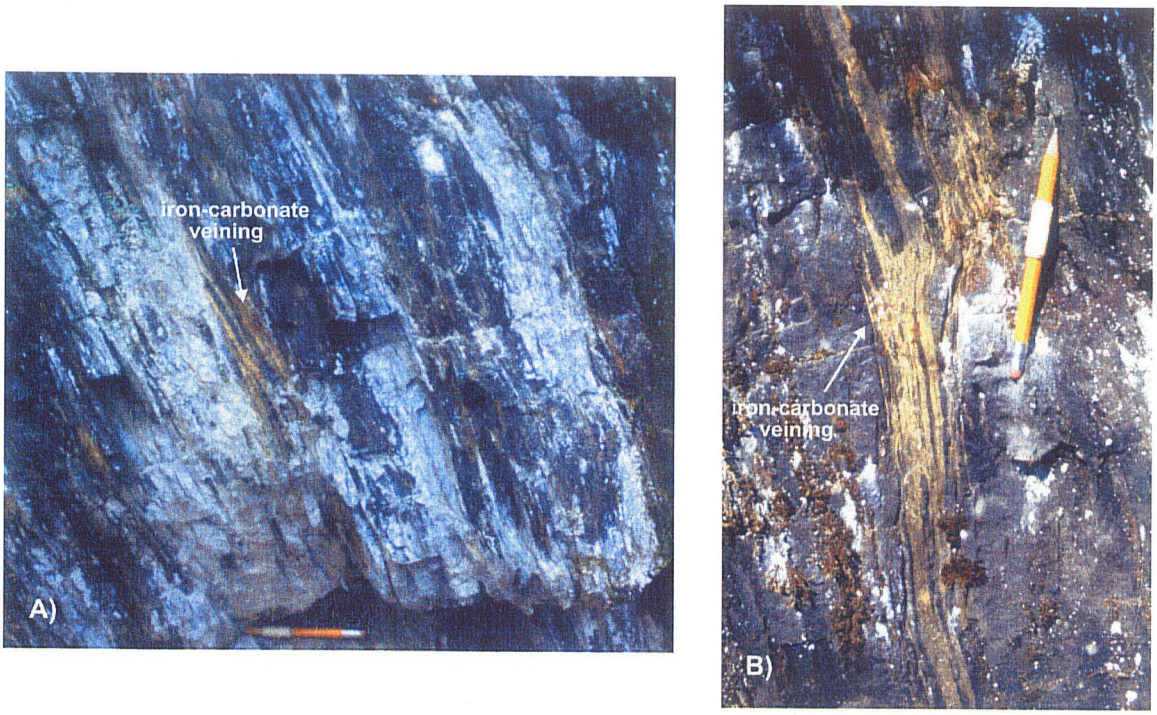

Figure 7.14 Iron-carbonate veining in high strain zone 4 metres in width and striking a minimum of 300m near the north shore of Gemmel Lake. Easting 361847, northing 6290050 (a); easting 361992, northing 6290061 (b); UTM Zone 14, NAD83.

Regions of VMS high potential occur just north of highway 396 from Digney to Stear Lakes. Other smaller high potential zones are found along the south shores of Pool and Boiley Lakes, and near Monique Lake (Figure 7.15). There are four known VMS occurrences in the Gemmel-Councell Lake area. Of these four occurrences two are located within high potential zones at Pool and Boiley Lakes. The other two occurrences lie outside of high potential zones, but are within 550 m of a high potential zone. One

sample containing 802 ppm Zn was found about 1 km north east of Stear Lake about 500 m from a high potential zone.

Ground work south of Pool Lake was completed during the 2000 field season. Pillow and massive basalts with moderate to high strain levels were seen in the area. Units comprising alternating mafic and felsic bands were found with quartz veining throughout. These veins are commonly rusted and have epidote rims. Abundant disseminated pyrrhotite was found at one location south of Pool Lake. Samples taken from this location included 112 and 261 ppm Cu and Zn respectively. About 1.5 km to the southwest of Pool Lake near Monique Lake pillowed and massive basalts are moderately strained. These rocks are strongly rusted locally and contain trace to 5% coarse and fine disseminated pyrite and pyrrhotite. Siliceous zones and 1-2 m wide quartz porphyry dikes occur throughout the area. Two samples collected in the area contained 489 and 638 ppm Cu.

South of Boiley Lake ground truthing completed during the 2001 field season had an emphasis on shear-hosted potential. However, it was apparent that the high strain zone also has VMS potential. Alteration zones containing chlorite-garnetÒmagnetite schist (Ferreira, 1993) and quartz epidote nodules have been discribed in the area (Figure 7.16). Also found in the Boiley Lake area were 2-3 m wide banded iron formations with strike lengths of over 100m (364000, 6284000: Figure 7.15). Disseminated sulphides up to 10% were found in a few locations. A sample from one such location contained 408 ppm Cu.

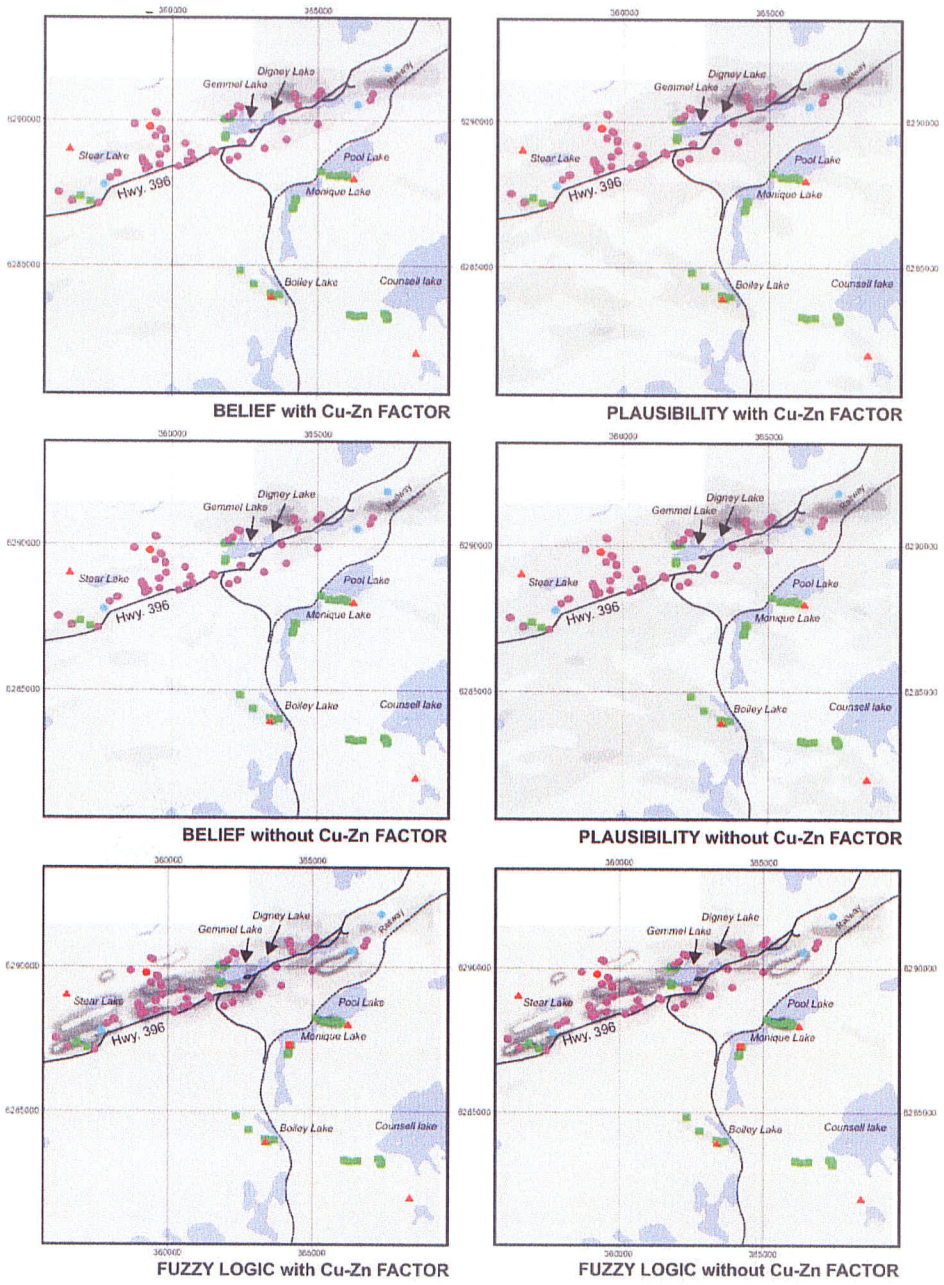

Figure 7.15 Dempster-Shafer and fuzzy logic combination VMS outputs for Gemmel-Councell Lake area. Grey-scale levels represent top 5% of pixel value distribution, with relative scale being linear. White indicates low relative potential; black indicates high relative potential. Includes ouputs with and without Cu-Zn factor. Triangle (red) - known occurrences; Square (green) - ground truth locations; Square (red) - Cu or Zn occurrence (>500ppm) from ground truth locations; Circle (purple) - Manitoba Geological Survey samples. Circle (blue) - Open File 99-13 samples. Circle (red) - Cu or Zn occurrence (>500ppm) from Manitoba Geological Survey and Open File 99-13 samples.

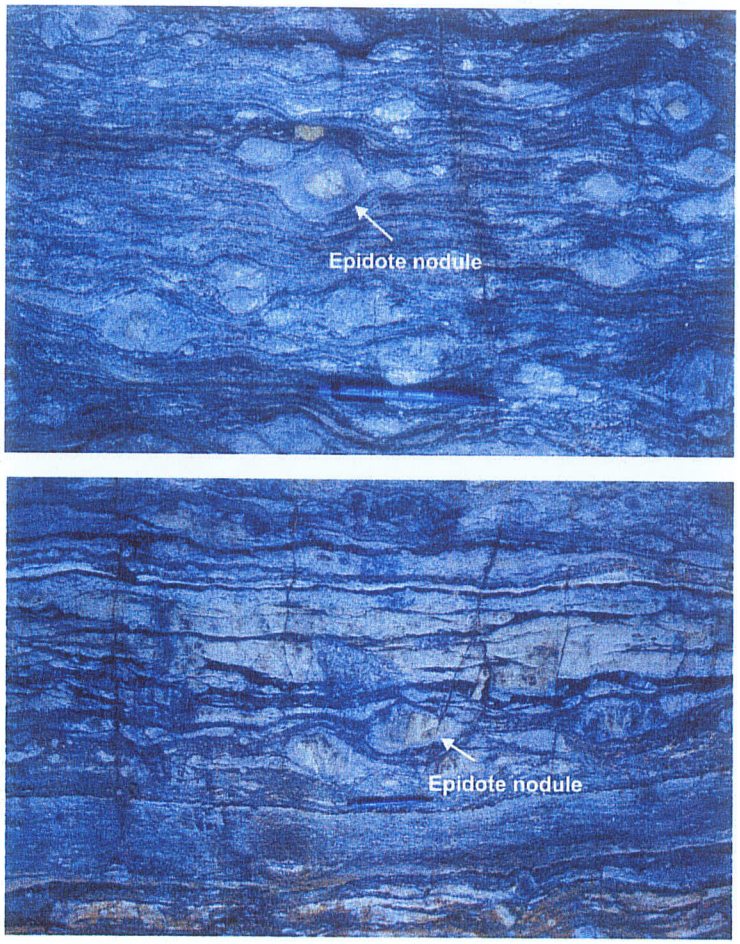

Figure 7.16 Quartz epidote nodules near Boiley Lake. Easting 362789, northing 6284356; UTM Zone 14, NAD83.

7.1.4 Area 3: Dunphy - Laurie Lake

Two main high potential zones occur in the Dunphy - Laurie Lake area. The first zone is between Laurie and Todd lakes. Access to this zone was poor, so no ground work was completed in the area. The second area of high potential includes a zone south of Dunphy Lake, to the east of Snake Lake, and a few patchy zones south of Fox Mine. Dempster-Shafer DL high potential maps (Figure 7.17 a and b) do not show a prominent high potential in the Fox Mine area. The high potential zone east of Snake Lake occurs

only in scenario 4. Ground truthing in the Dunphy-Laurie Lake area was limited to the high potential zone south of Dunphy Lake. Potential maps for scenarios 3 and 4 are shown in figure 7.17. Dempster-Shafer DFJ potential maps that use a exponential shear-stress function show no major high potential zone in the Dunphy-Laurie Lake area and are not included in figure 7.17.

Between Dunphy and Snake Lakes a high potential zone about 3 km in length trends west-southwest. An area of good exposure was documented along the southern shore of Dunphy Lake. The predominantly mafic rocks are highly strained and include quartz veining and boudin structures. Disseminated sulphides were found in a biotite-rich zone adjacent to a silicified zone. Closer to the shore several generations of strain fabrics were observed. Tight folds, fold noses, and boudin structures were observed (Figure 7.18). Silicification is common and disseminated sulphides up to 5% were found along the shore line over 200m of strike. Three samples were taken along the shore line containing nil, 30, and 368 ppb Au. The sample containing 368 ppb Au was taken from an angular fragment mixed together with other angular fragments all of the same rock type. These angular fragments were of the same rock type as the outcrop directly beneath or adjacent to the fragments.

North of Fox mine About 500m North of Fox mine moderate to high strain is observed in massive and pillow basalts and sedimentary units. In one location pillows had a length to width ratio of 20:1. Brittle quartzofeldspathic veining was documented throughout and zones of silicification occur locally. Boudinage quartz-carbonate veins and possible shear bands were also observed in the area (Figure 7.19).

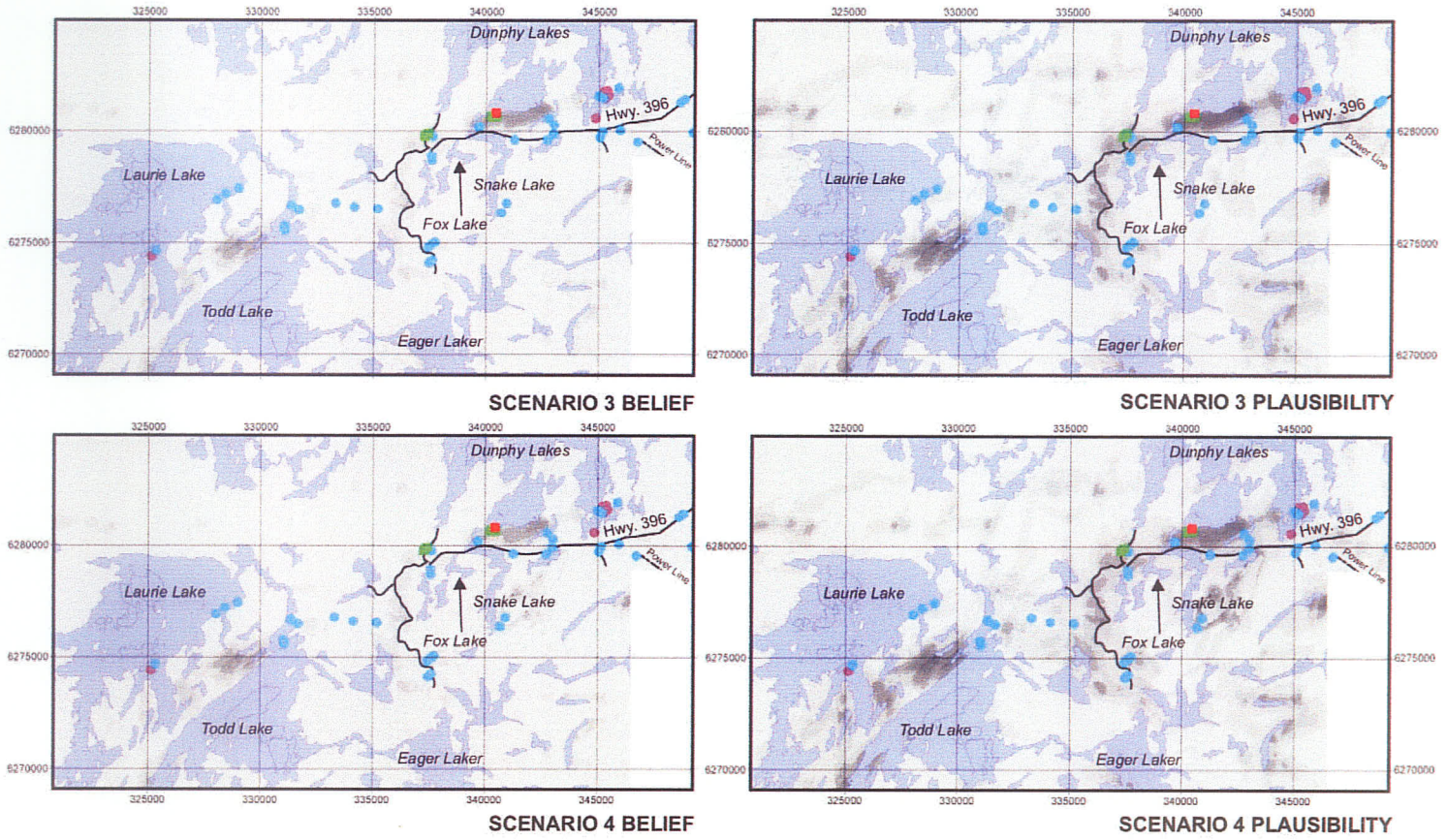

Figure 7.17a Dempster-Shafer combination outputs for Dunphy-Laurie Lake area. Grey-scale levels represent top 5% of pixel value distribution, with relative scale being linear. White indicates low relative potential; black indicates high relative potential. Structure component includes lineament deformation potential. Shear strain function is logarithmic. Triangle (red) - known occurrences; Square (green) - ground truth locations; Square (red) - gold occurrences (>10ppb) from ground truth locations; Circle (purple) - Manitoba Geological Survey samples. Circle (blue) - OF99-13 samples. Circle (red) - gold occurrences (>10ppb) from Manitoba Geological Survey samples.

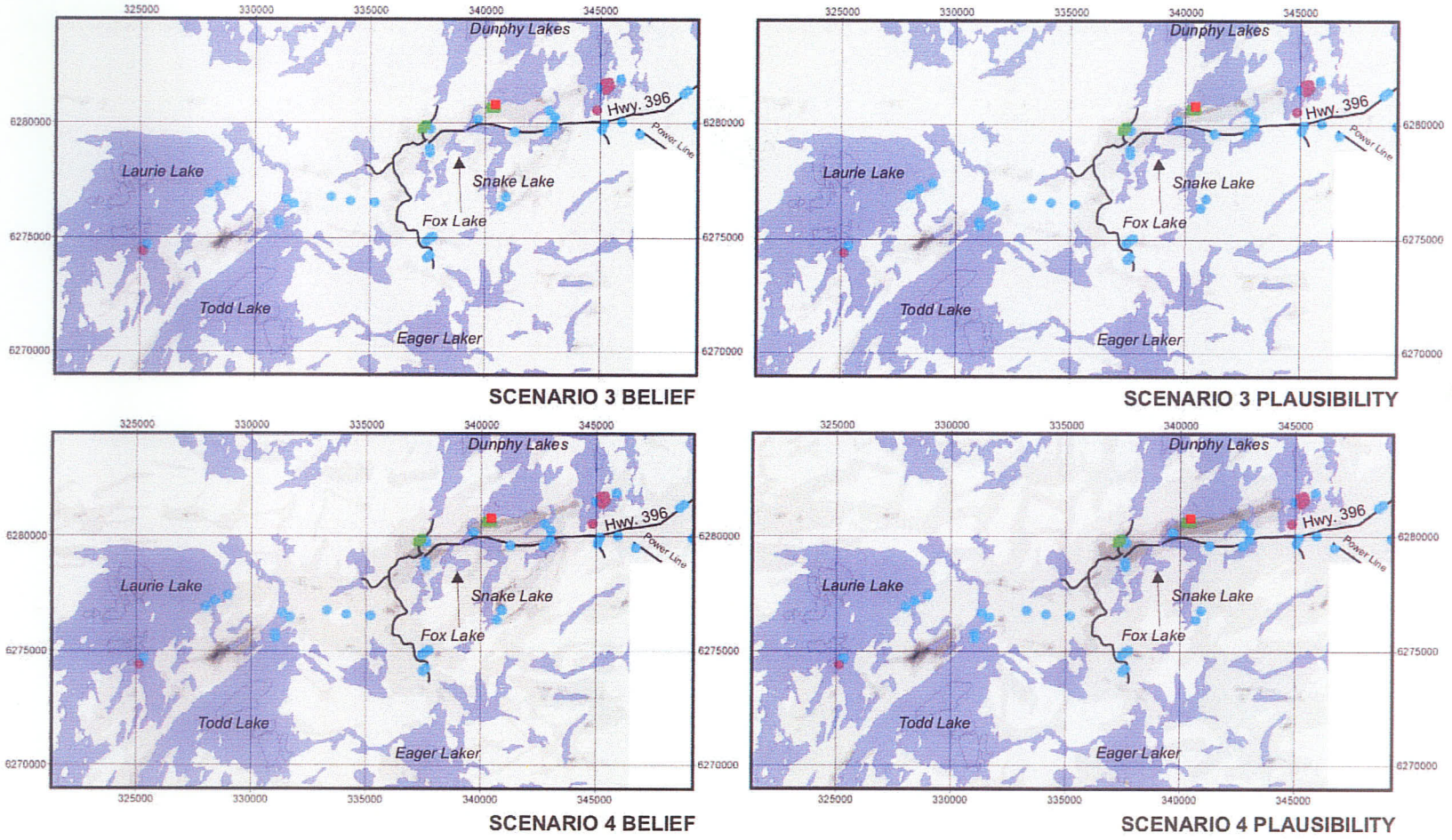

Figure 7.17b Dempster-Shafer combination. Structure component includes lineament deformation potential. Shear strain function is exponential.

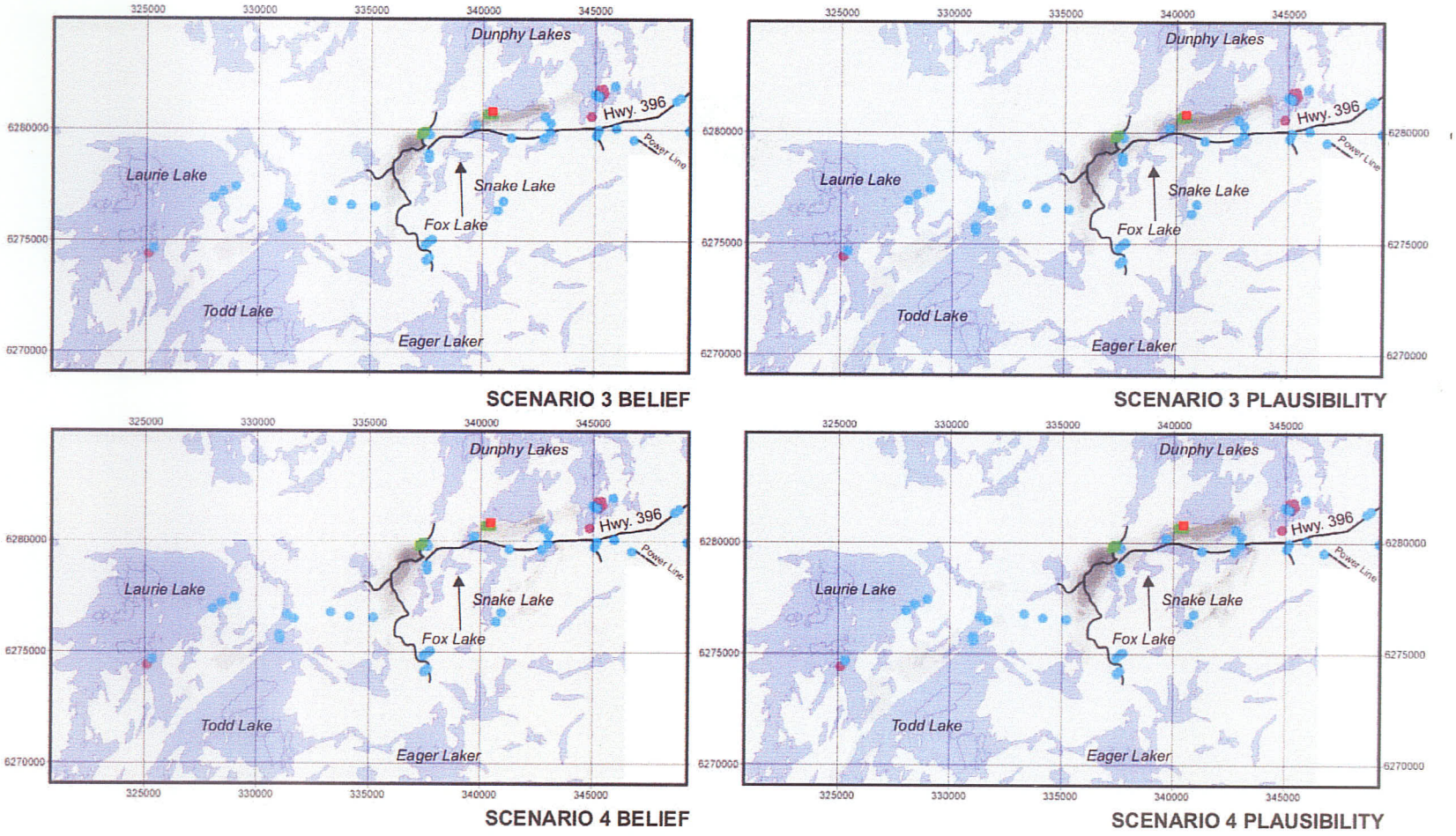

Figure 7.17c Dempster-Shafer combination. Structure component includes lineament deformation, faults, and JSZ potential. Shear strain function is logarithmic.

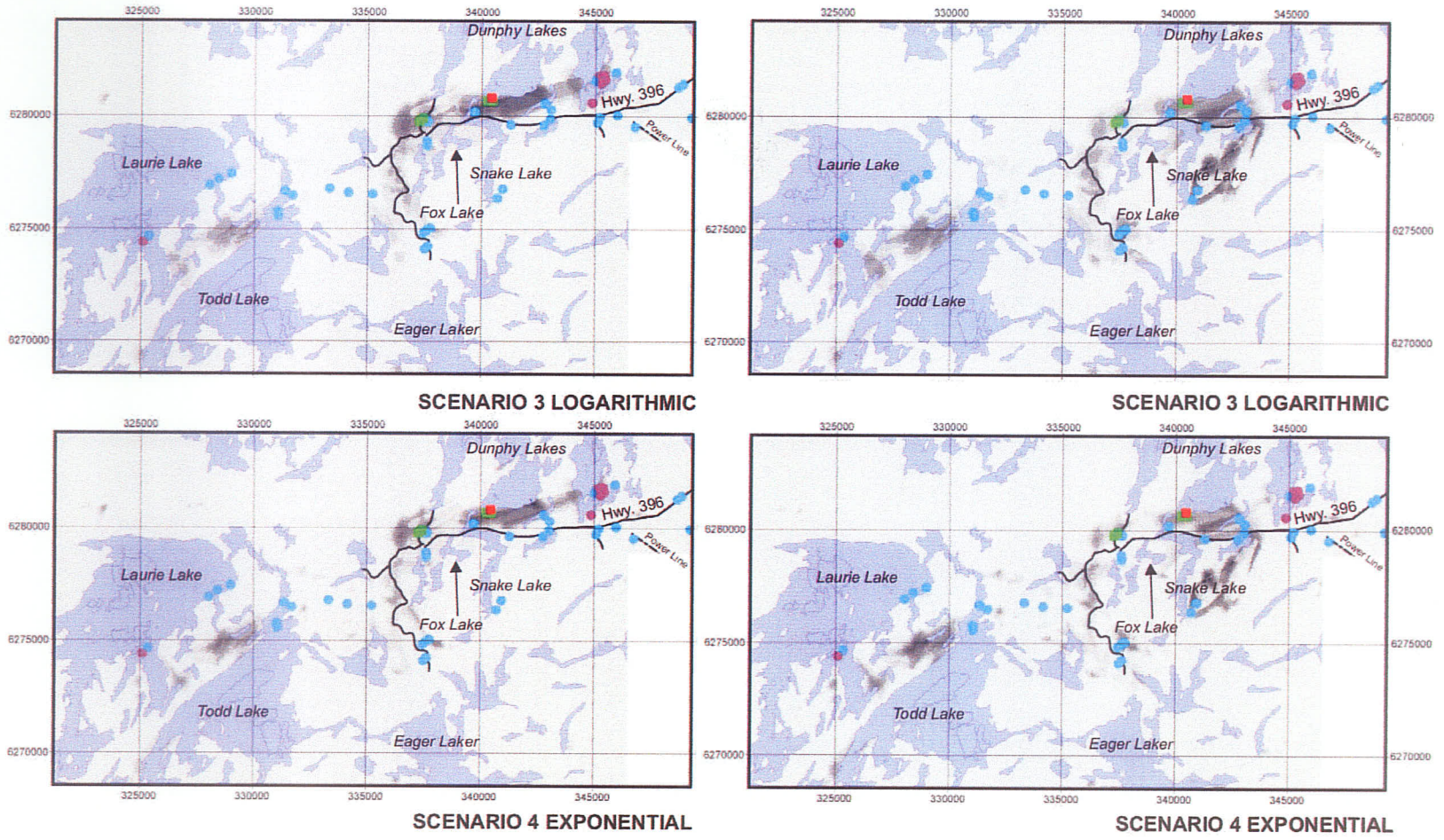

Figure 7.17d Fuzzy logic combination. Structure component includes lineament deformation potential. Shear strain logarithmic and exponential functions.

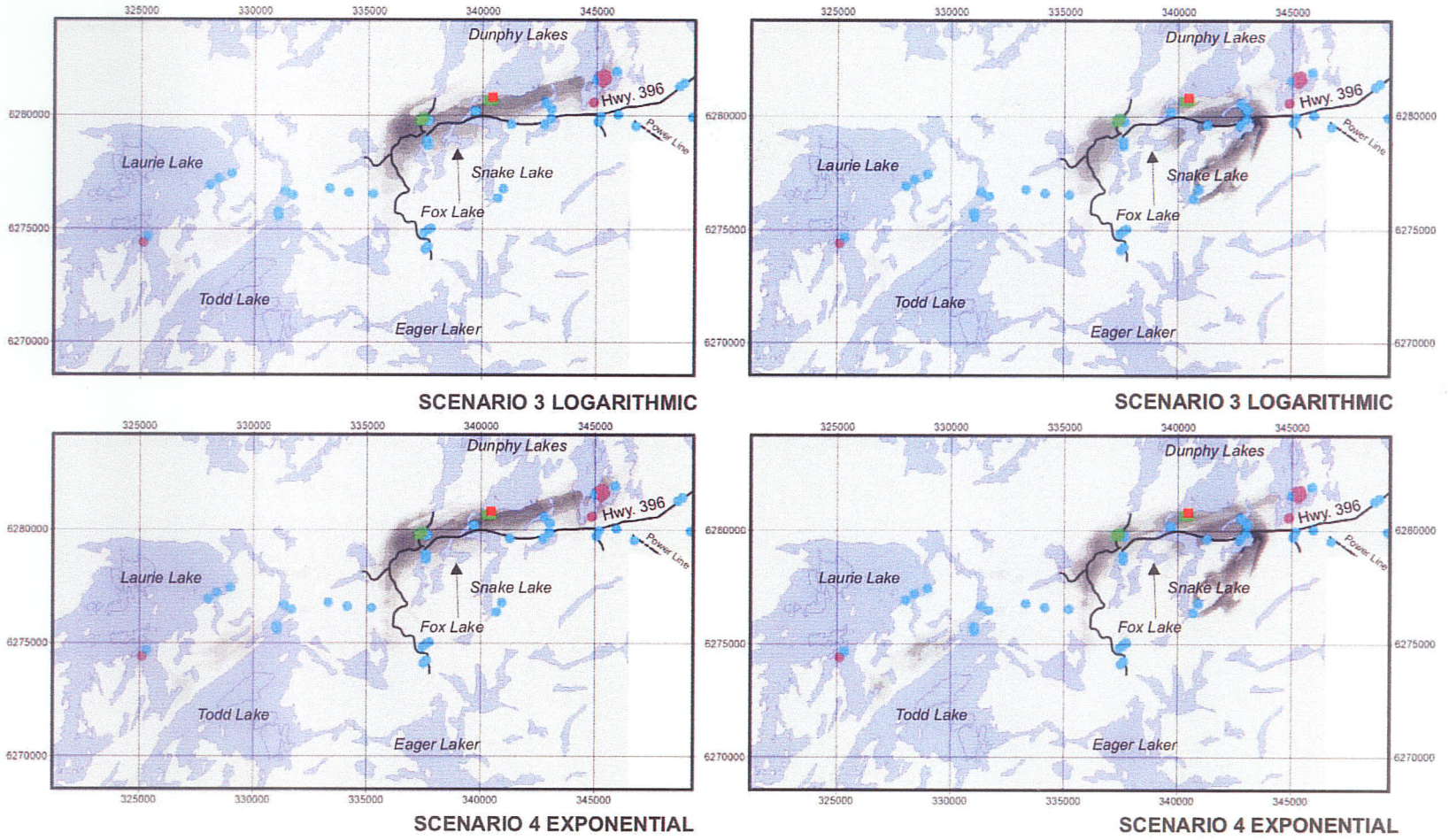

Figure 7.17e Fuzzy logic combination. Structure component includes lineament deformation, faults, and JSZ potential. Shear strain logarithmic and exponential functions.

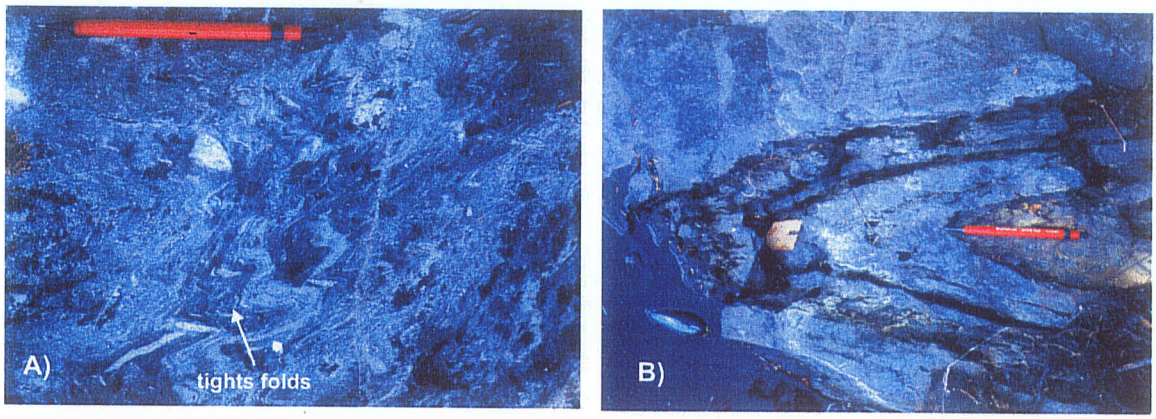

Figure 7.18 Tight folds (a) and fold noses (b) along the south shore of Dunphy Lakes. Easting 340439, northing 6280779; UTM Zone 14, NAD83.

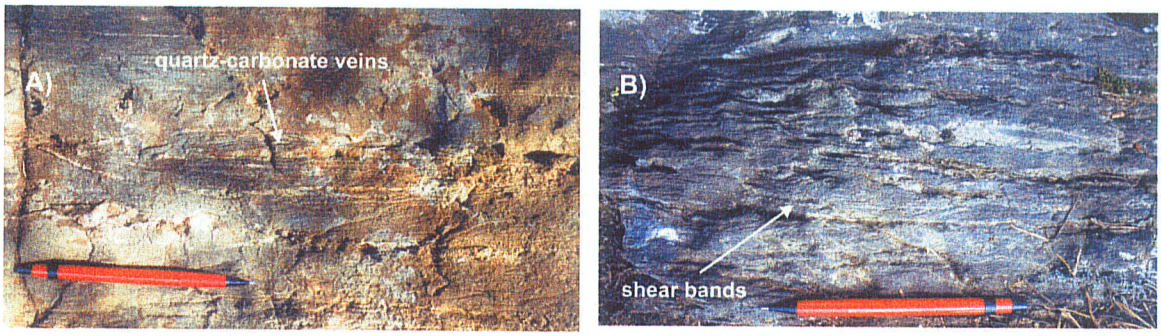

Figure 7.19 Boudinage quartz-carbonate veins and possible shear bands just north of the Fox Mine site. Easting 337269, northing 6279752; UTM Zone 14, NAD83.

The emphasis of ground truthing in the Dunphy and Laurie Lakes was on shear-hosted gold potential. However, in the area there are two VMS deposits, one of which is the Fox Mine and Lar deposit (see Appendix C); and four known occurrences (Figure 7.20). Dempster-Shafer and fuzzy logic potential maps, both with and without the Cu-Zn potential, show a major high potential zone located directly at the Fox Mine site. A total of 11 958 182 tonnes of ore were milled at the Fox Mine with average grades of 1.82% and 1.78% Cu and Zn respectively (Olson, 1987). The second deposit is the Lar deposit,

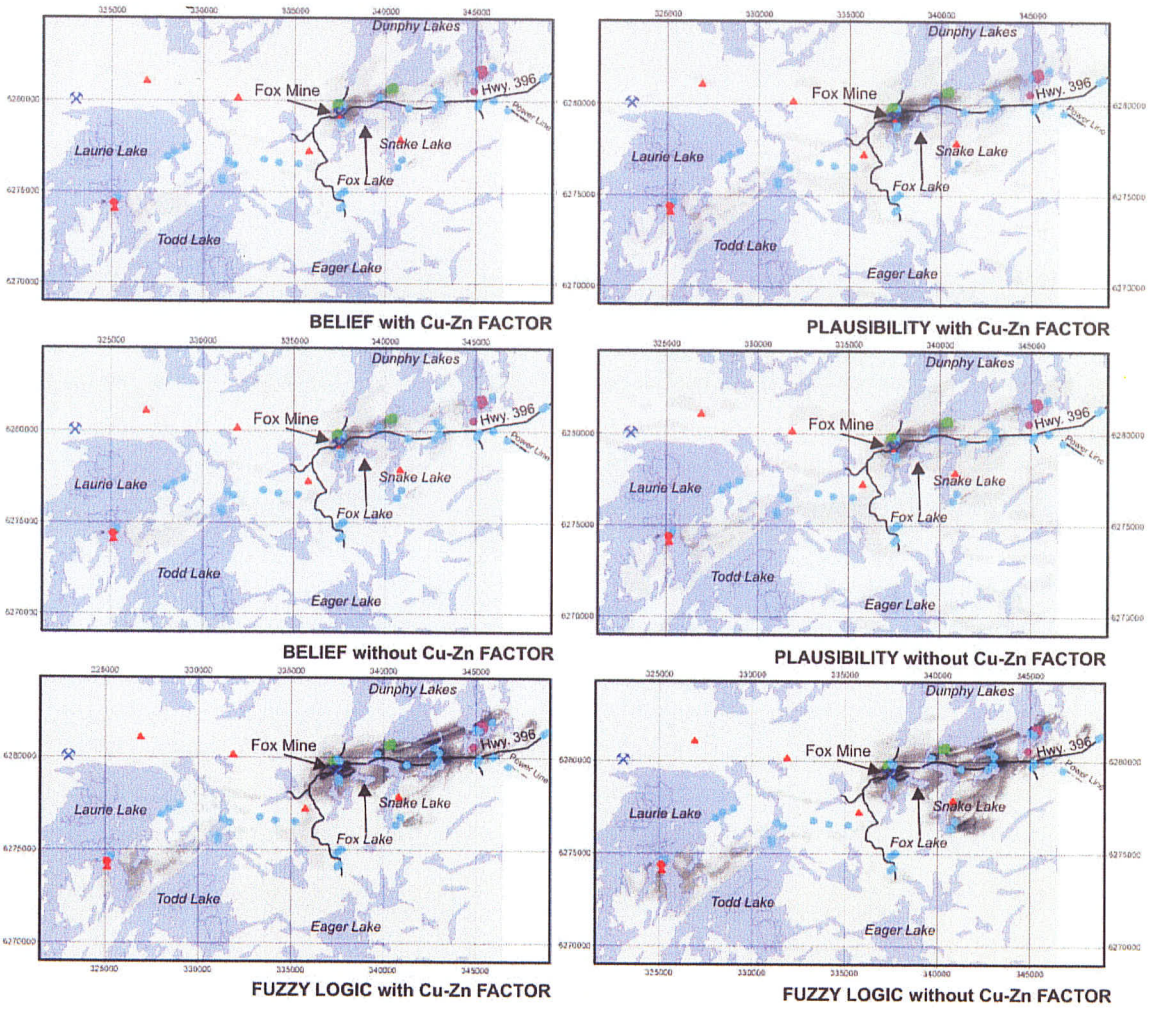

Figure 7.20 Dempster-Shafer and fuzzy logic combination VMS outputs for Dunphy - Laurie Lake area. Grey-scale levels represent top 5% of pixel value distribution, with relative scale being linear. White indicates low relative potential; black indicates high relative potential. Includes ouputs with and without Cu-Zn factor. Triangle (red) - known occurrences; Square (green) - ground truth locations; Square (red) - Cu or Zn occurrence (>500ppm) from ground truth locations; Circle (purple) - Manitoba Geological Survey samples. Circle (blue) - Open File 99-13 samples. Circle (red) - Cu or Zn occurrence (>500ppm) from Manitoba Geological Survey and Open File 99-13 samples.

which is estimated to contain 1 361 000 tonnes grading 0.8% Cu and 2.15% Zn. No high potential zone is associated with the Lar Deposit.

High potential zones other than the one at the Fox Mine site are located along the south shores of Dunphy Lakes, between Todd and Laurie Lakes, and at the southeast tip of Snake Lake. The Snake Lake area is most prominent in the fuzzy logic output maps. Two known occurrences are found north of Laurie Lake, one of which is associated with a small high potential zone in the Dempster-Shafer output maps. The occurrences just south of Fox Mine and to the east of Snake Lake lie within, or are directly adjacent to high potential zones in the fuzzy logic and Dempster-Shafer potential maps.

7.2 Accuracy and Prioritization

Section 7.1 discussed the main high potential zones defined in the Shear-hosted and VMS output potential maps. Ground truthing of a selection of high potential zones to verify the accuracy of the high potential maps. Overall the locations that were ground truthed showed moderate to high potential for shear-hosted gold and VMS deposits. Also in the previous section were known occurrences compiled from the Mineral Deposit Series. In this section accuracy of the high potential maps will be defined as the calculated percentage of known occurrences that lie within high potential zones. Potential maps shown in this chapter include only the top 5% of potential value distribution. The locations of known occurrences are given in UTM coordinates and are represented as a points. For testing, each occurrence is represented as a circle with a radius of 100m. Occurrences within the top 5% potential distribution are considered hits.

TABLE 7.1: Shear-Hosted Spatial Model Accuracy

Potential output map	Accuracy (%)	Potential output map	Accuracy (%)
Dempster-Shafer (DL (1) – Log (2))		Dempster-Shafer (DL – Exp (2))	
Scenario 5	42	Scenario 5	58
Scenario 4	50	Scenario 4	58
Scenario 3	42	Scenario 3	58
Scenario 1&2	50	Scenario 1&2	58
Dempster-Shafer (DFJ (1) – Log)		Dempster-Shafer (DFJ – Exp)	
Scenario 5	100	Scenario 5	67
Scenario 4	100	Scenario 4	67
Scenario 3	100	Scenario 3	67
Scenario 1&2	100	Scenario 1&2	100
Fuzzy Logic (DL - Log)		Fuzzy Logic (DL - Exp)	
Scenario 5	58	Scenario 5	67
Scenario 4	58	Scenario 4	58
Scenario 3	67	Scenario 3	58
Scenario 1&2	58	Scenario 1&2	58
Fuzzy Logic (DFJ – Log)		Fuzzy Logic (DFJ – Exp)	
Scenario 5	100	Scenario 5	92
Scenario 4	92	Scenario 4	92
Scenario 3	92	Scenario 3	92
Scenario 1&2	92	Scenario 1&2	92

(1) DL: Lineament deformation; DFJ – Lineament deformation, faults and JSZ.
(2) Log: Logarithmic shear-stress function; Exp: exponential shear-stress function.

TABLE 7.2: VMS Spatial Model Accuracy

Potential output map	Accuracy (%)	Potential output map	Accuracy (%)
Dempster-Shafer		Fuzzy Logic	
with Cu-Zn potential	67	with Cu-Zn potential	39
without Cu-Zn potential	67	without Cu-Zn potential	56

Table 7.1 and 7.2 shows the accuracy of the Dempster-Shafer and fuzzy logic potential maps for the two spatial models. Overall there is good correlation between known occurrences and potential maps. The 32 potential maps for the shear-hosted model show an accuracy range of 42% - 100% with an average of 74%. The 4 VMS potential maps have an accuracy range of 39% - 67% with an average of 57%. The lower accuracy of the VMS model may be related to the lack of an alteration data set. The VMS occurrences are classified as "volcanogenic massive sulphide" deposits in the Mineral Deposit Series. Accuracy of the shear-hosted potential maps are based on known occurrences classified as "vein type deposits" from the Mineral Deposit Series. However, descriptions of the occurrences show that mineralization is controlled by both ductile and brittle deformation.

For the shear-hosted spatial model the Dempster-Shafer accuracy average was 70%, whereas the fuzzy logic accuracy was 84%. The potential output that made use of lineament deformation and faults and JSZ data sets showed better correlation with known occurrences than that obtained using only lineament deformation. Comparisons were made between the logarithmic versus exponential shear-stress functions for deformation potential. Potential maps with a logarithmic function showed marginal, yet consistently, better accuracy. Scenarios 1&2 have the highest accuracy of 77% with scenarios 3, 4, and 5 about 73%. Scenario 1&2 do not include heat component.

For the VMS spatial model the potential maps obtained using the fuzzy logic combination method that did not include the Cu-Zn factor showed better correlation with known occurrences. For the Dempster-Shafer output both potential maps had an

accuracy of 67%. Dempster-Shafer potential maps were more accurate than the fuzzy logic maps with averages of 66.7% and 42.7% respectively.

Two mines, the Fox VMS and Burnt Timber gold mines, were found within high potential zones in all of the potential maps for the VMS and shear-hosted gold spatial models respectively. Regardless of the combination method, sub-potential models used, and shear-stress function used (shear-hosted model) the two mines, and many of the known occurrences, are associated with high potential zones. The known occurrences are probably not a complete selection of occurrences in the southern part of the Lynn Lake belt. Therefore the accuracy of the potential maps discussed in this section can only be considered an estimate based on the given occurrences.

Also worth noting is the fact that the BT open pit gold mine is located within high potential zones using lineament deformation without the JSZ input data set. The lineament deformation potential map shows good correlation with the defined JSZ and suggests that the combination of VLF, VG, and SAR data sets can be a useful tool for locating areas of high deformation. A discussion on the output from the lineament analysis is given in next chapter.

The potential maps produced from the shear-hosted spatial model show good correlation with known occurrences and deposits in the southern part of the Lynn Lake Greenstone Belt. The results should assist in prioritization of future exploration for shear-hosted gold deposits. These high potential maps have highlighted potential zones that occur where existing or past exploration has occurred. They also have highlighted new areas of for possible exploration, specifically in the Gemmel - Stear Lake, Monique Lake, Boiley-Pool Lake, Dunphy Lake, and Fox mine areas. Of key interest is the area

west of Gemmel Lake where the definition of the JSZ has been extended west towards Wilmot Lake. Further definition of the extention of the JSZ west of Gemmel Lake will have important implications on future exploration in the area.

VMS potential maps show relatively good correlation with known occurrences and deposits. Field work focused on the shear-hosted potential model, however, two areas were visited that should be considered for future VMS exploration. The first area is south of Foster Lake. This area comprises intermixed units of subaqueous basalts and rhyolite. Quartz-epidote alteration and disseminated sulphides are evident throughout the area. Outcrop exposure in the area should be good owing to a recent forest fire in June 2001. The second location is along the south shore of Boiley Lake. This area includes chlorite-garnet±magnetite and quartz-epidote alteration zones. Disseminated pyrrhotite and pyrite occur at the surface in concentrations up to 10% locally. The area has undergone recent drilling and surface exploration (Beaumont-Smith pers. com., 2001).

8 DISCUSSION

8.1 Introduction

The first stage in the process of developing the shear-hosted and VMS spatial models was to put together a conceptual model. The next major stage was the translation of the conceptual model into a spatial model. The translation stage can involve multiple modeling phases, allowing the development of different models. During each phase problems were encountered during processing and combination, such as translation of a component, missing data sets, and spatial and numerical errors. These problems are discussed below. Recognition of these problems generally occurred during processing. Each additional phase of modeling was used to address these problems. The following discussion is divided into three parts: 1) methodology, 2) data fusion methods; and, 3) output and future work.

8.2 Methodology

The translation of theoretical components from a conceptual model into a spatial model requires that, first and foremost, the components of the conceptual model are appropriate. So, ultimately the accuracy of the spatial model and its output is dependent on the conceptual model. The conceptual models defined in this project were compiled with the intent to include generally excepted principles of the deposit types. At this point the expert must decide how complex the conceptual model will be. If a conceptual model is too basic the potential maps may be of minimal use. On the other hand, a conceptual model that is too complex may not be able to be adequately represented in a spatially format. These factors must be considered even before translation begins.

The base data sets available can be the factor controlling which components of the conceptual model are translated into the spatial model. For instance, alteration is an important feature in locating both shear-hosted and VMS deposits. Alteration zones indicate interaction between fluid and wall rock, which commonly leads to mineralization. Unfortunately a regional scale alteration map does not exist for the Lynn Lake Greenstone Belt, and therefore, an alteration component cannot be included into the spatial model.

Base data sets are rarely all of the same spatial extent, resolution or scale, format, or of the same projection. Data sets that are used to represent a component of the conceptual model are also not without spatial errors. These errors can occur during the collection of data, such as the extrapolation of geological contacts, or during processing, such as changing from vector to raster format. Although existing errors in the data sets acquired for this project errors may not be able to be corrected, processing errors can be kept to a minimum. The potential maps produced in this project, and in other data fusion projects, are only as good as the information available in the original base data sets. The differences in the base data sets, such as same spatial extent, resolution or scale, format, and projection, and spatial errors, must be considered during translation and processing, otherwise the results from any combination will have little or no meaning.

Problems that can occur during translation include the inability to translate a theoretical component of the conceptual model into a spatially dependent variable. Specific types of data not mapped at a regional scale, such as alteration, are an integral part of both the shear-hosted and VMS conceptual models. Without a regional alteration data set this component of the conceptual models could not be included in the spatial

models. Alternatively, problems in translation involve the inability to present the variable accurately. If a variable cannot be represented accurately it should be excluded. Including the translated variable may reduce the accuracy of the output maps rather than improve them. In earlier phases of the project a rheology factor was used in the shear-hosted spatial model. It became obvious during earlier phases that a rheology factor could not be represented accurately and was subsequently excluded in later phases.

Combination does not occur in a single stage, but in multiple stages. The resulting spatial models comprise sub-potential models for each major component of the model, and are developed for two main reasons: 1) they allow for the modification of a sub-potential model without having to change or recombine the other sub-potential models; and 2) they allow the given sub-potential models to be combined in different ways. The ability to change these sub-potential models individually is especially important if numerical errors are found during combination. Incorrectly entered weights will commonly show up in the output maps during combination of the sub-potential models. These errors can be corrected before subsequent combination with the other sub-potential models. The other sub potential models are also not affected by the changes and do not have to be recombined. Combining individual sub-potential maps in different ways allows for specific components to be included or excluded from the spatial model potential output for a particular reason. For example, in the VMS spatial model the Cu-Zn component is considered to have a high uncertainty relative to the other components. For this reason the Cu-Zn potential was included in one output, but not in the second output. Another reason for combining individual components individually is the ability to test numerous scenarios, such as the tectonic scenarios used in the shear-hosted spatial

model. This approach also allows for a specific component may be added at a later stage once data becomes available. Weights are assigned to sub potential models before combination with the other sub potential models. These weights reflect the confidence level of the component as a whole, or in comparison with the other sub potential models.

When modifying base data sets factors such as repetition, assumptions, and project area extent will affect the accuracy of the output. Base data sets may be used more than once to represent two components of the conceptual model. An example of this would be using VG and VLF for deformation potential, and again as a geophysical factor. In this example the same information is used twice with only minor modification thus creating a bias. The bias results from repeatedly weighting the same feature. Another example of repetition would be using the geological map for fluid-heat potential and source zone potential in the shear-hosted spatial model. In this case little or no bias occurs because different information from the same base data set is used.

In order to translate components of the conceptual model into the spatial model the expert may be required to make broad assumptions during the modification of input data sets. In the case of the heat component in the VMS spatial model proximity maps were used to show heating of rocks adjacent to a cooling intrusive body. The heating effect decreases away from the intrusive body and, therefore, a maximum extent was set. In order to determine the maximum extent an assumption was made that all of the intrusive bodies were circular on the 2-dimensional surface. This assumption was made so that the area of the polygon could be used to determine the radius and, hence, a maximum extent. The assumption is made to be consistent in applying maximum extent

to all the intrusive bodies used. Two intrusive bodies, with one having a volume a full magnitude greater than the other, should not be treated the same with respect to heat loss. Another assumption was made with respect to the structure component of the shear-hosted model. In this case the length to width ratio of deformation for a fault, or shear zone, was set to 5:1. The assumption here is that the lateral extent of deformation for all faults, shear zones, and lineaments will be based on this ratio. The assumption is a generalization of the deformational characteristics of faults, shear zones, and lineaments. The result is a set of proximity maps for faults, the JSZ, and for the lineament analysis maps that are consistent with each other. Considering different deformational characteristics for faults, shear zones and lineaments in brittle and ductile regimes may improve the accuracy of the spatial model.

The assumptions made are based on the information available in the conceptual model and the data sets being used. If more information is available, or becomes available, fewer assumptions need to be made during the translation of a component of the conceptual model into the spatial model. However, depending on the scale, or objective, of the project, the additional information may not significantly improve the output. It is here that the expert must weight the pros and cons of a given assumption to determine if the output will improve significantly.

The spatial extent of a project area must be considered when producing proximity maps. Proximity zones can easily be created around faults within the extent of the area of interest. Faults that lie outside the given area of interest will have no effect on the output. Not including these faults could significantly affect the potential output maps (Figure 8.1). This problem can be solved by expanding the original area of interest to include all

faults. This approach creates proximity maps to go beyond the extent of the input data set. The proximity map could be subsequently cropped to the extent of the project area, but would now include any effects of the outer units. Objects just outside the area of interest should not be ignored when using proximity maps. If data does not exist outside the project area extent, features along the edges of the potential output maps must be interpreted cautiously.

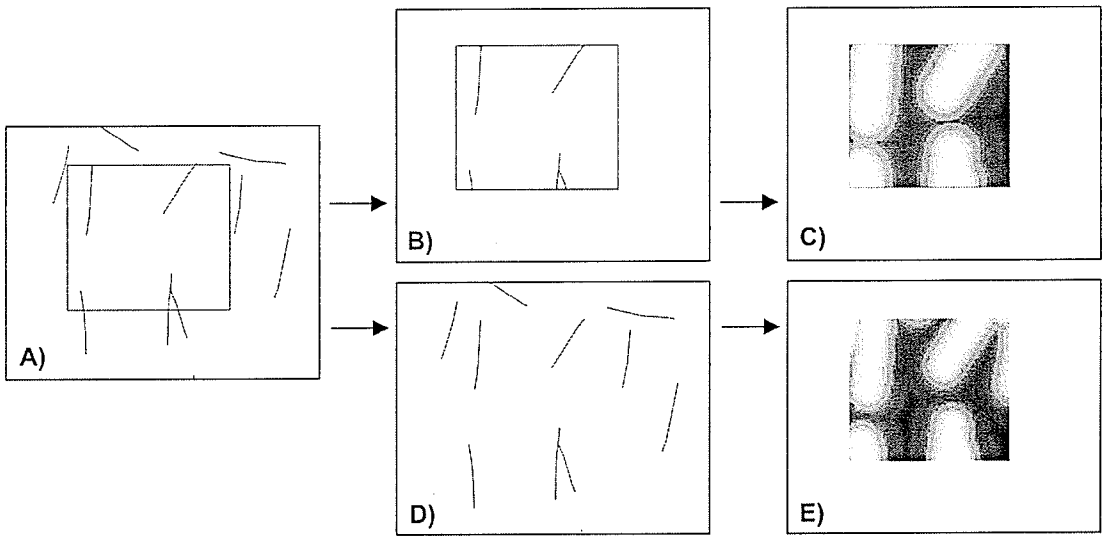

Figure 8.1 Fault data set (a) that includes the area of interest (blue). Faults within the area of interest (b) are used to create a proximity map (c). In (d) all faults from the given data set are used to create the proximity map (e). Note the differences specifically with respect to the edges of the proximity map.

Linear, logarithmic, and exponential decay functions were used to weight individual proximity zones for a given proximity map. The different decay functions were used to represent specific components of the shear-hosted and VMS conceptual model, such as strain rate across a fault or heat loss away from an intrusive body. One of the main questions that arose during the course of this project was the significance of

using different decay functions. Or would the use of a simple linear function result in the same output. Based on the output maps generated using the logarithmic and exponential functions for strain rate across a fault or shear zone, it was shown that significant differences do occur in the location and distribution of high potential zones. However, the differences in the output maps will have little meaning if the function used is incorrect. Another factor to consider is the scale of the project. Simple functions were used in this project, partly because of its regional scale. If a similar project was completed on one of the high potential areas defined for either spatial model, more complex functions could be used that are a more accurate representation of the conceptual model. The ability to test different decay functions is one of the advantages of the expert, or knowledge driven approach.

Different scenarios were used in the spatial models to represent the tectonic evolution of the Lynn Lake Greenstone belt. These scenarios were used primarily to determine which lithological units were present at the time of mineralization. All other units would not be included in the combination. For instance, in the shear-hosted spatial model five different scenarios were used to test differences in the output relative to different deformational events. For the VMS spatial model only syn-volcanic rocks and associated sediments were used in the stratigraphic factor. In each case the output maps generated did show differences in the location and distribution of high potential zones. If information specific to the project area is available, an exploration geologist will make extensive use of it. The same critical information must be applied to the data fusion approached used in this project. The difficulty for both manual and data fusion approaches is proper implementation of the information.

The last stage of processing involves weighting of the input maps. Weights are determined subjectively from the conceptual model. These values have no real quantitative meaning, however, they do represent relative differences. The actual weight of an element in an input map, or the component as a whole, is determined subjectively by the expert using the conceptual model. Subjective weighting allows for more flexibility than the statistical approach to data fusion. However, depending on the experience of the expert, subjective weighting can also lead to poor results. The key to subjective weighting is relative differences and not actual values. For the Dempster-Shafer method two independent belief functions must be chosen, belief and uncertainty. The belief function for the Dempster-Shafer method is the same as for the Fuzzy logic method, whereas uncertainty must be determined separately. Belief is considered to be an assessment that the evidence supports a proposition. The uncertainty value is determined by two factors: 1) the base data set, or sets; and 2) by the translation stage. It is important to make a strong distinction between the factors determining belief and uncertainty.

The weights applied to the various input maps generated during translation are combined using the fuzzy logic and Dempster-Shafer combination methods, which make use of the continuous scale between 0 and 1. These numerical combination methods produce results that are thorough, analytical, less subjective and more repeatable than manual methods. Errors can occur in the weighting of the input maps, which can produce results that are inaccurate. Before combination each of the input maps are checked for errors. However, in some cases errors are missed. During the initial combination stages numerical errors can also be detected. For example, a weight applied

to a specific proximity zone may be incorrect. If proximity zones are displayed in using grey levels, this type of error can be distinguished visually and corrected.

It was stated in section 5.4 that Belief + Disbelief + Uncertainty = 1. If this relationship is not satisfied the Dempster-Shafer method will not work correctly. Making sure that this relationship is satisfied can be tested prior to, and during combination. Prior to combination a simple calculation can be performed on the input data sets based on the above relationship. During combination errors can be found by checking the range of values for the pixels of an output map. If either belief, disbelief, or uncertainty are > 1, then an error exists.

Multiple combinations for both data fusion methods result in progressively smaller values, specifically for belief and disbelief in the Dempster-Shafer method. This in itself does not present a problem, however, ArcView's Spatial Analyst can not deal efficiently with values smaller than 10^{-6}. To deal with the problem, sub potential maps were reclassified to 64 levels before subsequent combination with other sub potential maps. Reclassification was done to reduce the number of decimal places of the output maps. Initially reclassification was considered to be a problem, however, after re-examination the reclassification may be warranted. The problem with reclassification is the inability to calculate disbelief and uncertainty for all combination stages. In earlier phases when a small number of input maps were used combination required only one stage. Belief, disbelief, and uncertainty output potential maps are generated for that combination. In subsequent phases multiple combination stages were required. After each stage belief, disbelief, and uncertainty output maps are generated, however, reclassification uses only the calculated belief function and the assigned uncertainty value

for that component of the spatial model. Disbelief is calculated from belief and uncertainty. The sub potential maps for each component of the spatial model are combined to produce the final potential map. Reclassification of the sub potential maps allows for the assigned uncertainty value to reflect the confidence level in the component as a whole, and not the base data sets and processing used for the sub potential models. In the case of the deformation potential in the shear-hosted spatial model there are multiple stages of combination and reclassification. In this case output at each stage becomes the base data set for the next stage of combination. This approach allows the user to treat each component independently. At each stage of combination the disbelief output map can be used to calculate plausibility, the optimistic assessment that the evidence supports a proposition.

8.3 Data Fusion Methods

Comparisons between the fuzzy logic and Dempster-Shafer data fusion methods show that the two methods generally resolve the same high potential zones. This result is considered reasonable and expected because of the fact that each method uses the same base data sets and weights. However, output potential maps are visually different. These differences are based on the range and distribution of potential values. The range of potential values is generally greater for the fuzzy method. The distribution for both methods show mean values skewed towards the lower potential values. However, there is a difference in the distribution of values. Figure 7.1 shows a selection of histograms showing typical distributions for fuzzy logic and Dempster-Shafer potential maps.

The two combination methods are significantly different. The Demspter-Shafer method is much more involved and more calculations are necessary. The Dempster-Shafer method combines input maps in a pairwise fashion, whereas the fuzzy method combines all inputs in one calculation. Overall the implementation of the fuzzy method is more straightforward than the Dempster-Shafer method. However, the fuzzy method does not include an uncertainty factor. The addition of an uncertainty factor is useful for two main reasons. First it allows for the generation of plausibility, or an upper quantitative assessment of a deposit occurring. Second it introduces the concept of uncertainty into combination. Uncertainty in the information available in a base data set, or in the processes involved in translation, can effect the location of high potential zones. A potential problem with the Demspter-Shafer method is conceptualizing belief, disbelief and uncertainty. As noted in the previous section in order to avoid confusion the concept of uncertainty and belief must be well defined. In this project belief is simply the positive degree of evidence for the existence of a deposit, which is the same value used in the fuzzy logic method. Uncertainty is defined as the confidence in the base data set, or sets, and by the translation and processing stage.

For the fuzzy logic method, missing data presents a serious problem when using the fuzzy gamma operation. Missing data must be given a weight of zero, which results in no output for that particular area. For instance, the geological map included areas of no data where thick overburden exists. This base data set was used for the source rock component of the shear-hosted spatial model. In this source rock component of the spatial model different scenarios were used. In each case particular units were not considered, based on the given scenario. A weight of zero must be set for all units that

are excluded, such as with missing data. Calculations on pixels that have a weight of zero result in that pixel having an output potential of zero. This problem was overcome by making use of proximity maps. Proximity maps assign weight to the entire project area, including areas of missing data or zero value data. This, results in an output with all pixels having a potential value greater than zero. This is not a complete solution, because high potential source rocks may still exist beneath the thick overburden. Choosing data sets that cover the majority of the project area will limit the areas of missing data. The Dempster-Shafer method, on the other hand, can deal with missing data (see section 6.4). However, the main purpose of using the Dempster-Shafer method was to make use of the uncertainty function, and to compare the results with the Fuzzy logic method.

Both methods would be useful tools if the same methodology was applied to another part of the Lynn Lake Greenstone Belt, or perhaps the La Ronge belt in eastern Saskatchewan. Choosing which method to use for another study depends on three main factors: 1) time, 2) scale, or accuracy required for the project; and, 3) missing data. If results are needed in a short period of time the Fuzzy logic method would be a good choice primarily because of its straightforward implementation. If the results are good, and further analysis is warranted the Dempster-Shafer method becomes a good option. Depending on the scale of the project the expert may wish to use the Fuzzy method for the entire project area to define a set of high potential zones. Then focus in on those zones and do a more detailed analysis using the Dempster-Shafer method. At a smaller scale with more detailed data sets uncertainty should become more useful to narrow potential economic targets. Missing data, as noted above, can be better dealt with using the Dempster-Shafer method. However, the percentage of missing data can also effect

which method is chosen. If only a small percentage of data is missing, for example 5-10%, either method should produce useful results. If the percentage of missing data is higher, for example 20-30%, the Dempster-Shafer method should be used. If missing data covers more than 50% of the project area the results should be interpreted cautiously.

8.4 Output and Future Work

Combination results in a set of sub-potential and potential maps. Potential is represent by numerical values. These values represent a relative potential scale based on the spatial model and the data sets used. However, the values do not represent the degree, in percent, that one is likely to find a deposit at a specific location. The accuracy, or the ability to find areas of potential economic interest using this spatial combination method, can be tested by comparing known deposits and occurrences of a specific deposit type and by ground truthing high potential sites.

Deposits and occurrences from the Mineral Deposit Series (see Baldwin, 1989; Ferreira 1993a; 1993b; 1993c; and, Ferreira and Baldwin, 1997) were used to test the potential maps for both models. The location of high potential zones was compared with the locations of known deposits or occurrences. The accuracy, or percentage, of the potential maps is given in Tables 7.1 and 7.2. This percentage is not based on all the occurrences and deposits within the project area, therefore, it is only an estimation of accuracy. Many occurrences have yet to be located. One such occurrence, near Stear Lake (see section 7.1.3), was not listed in the Mineral Deposit Series, but was found during the 1999 field season. This high potential zone is located at the site of the new

occurrence. In addition to this occurrence a new shear zone was found north of Stear Lake late in the summer of 2001 (Beaumont-Smith, pers. com., 2001). This shear zone was located in part using the high potential maps generated in this project. The potential maps in this project also located the sites of two former mines, the BT gold mine, and the Fox Lake VMS deposit. Although the accuracy of the potential maps is considered an estimate, the method of combination has successfully located existing occurrences and deposits. In addition to testing the accuracy of this method by comparing known occurrences with high potential zones, ground truthing of a section of high potential zones showed the ability of the method to successfully prioritize exploration projects.

Fieldwork completed during the summers of 2000 and 2001 focused on testing high potential sites from various phases of the project. During fieldwork sites were checked for characteristics that indicated potential for a particular deposit type and samples were taken for geochemistry and assay (Appendix A). For example, in the case of the shear-hosted spatial model, areas were checked primarily for high levels of strain and associated mineralization. It was not possible to check all high potential areas, primarily because of access, therefore a selection of sites was chosen along the length of the southern part of the belt.

Future work for shear-hosted gold deposits in the southern part of the Lynn Lake belt should include the Carwright-Hughes Lake, Wasekwan Lake, Gemmel-Counell Lake, and Dunphy-Laurie Lake areas. High strain zones in mafic and silicified rocks occur in the Cartwright-Hughes Lake high area. Ductile and brittle deformation in the area includes quartz iron-carbonate veining, disseminated sulphides, and gold. In the Waskwan Lake area high potential zones include the BT gold mine and several known

occurrences. The area includes highly strained rocks and quartz-carbonate veining, where deformation in the area is primarily associated with the JSZ. Sulphide mineralization and gold were found locally. The Gemmel-Councell Lake area includes a series of high potential zones all of which include high strain zones. These high strain zones include mineralization in quartz-carbonate veining, quartz-tourmaline veining, and mylonitic units in the Gemmel Lake, Monique, and Councell Lake areas respectively. Gold mineralization was found in during the 1999 field season southeast of Stear Lake in seritized and silicified volcaniclastic dacite intercalated with porphyritic basalt. The mineralization at this location is also deformation controlled. No known occurrence exist in the Dunphy-Laurie Lake area, however, highly strained rocks that include, boudin structures, tight folds and fold noses, and shear bands were found.

Major VMS high potential zones to be considered for future exploration projects are located in the Wasekwan, Gemmel-Councell Lake, and Dunphy-Laurie Lake areas. Ground truthing focused on the shear-hosted potential zones, however, the area south of Foster Lake and along the south shore of Boiley Lake were found to be potential VMS sites. Disseminated sulphides and chlorite-garnet and quartz-epidote alteration zones were commonly found in these areas. Host rocks included subaqueous basalts and felsic volcanic units. Future areas for VMS exploration include the area southwest of Foster Lake and along the south shore of Boiley Lake. More detailed analysis of the high potential zones defined in the VMS and shear hosted models, including high-resolution geophysics and alteration data, should be completed. With additional data more detailed potential maps can be created for each of the defined high potential zones. This method of combination described in this project can be applied at any scale. Overall the two

spatial models have produced potential maps that can prioritize sites for future exploration. The shear-hosted model showed good correlation with the known occurrences and ground truthing results. The VMS model, on the other hand was not as successful. This is considered to be attributed to the lack of an alteration data set.

8.5 Lineament Analysis

The main focus of the lineament analysis was to use remotely sensed data sets (VLF, VG, and SAR) to produce deformation potential maps which would form part of the structural component of the shear-hosted spatial model. The potential maps would be used in addition to the known faults and JSZ data sets, yet be independent of them. The resulting lineament map and potential maps have proven to be good indicators of the structural trends and deformation potential in the Lynn Lake Greenstone Belt respectively.

Figure 8.2 shows the lineament map and potential outputs for the Dempster-Shafer and Fuzzy logic combination methods using a logarithmic shear-stress function. Major linear trends are defined within the supracrustal rocks of the northern and southern portions of the Lynn Lake Belt. Other major structural trends include the contact between the Sickle group and plutonic and supracrustal rocks of the Lynn Lake and Keewatin River Belts. The supracrustal rocks of the Keewatin River Belt are also well defined in the lineament and deformation potential maps. Two other major trends are well defined in the maps and are associated with the JSZ and a northeast trending feature that forms part of the contact between the northern portion of the Lynn Lake Belt and the Southern Indian River Gniess Belt.

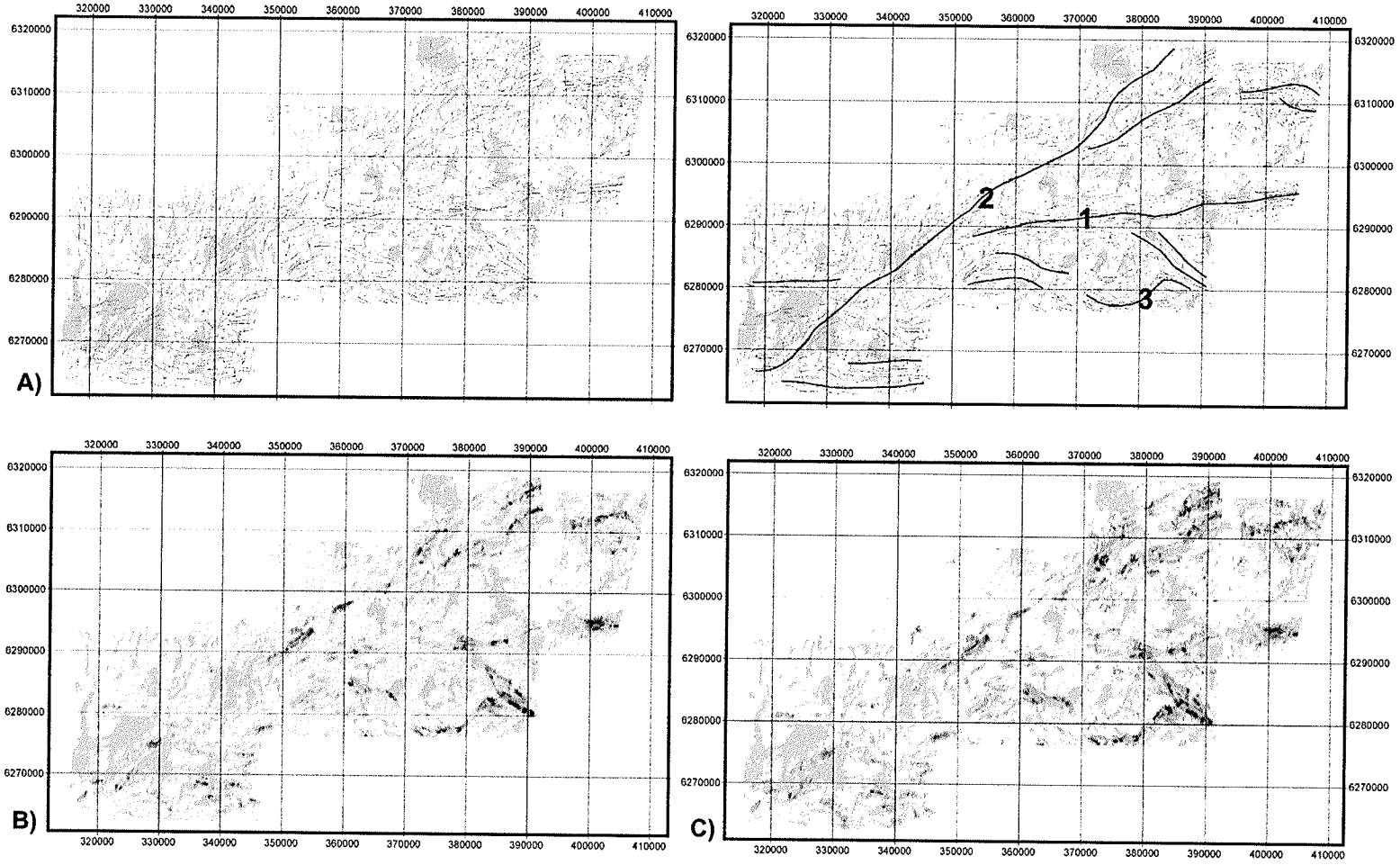

Figure 8.2 Lineament map (a) and potential outputs for the Dempster-Shafer (b) and Fuzzy logic (c) combination methods using a logarithmic shear-stress function. Inferred structural trends are shown for the lineament map: 1 - JSZ; 2 - Northeast trending feature; 3 - Sickle contact.. Lineaments are generated from VLF, VG, and SAR input data sets.

The JSZ trend appears to be 1) truncated by the northeast trending feature, 2) displaced by the northeast trending feature, or 3) splays in the Gemmel-Wilmot Lake area. In the first case the northeast trending feature can be followed from the northern belt south to the area between Laurie and Todd Lakes. Northwest of Wilmot Lake the JSZ trend appears to be truncated by the northeast trending feature. The northeast trending feature, which appears to pass through the Fox Mine area, may be interpreted to be a major structural feature associated with trust faulting in the area. A new U-Pb date of 1831 Ma (Turek et al., 2000) in the Fox Mine tonalite is much younger than the 1870 - 1915 dates obtained in other parts of the Lynn Lake Belt (Baldwin et al., 1987; Bickford and Van Schmus, 1985). The contrasting dates may be interpreted to be the result of a major structural break in the Laurie-Todd Lake area. This break is defined by the northeast trending feature. More work is necessary to determine the accuracy of this interpretation.

The second case also involves the northeast trending feature describe in 1). A linear trend is visible on the western side of the northeast trending feature and may be interpreted to be an extension of the JSZ, but displaced to the south. In last case the JSZ trend shows evidence of splaying in the Gemmel-Stear Lake area. If the JSZ does, in fact, splay at this location it could have major implications on locating shear-hosted gold deposits. The majority of shear-hosted gold deposits occur in areas of dilation, such as splays, rather than along the straight sections of shear zones (Hodgson, 1993). Representing splays spatially is a difficult task owing to the problem of distinguishing between small linear features and spays from the larger linear features such as the JSZ.

The lineament analysis has shown how remotely sensed platforms can be used to determine structural trends in an area. Combining the lineament deformation potential maps with the fault and JSZ data sets can improve the accuracy of locating potential areas of deformation, and in turn, shear-hosted gold deposits. If structural data is absent lineament deformation potential maps become a useful tool to locate major structural trends and high deformational zones.

9 SUMMARY AND CONCLUSIONS

Advancements in computer technology have made it possible for geologists to deal with the increasing size and availability of data sets. In order to gain a better understanding of various geological processes, geologists continue to combine multiple sets of data from various geological, geochemical, and geophysical platforms. The objective of this project was to develop mineralization potential maps for the southern part of the Lynn Lake Greenstone Belt, particularly with respect to the Johnson Shear Zone (JSZ) and associated structures. The emphasis of this project was on the processes involved in producing spatial deposit models with predictive power that we can test. Exploration geologists commonly combine information from various platforms to locate new deposits or prioritize areas for exploration. This project seeks to replicate what an exploration geologist does using their expert knowledge, but with more quantitative results that are less subjective and more reproducible than manual methods. The key problem with manual methods is the saturation of information. Manual combination limits the users ability to assess large quantities of data, weight the various data sets, accurately quantify spatial relations, and integration theoretical information. Today's computers and spatial data software allow the user to manipulate, combine, and display their results quickly and efficiently.

Data fusion is the framework of combining data sets to determine areas of potential economic interest. In this project combination makes use of theoretical principles, or a knowledge driven approach to locate potential areas for shear-hosted gold and VMS deposits in the southern portion of the Lynn Lake Greenstone Belt. To accomplish the objective five main stages were required: 1) the development of a

conceptual model; 2) compilation of a spatial database; 3) selection of a combination method; 4) a spatial deposit model and processing; and 5) probability output and testing.

Potential maps showing only the top 5% of potential value distribution were compared with known occurrences to test the accuracy of the spatial models. Overall there is good correlation between the known occurrences and potential maps with accuracy averaging 74% and 57% for the shear-hosted and VMS spatial models respectively. For the shear-hosted spatial model the Dempster-Shafer accuracy average was 70%, whereas the fuzzy logic accuracy was 84%. For the VMS spatial model Dempster-Shafer potential maps were more accurate than the fuzzy logic maps with averages of 66.7% and 42.7% respectively. Ground truthing of a selection of high potential zones was also completed to test the accuracy of the spatial models. Ground truthing showed that the high potential zones did include characteristics that are indicative of shear-hosted and VMS type deposits. High strain fabrics, quartz-carbonate veining, silicification, and samples containing anomalous concentrations of gold were typical of the high potential zones defined in the shear-hosted model. Features typical of VMS deposits included disseminated sulphides and chlorite-garnet and quartz-epidote alteration zones in subaqueous basalts and felsic volcanic units. Future areas for VMS exploration include the area southwest of Foster Lake and along the south shore of Boiley Lake. Sites for shear-hosted gold exploration in the Lynn Lake Greenstone Belt include the Gemmel-Stear Lake, Monique Lake, Boiley-Pool Lake, Dunphy Lakes, and Fox mine areas. The results have shown that the approach adopted for this study can accurately prioritize areas for exploration. Both the Burnt Timber gold mine and the Fox Lake VMS

deposit were located within high potential zones in the shear-hosted and VMS potential maps respectively.

In addition to the mineralization potential maps combination of data sets was also used to define major structural trends, specifically the JSZ, and high deformational zones. The lineament analysis made use remotely sensed data sets (VLF, VG, and SAR) to produce deformation potential maps which would form part of the structural component of the shear-hosted spatial model. The results from the lineament analysis correlate well with the extent of the JSZ and have defined other major trends within the belt. Of great interest is the extension of the JSZ west of Gemmel Lake and a major northeast trending structure in the western part of the belt. Interpretation of the potential maps indicate that the JSZ may splay west of Gemmel Lake. This will have major implications on future shear-hosted gold exploration in the belt.

In the process of producing the above results a number of conclusions have been drawn with respect to the methodology used. First and foremost is the aspect of correctness of the conceptual model. If a conceptual model is incorrect, then the spatial model and resulting potential maps will not be accurate. At this stage the expert must also determine the complexity of the conceptual model(s) to make the most use of the data sets available. If a component of the conceptual model cannot be represented accurately, then it should not be included. The availability of base data sets controls which components of the conceptual model can be translated. Without adequate data sets, producing potential maps using a spatial model is not possible. In this project sufficient data sets were available to develop the shear hosted and VMS spatial models. However, the addition of an alteration data set could have improved the overall accuracy of the two

spatial models, specifically the VMS spatial model. Alteration is likely the key component of locating a VMS deposit. The lower accuracy of the VMS spatial model can be interpreted to be the result of no alteration data. In addition to alteration, a second SAR scene with a look direction perpendicular to the first, improved resolution of the magnetic and VLF data, and a larger geochemical sample set, could greatly improve on the results shown here. The output potential maps are essentially only a good as the as the information in the base data sets. For this reason the compilation of various data sets with different resolution, scale, source, extent, projection, and data format must be done in a rigorous fashion, otherwise the results may be of minimal use. Translation is a major process that must consider not only the theoretical principles and data sets available, but also processing factors such as repetition, assumptions, and project extent.

The expert approach used in this project to producing mineralization potential maps allows for flexibility. This flexibility allows for experimentation and for numerous scenarios to be tested. Linear, logarithmic and exponential functions were used to represent weight in the proximity maps developed for the two spatial models. The use of different functions does effect the location and distribution of high potential zones in the output maps. However, the specific function used for a given component must be used correctly, otherwise the output may be inaccurate. For the structure component of the shear-hosted model logarithmic and exponential functions were used to represent finite strain across a plane. The logarithmic functions were used to represent ductile, or shear zone, characteristics. The potential maps that made use of the logarithmic functions did show better correlation with the known occurrences, and hence, should be adopted in future projects. More detailed functions can be used to improve the accuracy of the

output maps, specifically at smaller scales with more detailed data sets. For instance the exponential function used for heat loss from an intrusive body could be improved if more info becomes available.

Different scenarios based on the tectonic evolution of the belt were also tested in this project. The main purpose of these scenarios was the integration of good geological knowledge of the greenstone belt. The output maps generated using the different scenarios did show differences in the location and distribution of high potential zones. These differences indicate that this type of information can significantly effect the prioritization of exploration and should not be exclude form this type of combination. However, proper implementation of the information is essential to producing accurate potential maps. The main use of scenarios was in the shear-hosted spatial model. For the VMS spatial model only one scenario was used, owing to the fact that the relevant lithologies were syn-volcanic. Scenario 3 is considered to be the main mineralization event for the JSZ, however, results showed that scenario 1 had the highest correlation with known occurrences. This scenario did not make use of input from the heat component. This may be suggesting that additional heat from intrusive bodies is not a major factor in the distribution of shear-hosted gold. This project has demonstrated that the use of scenarios based on geological knowledge of the project area can be implemented and will effect the prioritization of future exploration.

The use of multiple scenarios and different proximity map functions in this approach to combination are more easily implemented if the components of the conceptual model are treated separately. Treating components separately allows for: 1) the modification of a sub-potential model without having to change or recombine the

other sub-potential models; and 2) they allow the given sub-potential models to be combined in different ways.

The Dempster-Shafer Belief theory and Fuzzy logic data fusion methods produce similar results, which is to be expected because the two methods use the same input data and weights. The main differences in the output maps primarily occurred locally with those high potential zones. The range and distribution of potential values for the two methods vary slightly with the fuzzy method have a greater range and distribution of values. Both methods have produced accurate output potential maps at the scale and complexity of the spatial models. The Fuzzy logic method showed better correlation with known occurrences than the Dempster-Shafer method. However, it is considered here that the addition of an uncertainty function in the Dempster-Shafer method allows for more control of the weighting of input maps. The uncertainty factor should become more important as spatial models become more complex. In order to take full advantage of the uncertainty factor the concept of uncertainty and belief must be well defined. Choosing which method to use in other locations will dependent on: 1) time, 2) scale, or accuracy required for the project; and, 3) missing data.

This project was completed at greenstone belt scale and made use of regional data sets compiled from Provincial and Federal agencies. Although the Lynn Lake Greenstone Belt has been explored off and on for over 50 years, other areas that have experience little or no exploration, but have regional data sets available, are prime candidates for this approach to prioritizing areas for exploration and land use management. This combination approach is not limited to regional data sets, but can be implemented at any scale. For example, a set of high potential zones determined at the

regional scale can be investigated and more detailed data sets can be collected for those areas. The process can be completed over again on the new data sets and exploration within regional high potential zones is further narrowed down to specific locations. This is, in essence, no different than exploration processes. Data fusion is simply a tool that makes use of the processing power of computers. However, as with any tool, there are specific processes that must be followed and problems that must be addressed.

This project has demonstrated how the expert system, or knowledge driven, approach can be used to translate theoretical principles defined in the conceptual model to produce a spatial model. In combination with the fuzzy logic and Dempster-Shafer data fusion methods this approach has the ability to accurately prioritize areas for exploration. Combination is not, however, limited to locating potential deposits, but may be a useful tool to remotely locate high deformation zones and major structural trends.

REFERENCES

An, P., Moon, W.M. and, Bonham-Carter, G.F. 1994a. An object-oriented knowledge representation structure for exploration data integration. Nonrenewable Resources, **3**: 132-145.

An, P., Moon, W.M. and, Bonham-Carter, G.F. 1994b. Uncertainty management in integration of exploration data using the belief function. Nonrenewable Resources, **3**: 60-71.

An, P., Moon, W.M., and Renez, A. 1991. Application of fuzzy set theory for integration of geological, geophysical, and remote sensing data. Canadian Journal of Exploration Geopysics, **27**: 1-11.

Ansdell, K.M., Corrigan, D., Stern, R., and Maxeiner, R., 1999. Shrimp U-Pb geochronology of complex zircons from Reindeer Lake, Saskatchewan: Implications for timing of sedimentation and metamorphism in the northwestern Trans-Hudson Orogen. *In* Geological Association of Canada - Mineralogical Association of Canada. Joint Annual Meeting, Abstract **24**: 3.

Argialas, D.P., and Harlow, C.A. 1990. Computational image interpretation models: An Overview and a perspective. Photogrammetric Engineering and Remote Sensing, **56**: 871 – 886.

Ascough, G. 1999. Geophysical characteristics of volcanogenic massive sulphide deposits. *In* Geophysics in mineral exploration: Fundamentals and case histories. *Edited by* C. Lowe, M.D. Thomas, and W.A. Morris. Geological Association of Canada, Short Course Notes, **14**: 41-62.

Baldwin, D.A. 1989. Mineral deposits and occurrences in the Lynn Lake Area, NTS 64C/14. Mineral Deposit Series Report No. 6, Manitoba Energy and Mines, Geological Services.

Baldwin, D.A., Syme, E.C., Zwanzig, H.V., Gordon, T.M., Hunt, P.A., and Stevens, R.D. 1987. U-Pb zircon ages from the Lynn Lake and Rusty Lake metavolcanic belts, Manitoba: two ages of Proterozoic magmatism. Canadian Journal of Earth Sciences, **24**,: 1053 – 1063.

Baldwin, D.A., Parbery, D., Boden, S., and Michielsen, A. 1985. Mineral deposit studies in the Lynn Lake and Barrington Lake areas. *In* Report of Field Activities 1985. Manitoba Energy and Mines, Geological Services, pp. 20-28.

Bateman, J.D. 1945. McVeigh Lake area, Manitoba. Geological Survey of Canada, Paper 45-14, pp. 34.

Beaumont-Smith, C.J. 2000. Structural analysis of the Johnson Shear Zone in the Gemmel Lake-Dunphy Lake area, Lynn Lake greenstone belt (parts of NTS 64C/11, /12). *In* Report on Activities 2000. Manitoba Trade, Industry and Mines, Manitoba Geological Survey, pp. 57-63.

Beaumont-Smith, C.J., and Edwards, C.D. 2000. Detailed structural analysis of the Johnson Shear Zone in the West Gemmel Lake area, Lynn Lake greenstone belt (parts of NTS 64C/11). *In* Report on Activities 2000. Manitoba Trade, Industry and Mines, Manitoba Geological Survey, pp. 64-68.

Beaumont-Smith, C.J., and Rogge, D.R. 1999. Preliminary structural analysis and gold metallogeny of the Johnson shear zone, Lynn Lake Greenstone Belt (Parts of NTS 64C/10, 11, 15). *In* Report of Activities, 1999. Manitoba Industry Trade and Mines, Geological Services, pp. 61-66.

Bickford, M.E., and Van Schmus, W.R. 1985. Preliminary U-Pb age data for the Trans-Hudson Orogen in northern Saskatchewan: new and revised results. *In* Summary of investigations 1985. Saskatchewan geological Survey, Saskatchewan Energy and Mines, Miscellaneous Report 85-4, pp. 63-66.

Bonham-Carter, G.F. 1994. Geographical Information Systems for Geoscientists: Modelling with GIS. Pergamon Press, Oxford, United Kingdom, pp. 398.

Bonham-Carter, G.F., Reddy, R.K.T., and Galley, A.G. 1993. Knowledge-driven modeling of volcanic massive sulphide potential with a geographical information system. *In* Mineral Deposit Modeling. *Edited by* R.V. Kirkham, W.D. Sinclair, R.I. Thorpe, and J.M. Duke. Geological Association of Canada, Special Paper 40, pp. 735–749.

Bursnall, J.T. 1989. Mineralization and shear zones. Geological Association of Canada, Short Course Notes, **6**.

Cann, J.R., Strens, M.R., and Rice, A. 1985. A simple magma-driven hydrothermal balance model for the formation of volcanogenic massive sulphides. Earth and Planetary Scinece Letters, **76**: 123-134.

Card, K.H., and Poulsen, K.H. 1998. Geology and mineral deposits of the Superior Province of the Canadian Shield. *In* Chapter 2, Geology of the Precambrian Superior and Grenville Provinces and Precambrian Fossils in North America. *Edited by* S. Lucus and M.R. St-Onge, Geological Survey of Canada, Geology of Canada, no.7, pp. 13-194.

Chung, C.F., and Fabbri, A.G. 1993. The representation of geoscience information for data integration. Nonrenewable Resources, **2**: 122-139.

Colvine, A.C., Fyon, J.A., Heather, K.B., Marmont, S., Smith, P.M., and Troop, D.G. 1988. Archean lode gold deposits in Ontario. Ontario Geological Survey, Miscellaneous Paper 139, pp. 136.

Dempster, A.P. 1968. A generalization of Bayesian inference. Journal Royal Statistical Society, ser. B, **30:** 205-247.

Elliot, S.R. 1986. Petrology, lithogeochemistry and metasomatic flux of the alteration zone associated with the Lar deposit, Lynn Lake area, Manitoba. University of Waterloo, M.Sc. thesis (unpublished), pp. 278.

Etheridge, M.A., Cox, S.F., Wall, F.J., and Vernon, R.H. 1984. High fluid pressures during regional metamorphism and deformation: Implications for mass transport and deformation mechanisms. Journal of Geophysical Research, **89**: 4344-4358.

Franklin, J.M. 1993. Volcanic-associated massive sulphide deposits. *In* Mineral Deposit Modeling. *Edited by* R. V. Kirkham, W.D. Sinclair, R.I. Thorpe, and J.M. Duke. Geological Association of Canada, Special Paper 40, pp. 315–335.

Fraser, D.C. 1969. Conturing of VLF-EM data. Geophysics, **34**: 958-967.

Fedikow, M.A.F., Ferreira, K.J., and Baldwin, D.A. 1991. The Johnson Shear Zone - A regional metallogenetic feature in the Lynn Lake area. Manitoba Energy and Mines, Mineral Deposit Thematic Map Series, Map 91-1.

Ferreira, K.J. 1993a. Mineral Deposits and Occurences in the McGavock Lake Area, NTS 64C/11. Mineral Deposit Series Report No. 26. Manitoba Energy and Mines, Geological Services.

Ferreira, K.J. 1993b. Mineral Deposits and Occurences in the Sickle Lake Area, NTS 64C/10. Mineral Deposit Series Report No. 23. Manitoba Energy and Mines, Geological Services.

Ferreira, K.J. 1993c. Mineral Deposits and Occurences in the Laurie Lake Area, NTS 64C/12. Mineral Deposit Series Report No. 9. Manitoba Energy and Mines, Geological Services.

Ferreira, K.J., and Baldwin, D.A. 1997. Mineral Deposits and Occurences in the Cockeram Lake Area, NTS 64C/15. Mineral Deposit Series Report No. 8. Manitoba Energy and Mines, Geological Services.

Ferreira, K.J. 1986. Geological investigations in the Foster Lake - Wasekwan Lake area. Manitoba Energy and Mines, Minerals Division, Report of Field Activities 1986. pp. 13 - 17.

Galley, A.G. 1993. Characteristics of semiconformable alteration zones associated with volcanogenic massive sulphide districts. Journal of Geochemical Exploration, **48**: 175-200.

George, H., and Bonham-Carter, G.F. 1989. Spatial modelling of geological data for gold exploration, Start Lake area, Saskatchewan. *In* Statistical applications in the Earth sciences, *Edited by* F.P. Agterberg, and G.F. Bonham-Carter. Geological Survey of Canada, Paper 89-9, pp. 157-169.

Gibson, H.L., Watkinson, D.H., and Comba, C.D.A. 1983. Silicification: Hydrothermal alteration in an Archean geothermal system within the Amulet rhyolite formation, Noranda, Quebec. Economic Geology, **78**: 954-971.

Gilbert, H.P. 1993. Geology of the Barrington Lake-Melvin Lake-Fraser Lake area. Manitoba Energy and Mines, Geological Report GR87-3, pp. 97.

Gilbert, H.P., Syme, E.C., and Zwanzig, H.V. 1980. Geology of the metavolcanic and volcaniclastic metasedimentary rocks in the Lynn Lake area. Geological Paper GP80-1, Manitoba Department of Energy and Mines, Mineral Resources Division, pp. 118.

Gordon, T.M., Hunt, P.A., Bailes, A.H., and Syme, E.C. 1990. U-Pb ages from the Flin Flon and Kisseynew belts, Manitoba: chronology of the crust formation at an Early Proterozoic accretionary margin. *In* The early Proterozoic Trans-Hudson Orogen of North America: *Edited by* J.F. Lewry, and M.R. Stauffer. Geological Association of Canada, Special Paper 37, pp. 177 – 199.

Henley, R.W., and Berger, B.R. 1993. What is an exploration model anyway? – An analysis of the cognitive development and use of models in mineral exploration. *In* Mineral Deposit Modeling. *Edited by* R.V. Kirkham, W.D. Sinclair, R.I. Thorpe, and J.M. Duke. Geological Association of Canada, Special Paper 40, pp. 41-50.

Hodgson, C.J. 1993. Mesothermal lode-gold deposits. *In* Mineral Deposit Modeling, (ed.) R.V. Kirkham, W.D. Sinclair, R.I. Thorpe and J.M. Duke; Geological Association of Canada, Special Paper 40, pp. 635–678.

Hodgson, C.J., and Lydon, J.W. 1977. The geological setting of volcanogenic massive sulfide deposits and active hydrothermal systems: Some implications for exploration. Canadian Institute of Mining and Metallurgy, Bulletin, **70**: 95-106.

Hoffman, P.F. 1990. Subdivisons of the Churchill Province and extent of the Trans-Hudson Orogen. *In* The Early Proterozoic Trans-Hudson Orogen of North America. *Edited by* J.F. Lewry, and M.R. Stauffer. Geological Association of Canada, Special Paper 37, pp. 15 – 39.

Hoffman, P.F. 1981. Autopsy of Athapuscow Aulacogen: a failed arm affected by three collisions. *In* Basins of Canada. *Edited by* F.H.A. Campbell. Proterozoic: Geological Survey of Canada, Paper 81-10, pp. 97 – 101.

Jackson, S.L. 1988. Alteration zones, structure and metamorphism of the Laurie Lake area. *In* Manitoba Energy and Mines, Report on Field Activities, 1988. pp. 178-182.

Jones, L.R., Beaumont-Smith, C.J., and Lafrance, B. 2000. Preliminary structural and gold metallogenic studies at the burnt timber mine and surrounding area, Lynn Lake Greenstone belt (NTS 64C/10). *In* Report of Activities 2000. Manitoba Industry Trade and Mines, Manitoba Geological Survey, pp. 82-90.

Kearey, P., and Brooks, M. 1991. An introduction to geophysical exploration 2nd Edition. Blackwell Science, Oxford, pp. 254.

Keating, P. 1999. Application of electromagnetic method in mineral exploration. *In* Geophysics in mineral exploration: Fundamentals and case histories. *Edited by* C. Lowe, M.D. Thomas, and W.A. Morris. Geological Association of Canada, Short Course Notes, **14**: 115-126.

Keays, R.R. 1984. Archean gold deposits and their source rocks: the upper mantle connection. *In* Gold'82. *Edited by* R.P. Foster. Geological Society of Zimbabwe, Special Publication Number 1, pp. 17-52.

Kenaley, D.S. 1982. Petrology, geochemistry and economic geology of the selected gold claims in rocks of the Wasekwan Lake area, Lynn Lake district, Manitoba, Canada. University of North Dakota, M.Sc. Thesis, pp. 306.

Kerrich, R. 1989a. Geodynamic setting and hydraulic regimes: Shear zone hosted mesothermal gold deposits. *In* Mineralization and shear zones. *Edited by* J.T. Bursnall. Geological Association of Canada, Short Course Notes, **6**: 89-129.

Kerrich, R. 1989b. Geochemical evidence on the sources of fluids and solutes for shear zone hosted mesothermal Au deposits. *In* Mineralization and shear zones. *Edited by* J.T. Bursnall. Geological Association of Canada, Short Course Notes, **6**: 129-198.

Lewry, J.F., and Collerson, K.D. 1990. The Trans Hudson Orogen: Extent, subdivisions, and problems. *In* The Early Proterozoic Trans-Hudson Orogen of North America. *Edited by* J.F. Lewry, and M.R. Stauffer. Geological Association of Canada, Special Paper 37, pp. 1 – 14.

Lewry, J.F., Macdonald, R., Livesey, C., Meyer, M.T., Van Schmus, W.R., and Bickford, M.E. 1987. U-Pb geochronology of accreted terranes in the Trans Hudson Orogen in northern Saskatchewan. *In* Geochemistry and Mineralization of Proterozoic Volcanic Suites. *Edited by* T.C. Pharaoh, R.D. Beckinsale and R. Rickards. Geological Society of London, Special Publication 33 33, pp. 147-166.

Lopes, A., Touzi, R., and Nezry, E. 1990. Adaptive speckle filters and scene heterogeneity. IEEE Transactions on Geoscience and Remote Sensing, **28**: 992-1000.

Lowe, C. 1999. Application of the magnetic method in mineral exploration: Fundamentals and recent developments. *In* Geophysics in mineral exploration:

Fundamentals and case histories. *Edited by* C. Lowe, M.D. Thomas, and W.A. Morris. Geological Association of Canada, Short course notes **14**: 131-162.

Lowell, R.P., and Rona, P.A. 1985. Hydrothermal models for the generation of massive sulphide deposits. Journal of Geophysical Research, **90**: 8769-8783.

Lydon, J.W. 1988a. Volcanogenic massive sulphide deposits, part 1: a descriptive model. *In* Ore Deposit Models. *Edited by* R.G. Roberts, and P.A. Sheahan. Geoscience Canada, Reprint Series 3, pp. 145–154.

Lydon, J.W. 1988b. Volcanogenic massive sulphide deposits, part 2: genetic models. *In* Ore Deposit Models. *Edited by* R.G. Roberts and P.A. Sheahan. Geoscience Canada, Reprint Series 3, pp. 155–182.

Milligan, G.C. 1960. Geology of The Lynn Lake district. Manitoba Mines and Natural Resources, Mine Branch Publication 57-1, pp. 317.

Moon, W.M. 1993. On mathimatical representation and integration of multiple spatial geoscience data sets. Canadian Journal of Remote Sensing, **19**: 63 – 67.

Moon, W.M. 1990. Integration of geophysical and geological data using evidential belief function. IEEE Transactions on Geoscience and Remote Sensing, **28**: 711-720.

Murphy, J.B. 1989. Tectonic environment and metamorphic characteristics of shear zones. *In* Mineralization and shear zones. *Edited by* J.T. Bursnall. Geological Association of Canada, Short Course Notes, **6**: 29 - 48.

Norman, G.W.H. 1933. Granville Lake district, northern Manitoba. Geological Survey of Canada, Summary Report, Part C, pp. 23-41.

Olson, P.E. 1987. The stratigraphy, structural geology and geochemistry of the Fox Lake massive sulfide deposit. University of Manitoba, M.Sc. Thesis (unpublished), pp. 220.

Palacky, G.J. 1987. Resistivity characteristics of geologic targets. *In* Electromagnetic methods in applied geophysics. *Edited by* M.N. Nabighian. Society of Exploration Geophysics, **1**: 53-130.

Peck, D.C., and Eastwood, A.M. 1997. Geochemical and structural analysis of gold mineralization at the Burnt Timber mine, Lynn Lake. *In* Report of Activities 1997. Manitoba Energy and Mines, geological Services, pp. 50-60.

Peck, D.C., Lin, S., Atkin, K., and Eastwood, A.M. 1998. Reconnaissance structural studies of the Au Metallotects in the Lynn Lake greenstone belt (parts of NTS 64C/10, C/11, C/15). *In* Report on Activities, 1998. Manitoba Energy and Mines, Geological Services, pp. 69-74.

Peck, D.C., and Smith, T.E. 1989. The geology and geochemistry of the Cratwright Lake area: Lynn Lake Greenstone Belt, northwestern Manitoba. Canadian Journal of Earth Science, **26**: 716-736.

Philpotts, A.R. 1990. Principles of igneous and metamorphic petrology. Prentice Hall, Englewood Cliffs, New Jersey, pp. 498.

RADARSAT International, 1996. RADARSAT Geology Handbook. RADARSAT International, unpublished.

Ramsay, J.G. 1980. Shear zone geometry: a review. Journal of Structural Geology, **2**: 83-99.

Ramsay, G.H., and Graham, R.H. 1970. Strain variation in shear belts. Canadian Journal of Earth Sciences, **7**: 786-813.

Ramsay, J.G., and Huber, M.I. 1987. The techniques of modern structural geology, Volume II: Folds and Fractures. Academic press, Orlando, pp. 700.

Rencz, A.N., Harris, J., Watson, G.P., and Murphy, B. 1994. Data integration for mineral exploration in the Antigonish Highlands, Nova Scotia: Application of GIS and RS. Canadian Journal of Remote Sensing 1994, **20**: 257-267.

Richards, J.A. 1993. Remote Sensing and digital image analysis: An introduction. Springer-Verlag, New York, pp. 340.

Richardson, D.J., and Ostry, G. 1996. Gold deposits of Manitoba. Manitoba Energy and Mines, Economic Report ER 86-1 (second edition), pp. 114.

Roberts, R.G. 1988. Archean lode gold deposits. *In* Ore Deposit Models. *Edited by* R.G. Roberts, and P.A. Sheahan. Geoscience Canada, Reprint Series 3, pp. 1–20.

Rogge, D.M. Halden, N.M., and Beamont-Smith, C.J. 2000. Mineralization potential mapping: A data fusion analysis. *In* Report of Activities 2000. Manitoba Industry Trade and Mines, Manitoba Geological Survey, pp. 82-90.

Saager, R., Meyer, M., and Muff, R. 1982. Gold distribution in supracrustal rocks in Archean greenstone belts in Southern Africa and from Paleozoic ultramafic complexes of the European Alps: Metallogenic and geochemical implications. Economic Geology, **77**: 1-24.

Seyfried, W.E., and Janecky, D.R. 1985. Heavy metal and sulfur transport during subcritical and supercritical hydrothermal alteration of basalt: Influence of fluid pressure and basalt composition and crystallinity. Geochimica et Cosmochimica Acta, **49**: 2545-2560.

Shafer, G. 1976. A mathematical theory of evidence. Princeton University Press, New Jersey, pp. 297.

Sharma, K.N.M. Singhroy, V.H., Madore, L., Levesque, J., Herbert, C., and Hinse, M. 1999. Use of radar images in the identification of major regional structures in the Grenville Province, western Quebec. Canadian Journal of Remote Sensing, **25**: 278-291.

Sherman, G.R. 1992. Geology, hydrothermal activity and gold mineralization in the Gemmell Lake area of the early Proterozoic Lynn Lake Greenstone Belt, Manitoba. M.Sc. thesis, University of Windsor, Windsor, Ontario, pp. 148.

Sherman, G.R., Samson, I.M., and Holm, P.E. 1989. Deformation, veining and gold mineralization along part of the Johnson Shear Zone, Lynn Lake Greenstone belt, Manitoba. *In* Manitoba Energy and Mines, Minerals Division, Report of Field Activities, 1989, pp. 16-18.

Shi, Z., and Fung, K.B. 1994. A comparison of digital speckle filters. Proceedings of IGARSS'94, **4**: 2129-2131.

Sibson, R.H. 1989. Earthquake faulting as a structural process. Journal of Structural Geology, **11**: 1-14.

Sibson, R.H., Robert, F., and Poulsen, K.H. 1988. High angle reverse faults, fluid pressure cycling, and mesothermal gold-quartz deposits. Geology, **16**: 551-555.

Singhroy, V., and Saint-John, R. 1999. Effects on the selection of RADARSAT-1 incidence angle for geological applications. Candian Journal of Remote Sensing, **25**: 211-217.

Spence, C.D., and de Rosen-Spence, A.F. 1975. The place of sulphide mineralization in the volcanic sequence at Noranda, Quebec. Economic Geology, **70**: 90-101.

Srivastav, S.K., Bhattacharya, A., Kamaraju, M.V.V., Sreenivasa Reddy, G., Shrimal, A.K., Metha, D.S., List, F.K., and Burger, H. 2000. Remote sensing and GIS for locating favourable zones of lead-zinc-copper mineralization in Rajpura-Dariba area, Rajasthan, India. International Journal of Remote Sensing, **21**: 3253-3267.

Syme, E.C. 1990. Stratigraphy and geochemistry of the Lynn Lake and Flin Flon metavolcanic belts, Manitoba. *In* The Early Proterozoic Trans-Hudson Orogen of North America. *Edited by* J.F. Lewry, and M.R. Stauffer. Geological Association of Canada, Special Paper 37, pp. 143 – 161.

Syme, E.C. 1985. Geochemistry of metavolcanic rocks in the Lynn Lake Belt. Geological Report GR84-1, Manitoba Energy and Mines, Geological Services.

Thom, A., Arndt, N., and Stauffer, M.R. 1990. Flin Flon and west La Ronge belts, Saskatchewan: products of Proterozoic sub-duction related volcanism. . *In* The Early Proterozoic Trans-Hudson Orogen of North America. *Edited by* J.F. Lewry, and M.R. Stauffer. Geological Association of Canada, Special Paper 37, pp. 163-175.

Thompson, J.F.H. 1993. Application of deposit models to exploration. *In* Mineral Deposit Modeling. *Edited by* R.V. Kirkham, W.D. Sinclair, R.I. Thorpe, and J.M. Duke. Geological Association of Canada, Special Paper 40, pp. 51-67.

Turek, A., Woodhead, J., and Zwanzig, H.V. 2000. U-Pb age of the gabbro and other plutons at Lynn Lake (Part of NTS 64C). *In* Report of Activities 2000. Manitoba Trade, Industry and Mines, Manitoba Geological Survey, pp. 97-104.

Van Schmus, W.R., Bickford, M.E., Lewry, J.F., and Macdonald, R. 1987. U-Pb geochronology in the Trans-Hudson Orogen, northern Saskatchewan, Canada. Canadian Journal of Earth Sciences, v. 24, pp. 407-424.

Wald, L. 1999. Some Terms of Reference in Data Fusion. IEEE Transactions on Geosceince and Remote Sensing, **37**: 1190-1193.

Watson, G.P., and Rencz, A.N. 1989. Data integration studies in northern New Brunswick. *In* Statistical applications in the Earth sciences. *Edited by* F.P. Agterberg, and G.F. Bonham-Carter. Geological Survey of Canada, Paper 89-9, pp. 185-191.

Watters, B.R., and Pearce, J. 1987. Metavolcanic rocks of the La Ronge Domain in the Churchill Province, Saskatchewan: geochemical evidence for a volcanic arc origin. *In* Geochemistry and mineralization of Proterozoic volcanic suites. *Edited by* T.C. Pharaoh, R.D. Beckinsale, and R. Rickards. Geological Society of London, Special Publication 33, pp. 167 – 182.

Wright, D.F., and Bonham-Carter, G.F. 1996. VHMS favourability mapping with GIS-based integration models, Chisel Lake–Anderson Lake area. *In* EXTECH I: A Multidisciplinary Approach to Massive Sulphide Research in the Rusty Lake–Snow Lake Greenstone Belts, Manitoba. *Edited by* G.F. Bonham-Carter, A.G. Galley, and G.E.M. Hall. Geological Survey of Canada, Bulletin 426, pp. 339–376, 387–401.

Zedeh, L.A. 1965. Fuzzy sets. IEEE Information and Control, **8**: 338-353.

Zimmermann, H., and Zysno, P. 1980. Latent connectives, human decision making. Fuzzy Sets and Syztems, **4**: 37-51.

Zwanzig, H.V., Syme, E.C., and Gilbert, H.P. 1999. Updated trace element geochemistry of ca. 1.9 Ga metavolcanic rocks in the Paleoproterozoic Lynn Lake Belt. Manitoba Industry, Trade and Mines, Geological Services, Open File Report OF99-13, pp. 46.

Zwanzig, H.V. 1990. Kisseynew gneiss belt in Manitoba: stratigraphy, atructure and tectonic evolution. *In* The Early Proterozoic Trans-Hudson Orogen of North America. *Edited by* J.F. Lewry, and M.R. Stauffer. Geological Association of Canada, Special Paper 37, pp. 95-120.

APPENDIX A

Compiled Data Sets for the Lynn Lake Greenstone Belt

Appendix A is a list of compiled data sets used in this project. All data sets are on the included on CD. Appendix A also lists output potential maps generated from the shear-hosted and VMS spatial models. Output potential maps generated using fuzzy logic and Dempster-Shafer methods are included. All potential maps are on the included CD.

Geological Map 1:50 000:	Revised 1980, digitized 1998 Geological Services, Manitoba Energy and Mines
Geochemical Units 1:250 000:	OF99-13-1 Lynn Lake Greenstone Belt, Geological Services, Manitoba Energy and Mines (1999)
Aeromagnetic Digital Data:	10500 Barrington lake (1) TF, VG, VLF-EM 13800 Lynn Lake 1982 (1) TF, VG, VLF-EM 18201 Lynn Lake 100 1985 (2) TF, VG, VLF-EM Geological Survey of Canada; Geological Services, Manitoba Energy and Mines
Syntetic Apature Radar Data:	RADARSAT_1, SAR Standard 3 Beam Mode, Canadian Space Agency, Manitoba Remote Sensing Centre (2000)
Geochemical Data:	Lynn Lake Greenstone Belt, Chris Beaumont-Smith, Manitoba Geological Survey (1999, 2000)
Geochemical Data:	Lynn Lake Greenstone Belt, Ground truthing, Derek Rogge and Manitoba Geological Survey (2000, 2001)

(1) A "Joint Agreement" program between the Government of Canada and the Province of Manitoba.
(2) The Canada-Manitoba Mineral Development Agreement (MDA), 1984 – 1989

Fuzzy Shear-Hosted Spatial Model

Potential Output

182fs5dll, 182fs5dle, 138fs5dll, 138fs5dle, 105fs5dll, 105fs5dle,
182fs4dll, 182fs4dle, 138fs4dll, 138fs4dle, 105fs4dll, 105fs4dle,
182fs3dll, 182fs3dle, 138fs3dll, 138fs3dle, 105fs3dll, 105fs3dle,
182fs1dll, 182fs1dle, 138fs1dll, 138fs1dle, 105fs1dll, 105fs1dle,
182fs5dfjl, 182fs5dfje, 138fs5dfjl, 138fs5dfje, 105fs5dfjl, 105fs5dfje,
182fs4dfjl, 182fs4dfje, 138fs4dfjl, 138fs4dfje, 105fs4dfjl, 105fs4dfje,
182fs3dfjl, 182fs3dfje, 138fs3dfjl, 138fs3dfje, 105fs3dfjl, 105fs3dfje,
182fs1dfjl, 182fs1dfje, 138fs1dfjl, 138fs1dfje, 105fs1dfjl, 105fs1dfje
abbreviations: fs fuzzy scenario; dl lineament deformation; dfj lineament, fault, and JSZ deformation; l logarithmic shear-stress function; e exponential shear-stress function.

Fluid-Heat Potential

ffhs5, ffhs4, ffhs3
abbreviations: ffh fuzzy fluid-heat scenario

Source Zone Potential

fszs5, fszs4, fszs3, fszs1
abbreviations: ffh fuzzy source zone scenario

Deformation Potential (Lineament)

182fdll, 182fdle, 138fdll, 138fdle, 105fdll, 105fdle
abbreviations: fdl fuzzy lineament deformation; l logarithmic shear-stress function; e exponential shear-stress function.

Deformation Potential (Lineament, Faults, JSZ)

182fdfjl, 182fdfje, 138fdfjl, 138fdfje, 105fdfjl, 105fdfje
abbreviations: fdfj fuzzy lineament, fault, and JSZ deformation; l logarithmic shear-stress function; e exponential shear-stress function.

Fault Potential

182ftl, 182fte, 138ftl, 138fte, 105ftl, 105fte
abbreviations: ft fuzzy fault; l logarithmic shear-stress function; e exponential shear-stress function.

JSZ Proximity Input

182fjszl, 182fjsze, 138fjszl, 138fjsze, 105fjszl, 105fjsze
abbreviations: fjsz fuzzy Johnson Shear Zone; l logarithmic shear-stress function; e exponential shear-stress function.

Deformation Potential VLF, VG, SAR

182fvlfl, 182fvlfe, 138fvlfl, 138fvlfe, 105fvlfl, 105fvlfe
182fvgl, 182fvge, 138fvgl, 138fvge, 105fvgl, 105fvge
182fsarl, 182fsare, 138fsarl, 138fsare, 105fsarl, 105fsare
abbreviations: f fuzzy; vlf very low frequency electromagnetics; vg vertical gradient magnetics; sar synthetic aperture radar; l logarithmic shear-stress function; e exponential shear-stress function.

VLF, VG, SAR lineaments

vlflqline182, vlflqline138, vlflqline105,
vlfoqline182, vlfoqline138, vlfoqline105,
vgline182, vgline138, vgline105,

sarline
abbreviations: vlf very low frequency electromagnetics; lq line quadrature; oq orthoquadrature; vg vertical gradient magnetics; sar synthetic aperture radar

Fuzzy VMS Spatial Model

Potential Output

105fvmsmcz, 138fvmsmcz, 105fvmsmcz, 182fvmsa, 138fvmsa, 105fvmsa
abbreviations: fvms fuzzy volcanogenic massive sulphide; mcz without CuZn potential; a with CuZn potential.

Stratigraphic Potential

fstrat, fburnt, fvolcsed, fvolcmafic, fvolcfelsic, fvolcinter
abbreviations: f fuzzy; strat stratigraphic potential, burnt Burntwood Sediments; volcsed volcanogenic sediments; volcmafic-felsic-inter mafic-felsic-intermediate volcanic rocks.

Heat Potential

fheat
abbreviations: fheat fuzzy heat.

CuZn Potential

fCuZn, fCu, fZn
abbreviations: fheat fuzzy; Cu copper; Zn zinc.

Geophysics

182ftfvlf, 138ftfvlf, 105ftfvlf
abbreviations: f fuzzy; vlf very low frequency electromagnetics; tf total field magnetics

Dempster-Shafer Shear-Hosted Spatial Model

Potential Output

Belief
182dbs5dll, 182dbs5dle, 138dbs5dll, 138dbs5dle, 105dbs5dll, 105dbs5dle,
182dbs4dll, 182dbs4dle, 138dbs4dll, 138dbs4dle, 105dbs4dll, 105dbs4dle,
182dbs3dll, 182dbs3dle, 138dbs3dll, 138dbs3dle, 105dbs3dll, 105dbs3dle,
182dbs1dll, 182dbs1dle, 138dbs1dll, 138dbs1dle, 105dbs1dll, 105dbs1dle,
182dbs5dfjl, 182dbs5dfje, 138dbs5dfjl, 138dbs5dfje, 105dbs5dfjl, 105dbs5dfje,
182dbs4dfjl, 182dbs4dfje, 138dbs4dfjl, 138dbs4dfje, 105dbs4dfjl, 105dbs4dfje,
182dbs3dfjl, 182dbs3dfje, 138dbs3dfjl, 138dbs3dfje, 105dbs3dfjl, 105dbs3dfje,
182dbs1dfjl, 182dbs1dfje, 138dbs1dfjl, 138dbs1dfje, 105dbs1dfjl, 105dbs1dfje
Plausibility
182dps5dll, 182dps5dle, 138dps5dll, 138dps5dle, 105dps5dll, 105dps5dle,
182dps4dll, 182dps4dle, 138dps4dll, 138dps4dle, 105dps4dll, 105dps4dle,
182dps3dll, 182dps3dle, 138dps3dll, 138dps3dle, 105dps3dll, 105dps3dle,
182dps1dll, 182dps1dle, 138dps1dll, 138dps1dle, 105dps1dll, 105dps1dle,
182dps5dfjl, 182dps5dfje, 138dps5dfjl, 138dps5dfje, 105dps5dfjl, 105dps5dfje,
182dps4dfjl, 182dps4dfje, 138dps4dfjl, 138dps4dfje, 105dps4dfjl, 105dps4dfje,
182dps3dfjl, 182dps3dfje, 138dps3dfjl, 138dps3dfje, 105dps3dfjl, 105dps3dfje,
182dps1dfjl, 182dps1dfje, 138dps1dfjl, 138dps1dfje, 105dps1dfjl, 105dps1dfje

abbreviations: dbs Dempster-Shafer belief scenario; dps Dempster-Shafer plausibility scenario; dl lineament deformation; dfj lineament, fault, and JSZ deformation; l logarithmic shear-stress function; e exponential shear-stress function.

Fluid-Heat Potential

dfhs5, dfhs4, dfhs3

abbreviations: dfh Dempster-Shafer fluid-heat scenario

Source Zone Potential

dszs5, dszs4, dszs3, dszs1

abbreviations: dfh Dempster-Shafer source zone scenario

Deformation Potential (Lineament)

182ddll, 182ddle, 138ddll, 138ddle, 105ddll, 105ddle

abbreviations: ddl Dempster-Shafer lineament deformation; l logarithmic shear-stress function; e exponential shear-stress function.

Deformation Potential (Lineament, Faults, JSZ)

182ddfjl, 182ddfje, 138ddfjl, 138ddfje, 105ddfjl, 105ddfje

abbreviations: ddfj Dempster-Shafer lineament, fault, and JSZ deformation; l logarithmic shear-stress function; e exponential shear-stress function.

Fault Potential

182dtl, 182dte, 138dtl, 138dte, 105dtl, 105dte

abbreviations: dt Dempster-Shafer fault; l logarithmic shear-stress function; e exponential shear-stress function.

JSZ Proximity Input

182djszl, 182djsze, 138djszl, 138djsze, 105djszl, 105djsze

abbreviations: djsz Dempster-Shafer Johnson Shear Zone; l logarithmic shear-stress function; e exponential shear-stress function.

Deformation Potential VLF, VG, SAR

182dvlfl, 182dvlfe, 138dvlfl, 138dvlfe, 105dvlfl, 105dvlfe

182dvgl, 182dvge, 138dvgl, 138dvge, 105dvgl, 105dvge

182dsarl, 182dsare, 138dsarl, 138dsare, 105dsarl, 105dsare

abbreviations: d Dempster-Shafer ; vlf very low frequency electromagnetics; vg vertical gradient magnetics; sar synthetic aperture radar; l logarithmic shear-stress function; e exponential shear-stress function.

VLF, VG, SAR lineaments

vlflqline182, vlflqline138, vlflqline105,

vlfoqline182, vlfoqline138, vlfoqline105,

vgline182, vgline138, vgline105,

sarline

abbreviations: vlf very low frequency electromagnetics; lq line quadrature; oq orthoquadrature; vg vertical gradient magnetics; sar synthetic aperture radar

Dempster-Shafer VMS Spatial Model

Potential Output

105dpvmsmcz, 138dpvmsmcz, 105dpvmsmcz, 182dpvmsa, 138dpvmsa, 105dpvmsa,
105dbvmsmcz, 138dbvmsmcz, 105dbvmsmcz, 182dbvmsa, 138dbvmsa, 105dbvmsa
abbreviations: dpvms Dempster-Shafer plausibility; dbvms Dempster-Shafer belief; volcanogenic massive sulphide; mcz without CuZn potential; a with CuZn potential.

Stratigraphic Potential

dstrat, dburnt, dvolcsed, dvolcmafic, dvolcfelsic, dvolcinter
abbreviations: d Dempster-Shafer; strat stratigraphic potential, burnt Burntwood Sediments; volcsed volcanogenic sediments; volcmafic-felsic-inter mafic-felsic-intermediate volcanic rocks.

Heat Potential

dheat
abbreviations: dheat Dempster-Shafer heat.

CuZn Potential

dCuZn, dCu, dZn
abbreviations: dheat Dempster-Shafer; Cu copper; Zn zinc.

Geophysics

182dtfvlf, 138dtfvlf, 105dtfvlf
abbreviations: vlf very low frequency electromagnetics; tf total field magnetics

APPENDIX B

Appendix B is a list of the shear-hosted deposits and occurrences in the southern part of the Lynn Lake Greenstone belt is compiled from the Mineral Deposit Series, Manitoba energy and Mines, including the West Gemmel Lake occurrence.

Lodestone Occurrence (NTS 64C/15 Location 44)

The Lodestone occurrence is located just west of Gold Lake, which is about 1 km south of Hughes Lake. Felsic to intermediate tuff, andesite, and minor argillite comprise the lithological units around the occurrence. The occurrence, located within intensely sheared rocks, lies just north of the interpreted northern edge of the JSZ. The deformation forms a zone about 15 - 30 m in width and is considered to be part of the JSZ (Gilbert et al., 1980). Milligan (1960) noted the presence of pyrite, chalcopyrite, galena, and visible gold, whereas Baldwin et al., (1985) described disseminated pyrite, arsenopyrite, and galena.

Cartwright Lake Area (NTS 64C/15 Locations 3,4 and 43)

A volcanic sequence about 2 km thick occurs at Cartwright Lake comprising basal tholeiitic Cockeram Basalts, overlain by tholeiitic basalts, felsic volcanic rocks, and turbitites of the Cartwright Lake bimodal suite. Hughes Lake Calc-alkaline andesites comprise the upper series. This sequence is intruded by pre-Sickle Group massive and foliated diorite, quartz diorite and tonalite. The regional metamorphic grade is greenschist with locally developed epidote amphibolite assemblages.

The main gold occurrence in the area is the Bonanza Claim on the east side of the southern arm of Cartwright Lake. Gold occurs in a vein network associated with a fractured porphyry dyke. The veins commonly contain up to 30% pyrite with l esser concentrations of galena, chalcopyrite, arsenopyrite, and bornite (Peck and Smith, 1989). Interbedded mafic flows and pyroclastic rocks occur north of the occurrence, whereas to the south rock exposures are quartz poor mudstone. Intensive silicification, carbonatization and epidotization are seen in adjacent rocks suggesting extensive hydrothermal circulation (Peck and Smith, 1989). Deformation in the area is observed at

the ductile - brittle contact between volcanic and sedimentary units with the granitic intrusions to the south. These contrasting units exhibit shearing and cataclastic textures consistent with the JSZ.

Burnt Timber Deposit (NTS 64C/15 Locations 6 and 36)

The Burnt Timber deposit is located approximately 13 km southwest of the town of Lynn Lake. The deposit produced 80 000 ounces of gold from 1993 - 1996 as an open pit operation. Shear laminated silicified and carbonatized volcanic and sedimentary rocks in the hanging wall of a post mineralization fault (T1) host the gold. Variably altered basalt, gabbro, and metasediments, or metavolcanic tuff, comprise the rocks on the south side of the T1 fault. This fault, located along the southern margin of the JSZ, strikes east-northeast and dips steeply to the north. Alteration associated with mineralization forms a 100 m wide zone within the JSZ (Jones et al., 2000). Silicification, carbonitization, and pyritic alteration increases towards the fault. Mineralization is fracture controlled and occurs as breccia zones and quartz veinlets; and as high grade, intensely silicified laminated shear zones. A spatial relationship has also been noted with felsic porphyry dykes observed on outcrop and from diamond drill core.

Foster Lake Area (NTS 64C/14 Location 9 and NTS 64C/15 Location 35)

The first description of a quartz sulphide-gold vein associated with the JSZ was given by Bateman (1945) north of Foster Lake towards Franklin Lake. Foster Lake is about 12 km southeast of Lynn Lake and only about 1 - 2 km west of the Burnt Timber open pit mine. A fine-grained granite along the north shore of the lake is flanked by a sequence of mafic, intermediate, and felsic sedimentary rocks that are subsequently overlain by mafic volcanic and intrusive rocks. These supracrustal rocks form an east-striking, north dipping layered sequence. Silicification occurs throughout the felsic sedimentary rocks, whereas chloritization is common in the mafic sedimentary rocks. The strongest alteration is associated with areas where fracture cleavage is well developed (Ferreira, 1986). Alteration is minimal in the fine-grained granite, mafic volcanic and intrusive rocks. Gold mineralization is located siliceous lenses enveloped in

deformed sulphide bearing felsic sedimentary rocks. Quartz-chlorite veins with coarse native gold, galena, and pyrite transect the sedimentary sequence.

Brown - Ace Vein Occurrence (NTS 64C/14 Location 8)

The Brown - Ace Vein occurrence is located 1.15 km west-north west from the west end of Franklin Lake. Plagioclase-phyric basaltic rocks of the Fox Mine - Gemmel Lake succession are found in the immediate vicinity to the occurrence. To the northeast aphyric basaltic rocks of the Cockeram Lake Basalts are only a few tens of away. Basalt flows, breccia, lapilli tuff and altered siliceous sedimentary rocks overly the occurrence. The silicified sedimentary rocks are intruded by a plagioclase porphyry dyke. Fracture zones, which host sulphide and gold mineralization, follow the "drag-folded trend" of the surrounding wall rocks. These fractures commonly occur within the siliceous rock and the plagioclase porphyry and comprise quartz veins with galena, sphalerite, pyrite, pyrrhotite and gold. Broad drag folds and complex shear zones within the area were noted by Bateman (1945) and Kenaley (1982), similar features are observed within other gold occurrences associated with the JSZ.

Finlay McKinlay and Prospector Occurrences (NTS 64C/11 Location 5)

These two gold occurrences occur within 200 m of each other about 16 km southwest of Lynn Lake. At both locations the precipitation of gold occurred after ductile deformation within late vein sets. Gold is associated with sulphides in the late vein sets and disseminations in the wall rock (Sherman et al., 1989).

The Finlay McKinlay occurrence is located within a quartz diorite close to the contact with the Sickle Group Conglomerate. Veins are coarse grained and highly fractured quartz with minor carbonate, biotite, chlorite and tourmaline. These veins occur within a relatively discrete shear zone, considered to part of the larger JSZ. They exhibit protomylonitic, mylonitic, and locally developed ultramylonitic textures. Sherman et al., (1989) noted three sets of vein types, however, gold is only associated with the quartz - sulphide veins that occupy the center of the shear zone. Alteration haloes comprise biotite, tourmaline, chlorite, carbonate, potassium feldspar, and pyrite

and are associated with the veins. Mineralization includes free gold, pyrite, chalcopyrite, pyrrhotite, arsenopyrite and magnetite.

The Prospector gold occurrence is hosted by felsic and mafic sedimentary rocks that form a thin unit between felsic and overlying mafic volcanic units. Ductile deformation includes tight folds, asymmetric folds, and boudinaged quartz veins, whereas brittle deformation is characterized by fracturing, brecciation, pseudotachylyte development, and faulting in narrow zones. Alteration haloes consisting of chlorite, quartz, biotite, tourmaline, carbonate, garnet, and potassium feldspar occur adjacent to the veins. Gold mineralization is minimal and there are no visible sulphides within these veins, however, pyrite, pyrrhotite, arsenopyrite, and magnetite do occur in minor amounts within the wall rock.

1.1 West Gemmel Lake Occurrence

Gold mineralization west of Gemmel Lake was identified in 1999 and occurs within sericitized and silicified volcaniclastic dacite intercalated with porphyritic gabbro (Beaumont-Smith and Edwards, 2000). The gold is associated with fine-grained acicular disseminated arsenopyrite and less abundant pyrite. The fine-grained dacite is intensly foliated and occurs in tight isoclinal folds within variably deformed gabbro. Mylonitic fabrics are commonly preserved in the dacite and finely laminated mafic tectonite units and narrow protomylonitic zones occur within the gabbro unit. Although the occurrence is part of the extended JSZ (Beaumont-Smith and Rogge, 1999) it displays a different structural, mineralization and alteration characteristics than other occurrences previously describe along the JSZ (Beaumont-Smith and Edwards, 2000).

Lasthope Occurrence (NTS 64C/10 Location 1)

This occurrence is located within the Miskwa Belt about 10 km south of the JSZ just west of a major fault. Magnetite bearing quartzite, feldspathic quartzite, mafic tuff, and quartz-feldspar porphyry compose a northwest-trending sequence that hosts the gold occurrence. Two major veins occur in the area, however, only the southern quartz-sulphide vein is mineralized. It includes sugary quartz with minor pyrite, chalcopyrite,

sphalertite, and trace galena. The vein cuts quartz stringers in the silicified wall rock (Milligan, 1960).

APPENDIX C

Appendix C is a list of the VMS known occurrences and deposits in the southern part of the Lynn Lake Greenstone belt is compiled from the Mineral Deposit Series, Manitoba energy and Mines.

1.2 VMS Deposits

Between 1970 and 1985 the Fox mine milled a total of 11 958 182 tonnes of ore with Cu and Zn grades of 1.82% and 1.78% respectively (Olson, 1987). The Fox mine (NTS 64C/12 location 1) is located southwest of Lynn Lake along Provincial road 396 about 1 km west of Mukasew Lake, formally known as Fox Lake. The deposit is within the Fox Mine succession (see chapter 2), which comprises mafic to felsic volcanic and sedmimentary rocks. South of the deposit is a tonalite intrusion and to the north is Sickle group arkosic sandstone and mafic and intermediate volcanic rocks. The sulphide lenes are laterally continuous within a 500 m thick sequence that was deposited in a subaqueous environment. Pyrite, chalcopyrite, sphalerite, and pyrrhotite are the major sulphide minerals in the deposit, which extends from the surface to a depth of 855 m. An alteration zone spatially associated with the sulphide lenses comprises qua rtz-sericite, quartz biotite, cordierite-anthophyllite, and biotite-phlogopite-talc-chlorite mineral assemblages (Ferreira, 1993).

The L ar de posit (NTS 64C /12 location 21), located on the northwest shore of Laurie Lake, is estimated to have 1 361 000 tonnes grading 0.8% Cu and 2.15% Zn. The deposit lies in a sequence of mafic fragmental and flows, felsic volcanic rocks, and greywackes; and, is underlain by greywacke, siltstone, mudstone and mafic volcanic rocks. To the north and south are granodioritic to tonalitic plutons. The deposit comprises two lenses enclosed predominantly in rhyodacitic rocks (Elliott, 1986) of near solid-to-solid sulphide, which includes pyrrhotite + pyrite ± sphalerite ± chalcopyrite ± magnetite ± tetrahedrite. The alteration zone spatially associated with the Lar deposit consists of coarse-grained cordierite-anthophyllite or anthopyllite-garnet-cordierite (Ferreira, 1993).

1.3 NTS 64C/12 VMS Occurrences

The Bag occurrence is on the east shore of Snake Lake and is underlain by a small enclave of Snake Lake Dacite, which is surrounded by mafic intrusive rocks (Location 8). Grab samples from outcrop exposure and pits give Cu and Zn values up to 3080 ppm and 6180 ppm respectively. The zone of mineralization comprises disseminated pyrite and chalcopyrite in a siliceous anthophyllite + cordierite + biotite ± garnet porphyroblastic schist (Ferreira, 1993).

Location 15 is southeast of Hatchet Lake and is underlain by mafic to intermediate volcanic rocks with greywacke, silstone, mudstone and tuff to the north. Garnetiferous biotitic intermediate volcanic rocks host the near solid to solid sulphide mineralization. Only trace Cu and Zn was noted from drill core samples (Ferreira, 1993).

The New Fox occurrence (Location 18) is 1.75 km south of Vaughan Lake and is underlain by greywacke, silstone, mudstone and lesser mafic volcanic rocks with a tonalitic intrusion to the north. Gilbert (1980) noted an alteration zone of porphyroblastic schist with assemblages of anthopyllite + gedrite ± garnet ± cordierite ± sillimanite ± staurolite. Mafic to intermediate volcanic flows and volcaniclastic rocks host the alteration zone, which has similar alteration assemblages as the Fox Mine deposit. Cu values are as high as 3789 ppm in rock samples, whereas core values are 1.14% cu and 0.02% Zn (Ferreira, 1993).

Interlayered mafic volcanic and sedimentary rocks underlie the Gran occurrence located between Laurie and Craig Lakes (Location 20). Four main units comprise the area and include mafic volcanic and volcaniclastic rocks, fine to medium grained feldspar + biotite ± quartz schist/gneiss, garnet + anthophyllite ± cordierite ± chlorite + biotite in a quartzofeldspathic matrix, and a weakly foliated medium to coarse-grained biotite granodiorite. The mineralized zone comprises seritizied siliceous rock with pyrite and pyrrhotite in quartz-biotite-garnet gneiss and mafic tuffaceous or volcaniclastic host rocks. Samples taken from the area contain up to 142 ppm Cu and 116 ppm Zn (Ferreira, 1993).

At the southern end of Laurie Lake is Location 24. This occurrence is underlain by mafic and felsic volcanic rocks, greywacke, siltstone, mudstone, conglomerate and Sickle sediments. To the north of the occurrence is mafic tuffs, deformed pillows and mafic breccia, whereas to the south lies Sickle sediments. Alteration zones in mafic to intermediate volcanic rocks are Fe-Mg-Al enriched and Ca-Na-K depleted (Jackson, 1988). The mineralized zone occurs within a weathered garnet-anthophyllite-porphyroblastic rock and includes pyrite and chalcopyrite with up to 2840 ppm Cu and 169 ppm Zn (Ferreira, 1993).

NTS 64C/11 VMS Occurrences

North of Wilmot Lake two occurrences (Location 4) are underlain by greywacke, siltstone and mudstone, mafic and felsic volcanic rocks and minor gabbroic intrusions. The first occurrence is the Wilmot west occurrence and is in a sequence of mafic heterolithic breccia, mafic and felsic tuff, and biotite- and hornblende-wackes and sandstone. Mineralization in the second occurrence, Wilmot east, is within a succession of sedimentary rocks, specifically siltstone. A mineralized intersection in core had assay values of 0.01% Cu and 0.17% Zn (Ferreira, 1993).

The Boiley Lake occurrence (Location 8) lies within a sequence of basalt and mafic dykes, intermediate tuffs interlayered with volcaniclastic rocks, rhyolite, felsic to intermediate tuff, discontinuous magnetite-chert iron formation, and a kyanite-sericite-quartz biotite schist + chert layer. Minor amounts of staurolite, anthophyllite, kyanite, sillimanite, and cordierite occur within a coarse-grained chlorite-garnet ± magnetic schist alteration zone. Pyrite and chalcopyrite are the dominant type of mineralization. Assay values from one drill core showed 3.7% Cu over 0.7 m (Ferreira, 1993).

Magnetic data shows a strong linear from Boiley Lake trending southeast towards Counsell Lake and location 11. Mafic to felsic volcanic, volcaniclastic and sedimentary rocks underlie a coarse-grained chlorite-garnet ± magnetite schist alteration zone, which hosts the Counsell Lake occurrence. Cu values from DDH samples range from 0.14% over 25.4 cm to 3.65% over 3.8 m (Ferriera, 1993).

North of Counsell Lake is the Pool Lake occurrence (Location 9), which is underlain by mafic flow and fragmental rocks and lenses of rhyolite to dacite volcanic rocks. To the north and southeast are felsic and intermediate plutonic rocks. To the west are Sickle sedimentary rocks. Mineralization is within oxidized, partly garnetiferous, and chloritic lens of felsic tuff and lapilli tuff, which is overlain by pillowed flows. Pyrite, arsenopyrite, pyrrhotite, and fine-grained chalcopyrite are the dominant mineralization with DDH assay values close to 1% Cu and Zn (Ferriera, 1993).

Location 18 is about 4 km east of Irene Lake and is underlain by mafic to intermediate flows and fragmental rocks, massive porphyritic rhyolite, greywacke, siltstone and mudstone. To the north is a tonalitic to granodioritic intrusion. Mineralization comprises minor amounts disseminated pyrrhotite, pyrite ± chalcopyrite ± sphalerite ± galena on outcrop and within core. DDH assay values contained 0.01 to 0.16 Cu and nil to 0.17% Zn. The Stear Lake occurrence (Location 19), just east of location 18, is located in a similar setting to location 19. DDH mineralized intersections include 0.08% Cu and 3.01% Zn over 6 cm, nil - 0.03% Cu and 0.04 - 0.015% Zn over 30 cm, and nil – 0.08% Cu and nil – 0.04% Zn (Ferriera, 1993).

1.4 NTS 64C/10 VMS Occurrences

Location 13 is located at Wiley Lakes and is underlain by tonalite and dioritic intrusions, aphyric and porpyritic basalt, and minor rhyolitic tuff. Siliceous and chloritic sections were found in core. Pyrite, pyrrhotite, and chalcopyrite mineralization in core is hosted by andesite, dacite, chlorite ± sericite schist and minor dacite porphyry. No geochemical data is available (Ferriera, 1993).

1.5 NTS 64C/14 VMS Occurrences

Southwest of Lynn Lake is Location 13 (NTS 64C/14) that lies within supracrustal volcanic, volcaniclastic and sedimentary rocks and is underlain by the Fraser Lake Gabbro. Pyrite, Pyrrhotite, chalcopyrite, and sphalerite are disseminated within a hornfels inclusion in the supracrustal rocks (Baldwin, 1989).

Location 14 is south of Eldon Lake and is underlain by greywacke, siliceous argillite, siltstone and chert, which are intruded by diorite, granodiorite, granite and

gabbro. Mineralization includes pyrrhotite, pyrite, sphalerite, and chalcopyrite with assay values ranging from 11 ppm and 123 ppm to 855 ppm and 3530 ppm Cu and Zn respectively (Baldwin, 1989).

Rhyolitic flows and tuff with minor intercalated mafic tuff underlies an occurrence 1.5 km west from the south end of Eldon Lake (Location 48). Felsic rocks and a sequence of mafic volcanic flows occur to the north of location 48, whereas a quartz diorite is intruded into felsic volcanic and sedimentary rocks to the south. Mineralization found in core included solid pyrrhotite associated with a quartz vein. Assay values from the core gave nil – 0.1% Cu and nil – 0.2% Zn (Baldwin, 1989).

Mineralization at location 53 is disseminated pyrite and pyrrhotite within a mafic tuff. The occurrence is underlain by conglomerate, hornblende-bearing and biotite-bearing greywacke, siltstone and mudstone. No geochemical data is available, however, a solid sulphide lens of pyrite, chalcopyrite, sphalerite and pyrrhotite was found (Baldwin, 1989).